LEIBNIZ INSTITUTE FOR
TROPOSPHERIC RESEARCH

# Biennial Report

## Zweijahresbericht

## 2010 / 2011

Leibniz Institute for Tropospheric Research

# Biennial Report

## Zweijahresbericht

# 2010 / 2011

LEIBNIZ INSTITUTE FOR
TROPOSPHERIC RESEARCH

## Imprint

***Published by***
Leibniz Institute for Tropospheric Research (IfT)
Leibniz-Institut für Troposphärenforschung e.V. Leipzig (IfT)

Member of the Leibniz Association (WGL)

*Postal address:* Permoserstr. 15
04318 Leipzig
Germany

*Phone:* ++49 - 341-235-3210
*Fax:* ++49 - 341-235-2361
*E-mail:* dir-sekretariat@tropos.de
*Internet:* http://www.tropos.de

***Copy Editors***
Katja Schmieder, Konstanze Kunze, Kerstin Müller, Heike Scherf, Beate Richter

***Editorial Board***
Andreas Macke, Hartmut Herrmann, Ina Tegen

# Table of contents

# Introduction / Einleitung
## Overview / Übersicht

## Introduction

In the “Research Park Leipzig/Permoserstraße” close to the Helmholtz Centre for Environmental Research, the Leibniz-Institute for Surface Modification and other research establishments and related businesses you find the Leibniz Institute for Tropospheric Research (IfT). Its name identifies the IfT as a member of the Leibniz Association. The institute was founded for the investigation of physical and chemical processes in the polluted troposphere.

***Fig. / Abb. 1:*** *IfT main building. / IfT-Hauptgebäude.*

A well-defined and globally unique research profile of IfT emerged, with a focus the physical and chemical relations between atmospheric small airborne (aerosols) and cloud particles. Despite their minute absolute amount, aerosol particles and cloud droplets are essential parts of the atmosphere because they control the budgets of energy, water and trace substances of the Earth System. Human activities can change these highly disperse systems and thus feed back on human beings. This may happen via health effects caused by inhaled particles and fog droplets and through regional and global climate change.

Despite these strong connections between human beings, aerosols, and clouds, important

***Fig. / Abb. 2:*** *IfT cloud laboratory. / IfT-Wolkenlabor.*

## Einleitung

Auf dem Gelände des „Wissenschaftsparks Leipzig/Permoserstraße“, in Nachbarschaft zum Helmholtz-Zentrum für Umweltforschung, zum Leibniz-Institut für Oberflächenmodifizierung sowie weiteren Einrichtungen befindet sich seit 1992 das Leibniz-Institut für Troposphärenforschung e. V. (IfT). Sein Name weist es als Mitglied der Wissenschaftsgemeinschaft Gottfried Wilhelm Leibniz aus. Gegründet wurde es zur Erforschung physikalischer und chemischer Prozesse in der belasteten Troposphäre.

Es hat sich ein klares und weltweit einzigartiges Forschungsprofil herausgebildet, in dessen Mittelpunkt die physikalischen und chemischen Beziehungen zwischen atmosphärischen Schwebeteilchen (Aerosolen) und Wolkenpartikeln stehen. Trotz geringster absoluter Mengen sind diese Partikel wesentliche Bestandteile der Atmosphäre, weil sie den Energie-, Wasser- und Spurenstoffhaushalt des Erdsystems beeinflussen. Menschliche Aktivitäten können die Eigenschaften dieser hochdispersen Systeme verändern und direkt sowie indirekt auf den Menschen zurück wirken. Das kann sowohl über die gesundheitlichen Wirkungen eingeatmeter Partikel

***Fig. / Abb. 3:*** *IfT multi-purpose building. / IfT-Mehrzweckgebäude.*

und Nebeltröpfchen als auch über regionale und globale Klimaänderungen geschehen.

Trotz dieser wichtigen Beziehungen zwischen Mensch auf der einen und Aerosol/Wolken auf der anderen Seite sind die physiko-chemischen Prozesse von Aerosol- und Wolkenbildung und die Wechselwirkungen mit Gesundheit und Klima noch wenig verstanden. Dies liegt vor allem an Schwierigkeiten bei der Analyse der beteiligten kleinsten Stoffmengen und an dem komplexen Verhalten troposphärischer Mehrphasensysteme, deren Einzelprozesse in der Atmosphäre nicht klar getrennt beobachtet werden können. In der gegenwärtigen Klimadiskussion zum globalen

physico-chemical processes of aerosol and cloud formation and the relationships with climate and health are poorly understood. This limitation is mainly due to difficulties with analyzing the very small samples and with the complex behavior of tropospheric multiphase systems, in which individual processes seldom can clearly be distinguished. In climate research this limitation is reflected in much larger uncertainties in predicted anthropogenic aerosol and cloud effects in comparison to numbers published by the Intergovernmental Panel on Climate Change for additional greenhouse gases.

Rapid advances in our understanding of tropospheric multiphase processes and an application of this process understanding to the prediction of the consequences of human impacts can only be expected from concerted approaches from several directions. Consequently, the Leibniz Institute for Tropospheric Research conducts field studies in several polluted regions parallel to the development of analytical methods for aerosol and cloud research.

These tools are not only applied in field experiments but also in extensive laboratory investigations, which form a second major activity. A third approach consists of the formulation and application of numerical models that reach from process models to regional simulations of the formation, transformation and effects of

***Fig. / Abb. 4:*** *Laser beams transmitted at IfT by Polly (2-channel lidar), two Polly$^{XT}$ (6-channel lidars), and the EARLINET lidar (9-channel lidar). / Laserstrahlen über dem IfT von Polly (2-Kanal-Lidar), zwei Polly$^{XT}$ (6-Kanal-Lidar) und dem EARLINET-Lidar (9-Kanal-Lidar).*

***Fig. / Abb. 5:*** *IfT research station Melpitz near Leipzig. / IfT-Forschungsstation Melpitz bei Leipzig.*

Wandel spiegelt sich diese Kenntnislage in den sehr viel größeren Unsicherheiten in allen zu Aerosol- und Wolkenwirkung veröffentlichten Zahlen im Verhältnis zu Treibhauseffekten der Gase wider.

Rasche Zuwächse im Verständnis troposphärischer Mehrphasenprozesse und eine Anwendung dieses Prozessverständnisses auf die Vorhersage der Folgen menschlicher Eingriffe lassen sich nur durch ein konzertiertes Vorgehen in mehreren Richtungen erwarten. Das Leibniz-Institut für Troposphärenforschung betreibt daher neben Feldstudien in belasteten Regionen auch die Entwicklung eigener physikalischer und chemisch-analytischer Verfahren zur Untersuchung von Aerosolen und Wolken. Diese Verfahren werden auch in ausgedehnten Laboruntersuchungen eingesetzt, der zweiten Hauptarbeitsrichtung des Instituts. Ein dritter Arbeitsbereich entwickelt und wendet numerischer Modelle von der Prozessbeschreibung bis zur Beschreibung der regionalen Bildung, Umwandlung und Wirkung troposphärischer Mehrphasensysteme an und bildet den Rahmen für ein umfassendes Prozessverständnis atmosphärischer Multiphasensysteme.

## Feldexperimente

Die Feldexperimente des Instituts dienen der Aufklärung des atmosphärischen Kreislaufs der Aerosolpartikel und Wolkentropfen und der damit verbundenen Prozesse. Die Komplexität des Systems wird dabei unter anderem dadurch bestimmt, dass in der Atmosphäre Partikel und Tropfen auftreten, deren Größe sich im Nano- und Mikrometerbereich um mehr als sechs Zehnerpotenzen unterscheiden kann, die dementsprechend auch unterschiedlichen Umwandlungsprozessen unterliegen. Außerdem kann man im Aerosol alle kondensationsfähigen Stoffe des Erdsystems finden, von denen eine große Zahl das Klima und die Biosphäre und deren Wirkung beeinflussen. Als Folge dieser

***Fig. / Abb. 6:*** *Arterial road in Leipzig. / Hauptverkehrsader in Leipzig.*

tropospheric multiphase systems. This approach provides the framework for an overall process understanding of tropospheric multiphase systems.

**Field experiments**

Field experiments elucidate the atmospheric life cycle and related processes of aerosol particles and cloud droplets. This task is vastly more difficult than comparable trace gas studies because particle and droplet diameters in the nano and micrometer size range over more than six orders of magnitude in atmospheric aerosols and clouds, all of which play an important role in certain processes. Furthermore, all atmospheric condensable substances can be found in the aerosol and a large number of them contribute to climate and biospheric effects. Essential properties of aerosol particles and cloud droplets of this multidimensional system are not well established on a global scale yet.

This uncertainty and thus the research efforts of the Leibniz Institute for Tropospheric Research start with particle sources. The combustion of fossil and contemporary fuels is one of the most prominent aerosol sources. However, these sources are still

***Fig. / Abb. 7:*** *View from the Campus of Peking University on a heavily polluted day. / Blick vom Gelände der Peking Universität an einem stark verschmutzten Tag.*

Vielfalt und der mengenbedingten analytischen Schwierigkeiten sind wesentliche globale Aerosol- und Wolkeneigenschaften noch wenig bekannt.

Diese Unsicherheit beginnt schon bei den Partikelquellen, die ebenfalls Forschungsgegenstand am Leibniz-Institut für Troposphärenforschung sind. Die Verbrennung fossiler und nachwachsender Brennstoffe zur Energieerzeugung und im Verkehr sind wichtigste Aerosolquellen. Wie sich aus Messungen des Instituts an vielen urbanen Messstellen und kontinentalen Hintergrundstationen ergab, unterliegen die Emissionen von Partikeln und deren Vorläufern enormen physikalischen und chemischen Umwandlungen, die mit hoher zeitlicher Auflösung verfolgt werden müssen, um die beteiligten Prozesse aufzuklären.

Selbst die am höchsten verunreinigten Regionen über Nordamerika, Europa, Afrika, dem

***Fig. / Abb. 8:*** *Monitoring station Leipzig, Eisenbahnstraße (red building). / Messstation Leipzig, Eisenbahnstraße (rotes Gebäude).*

indischen Subkontinent, dem Amazonasgebiet und Ostasien sind noch bei weitem nicht hinreichend bezüglich ihrer Aerosolbelastungen und den daraus resultierenden Klimawirkungen charakterisiert. Auf diese Regionen konzentrieren sich daher in internationaler Zusammenarbeit die Feldexperimente des Instituts. Das Institut beteiligt sich deshalb an internationalen Messkampagnen und Langzeitmessungen in Asien, Südamerika und der maritimen Troposphäre über dem südlichen und nördlichen Atlantik. Seit einigen Jahren nehmen Untersuchungen zum Mineralstaub und dessen Wirkung auf den Strahlungshaushalt und Wolkenbildung im Quellgebiet der Sahara, aber auch im Fernfeld über dem Nordatlantik wachsenden Raum ein. Durch Nutzung eines kommerziellen Verkehrsflugzeuges der Lufthansa werden auch Aerosolverteilungen in der belasteten oberen Troposphäre auf regelmäßig beflogenen interkontinentalen Routen vermessen.

Auf kleineren Skalen werden Untersuchungen zur Partikelbildung und Wechselwirkung zwischen Aerosolpartikeln und Wolken und der

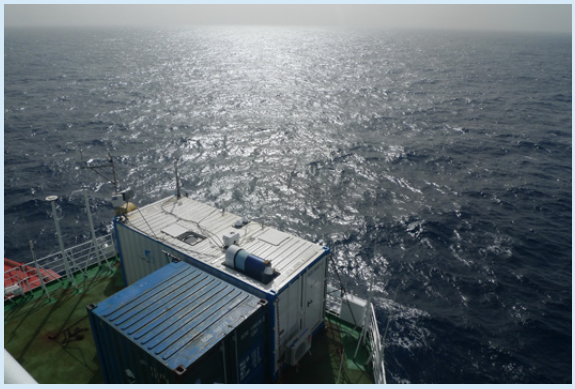

***Fig. / Abb. 9:*** *Container based OCEANET Atmospheric Observatory on its first mission onboard Research Vessel Polarstern in the North and South Atlantic. / Containerbasiertes OCEANET Atmosphärenobservatorium auf der ersten Mission an Bord des Forschungsschiffes Polarstern im Nord- und Südatlantik.*

poorly characterized in terms of climate-relevant aerosol parameters. According to long-term urban and rural measurements of the institute emissions of particles and their precursor gases are subject to strong physical and chemical transformations that need to be followed with high-resolution sensors in order to identify the underlying processes.

Not even the largest highly polluted regions in the plumes of North America, Europe, Africa, the Indian subcontinent, Amazonia, and Eastern Asia are sufficiently characterized in terms of aerosol burdens and ensuing climate effects. The institute focuses thus its participation in international field campaigns and dedicated long-term studies in Asia, South America and the marine troposphere over the northern and southern Atlantic. In recent years, the study of climate-relevant aspects of mineral dust near its most important Saharan source and in the far field over the Atlantic have gained more weight in the institute's research. By means of a commercial aircraft operated by Lufthansa on intercontinental routes, aerosol measurements are conducted even in the polluted upper troposphere.

On smaller scales, investigations concerning new particle formation, the interactions between

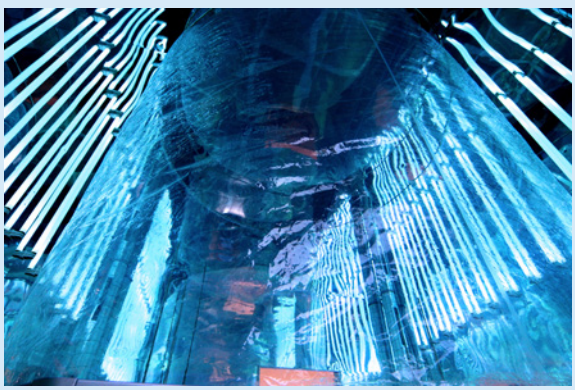

***Fig. / Abb. 10:*** *The IfT aerosol chamber (LEAK) with UV lamps. / Die IfT-Aerosolkammer (LEAK) mit UV-LAMPEN.*

Einfluss turbulenter Mischungsprozesse auf die Wolkenentwicklung mit Hilfe der hubschrauber-getragenen Messplattform ACTOS durchgeführt. Zusätzlich werden Bergstationen zu Prozessstudien genutzt die sich dem Verständnis von Einzelprozessen, wie der Partikelneubildung, der physiko-chemischen Veränderung des Aerosols beim Wolkendurchgang und dem Einfluss von Aerosolen auf die Entwicklung von Wolken widmen.

Das IfT ist maßgeblich an regionalen, nationalen und Europäischen Messnetzen zur Erfassung des Aerosols und der Bewölkung beteiligt. Das Institut betreibt weiterhin das Weltkalibrierzentrum der WMO für physikalische Aerosolmessungen zur Qualitätssicherung von in-situ Messungen an nationalen und internationalen Messstationen.

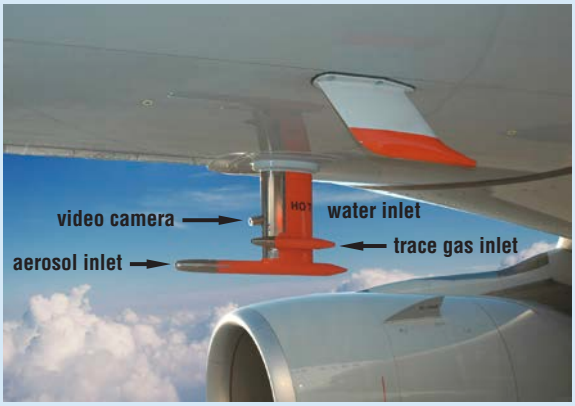


***Fig. / Abb. 11:*** *CARIBIC inlet system at the lower fuselage of a Lufthansa Airbus A340-600. In CARIBIC regular measurements of trace gases and aerosol particles are carried out in the free troposphere since 1997 using commercial aircraft. / CARIBIC-Einlasssystem an der Rumpfunterseite eines Lufthansa-Airbus A340-600. Im Projekt CARIBIC werden mit Hilfe eines kommerziellen Flugzeugs seit 1997 regelmäßige Messungen von Spurengasen und Aerosolpartikeln in der freien Troposphäre durchgeführt.*

**Laborexperimente**

In der Atmosphärenforschung werden kontinuierlich physikalisch-chemische Modelle zur Beschreibung der wesentlichen Prozesse entwickelt. Grundlage derartiger Modelle sind stets Prozessparameter, die in Laborexperimenten unter bekannten Umgebungsbedingungen ermittelt werden.

In der Abteilung Physik werden im Bereich der Laborexperimente zahlreiche Messmethoden entwickelt, die zur Partikelcharakterisierung in boden- und luftgestützten Feldmesskampagnen eingesetzt werden. Im Einzelnen betreffen diese Arbeiten die Weiterentwicklung von DMA-basierenden (Differentieller Mobilitätsanalysator) Größenspektrometern sowie Sammelsysteme zur physikalischen und chemischen Charakterisierung von Wolkentröpfchen und dem interstitiellen Aerosol, also denjenigen Aerosolpartikeln, die

aerosol particles and clouds, and the influences of turbulent mixing processes on cloud development are carried out with help of the helicopter-borne measurement platform ACTOS. In addition, process studies are conducted at suitable locations such as mountain observatories to study particle nucleation, particle processing through clouds and the influence of anthropogenic aerosols on the optical properties of clouds.

The IfT leads several regional, national and European meausrements networks to monitor aerosols and cloudiness. The IfT hosts the WMO World Calibration Centre for physical in-situ aerosol measurements to assure high quality standards at national and international observatories.

***Fig. / Abb. 13:*** *Mini Raman lidar Polly $^{XT}$ in an air-conditioned cabinet. / Mini-Ramanlidar Polly $^{XT}$ im klimatisierten Gehäuse.*

### Laboratory experiments

In atmospheric research, there is a continuous development of physico-chemical models for the description of the most relevant process. These models are based on process parameters, which need to be determined in laboratory experiments under controlled environmental conditions.

In the physics section of the institute, laboratory experiments cover the development of a large number of methods to characterize atmospheric particles and droplets. In particular, DMA-based (Differential Mobility Analyzer) size spectrometers

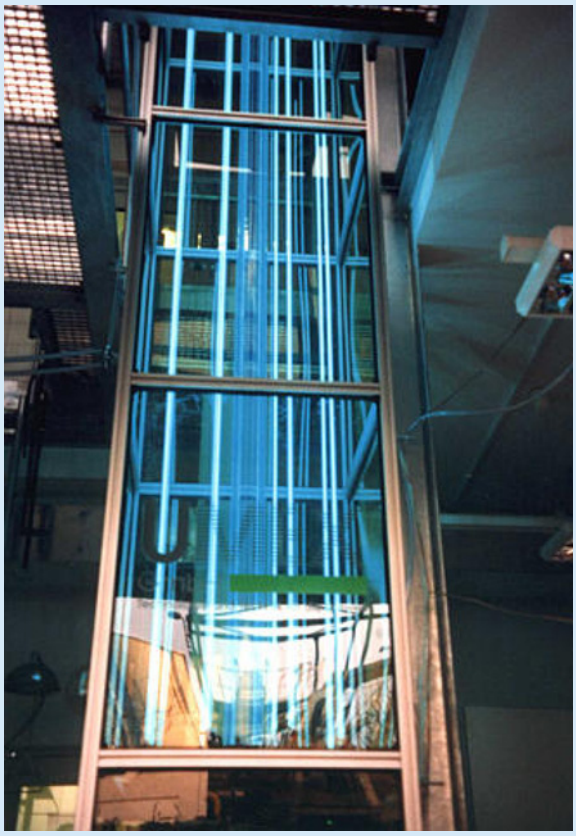

***Fig. / Abb. 12:*** *The IfT laminar flow tube reactor (IfT-LFT). / Der laminare Rohrreaktor des IfT.*

innerhalb von Wolken neben den Wolkentröpfchen selbst in der Gasphase suspendiert sind.

Optische Messmethoden werden zur Bestimmung der Extinktion von Partikeln und der Absorption von Spurengasen und Radikalen mittels der differentiellen Absorptionsspektroskopie (DOAS) angewendet. Mehrwellenlängenlidare und ein Windlidar werden zur Bestimmung von Aerosoleigenschaften, Aerosolflüssen und meteorologischen Parametern wie Temperatur, Feuchte und Wind im Labor weiterentwickelt und im Feld eingesetzt. Die Anteile „schwarzen Kohlenstoffs“ und mineralischer Aerosolkomponenten in Aerosolproben werden durch spektrale Absorptionsmessungen bestimmt.

In zwei Bereichen werden prozessorientierte Laboruntersuchungen gemeinsam von den Abteilungen Physik und Chemie durchgeführt. Diese abteilungsübergreifenden Aktivitäten betreffen einen als Laminarströmungsrohr ausgeführten Reaktor, an dem die Bildung von Partikeln aus $SO_2$ untersucht wird. Im Jahr 2005 nahm das IfT das neue Wolkenlabor rund um den Strömungsreaktor LACIS in Betrieb. Untersuchungen von LACIS betreffen das hygroskopische Wachstum von Aerosolpartikeln unterschiedlichster chemischer Zusammensetzung, deren Aktivierung zu Wolkentröpfchen sowie deren Gefrieren. Ziele dieser Untersuchungen sind die Erlangung eines besseren Prozessverständnisses auf fundamentaler Ebene, die Identifikation kritischer und kontrollierender Parameter und die Entwicklung geeigneter Parametrisierungen zur Beschreibung von Tröpfchen- und Niederschlagsbildung sowie Partikelalterungsprozesse in dynamischen Modellen.

In der Abteilung Chemie werden Gasphasenreaktionen der Radikale OH und $NO_3$ in Strömungsreaktoren und der Leipziger Aerosolkammer (LEAK) untersucht. Diese Reak-

and sampling systems for the characterization of cloud droplets and interstitial aerosol particles are designed. Spectroscopic techniques such as the Differential Optical Absorption Spectroscopy have been developed for the analysis of trace gases and aerosol particles. Multi-wavelength aerosol LIDAR (Light Detection and Ranging) systems are developed in the field for measuring atmospheric state parameters such as temperature, wind and relative humidity besides aerosol-optical characteristics and aerosol fluxes. Black carbon and mineral, light absorbing aerosol components are quantified with spectroscopic methods in aerosol and cloud samples.

The physics and chemistry sections are jointly carrying out process-oriented laboratory studies in two main areas. The first of these activities concerns a laminar flow tube reactor in which particle formation from $SO_2$ is being investigated. With the large Leipzig Aerosol Cloud Simulator LACIS founded in 2005, the hygroscopic growth of aerosol particles, their activation to cloud droplets and the freezing of cloud droplets are considered. Goals of these investigations are achieving a better understanding concerning the underlying fundamental processes, the identification of critical and controlling parameters, and the development of parameterizations of cloud and precipitation formation as well as particle aging processes for use in dynamical models.

The chemistry department conducts several process-oriented laboratory studies. Gas phase reactions of the radicals OH and $NO_3$ are being investigated in flow reactors. These reactions are important for ozone and particle formation caused by biogenic and anthropogenic emissions of volatile hydrocarbons. These investigations are also done in collaboration with the Physics Department determining hygroscopic growth and

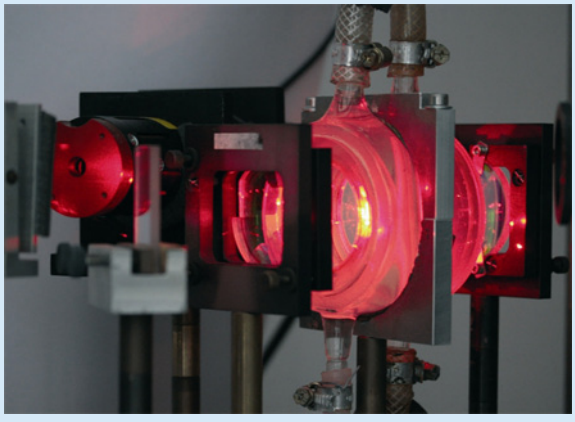

***Fig. / Abb. 14:*** *Experimental set-up including White cell optics, reaction cell and solid state laser for the kinetic investigation of nitrate-radical ($NO_3$) reactions in aqueous solution. / Versuchsaufbau zur Messung der Kinetik von Nitratradikalreaktionen ($NO_3$) in wässriger Lösung mit Festkörperlaser, Whitespiegel-Konfiguration und Reaktionszelle.*

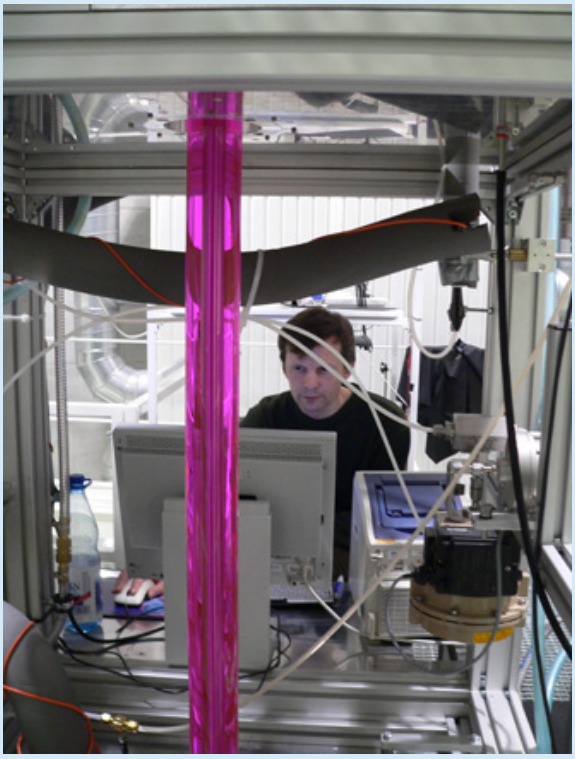

***Fig. / Abb. 15:*** *The "Leipzig Aerosol Cloud Interaction Simulator" (LACIS). / Der Wolkenkanal (LACIS).*

tionen sind von Interesse für die Ozon- und Partikelbildung, verursacht durch anthropogene oder biogene flüchtige Kohlenwasserstoffe. Die Untersuchungen laufen auch in Zusammenarbeit mit der Abteilung Physik zur Bestimmung des Feuchtewachstums und der Tropfenaktivierung der erzeugten Partikel.

In einem Einzeltropfenexperiment werden Phasentransferparameter für Spurengase und Radikale untersucht. Die Bestimmung von Phasentransferparametern und reaktiven Aufnahmekoeffizienten wird dabei auf bisher nicht betrachtete chemische Spezies und komplexe Oberflächen ausgeweitet. Im Bereich von Flüssigphasenmechanismen werden Reaktionen von vorwiegend radikalischen Oxidantien mit zeitaufgelösten optischen Nachweistechniken untersucht. Diese Reaktionen laufen in den Tröpfchen von Wolken, Regen und Nebel sowie in wässrigen Aerosolpartikeln ab. Hier werden zum Verständnis der Oxidation organischer Spurengase im troposphärischen Mehrphasensystem eine Vielzahl von Reaktionen der Radikale OH und $NO_3$ sowie Reaktionen von halogenhaltigen Oxidantien untersucht. Letztere Spezies sind von Interesse bei der Freisetzung von Halogenverbindungen aus maritimen Seesalzpartikeln, der so genannten Halogenaktivierung.

In der analytischen Messtechnik werden in Laborexperimenten Verfahren zur besseren chemischen Charakterisierung der organischen Bestandteile von Aerosolpartikeln entwickelt und

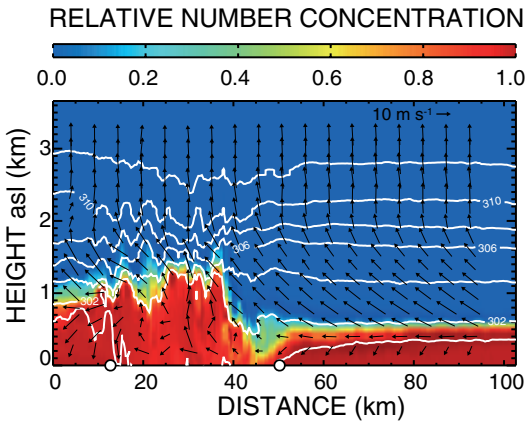


***Fig. / Abb. 16:*** *The Image shows the vertical distribution of a passive tracer above the Cape Verdean island of Santiago, located between the two dots at 12 km and 50 km. The arrows show the horizontal wind direction. / Das Bild zeigt die vertikale Verteilung eines passiven Tracers über der kapverdischen Insel Santiago, die sich zwischen den beiden Punkten bei 12 km und 50 km erstreckt. Die Pfeile zeigen die horizontale Windrichtung.*

cloud droplet activation of the particles formed. The chemical identity of atmospheric particles is being characterized in the Leipzig Aerosol Chamber (LEAK). In a single drop experiment, phase transfer parameters of trace gases and radicals are being determined for different chemical species and surfaces. Experiments with radical reactions in the liquid phase form a core activity of the laboratory experiments, because of their importance for processes in haze particles, fog and cloud droplets as well as in deliquescent aerosol particles. For the understanding of the oxidation of organic trace gases in the tropospheric multi-phase system, a large number of reactions with the OH and $NO_3$ radicals are being studied as well as reactions of halogenated oxidants. The latter species are of interest for the emission of reactive halogen compounds from sea salt particles.

Several laboratory experiments are dedicated to the chemical characterization of atmospheric organic aerosol components. Besides the conventional combustion techniques, mass spectroscopic and chromatographic techniques coupled directly to analysis by mass spectrometry or capillary electrophoresis with different sampling and segregation techniques are being developed.

## Modeling

For the description of complex atmospheric processes, model systems of varying dimensions and complexity for micro- and mesoscale problems are developed, tested and applied using data of field experiments and satellite measurements.

One focus of research is the description of cycles, interactions and phase transfer between aerosol particles, gases and clouds. The aim is an

getestet. Diese Techniken beruhen zumeist auf massenspektrometrischen Verfahren, die in verschiedenen Kopplungstechniken eingesetzt werden. Im Bereich der Probenahmetechniken gibt es auch hier eine enge Kooperation mit der Abteilung Physik zur Entwicklung einer gezielten Abscheidung von Partikeln bestimmter Größe und deren chemischer Analyse.

## Modellierung

Zur Beschreibung der komplexen atmosphärischen Vorgänge werden Modellsysteme verschiedener Dimension und Komplexität für die Mikro- bis Mesoskala entwickelt, überprüft und angewendet; auch in Kombination mit Daten aus Feldmessungen und aus satellitengestützten Fernerkundungen.

Ein Forschungsschwerpunkt ist, die Kreisläufe, Wechselwirkungen und Phasenübergänge zwischen Aerosolpartikeln, Gasen und Wolken zu beschreiben, um so zu einer Verbesserung des Verständnisses klimarelevanter Prozesse in troposphärischen Mehrphasensystemen zu gelangen.

Chemie-Transportmodellierung wird durch das am IfT entwickelte 3D-Modellsystem COSMO-MUSCAT realisiert. Seine Brauchbarkeit zur Simulation des Ausbreitungsverhaltens von Partikeln und Gasen auf regionaler Skala wurde in mehreren internationalen Modellvergleichen und bei der Bearbeitung von Fragen zur

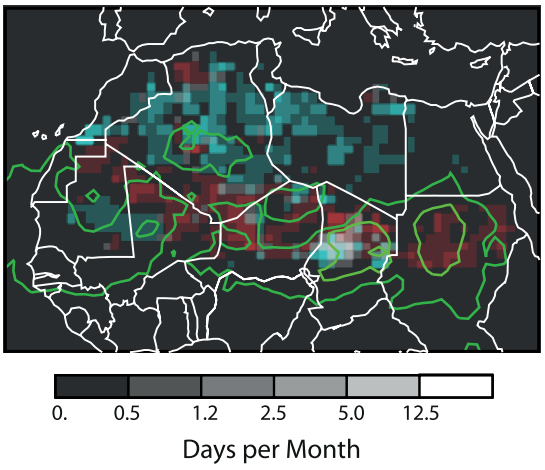


***Fig. / Abb. 17:*** *Annual average number of days per month of Saharan dust source activation for the year 2007. The red color scale represents dust source activation derived from the Meteosat Second Generation infrared dust index, the turquois shading represents model results from COSMO-MUSCAT. The contour lines indicate the occurrence of nocturnal low-level jets. / Durchschnittliche Anzahl von Tagen pro Monat im Jahr 2007, an denen eine Aktivierung von Saharastaubquellen stattfindet. Die rote Farbskala repräsentiert Ereignisse, die vom ‚Meteosat Second Generation'-Staubindex abgeleitet wurden; die türkisfarbene Skala repräsentiert Ergebnisse des COSMO-MUSCAT-Modells. Die Konturlinien beschreiben das Auftreten von nächtlichen Grenzschichtstrahlströmen.*

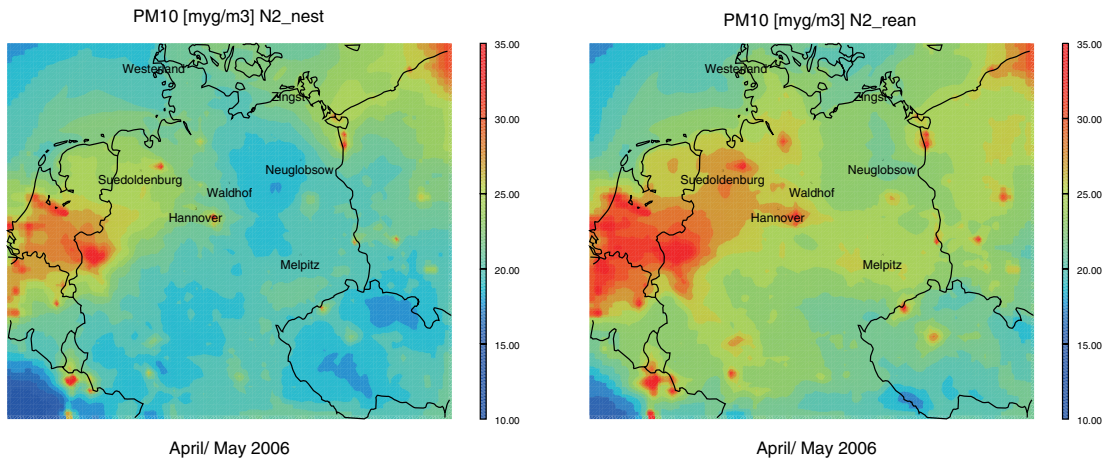


***Fig. / Abb. 18:*** *Comparison of averaged PM10 concentrations for different model setups: Meteorological forcing by nesting (left) and by reanalysis data (right). / Vergleich der mittleren PM10-Konzentrationen für unterschiedliche Modellkonfigurationen: Meteorologischer Antrieb durch Modell-Nestung (links) und mit Reanalyse-Daten (rechts).*

improvement in understanding of climate-relevant processes in the troposphere.

Chemistry-transport modeling is realized with the three-dimensional modeling system COSMO-MUSCAT that has been developed at the IfT and used for simulation of transport of photo oxidants and particles in a mesoscale region.

The model system was successfully tested in international model intercomparison studies and was applied for air quality studies. In several projects the dynamics of primary and secondary particles was simulated and their feedback on the radiative budget was investigated. For further investigations an “urbanized” version of COSMO-MUSCAT has been be developed and can be used with a horizontal grid resolution up to 180x180m. It will be applied for studies of the influence of future climate change on the budget of trace elements.

The model ASAM (All Scale Atmospheric Model) indicates future developments, applicable from the micro to the global scale. It realized cut cells in a Cartesian grid for the description of orography and obstacles. It is currently mainly used for simulations of transport of particles in the microscale domain (urban canyons and urban districts).

One- and two-dimensional process models are also developed and applied. SPECS (SPECtral bin cloud microphysicS) can be used for the investigation of cloud processes with a detailed description of condensation, collision or freezing. SPACCIM (SPectral Aerosol Cloud Chemistry Interaction Model) is a parcel model, which combines detailed microphysics with a complex multiphase chemistry. Both modules can be applied to for process modeling as one-dimensional box model version as well as coupled with the mesoscale model COSMO for the investigation of real situations. The process modeling studies are realized in connection with

Luftqualität im legislativen Bereich gezeigt. In mehreren Projekten wird die Dynamik primärer und sekundärer Aerosolpartikel simuliert und deren Rückkopplungseffekte auf die Strahlung untersucht. Für weitere Anwendungsmöglichkeiten wird zusätzlich eine „urbanisierte“ Version von COSMO-MUSCAT entwickelt, die eine horizontale Gitterauflösung bis hinab zu 180x180 m nutzt. Damit werden auch Untersuchungen zum Einfluss der regionalen Klimavariabilität auf Spurenstoffhaushalte durchgeführt.

Mit ASAM (All Scale Atmospheric Model) steht ein zukunftsweisendes, noch in der Weiterentwicklung befindliches Modell zur Verfügung, dessen dynamischer Kern für Anwendungen vom mikroskaligen bis zum globalen Maßstab eingesetzt werden kann und das in einem kartesischen Gitter mit angeschnittenen Zellen für die Darstellung von Orographie und Hindernissen realisiert wurde. Es wird gegenwärtig vor allem zur Simulation der Ausbreitung von Partikeln im mikroskaligen Bereich (Straßenschluchten, Stadtquartiere) genutzt.

Daneben wurden und werden ein- und zweidimensionale Prozessmodelle entwickelt bzw. weiterentwickelt. SPECS (SPECtral bin cloud microphysicS) dient zur Beschreibung von Wolkenprozessen. Es erlaubt eine explizite und sehr genaue Berechnung der Prozesse Kondensation, Kollision oder Gefrieren. SPACCIM (SPectral Aerosol Cloud Chemistry Interaction Model) ist ein Paketmodell zur gekoppelten größenaufgelösten Beschreibung von Mikrophysik und Mehrphasenchemie. Beide Module können sowohl als Boxmodell zur Prozessmodellierung als auch gekoppelt an das mesoskalige COSMO-Modell zur Untersuchung von realen Situationen verwendet werden. Die Prozessmodellierungen

field studies and experiments at LACIS (Leipzig Aerosol Cloud Simulator).

The model simulation of tropospheric multiphase systems is numerically highly demanding. The models need to be sufficiently accurate and numerically efficient to be used productively on existing computer systems. Ongoing developments within the modeling department aim at an increase in the model efficiencies.

werden im Zusammenhang mit Feldstudien sowie mit den Experimenten am Wolkenkanal LACIS durchgeführt.

Die modelltechnische Behandlung eines so umfassenden atmosphärischen Systems ist numerisch sehr aufwendig. Die zu entwickelnden Modelle müssen hinreichend genau sein und numerisch sehr effizient den jeweils zur Verfügung stehenden Rechnerarchitekturen angepasst werden. Zur Optimierung der verwendeten numerischen Verfahren und Parallelisierungsstrategien liefert die Abteilung Modellierung ebenfalls wesentliche Beiträge.

## Overview of the individual contributions

The institute's work is structured into three major research themes:

1. *Evolution, transport and spatiotemporal distribution of tropospheric aerosol*
2. *Effect of tropospheric aerosol on clouds and on the radiation budget*
3. *Chemical processes in tropospheric multiphase systems*

The aim of the corresponding studies is to explore significant processes in the troposphere and to improve the forecast of tropospheric multiphase systems by means of detailed process studies.

The work in the departments "Physics" and "Atmospheric Modelling" are aiming in about equal parts mostly at the first two research topics whereas the "Chemistry" department mainly mostly covers topic 1 and 3. On top of that a number of inter-department studies exist in all departments and for all research topics.

The present annual report introduces the work of the IfT in the time period 2010-2011 by means of 3 extended and 18 short contributions.

The DFG research group SAMUM (Saharan Mineral Dust Experiment) was successfully completed in 2011 after a 7 years term. Exemplarily for numerous publications **Tegen et al.** report on the successful combination of laboratory and field measurements on the one hand and the development and application of an aerosol transport model for integrative process understanding on the other hand. This combination represents a special quality of the institute. The results provide the base for the next step: the research of dispersion and aging of African aerosol along its way over the Atlantic, and the resulting impact on weather and climate, especially with respect to cloud formation processes.

## Übersicht der Einzelbeiträge

Die Arbeiten des Instituts gliedern sich in drei übergeordnete Forschungsthemen:

1. *Evolution, Transport und raumzeitliche Verteilung des troposphärischen Aerosols*
2. *Einfluss des troposphärischen Aerosols auf Wolken und Strahlungshaushalt*
3. *Chemische Prozesse in troposphärischen Mehrphasensystemen*

Das Ziel der damit verbundenen Arbeiten ist es, signifikante Prozesse in der Troposphäre zu erkunden und durch detaillierte Prozess-Studien die Vorhersage troposphärischer Mehrphasensysteme zu verbessern.

Die Arbeiten der Abteilungen „Physik" und „Atmosphärische Modellierung" zielen zu etwa gleichen Teilen zumeist auf die ersten beiden Forschungsthemen ab, während die Abteilung „Chemie" hauptsächlich die Themen 1 und 3 abdeckt. Darüber hinaus gibt es eine Vielzahl abteilungsübergreifender Arbeiten in allen Abteilungen und zu allen Themenbereichen. Der vorliegende Jahresbericht stellt in drei längeren und 18 Kurzbeiträgen einige ausgewählte Arbeiten des IfT im Zeitraum 2010 bis 2011 vor.

Nach sieben erfolgreichen Arbeitsjahren fand die DFG-Forschergruppe SAMUM **(Saharan Mineral Dust Experiment)** in 2011 ihren Abschluss. Exemplarisch für zahlreiche Publikationen berichten **Tegen et al.** über die gelungene Verbindung von Labor- und Feldmessungen auf der einen Seite und die Entwicklung und Anwendung von Modellen für ein integratives Prozessverständnis auf der anderen Seite. Diese Verbindung stellt eine besondere Qualität des Instituts dar. Die Ergebnisse legen die Basis für den nächsten Schritt: die Erforschung der Ausbreitung und Alterung des afrikanischen Aerosols auf seinem

Generally, numerous interactions between gas phase, aerosol particles and liquid phase occur in clouds. Field experiments on orographic clouds enable a ground-based in-situ measurement of these interactions in the real atmosphere.

A corresponding project to this issue was Hill Cap Cloud Thuringia 2010 (HCCT-2010), successfully performed in September/October 2010 on Mount Schmücke in Thuringia. Gas phase, particles and cloud droplets were physically and chemically characterized in detail based on three measurement sites on the up- and downwind valley sides and on the Schmücke summit. **Pinxteren et al.** introduce the first results of this international measurement campaign that was lead by the IfT. A first highlight was the detection of a stronger hygroscopic growth of aerosol particles after the cloud passage. Field experiments and modelling activities were strongly cooperating in this campaign.

Measurements of particles in clouds are a technical and logistical challenge.

For detailed investigation of microphysical and dynamic characteristics of surface remote clouds the IfT utilizes the helicopter-borne measurement payload ACTOS (Airborne Cloud Turbulence Observation System). In November 2010 and April 2011 two measurement campaigns with ACTOS were performed over Barbados in shallow trade wind clouds, accompanied by ground-based remote sensing from the department of the Max-Planck-Institute of Meteorology and the radiation measurement department of the Leipzig Institute of Meteorology. **Siebert et al.** summarize the most important results of the first two campaigns. The detection of so-called giant cloud condensation nuclei, which may play a key role in explaining precipitation in shallow maritime cumulus is noted here as an example.

Without any doubt the 2010 eruption of the Eyjafjallajökull volcano and the resulting transport of volcanic ash over Europe was a significant incident within the reporting period. As a leading member in the European Aerosol Research Lidar Network (EARLINET) the IfT was the first institute able to evaluate the ash concentration and hence published the worldwide first scientific publication relating to this topic. In the present report **Seifert et al.** demonstrate how mass concentrations of volcanic and non-ash aerosol can be separated from combined polarization lidar and sun photometer measurements, which will become a standard for a European network in the long term. They also show that volcanic ash is a very efficient ice nuclei and thus plays an important role in the onset of precipitation in supercooled clouds.

The intensive discussion about “no-flight-zones” caused by volcanic ash emphasizes the importance of a reliable large-scaled modelling of ash transport. In a comprehensive study **Heinold et al**. point to the

Generell finden in Wolken zahlreiche Wechselwirkungen zwischen Gasphase, Aerosolpartikeln und flüssiger Phase statt. Feldexperimente an orographischen Wolken erlauben eine bodengestützte in-situ Untersuchung dieser Wechselwirkungen in der realen Atmosphäre. Hill Cap Cloud Thuringia 2010 (HCCT-2010) war ein solches Experiment, das im September/Oktober 2010 an der Schmücke im Thüringer Wald erfolgreich durchgeführt wurde. Gasphase, Partikel und Wolkentropfen wurden an drei Messpunkten im Luv, auf dem Gipfel und im Lee der Schmücke umfassend chemisch und physikalisch charakterisiert. **Van Pinxteren et al.** stellen die ersten Ergebnisse dieser vom IfT angeführten internationalen Messkampagne vor. Ein erstes Highlight ist die Entdeckung einer erhöhten Hygroskopizität von Aerosolpartikeln nach dem Passieren der Wolkenphase. Auch in diesem Großexperiment wirken Feldexperimente und Modellierung zusammen. Die Messung von Partikeln in Wolken stellt eine besondere technische und logistische Herausforderung dar. Zur detaillierten Erfassung der mikrophysikalischen und dynamischen Eigenschaften bodenferner Wolken steht dem IfT seit einigen Jahren die Hubschrauberschleppsonde ACTOS zur Verfügung. Im November 2010 und April 2011 wurden über Barbados zwei Messkampagnen mit ACTOS in flachen Passatwindwolken durchgeführt und von der bodengebundenen Wolkenfernerkundung des Max-Planck Instituts für Meteorologie sowie Strahlungsmessungen des Leipziger Instituts für Meteorologie begleitet. **Siebert et al.** fassen die wichtigsten ersten Ergebnisse beiden Kampagnen vor. Erwähnt sei hier exemplarisch die Messung von sogenannten gigantischen Wolkenkondensationskernen, die ein Schlüssel zur Erklärung von Niederschlagsbildung in flachen maritimen Kumuluswolken sein können.

Ein wichtiges Ereignis im Berichtszeitraum war zweifellos der Ausbruch des Vulkans Eyjafjallajökull auf Island und der damit verbundene Transport von Vulkanasche über Europa. Als führendes Mitglied im Europäischen Lidarnetzwerk EARLINET war das IfT als erstes Institut in der Lage, die Aschekonzentrationen abzuschätzen und hat folgerichtig die weltweit erste internationale Fachpublikation zu diesem Ereignis veröffentlicht. Im vorliegenden Bericht demonstrieren **Seifert et al.**, wie aus der Kombination von Lidar- und Sonnenphotometermessungen - die langfristig zum Standard eines europäischen Messnetzes werden – die aus Messungen abgeleiteten Massekonzentrationen von Asche

significance of model initialization for the accurate calculation of ash dispersion. These simulations show which emission heights contributed to the observed spatiotemporal dispersion of volcanic ash over Europe. They further find that emission heights derived from satellite remote sensing are able to provide promising model initializations.

Rain in the mid und high latitudes nearly exclusively evolve from the ice phase. In this process so called ice nuclei activate the freezing mechanism. Which ice nuclei generates which nucleation rate and how the relevant mechanisms look like are elementary questions of cloud physics. To address these questions is a central task of the IfT. The following three studies investigate this topic from different points of view. Biological particles, especially bacteria belong to the most effective ice nuclei, as found in the atmosphere or in rain samples. **Hartmann et al.** were able to specifically prove this by measurements at the Leipzig Aerosol Cloud Interaction Simulator (LACIS) for the bacterial strain Pseudomonas Syringae.

Due to the different land/sea distribution in the northern and southern hemisphere and the correspondingly different origins of aerosol particles ice formation in clouds may differ as well. In fact, by means of lidar observations in Punta Arenas, Cape Town, on the research vessel Polarstern and in Leipzig **Kanitz et al.** found that the stronger maritime southern hemisphere aerosol produces significant less ice than the more anthropogenic northern hemisphere aerosol.

The process of heterogeneous ice nucleation has been described alternatively in the literature as being stochastic or deterministic. A ground-braking theoretical study of **Niedermeier et al.** proves that the first assumption as generally true, but they also show that ice nuclei with typically strongly variable surface area properties in reality show deterministic freezing behaviour.

Observing the tropospheric aerosol by means of state-of-the-art measurement technique is a core competence of the IfT. By means of measurement networks large scale pattern in the polluted troposphere become visible. A typical example for this is the wintertime smog episode. For the geographical area of Saxony **Birmili et al.** detect local and East European main source areas for particulate matter pollution. A statistical analysis for the time period 1990 - 2010 shows that the number of threshold exceedances is climatologically coupled to low temperatures.

Since 1997 the IfT participates in measurement flights on a board an airliner on a regular basis. For the first time **Hermann et al.** could establish a climatology of the upper tropospheric aerosol from the collected measurement data and compared these to results from climate model calculations. The differences found provide important information

und aschefreiem Aerosol getrennt werden können. Sie zeigen ebenso, dass Vulkanasche einen extrem geeigneten Eisbilder und damit Niederschlagsauslöser in unterkühlten Wasserwolken darstellt.

Die intensive Diskussion um die mit dem Vulkanaschetransport verursachten Flugverbotszonen unterstreicht die Bedeutung einer zuverlässigen großräumigen Modellierung des Aschetransports. In einer umfangreichen Modellstudie weisen **Heinhold et al.** auf die Bedeutung der Modellinitialisierung aus Beobachtungen für die Genauigkeit der Ausbreitungsrechnungen hin. Die Simulationen zeigen, welche Emissionshöhen zur tatsächlichen raumzeitlichen Verteilung der Vulkanasche über Europa beigetragen haben, und dass Emissionshöhen aus Satellitenmessungen vielversprechende Modellinitialisierungen liefern können.

Regen in den mittleren und hohen Breiten entsteht fast ausschließlich über die Eisphase. Dabei lösen sogenannte Eiskeime den Gefrierprozess aus. Welche Eiskeime welche Gefrierraten erbringen und welche Mechanismen dabei zum Tragen kommen sind sehr elementare Fragestellung der Wolkenphysik. Deren Beantwortung ist eine der zentralen Aufgaben des IfT. Die folgenden drei Arbeiten behandeln diese Thematik unter verschiedenen Gesichtspunkten. Biologische Partikel, insbesondere Bakterien, gehören zu den effektivsten Eiskeimen, die in der Atmosphäre bzw. in Niederschlagsproben gefunden werden. **Hartmann et al.** konnten dies mit Messungen am Leipzig Aerosol Cloud Interaction Simulator (LACIS) konkret für den Bakterienstamm Pseudomonas Syringae nachweisen.

Aufgrund der unterschiedlichen Land/See-Verteilung auf Nord- und Südhemisphäre unseres Planeten und den damit verbundenen hemisphärisch unterschiedlichen Aerosolquellen könnte auch die Eiskeimfähigkeit verschiedenen sein. Tatsächlich konnten **Kanitz et al.** anhand von Lidarmessungen in Punta Arenas, Kapstadt, auf dem Forschungsschiff Polarstern sowie in Leipzig nachweisen, dass das stärker maritim geprägte südhemisphärische Aerosol bei vergleichbaren meteorologischen Bedingungen deutlich weniger Eis produziert als das mehr kontinental und anthropogen geprägte nordhemisphärische Aerosol.

Der eigentliche Prozess der heterogenen Eisbildung wird in der Literatur wahlweise als zufälliger oder deterministischer Mechanismus dargestellt. In einer bahnbrechenden theoretischen Arbeit können **Niedermeier et al.** nachweisen, dass ersteres grundsätzlich der Fall ist, jedoch Eiskeime mit typischerweise sehr variablen Oberflächeneigenschaften in der Praxis ein deterministisches Gefrierverhalten aufweisen.

for model improvements and for our general understanding of aerosol transport and production processes.

Within the reporting period the ground-based remote sensing of the troposphere has made a major step towards the mobile aerosol-cloud remote sensing by purchasing and commissioning a cloud radar and complimentary instruments. **Wandinger et al.** introduce the new "Leipzig Aerosol and Cloud Remote Sensing Observations System" LACROS and show first impressive measurements of ice formation in mixed phase clouds. The first mobile task will take place in the framework of an intensive measurement campaign in Jülich in spring 2013.

Organic and inorganic atmospheric matter react fundamentally different in aerosol and water particles compared to the dry atmosphere. Interestingly, often it is the processing in the aqueous solution that enables the detectability. **Van Pinxteren et al.** developed a method to retrieve smallest concentrations of carbonic acid in aqueous particle extracts from which important conclusions can be drawn about atmospheric oxidation processes.

A highly topical aspect of chemical processing is the usage of amine wash for $CO_2$ separation from power plant smoke gas as part of the Carbon Capture and Storage (CCS) technology. Based on laboratory and modelling work **Weller et al.** investigate the chemical degradation and the transformation of various amines and their potential secondary products. This work constitute a very successful example for the interplay between laboratory-based analytics and chemical process modelling at the IfT.

For the chemistry of marine particles **Bräuer et al.** have coupled a new complex liquid phase chemistry mechanism to a gas phase mechanism that enables to study complex multiphase processes of an air parcel along its trajectory and thus the corresponding time resolved retrieval of source and sink-fluxes of tropospheric compounds.

As mentioned earlier the tropospheric ice formation plays an increasing role in the observational strategies and laboratory works at the IfT. By means of a conceptual theoretical study **Hellmuth et al.** introduce a new mechanism for sulfate coating at mineral dust particles, which is relevant for aging processes and the corresponding radiative and microchemical properties of dust particles. This kind of studies may provide important momentum for future laboratory and fieldwork.

Odorous substances are part of the organic matter in the troposphere and thus underlay transport and oxidation processes. Odour contamination in the border-near regions of the Ore Mountains and in the Vogtland area is a well-known problem for several decades. **Jähn et al.** managed to explain a particular strong contamination in

Die Anwendung modernster Messtechnik zur Erfassung des troposphärischen Aerosols ist eine Kernkompetenz des IfT. Mithilfe von Messnetzen lassen sich großräumige Strukturen in der belasteten Troposphäre sichtbar machen. Ein klassisches Beispiel hierfür ist die winterliche Smog-Episode. **Birmili et al.** weisen für die Region Sachsen lokale und osteuropäische Hauptquellgebiete der Feinstaubbelastung nach. Eine statistische Betrachtung des Zeitraums 1999-2010 zeigt, dass die Zahl der Feinstaub-Grenzwertüberschreitungen in Sachsen klimatisch an tiefe Temperaturen gekoppelt ist.

Seit 1997 ist das IfT an regelmäßigen Messflügen auf einem Passagierflugzeug beteiligt. Die damit gewonnenen Beobachtungsdaten konnten **Hermann et al.** erstmalig zur Erstellung einer Klimatologie des hochtroposphärischen Aerosols nutzen und mit Ergebnissen von Klimamodellrechnungen vergleichen. Die gefundenen Unterschiede liefern wichtige Informationen zur Modellverbesserung und zu unserem generellen Verständnis von Aerosoltransport- und Bildungsprozessen.

Die bodengebundene Troposphärenfernerkundung hat im Berichtszeitraum mit der Anschaffung und Inbetriebnahme eines Wolkenradars und ergänzender Instrumente einen entscheidenden Schritt in Richtung mobiler Aerosol-Wolken-Erfassung gemacht. **Wandinger et al.** stellen das neue „Leipzig Aerosol and Cloud Remote Sensing Observations System" LACROS und erste beeindruckende Messungen zur Eisbildung in Mischphasenwolken vor. Der erste mobile Einsatz wird im Rahmen einer Intensivmesskampagne in Jülich im Frühjahr 2013 stattfinden.

Organische und anorganische Substanzen in der Atmosphäre reagieren im Aerosol und im Wassertröpfchen grundsätzlich anders als in der trockenen Atmosphäre. Interessanterweise ermöglicht die Prozessierung in der wässrigen Lösung oft erst die Detektierbarkeit. **Van Pinxteren et al.** entwickelten eine Methode zur Erfassung kleinster Konzentrationen von Carbonsäuren in wässrigen Partikelextrakten, aus denen wichtige Schlüsse über atmosphärische Oxidationsprozesse getroffen werden können.

Ein hochaktueller Aspekt chemischer Prozessierung ist die Verwendung von Aminwäsche zur $CO_2$ Abscheidung aus Rauchgas von Kraftwerken als Teil der Carbo Capture and Storage (CCS) Technologie. **Weller et al.** untersuchen im Labor und mit Modellstudien den chemische Abbau und die Umwandlung verschiedener Amine und deren mögliche Folgeprodukte. Die Arbeiten sind ein sehr gelungenes Beispiel für das Zusammenspiel von Labor-Analytik und chemischer Prozessmodellierung am IfT.

in the year 2011 with an orographically induced concentration of the odour substances followed by a mountain overflow, and thus provided the mechanism for extreme odour contamination, which in turn may help forcasting these events.

The realistic modelling of small-scale atmospheric processes requires an equal realistic handling of the fundamental problem of turbulence. **König and Knoth** developed a method to generate turbulence within the air mass that flows into a model domain. With this method it is possible, for example to more realistically simulate the circulation around buildings. Corresponding potential application fields are the simulations of pollutant transport in urban areas.

At the particle accelerator of the CERN in Switzerland together with international partners the IfT investigates the influence of ionized particle radiation on the activation and nucleation behaviour of atmospheric aerosols. In order to characterize the measurement chambers again small-scale simulations of the circulation and the particle dynamics have been performed. **Voigtländer et al.** demonstrate the design of a future circulation system to ensure an optimal mixing, which in turn is required to obtain valid conclusions about the influence of cosmic rays on the cloud formation on our planet.

Since a few years the marine troposphere moves stronger into the focus of the work at the IfT. Besides purely climatological aspects of radiative effects and cloud formation, biological respectively organic-chemical problems prove increasingly interesting. **Van Pinxteren et al.** introduce measurements of the organic composition of oceanic surface films made on board the German research vessel Polarstern. Marine surface films are little investigated up to know but form a prominent source of organic components in the troposphere that can also be found in the aerosol.

With a fraction of 60% of the natural emission Dimethyl Sulphate (DMS) is the largest sulphur-compound that is biogenic emitted into the atmosphere. DMS is produced from phytoplankton in the oceans. By means of chemical process modelling studies and laboratory experiments **Berndt el al.** provided important evidence for the degradation of DMS and especially for DMS-induced aerosol formation in the troposphere.

Clouds remain the largest uncertainty in modelling our climate system. Clouds exhibit their largest climatic effect above oceans where they most strongly contrast from the dark and warm surface. Based on multi-year ship measurements **Macke et al.** tested the capability of climate models to reproduce the effect of clouds on the radiation budget. They find substantial deficiencies in modelling the natural radiation variability.

In einer Arbeit von **Bräuer et al.** wurde ein neuer komplexer Flüssigphasenchemiemechanismus für die Chemie mariner Partikel an einen Gasphasenmechanismus gekoppelt, und erlaubt so komplexe Multiphasenprozessstudien eines Luftpaketes entlang seiner Trajektorie und damit verbunden die zeitaufgelöste Erfassung von Quell- und Senkenflüssen troposphärischer Verbindungen.

Wie bereits erwähnt spielt die troposphärische Eisbildung in den Beobachtungsstrategien und Laborarbeiten eine wachsende Rolle in den Arbeiten aller Bereiche am IfT. **Hellmuth et al.** stellen in einer konzeptuellen theoretische Studie einen neuen Mechanismus zur Sulfatbeschichtung auf Mineralstaubpartikeln vor, der wichtig für Alterungsprozesse auf Staubpartikeln und den damit verbundenen strahlungsoptischen und mikrochemischen Aerosoleigenschaften sein kann. Derartige Studien können wichtige Impulse für zukünftige Labormessungen und Feldstudien liefern.

Geruchsstoffe sind Teil der organischen Materials der Troposphäre und unterliegen damit Transport- und Oxidationsprozessen. Geruchsbelastung ist seit Jahrzehnten ein bekanntes Problem in den grenznahen Gebieten des Erzgebirges und des Vogtlandes. Ausbreitungsmodellstudien von **Jähn et al.** konnten die besonders starken Belastungen im Jahr 2011 auf eine orographisch verursachte Verdichtung der Geruchsstoffe gefolgt von einer Gebirgsüberströmung zurückführen und damit den Mechanismus für extreme Geruchsbelastungen in diesem Gebiet aufklären sowie Möglichkeiten zur Vorhersage anbieten.

Die realistische Modellierung kleinskaliger atmosphärischer Prozesse erfordert einen ebenso realistischen Umgang mit dem fundamentalen Problem der Turbulenz. **König und Knoth** entwickelten eine Methode zur Turbulenzgeneration der in ein Modellgebiet einströmenden Luftmasse. Mit dieser Methode ist es z.B. möglich, Umströmungen um Gebäude realistischer zu simulieren. Anwendungen hierzu können Schadstofftransportsimulationen für Stadtbereiche sein.

Das IfT untersucht mit internationalen Partnern am Teilchenbeschleuniger des CERN in der Schweiz den Einfluss von ionisierender Partikelstrahlung auf das Aktivierungs- und Nukleationsverhalten atmosphärischer Aerosole. Zur Charakterisierung der Messkammer wurden ebenfalls kleinskalige Strömungs- und partikeldynamische Simulationen durchgeführt. **Voigtländer et al.** zeigen auf, wie ein zukünftiges Strömungssystem für eine optimale Durchmischung konzipiert sein muss, um zuverlässige Aussagen über den Einfluss kosmischer Strahlung auf die Wolkenbildung auf unserem Planeten zu erhalten.

Die marine Troposphäre rückt seit einigen Jahren stärker in den Fokus der Arbeiten am IfT. Neben den rein klimatologischen Betrachtungen zur Strahlungswirkung und Wolkenbildung erweisen sich die biologischen bzw. organisch-chemischen Fragestellungen als zunehmend interessant. **Van Pinxteren et al.** stellen Messungen der organischen Zusammensetzung des ozeanischen Oberflächenfilmes an Bord des deutschen Forschungsschiffes Polarstern vor. Marine Oberflächenfilme sind eine bislang wenig untersuchte, aber bedeutende Quelle für die organischen Bestandteile der Troposphäre, die sich auch im Aerosol wiederfinden lassen.

Die bedeutendste biogene in die Atmosphäre emittierte Schwefelverbindung mit einem Anteil von etwa 60% der natürlichen Emissionen ist Dimethylsulfid (DMS). DMS wird durch Phytoplankton in den Ozeanen produziert. **Berndt et al.** konnten aus der Chemieprozessmodellierung und mittels Experimenten wichtige Hinweise auf den Abbau des DMS und insbesondere auf die DMS-induzierte Aerosolbildung in der Troposphäre liefern.

Wolken stellen nach wie vor die größte Unsicherheit in der Modellierung unseres Klimasystems dar. Ihre größte Klimawirksamkeit entfalten sie über den Ozeanen, wo sie sich am kräftigsten vom dunklen warmen Untergrund abheben. **Macke et al.** prüften anhand mehrjähriger Schiffsbeobachtungen die Güte von Klimamodellen, den Einfluss von Wolken auf den Strahlungshaushalt zu reproduzieren, und fanden dabei erhebliche Defizite in der Modellierung der natürlichen Strahlungsvariabilität.

# Articles

# Saharan Mineral Dust Experiment SAMUM–2: Transport of Saharan dust and biomass burning smoke to Cape Verde

Ina Tegen[1], Albert Ansmann[1], Bernd Heinold[1,3], Dietrich Althausen[1], Stefan Bauer[2], Ronny Engelmann[1], Stefan Horn[1], Detlef Müller[1], Thomas Müller[1], Matthias Tesche[1,4], Alexander Schladitz[1], Manfred Wendisch[2], Alfred Wiedensohler[1]

[1] Leibniz Institute for Tropospheric Research (IfT), Leipzig, Germany
[2] Leipzig Institute for Meteorology, University of Leipzig, Germany
[3] Now at University of Leeds, UK
[4] Now at Stockholm University, Sweden

*Die DFG-Forschergruppe SAMUM (Saharan Mineral Dust Experiment) untersuchte von 2004 bis 2011 die physikalischen Eigenschaften und die Verteilung des Saharastaubes sowie seiner Wirkung auf Strahlungshaushalt und atmosphärische Dynamik. In der zweiten Phase von SAMUM, die von 2007 bis 2011 stattfand, wurden Aerosoleigenschaften in der Region der Kapverdischen Inseln untersucht. In-situ Messungen von optischen und mikrophysikalischen Partikeleigenschaften von Boden- und Flugzeugmessungen sowie Charakterisierung der Aerosoleigenschaften durch Mehrwellenlängenlidar-messungen erlaubten es, Saharastaubschichten, Rauchpartikel aus Biomasseverbrennung und marines Grenzschichtaerosol im Einzelnen zu untersuchen. Im Rahmen von SAMUM wurde ein regionales Transportmodell für Saharastaub und Biomasseverbrennungsaerosol in der Sahelregion entwickelt. Das Modell ermöglicht die Untersuchung der Auswirkungen der Aerosolverteilung auf die atmosphärische Schichtungsstabilität und atmosphärische Zirkulation der westafrikanischen Tropen und Subtropen.*

## Introduction

Soil dust particles directly emitted from deserts are a major contribution to the global aerosol load. They are frequently transported from the source regions towards Europe and the tropical North Atlantic Ocean as far as the Caribbean. Desert aerosol particles impact on climate in different ways. The magnitude of direct radiative effect of dust depends on its optical properties, its vertical distribution, the presence of cloud cover, and the spectral albedo and temperature of the underlying surface. Dust aerosol influences the Earth's climate also indirectly by modifying cloud optical properties and lifetimes. The research group 'SAharan Mineral dUst experiMent' (SAMUM) (supported by the Deutsche Forschungsgemeinschaft, 2004–2011) focused on determining the properties and transport of Saharan dust particles and their interaction with solar and terrestrial radiation [*Heintzenberg*, 2009; *Ansmann et al.*, 2011]. Two major field campaigns were carried out in the SAMUM timeframe. The first took place in 2006 in Morocco (SAMUM–1). In the second phase of SAMUM Saharan dust transported to the Cape Verde Islands in 2008 (SAMUM–2) was investigated. Together with dust transported from the Sahara, marine aerosol in the boundary layer and smoke aerosol transported from biomass burning sources in the Sahel in elevated layers contribute to the aerosol load In the Cape Verde region (Fig. 1). The main results of the SAMUM campaigns are described in two special issues of *Tellus B* in 2009 and 2011.

Field observations (ground-based, airborne, remote sensing) and modeling results were part of dust closure experiments with a strong focus on vertical profiling. A major strength of the SAMUM project was the close interaction between projects involving field and laboratory measurements, and the regional dust model development and application. One goal of SAMUM was the development of appropriate dust parameterizations for regional models describing dust emission, transport and deposition as well as its radiative impact.

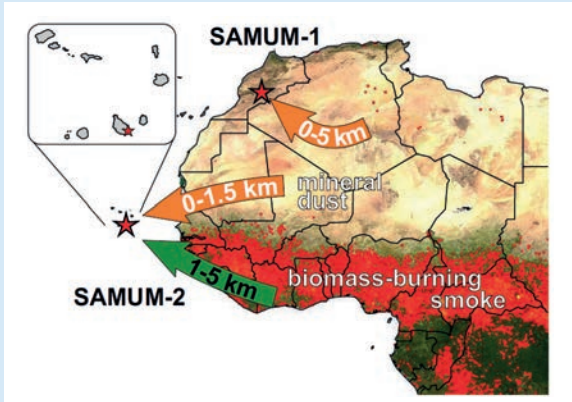


***Fig. 1:*** *SAMUM–1 and SAMUM–2 field sites (stars) in southern Morocco and at Cape Verde. While during SAMUM–1 dust was advected within a dust layer from the surface to about 5 km height, during SAMUM–2 (winter campaign) a shallow dust layer up to about 1.5 km height and an extended lofted aerosol layer from about 1.5 km height consisting of biomass burning smoke and mineral dust were frequently observed (from Ansmann et al. [2011]).*

## Scope of SAMUM–2 observations

The SAMUM–2 experimental activities consisted of multi-instrument ground-based and airborne

| | | |
|---|---|---|
| Airborne measurements (Falcon) | In situ: Profiling of physical, chemical, optical, and radiative properties | *Weinzierl et al.* [2011], *Petzold et al.* [2011], *Lieke et al.* [2011], *Bauer et al.* [2011] |
| | HSR lidar: Profiling of extinction coefficient and depolarization ratio at 532 nm, and backscatter coefficients at 532 and 1064 nm | *Petzold et al.* [2011], *Weinzierl et al.* [2011] |
| Ground-based measurements (Praia) | In situ: Physical, chemical, and optical characterization at ground | *Kandler et al.* [2011a,b], *Schladitz et al.* [2011a,b], *Müller et al.* [2011] |
| | Raman lidar: Profiling of extinction and backscatter coefficients and depolarization ratio at several wavelengths | *Tesche et al.* [2011a], *Groß et al.* [2011a,b] |
| | Doppler lidar: Profiling of horizontal and vertical wind components | *Engelmann et al.* [2011] |
| | Sun photometers: Optical depth at several wavelengths | *Toledano et al.* [2011] |
| | Radiosonde: Temperature, pressure, humidity, horizontal wind velocity and direction | *Tesche et al.* [2011a] |
| | Radiation observations: Radiative fluxes at visible and IR wavelengths | *Bauer et al.* [2011], *Köhler et al.* [2011] |

***Tab. 1:*** *Overview of SAMUM–2 observations and corresponding publications in the Tellus B special issue [2011], in which the instruments are described.*

measurements summarized in Tab. 1 (modified from *Ansmann et al*. [2011]). At the Praia site on the island of Santiago, Cape Verde (15°N, 23.5°W, 110 m asl), in-situ observations of physico-chemical and optical properties of the boundary layer aerosol and radiation measurements were conducted. Measurements taken on board the research aircraft Falcon 20-E of the Germany Aerospace Center (DLR) characterized the mixed plume of Saharan dust and biomass burning particles complementing the ground-based measurements. Special emphasis was on profiling of aerosol extinction coefficients at ambient conditions with advanced lidars, profiling of the particle-shape sensitive depolarization ratio at several wavelengths, and on airborne in situ observations of the dust size distribution. The analyses of the observations were supplemented by a variety of models for the computation of the optical properties from the observed chemical composition, size distribution, and morphology for the calculation of the impact of dust fields on the radiation budget and for the simulation of regional dust and smoke transport [*Gasteiger et al.*, 2011*; Bauer et al.*, 2011*; Köhler et al.*, 2011*; Heinold et al.*, 2011a,b].

**Meteorological situation**

The SAMUM–2 winter campaign was carried out between January 15 and February 14 2008 in Praia, Cape Verde. During the campaign several high pressure systems moved across Western Europe and the Mediterranean Sea, causing large south-north pressure gradients across the Sahel, followed by widespread dust emission [*Knippertz et al.*, 2011]. Dust emitted in Mauritania, Mali and Niger was transported westward toward the Cape Verdes within a few days. In that time of the year the dust layer over Cape Verde is usually restricted to the lowest 1.5 km of the atmosphere. A maritime aerosol layer developing near-ground often mixes with the transported dust. To the south, synoptic-scale midlevel easterlies led to an efficient transport of biomass burning aerosol from vegetation-fires over southern West Africa [*Knippertz et al.*, 2011]. Dust is also advected southwards by the Harmattan winds and then mixed upwards by convection. South of about 11°N, where biomass–burning activity is most intensive, smoke is equally mixed to higher altitudes and transported westwards towards the tropical Atlantic at 1.5 to 5 km height. Based on the observations during SAMUM–2, three phases of interest were distinguished when dust was dominating (surface aerosol concentration >200 µg $m^{-3}$), and a period of no pure dust in February when the high-pressure influence weakened. Low aerosol optical thickness (AOT), high Ångström exponents, and surface aerosol concentrations <60 µg $m^{-3}$ characterized that period. During this phase, dust only occurred in the elevated mixed dust and smoke layer.

Doppler wind measurements at Praia revealed effects of the differential heating of the island and the surrounding ocean and together with the

impact of the island topography [*Engelmann et al.*, 2011]. Horizontal and vertical winds were measured in the disturbed maritime boundary layer and compared to local radiosoundings. Interpretation of the measurements was supported by Large Eddy Simulations (LES) that computed the effects of heat islands and dynamic mixing mechanisms. The islands were modeled as flat heating surfaces in the ocean, only. The model is based on the All-Scale Atmospheric Model (ASAM) [*Hinneburg and Knoth*, 2005] and runs on graphical processor units. The model simulates meteorological fields on a 256×256×64 grid. Indications are found that the island effects can widely control the downward mixing from greater heights to the surface of African aerosols, mainly Saharan dust and biomass-burning smoke, which were detected in a complex layering over the Cape Verde region

Figure 2 (left panels) shows the Doppler lidar observations for the example of January 25, 2008. Distinct features of up-and downward motions occurred on time periods longer than the typical eddy turnover time. LES supported the interpretation of these flow patterns. The LES results indicate that convective rolls develop over the island in this simulation at distances of 5–10 km inland of the east coast. Figure 2 (right panel) shows the data on the cut plane across the model domain at 15:30 UTC. A defined non-convective clear area of subsiding air developed about 5 km inland above the lidar site. This feature is rather consistent with the observations for many other days with similar surface winds. Even with the limitation that the orography was not included in the model, the LES indicates the strong influence of the heat islands on the airflow and aerosol transport and vertical mixing.

## Aerosol transport model

The regional dust model system that was further developed in the framework of SAMUM is described in detail by *Heinold et al*. [2011a]. It is based on the COSMO model, which is the operational weather prediction model of the German Weather Service (DWD), the online-coupled Chemistry-Transport-Model MUSCAT [*Wolke et al.*, 2004], and dust and smoke emission schemes. For the SAMUM–2 simulations a horizontal grid resolution of 28 km is used. The vertical grid has 40 layers from surface to tropopause with a first-layer depth of about 68 m. The model domain includes relevant Saharan dust emission areas, West African vegetation fires and the eastern Tropical Atlantic Ocean.

The SAMUM dust model utilizes the location of dust sources derived from Meteosat Second Generation (MSG) satellite observations [*Schepanski et al.*, 2007] for dust emission calculations. The model-predicted dust is transported as dynamic tracer in five independent size classes with radius limits at 0.1 µm, 0.3 µm, 0.9 µm, 2.6 µm, 8 µm and 24 µm. Dust is removed from the atmosphere by dry and wet deposition processes. Dust optical thicknesses are computed from simulated dust concentrations, particle size distributions and extinction efficiencies.

The emission of aerosol particles with diameter smaller than 2.5 µm (PM2.5) that originate from biomass burning are computed for individual fire pixels as a product of the daily burnt area, the burning efficiency, an empirical emission factor, and the available fuel load or biomass density. The location and the temporal variability of fires were derived from observations of the Moderate-Resolution Imaging Spectroradiometer (MODIS) fire detection products (https://lpdaac.usgs.gov).

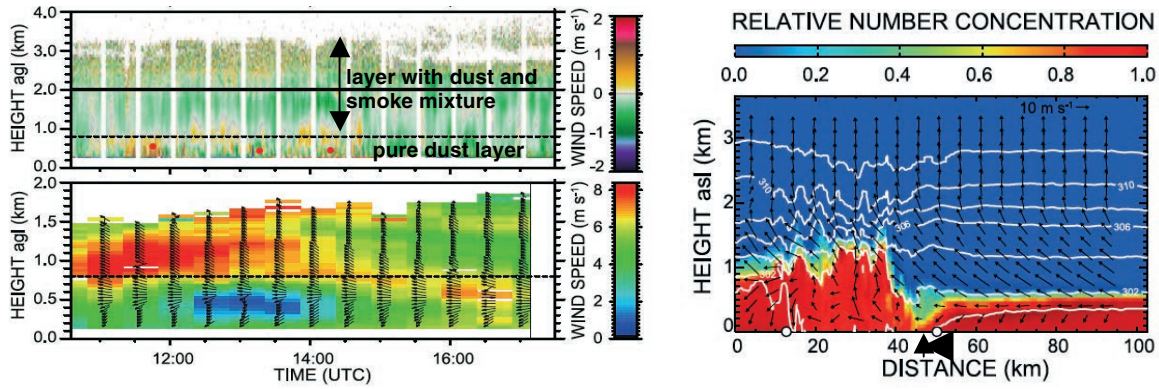


***Fig. 2:*** *Doppler lidar observations on January 25, 2008 at Praia. Temporal development of the logarithm of the vertical wind (left, top panel) and horizontal wind (left, lower panel) from 1200–1900 UTC. LES output of the relative number concentration of a passive boundary-layer aerosol tracer, isentropic levels and horizontal wind speed and direction (arrows) at a cut plane across the model domain for January 25, 2008, 1530 UTC (right panel) (the arrow marks the location of the lidar site and the white dots indicate the island boundaries at 15.1°N, 23.8°W and 14.9°N, 23.5°W). The initial tracer profile at the domain boundaries was 1 for heights <700 m and 0 for heights >700 m (from Engelmann et al. [2011].*

Smoke particles are effectively lifted from surface by convective transport.

The parameterization of radiative transfer of short- and longwave radiation in COSMO takes into account effects of scattering, absorption, and emission by aerosols, cloud droplets, and gases [*Tanre et al.*, 1984]. The constant distribution of desert dust and soot aerosol in the radiation scheme is replaced by the size-resolved optical thickness of dust and biomass smoke, respectively, that are simulated by the transport scheme MUSCAT, thus the computation of radiation fluxes accounts for a spatially and temporally varying atmospheric dust load.

### Dust and smoke transport

The dry synoptic-scale dynamics that cause dust events during the winter season are reproduced well by the meteorological model. The spatial and temporal evolution of dust and smoke transport in the transport model is illustrated for the example day February 4 2008 in Fig. 3. The transport of the mixed plume from West Africa towards Cape Verde is well reproduced in the model results and the computed hot spots of biomass burning aerosol over northern central Africa also agree well with satellite observations. Modeled winds and dust distributions are not always reproduced when dust mobilization is influenced by small-scale topography not resolved by the model. Over the western Gulf of Guinea the modeled particle optical depth was often lower than the observations as the fire maps used for model initialization were frequently contaminated by clouds and the simulated Bodélé dust emissions were too low.

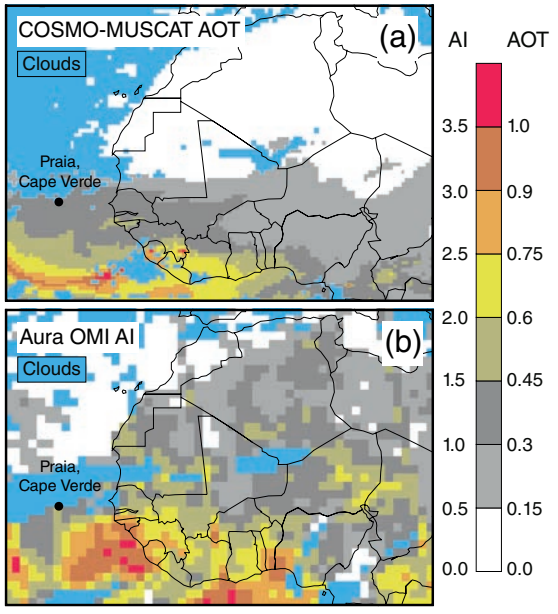


***Fig. 3:*** *Horizontal distribution of Saharan dust and biomass burning aerosol on February 4, 2008: Aerosol optical thickness at 550 nm retrieved from (a) model simulations and (b) OMI aerosol index providing semi-quantitative information on absorbing aerosol load. Cloudy areas are shown in light blue (Figure from Ansmann et al., [2011]).*

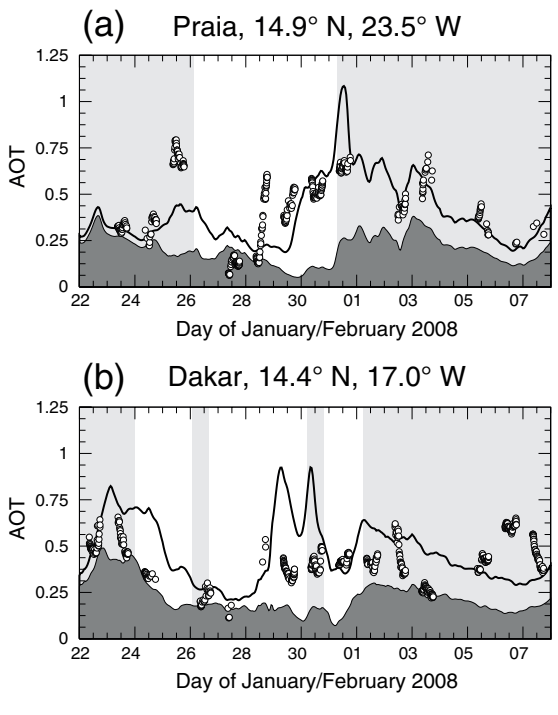


***Fig. 4:*** *Aerosol optical thickness (440 nm) at Praia/Santiago and Dakar on January 22 to February 7, 2008. Compared are sun photometer measurements provided by AERONET (black circles) and optical thickness of modelled smoke (dark grey shaded area) and the mixed plume of dust and smoke (solid black line). Grey shaded areas denote the days, on which the Ångström exponent from AERONET measurements is higher than 0.3, indicating a smoke-dominated aerosol layer (modified from Heinold et al. [2011a]).*

The simulated AOT are compared to sun photometer measurements at several locations (shown for the sites Praia and Dakar in Fig. 4). The Ångström exponent, which describes the spectral dependency of measured optical depth, is used as an indicator whether dust or smoke was dominant. It is close to zero for large dust particles, while values larger than one indicate the presence of very small particles as in vegetation fire smoke. Here, Ångström exponents larger than 0.3 define a smoke-dominated aerosol layer. Figure 4 shows the model-derived AOT due to biomass burning particles and the total of dust and smoke aerosol. The ratio of dust to vegetation-fire smoke simulated by the model agrees in general very well with the temporal evolution of the measured Ångström exponents.

Lidar observations close to Praia show complex aerosol structures throughout the troposphere up to 5 km height on most days of the campaign [*Engelmann et al.*, 2011*; Weinzierl et al.*, 2011 *and Tesche et al.*, 2011a]. In addition to airborne lidar observations onboard the Falcon aircraft, three

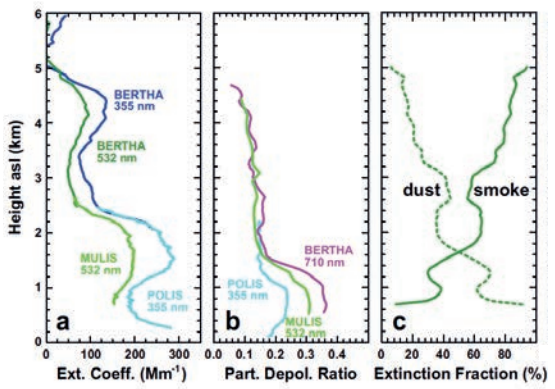


***Fig. 5:*** *(a) Raman lidar measurement of the volume extinction coefficient of particles at Praia, Cape Verde, from the dust-laden marine boundary layer to the top of the dust-smoke layer at 5 km height on January 31, 2008; (b) particle depolarization ratio; (c) dust and smoke contributions to the total volume extinction coefficients of particles. The measurements of three lidars (POLIS, MULIS, BERTHA) are combined. Light scattering and depolarization by mineral dust dominates up to 1.3 km. A homogeneous layer of aged smoke (a low smoke depolarization ratio <0.05 is assumed) and dust is present above about 1.3 km height. Figure modified from Ansmann et al. [2011].*

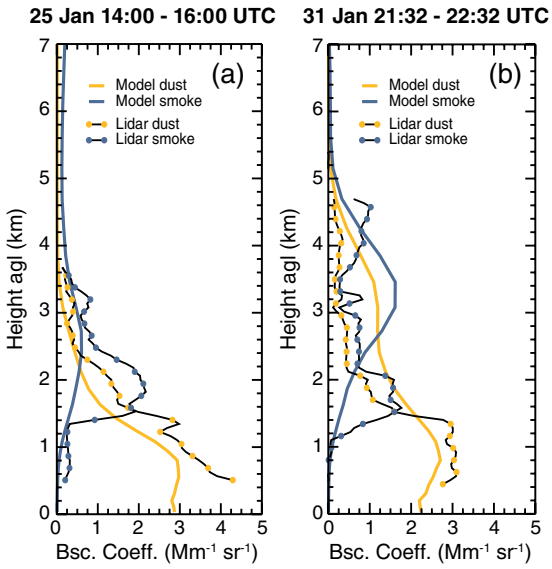


***Fig. 6:*** *Vertical profiles of dust (orange) and smoke (blue) particle backscatter coefficient (532 nm) at Praia on January 25 and 31, 2008. Shown are modeled profiles (solid colored lines) in comparison to lidar data (black lines with colored circles) (from Heinold et al. [2011a]).*

ground-based Raman lidars observed aerosol layers and provide vertically-resolved statistics of particle properties. *Tesche et al.* [2009] demonstrate that dust and smoke dominated layers can be separated because the large non–spherical dust particles cause high linear particle depolarization ratios, which is wavelength-dependent with values around 0.3 at 532 nm [*Tesche et al.*, 2011a] (see Fig. 5). Biomass–burning particles cause low depolarization ratios of around 0.05 [*Tesche et al.*, 2009b]. A maritime boundary layer with depolarization ratios close to zero made up the lowermost 0.4–1.0 km of the atmospheric column. A mineral dust layer was present over the maritime boundary layer (or even from the surface in cases of strong dust outbreaks) to a height of 1.5 km. Above the mineral dust layer, a mixed layer of mineral dust from North Africa and biomass–burning smoke from southern West Africa was observed during most of the time.

In agreement with the observations, the model simulates Saharan dust transport towards the Cape Verde islands mainly below 1–1.5 km height (Fig. 6). The computed smoke plume from the Tropical West Africa arrives above 1–2 km height at the Cape Verdes. Thus the observed aerosol layering of dust and biomass smoke particles is captured by the model, which is an important prerequisite for follow-up studies on the radiative aerosol effects, including their influence on atmospheric dynamics. Nevertheless, discrepancies exist because of a too intense vertical mixing of dust and smoke, which causes an underestimation of maximum particle concentrations at specific layers and explains the absence of detailed structures in modeled aerosol profiles (Fig. 6).

## Optical properties

A major goal of the SAMUM–2 project was to clarify the uncertainties in radiative properties of the mixed plume of Saharan dust and biomass burning smoke particles by different independent measurements.

Optical and microphysical aerosol properties were measured at Praia [*Kandler et al.*, 2011a; *Schladitz et al.*, 2011a; *Müller et al.*, 2011] and aboard the Falcon [*Petzold et al.*, 2011; *Weinzierl et al.*, 2011]. For particles smaller than 1 µm diameter, the dust aerosol size distributions measured during SAMUM–2 agree with earlier observations made during SAMUM–1. In contrast, differences are found for sizes larger than 10 µm. During SAMUM–1, in all cases particles larger than 10 µm were present, and in 80% of the cases the particles were smaller than 40 µm [*Weinzierl et al.*, 2011]. In contrast, no particles with diameters close to 30 µm were found during SAMUM–2 and in several cases particles larger than 10 µm were not detected. Gravitational settling during long-range transport causes the depletion of large coarse mode dust particles. The tropical biomass-burning aerosol layers measured during SAMUM–2 contain a significant amount of 10 µm particles, which is not present in the boreal biomass-burning layers. This difference is explained by the fact that the tropical biomass-burning layers contained mineral dust particles originating from the region north of 11°N [*Knippertz et al.*, 2011].

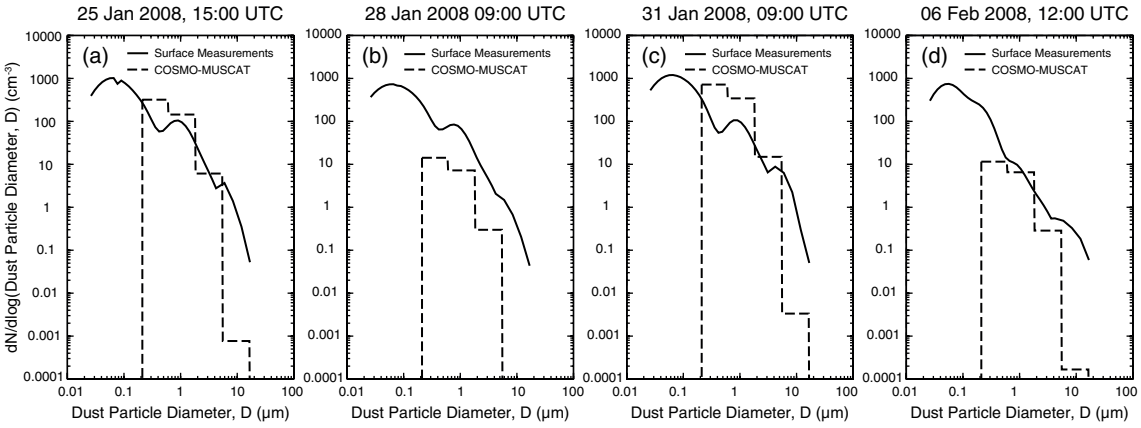


***Fig. 7:*** *Ground-level number size distribution at the SAMUM–2 site Praia on January 25 (15:00 UTC), 28 (09:00 UTC) and 31 (09:00 UTC), and February 6 (12:00 UTC) 2008. Model results for the first layer at about 34 m height (dashed line), measurements from a combined DMPS/APS system at about 5 m height (solid line). The observation data are truncated at 20 µm to exclude locally emitted large particles (from Heinold et al. [2011a]).*

The measurements of the particle size distribution serve as an additional indicator as to whether the dust production and transport processes are correctly simulated by the regional dust model (Fig. 7, [*Heinold et al.*, 2011a]). Reliable size distributions are needed to compute dust optical quantities. Mineral dust particles are generally found in the size range larger than 0.1 µm diameter. High number concentration of particles larger than 15 µm indicates locally emitted aerosol particles [*Kandler et al.*, 2011b]. Dust particles larger than 10 µm have mostly been removed by mainly dry deposition during long-range transport towards the Cape Verde Islands. Large discrepancies between modeled dust particle numbers and ground-based size measurements are only found for the dust outbreak on January 28, indicating misrepresentation of the dust outbreak across the tropical Atlantic Ocean in the model. In general, the agreement between model-derived dust particle number size distributions and ground-based size observations is best when the spatio-temporal dust distribution is also modeled correctly (based on comparisons of optical thickness and backscatter/extinction coefficients).

Inversion of lidar measurements of the smoke layer results in a range of single scattering albedo (SSA) values of 0.65–0.9 (mean value of 0.75) for pure smoke. This range of values is characteristic for the entire SAMUM–2a campaign [*Tesche et al.*, 2011b]. Inversion of the SAMUM–2 Sun photometer observations indicated values of about 0.84 for SSA (550 nm) when the optical depth was dominated by smoke (fine mode optical depth >0.5, *Toledano et al*. [2011]) but dust particles were present as well.

Optical closure studies based on the surface observations at Praia, regarding scattering, absorption and extinction coefficients of particles (including the dependence of the optical properties on relative humidity) are presented by *Schladitz et al.* [2011a,b]. The knowledge of the spectral dependence of absorption by desert dust particles and the respective complex refractive index is a pre-requisite for the modeling of the direct dust radiative effect. Absorption by dust depends on the size and shape of the particles and their mineralogical composition. Spectral absorption coefficients were measured with an absorption photometer from 300 to 800 nm during SAMUM–1 and from 300 to 960 nm during SAMUM–2 [*Müller et al.*, 2011]. The spectral dependence suggests a higher amount of iron in the dust particles over Cape Verde than in southern Morocco. At longer wavelengths the imaginary part of the refractive index differs between both campaigns. These observations points to different origins and mineralogical composition of dust observed during SAMUM–1 and SAMUM–2.

## Aerosol forcing and effects

In the regional dust transport model, the coupled dynamic-radiation model allows the modeled dust and smoke particle concentration to interact with the solar and terrestrial radiation and with the model dynamics [*Heinold et al.*, 2011b]. The optical properties of mineral dust were computed from the size-resolved dust load assuming a mineral composition containing 2% hematite, which is highly absorbing at solar wavelengths. The prescribed dust refractive indices were chosen in accordance with measurements in the vicinity of dust sources during the SAMUM–1 field campaign. High values of absorption were also assumed for biomass burning particles that are representative for freshly emitted smoke particles from African savanna fires. Thus the findings on the smoke radiative feedback should be considered as the maximum effects.

Clear-sky net radiative forcing of the mixture of mineral dust and biomass smoke are negative on

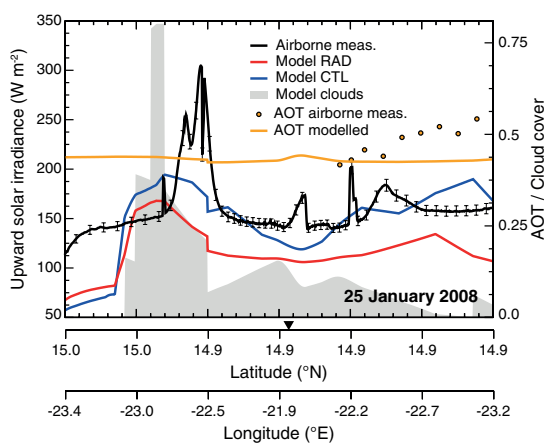


***Fig. 8:*** *Modeled aerosol optical thickness and upward solar irradiance compared with measurements taken during the Falcon flight west of Santiago Island on January 25, 2008 (14:50–15:20 UTC). The airborne radiation measurements were conducted under clear-sky conditions. The grey-shaded area indicates cloud coverage below the flight level in the model (from Heinold et al. [2011b]).*

daily average reaching -39 $Wm^{-2}$ for the 14-day period. At TOA and for the atmosphere, the values are positive with up to +19 $Wm^{-2}$ and +58 $Wm^{-2}$, respectively [*Heinold et al.*, 2011b].

Modeled upward solar irradiances were evaluated against airborne radiative measurements [*Bauer et al.*, 2011] from the Falcon over the Atlantic Ocean for a case of biomass burning aerosol above desert dust on January 25, 2008 (Fig. 8). The modeled AOT of 0.4 agrees with measured AOT ranging from 0.4 to 0.6. The measured upward solar irradiances slowly increase reaching values around 150 $Wm^{-2}$ with peaks up to 305 $Wm^{-2}$ due to underlying clouds. The modeled upward solar irradiances are 40% lower than the radiation measurements during the first minutes when the aircraft flew below 5 km altitude. This is because, in contrast to the observations, clouds are simulated at higher levels and therefore reduce the simulated incident solar radiation at this altitude. The model results including aerosol-radiation interaction (RAD) are on average 10 $Wm^{-2}$ higher than the values from the control run without radiative feedback (CTL). An increase in the effective albedo over the Atlantic ocean due to the presence of dust and smoke aerosol particles leads to an enhanced amount of upward solar radiation.

The comparison of modeled and observed upward solar irradiances demonstrates, that the coupled dynamic and radiation simulations give reasonable results for the following studies on radiative effects of dust and biomass burning smoke particles, even though the aerosol distribution is not always correctly reproduced.

The atmospheric response to dust and smoke radiative effects is presented in terms of temperature and air pressure changes in Fig. 9. Shown are differences of the 500 hPa and 950 hPa temperature and the surface pressure computed from model results of radiative feedback and non-feedback runs. The maps show difference values for 12:00 UTC and 24:00 UTC and for the daily means, each averaged over the period January 25 to February 7. The yield of radiative energy in the atmospheric column is caused by the absorption of solar and terrestrial radiation within the plume of mineral dust and biomass burning smoke. This effect is evident throughout the day in the overall increase in the 500 hPa temperature reaching up to +1.1 K over the southern West African coast (Fig. 9, upper panel). The differences in the horizontal distribution of atmospheric response during different times of the day are mainly related to the spatial and temporal evolution of the aerosol plume. The negative surface forcing results in a decrease in the near-surface (950 hPa) temperature over land (Fig. 9, center panels). Strongest reductions of locally up to 2.7 K occur in regions with highest AOT at noontime. The main daytime effect of the mixed dust and biomass burning smoke plume is to redistribute radiative heating from the surface to the atmospheric column over land [*Heinold et al.*, 2011b].

The radiative impact of dust and smoke particles on temperature fields corresponds to variations of the air pressure as shown in Fig. 9 (lower panels). The aerosol radiative heating within the aerosol plume extends over several vertical layers and induces rising motion and negative pressure perturbations near the surface. Because of the pronounced radiative cooling near the aerosol layer top (not shown) and at the surface, the simulations result in sinking motion and pressure increase over the biomass burning area at night. For the remaining domain, the negative radiative effect on surface pressure prevails. The air-flow patterns are locally modified as indicated by white arrows in Fig. 9 (lower panels).

The differences in the north-south gradient of pressure at the surface and 500 hPa indicate a systematically enhanced Hadley circulation, which leads to stronger upper-level air transport. Flow patterns in Fig. 9 (lower panels) show a cyclonic circulation west of the African continent induced by the dust and smoke radiative forcing. Therefore, the transport of Saharan dust is more focused towards the Cape Verde region compared to the model results without radiative feedback.

The separation of the dust and smoke signal in the lidar measurements (Fig. 5; *Tesche et al.* [2011b]) allows for individual evaluation of modeled dust and smoke aerosol profiles simulated with and without radiative feedback in the model. The lidar profile in Praia on January 31 (Fig. 10) indicates the presence of smoke particles between 1 km and 5 km with maximum extinction coefficients of about 105 $Mm^{-1}$ and 75 $Mm^{-1}$ at 1.8 km and 4.2 km

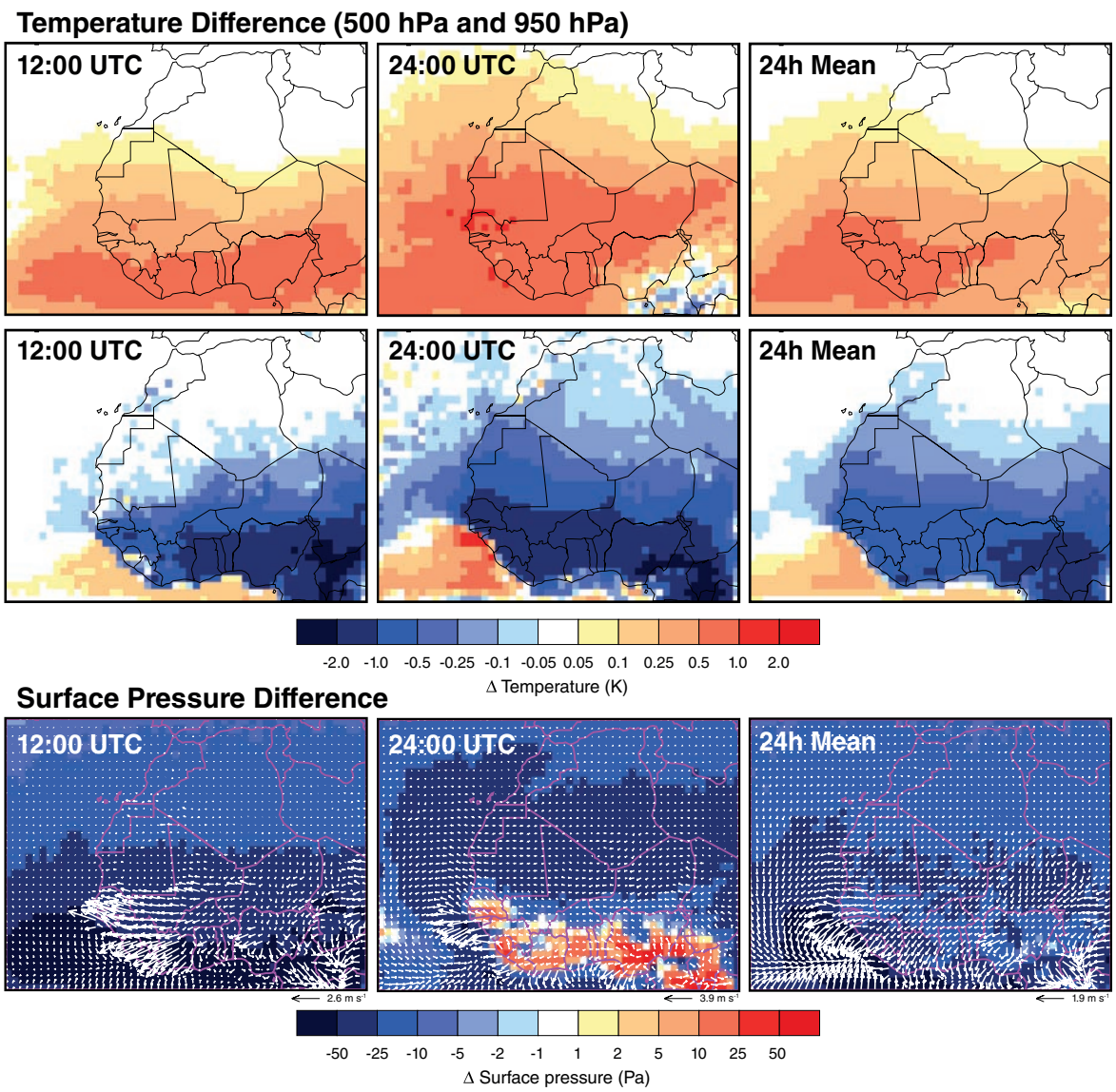


***Fig. 9:*** *Difference maps of the modeled temperature between the experiment including aerosol radiative forcing (RAD) and results when the feedback is not included (CTL), averaged over the period from January 25 to February 7, 2008. Top panels: 500 hPa level, center panels: 950 hPa level. Left panels: 12:00 UTC, middle panels: 24:00 UTC and right panels: daily mean. Lower panels: corresponding mean difference in modeled surface pressure. White arrows denote changes in surface winds induced by dust and smoke radiative forcing (zonal and meridional wind speed differences between case RAD and CTL) (from Heinold et al. [2011b]).*

height, respectively. In the model run without radiative feedback only the location of the observed lower smoke maximum is reproduced at height of 1.6 km. When radiative feedback is considered, the simulated smoke layer is centered at a higher level in about 3.5 km height. As mentioned above, the transport of mineral dust is more directed towards the Cape Verde Islands when the radiative feedback is included. However, this increases the tendency to overestimate the dust load above 1.5 km height caused by a too strong vertical mixing in the model [*Heinold et al.*, 2011b]. It is notable that there is a tendency for developing more defined dust layers when radiative feedback is considered compared to the simulation without dust forcing influence on atmospheric dynamics.

The model results show that including the radiative forcing in dust and biomass burning simulations makes a difference to atmospheric dynamics. An improvement of the model representation of vertical smoke distribution was found locally. The impact of Saharan dust and smoke particles on the radiation budget is part of the complex West African circulation. It influences the meteorological conditions at different scales, but also affects the aerosol transport itself. However, it is difficult to show if model runs with aerosol-radiation interaction generally agree better with aerosol observations than those without radiative feedback given the uncertainties in the model. Measurements cannot be used to directly validate the dynamic feedbacks.

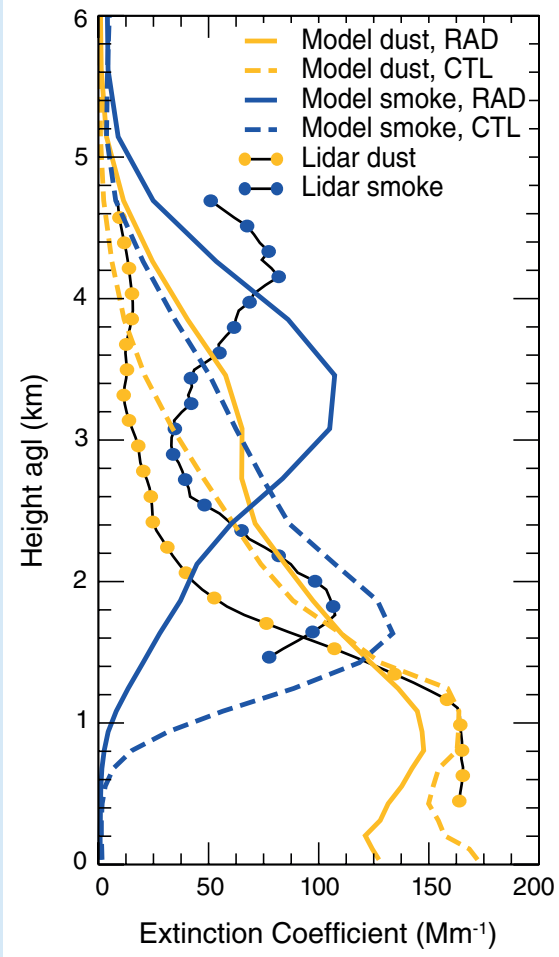


***Fig. 10:*** *Vertical profiles of dust (orange) and smoke (blue) backscatter coefficients (532 nm) at Praia site on January 31, 2008 (21:32–22:32 UTC). Comparison of modeled profiles from feedback simulation (solid lines) and from control run (dashed lines) with lidar data (lines with colored circles) (from Heinold et al. [2011b]).*

## Summary and Conclusion

While the first SAMUM campaign focused on Saharan dust near the sources, SAMUM–2 studied dust transported away from the sources, together with aerosol layers dominated by marine aerosol and smoke aerosol from biomass burning sources in the Sahel region. The comprehensive in-situ characterization of the aerosol particles from samples taken at the surface and from aircraft included measurements of the chemical, mineralogical and morphological properties of the spectral absorption coefficient [*Kandler et al.*, 2009, 2011a,b; *Lieke et al.*, 2011; *Müller et al.*, 2009b, 2011; *Scheuvens et al.*, 2011]. The strong emphasis on measurements of the atmospheric with ground-based and airborne Raman lidars as well as a Doppler lidar for vertical mixing studies allowed to evaluate the optical properties of the different aerosol layers separately [*Tesche et al.*, 2011a,b; *Groß et al.*, 2011; *Engelmann et al.*, 2011]. The combination of airborne lidar and in situ observations allowed to characterize the aerosol type (smoke, dust, marine particles and mixtures) by combining the depolarization ratio, lidar ratio and absorption Ångström exponent information [*Weinzierl et al.*, 2011].

A major strength of the SAMUM project was the close interaction between projects involving field and laboratory measurements, and the development and application of the regional aerosol transport model. Based on existing model components, the new model design of COSMO-MUSCAT includes dust and smoke aerosol as radiatively active components of the atmosphere. This setup allowed to test the impact of changes in boundary layer stability and atmospheric dynamics by the absorbing aerosol particles [*Heinold et al.*, 2011a,b]. As a result of SAMUM, the model has become a useful tool to study processes of atmospheric dust transport and effects, and to provide a spatiotemporal context to field studies dedicated to Saharan dust.

Future field campaigns may focus on the dust source regions to cover dust emission issues, and on the far range of the long-range transport regime towards North America in summer and South America in winter. Future field campaigns should also consider effects of dust and smoke particles on cloud evolution and formation of precipitation in the intertropical convergence zone over the tropical Atlantic.

## References

Ansmann, A., A. Petzold, K. Kandler, I. Tegen, M. Wendisch, D. Müller, B. Weinzierl, T. Müller, and J. Heintzenberg (2011), Saharan Mineral Dust Experiments SAMUM-1 and SAMUM-2: What have we learned?, *Tellus B*, *63*(4 (Special Issue)), 403-429, doi: doi:10.1111/j.1600-0889.2011.00555.x.

Bauer, S., E. Bierwirth, M. Esselborn, A. Petzold, M. A, T. Trautmann, and M. Wendisch (2011), Airborne spectral radiation measurements to derive solar radiative forcing of Saharan dust mixed with biomass burning smoke particles, *Tellus B*, *63*, doi: 10.1111/j.1600-0889.2011.00567.x.

Engelmann, R., A. Ansmann, S. Horn, P. Seifert, D. Althausen, M. Tesche, M. Esselborn, J. Fruntke, K. Lieke, V. Freudenthaler, and S. Gross (2011), Doppler lidar studies of heat island effects on vertical mixing of aerosols during SAMUM-2, *Tellus B*, *63*, 448-458.

Gasteiger, J., M. Wiegner, S. Gross, V. Freudenthaler, C. Toledano, M. Tesche, and K. Kandler (2011), Modelling lidar-relevant optical properties of complex mineral dust aerosols, *Tellus B*, *63*, 725-741.

Gross, S., M. Tesche, V. Freudenthaler, C. Toledano, M. Wiegner, A. Ansmann, D. Althausen, and M. Seefeldner (2011a), Characterization of Saharan dust, marine aerosols and mixtures of biomass-burning aerosols and dust by means of multi-wavelength depolarization and Raman lidar measurements during SAMUM 2, *Tellus B*, *63*, 706-724, doi: doi:10.1111/j.1600-0889.2011.00556.x.

Gross, S., J. Gasteiger, V. Freudenthaler, M. Wiegner, A. Geiss, A. Schladitz, C. Toledano, K. Kandler, M. Tesche, A. Ansmann, and A. Wiedensohler (2011b), Characterization of the planetary boundary layer during SAMUM-2 by means of lidar measurements, *Tellus B*, *63*, 695-705, doi: doi:10.1111/j.1600-0889.2011.00557.x.

Heinold, B., I. Tegen, K. Schepanski, M. Tesche, M. Esselborn, V. Freudenthaler, S. Gross, K. Kandler, P. Knippertz, D. Müller, A. Schladitz, C. Toledano, B. Weinzierl, A. Ansmann, D. Althausen, T. Müller, A. Petzold, and A. Wiedensohler (2011a), Regional modelling of Saharan dust and biomass-burning smoke Part 1: Model description and evaluation, *Tellus B*, *63*(4 (Special Issue)), 781-799, doi: doi:10.1111/j.1600-0889.2011.00570.x.

Heinold, B., I. Tegen, S. Bauer, and M. Wendisch (2011b), Regional modelling of Saharan dust and biomass-burning smoke Part 2: Direct radiative forcing and atmospheric, *Tellus B*, *63*(4 (Special Issue)), 800-813, doi: doi:10.1111/j.1600-0889.2011.00574.x.

Heintzenberg, J. (2009), The SAMUM-1 experiment over Southern Morocco: Overview and introduction, *Tellus B*, *61*(1 (Special issue on SAMUM-1)), 2-11.

Hinneburg, D., and O. Knoth (2005), Non-dissipative cloud transport in Eulerian grid models by the volume-of-fluid (VOF) method, *Atmos. Environ.*, *39*(23-24), 4321-4330.

Kandler, K., L. Schütz, S. Jäckel, K. Lieke, C. Emmel, D. Müller-Ebert, M. Ebert, D. Scheuvens, A. Schladitz, B. Segvic, A. Wiedensohler, and S. Weinbruch (2011a), Ground-based off-line aerosol measurements at Praia, Cape Verde, during the Saharan Mineral Dust Experiment: Microphysical properties and mineralogy, *Tellus B*, *63*(4), 459-474, doi: doi:10.1111/j.1600-0889.2011.00546.x.

Kandler, K., K. Lieke, N. Benker, C. Emmel, M. Kupper, D. Müller-Ebert, M. Ebert, D. Scheuvens, A. Schladitz, L. Schütz, and S. Weinbruch (2011b), Electron microscopy of particles collected at Praia, Cape Verde, during the Saharan Mineral Dust Experiment: Particle chemistry, shape, mixing state and complex refractive index, *Tellus B*, *63*(4), 475-496, doi: doi:10.1111/j.1600-0889.2011.00550.x.

Knippertz, P., M. Tesche, B. Heinold, K. Kandler, C. Toledano, and M. Esselborn (2011), Dust mobilization and aerosol transport from West Africa to Cape Verde - A meteorological overview of SAMUM-2, *Tellus B*, *63*, 430-447, doi: doi:10.1111/j.1600-0889.2011.00544.x.

Köhler, C., T. Trautmann, E. Lindermeir, W. Vreeling, K. Lieke, K. Kandler, B. Weinzierl, S. Gross, M. Tesche, and M. Wendisch (2011), Thermal IR radiative properties of mixed mineral dust and biomass aerosol during SAMUM-2, *Tellus B*, *63*(4 (Special Issue)), 751-769, doi: 10.1111/j.1600-0889.2011.00563.x.

Lieke, K., K. Kandler, D. Scheuvens, C. Emmel, C. Von Glahn, A. Petzold, B. Weinzierl, A. Veira, M. Ebert, and S. Weinbruch (2011), Particle chemical properties in the vertical column based on aircraft observations in the vicinity of Cape Verde Islands, *Tellus B*, *63*(4 (Special Issue)), 497-511, doi: 10.1111/j.1600-0889.2011.00553.x.

Müller, T., A. Schladitz, K. Kandler, and A. Wiedensohler (2011), Spectral particle absorption coefficients, single scattering albedos and imaginary parts of refractive indices from ground based in situ measurements at Cape Verde Island during SAMUM-2, *Tellus B*, *63*(4), 573-588, doi: doi:10.1111/j.1600-0889.2011.00572.x.

Petzold, A., A. Veira, S. Mund, M. Esselborn, C. Kiemle, B. Weinzierl, T. Hamburger, G. Ehret, K. Lieke, and K. Kandler (2011), Mixing of mineral dust with urban pollution aerosol over Dakar (Senegal): impact on dust physico-chemical and radiative properties, *Tellus B*, *63*(4 (Special Issue)), 619-634, doi: 10.1111/j.1600-0889.2011.00547.x.

Schepanski, K., I. Tegen, B. Laurent, B. Heinold, and A. Macke (2007), A new Saharan dust source activation frequency map derived from MSG-SEVIRI IR-channels, *Geophys. Res. Lett.*, *34*(18), L18803, doi:18810.11029/12007GL030168.

Scheuvens, D., K. Kandler, M. Küpper, K. Lieke, S. Zorn, M. Ebert, L. Schütz, and S. Weinbruch (2011), Individual-particle analysis of airborne dust samples collected over Morocco in 2006 during SAMUM 1, *Tellus B*, *63*(4 (Special Issue)), 512-530, doi: 10.1111/j.1600-0889.2011.00554.x.

Schladitz, A., T. Müller, A. Nowak, K. Kandler, K. Lieke, A. Massling, and A. Wiedensohler (2011a), In situ

aerosol characterization at Cape Verde Part 1: Particle number size distributions, hygroscopic growth and state of mixing of the marine and Saharan dust aerosol, *Tellus B*, *63*(4), 531-548, doi: doi:10.1111/j.1600-0889.2011.00569.x.

Schladitz, A., T. Müller, S. Nordmann, M. Tesche, S. Gross, V. Freudenthaler, J. Gasteiger, and A. Wiedensohler (2011b), In situ aerosol characterization at Cape Verde Part 2: Parametrization of relative humidity- and wavelength-dependent aerosol optical properties, *Tellus B*, *63*, 549-572, doi: doi:10.1111/j.1600-0889.2011.00568.x.

Tanré, D., J. F. Geleyn, and J. Slingo (1984), First results of the introduction of an advanced aerosol/radiation interaction in the ECMWF low resolution global model, in *Aerosols and their Climatic Effects*, edited by H. E. Gerber and A. Deepak, pp. 133-177, Deepak Publishing, Hampton, Virginia.

Tesche, M., A. Ansmann, D. Müller, D. Althausen, R. Engelmann, V. Freudenthaler, and S. Groß (2009), Vertically resolved separation of dust and smoke over Cape Verde by using multiwavelength Raman and polarization lidars during Saharan Mineral Dust Experiment 2008, *J. Geophys. Res. - Atmos.*, *114*(D13), D13202, doi:13210.11029/12009JD011862.

Tesche, M., S. Gross, A. Ansmann, D. Müller, D. Althausen, V. Freudenthaler, and M. Esselborn (2011a), Profiling of Saharan dust and biomass-burning smoke with multiwavelength polarization Raman lidar at Cape Verde, *Tellus B*, *63*, 649-676, doi: doi:10.1111/j.1600-0889.2011.00548.x.

Tesche, M., D. Müller, S. Gross, A. Ansmann, D. Althausen, V. Freudenthaler, B. Weinzierl, A. Veira, and A. Petzold (2011b), Optical and microphysical properties of smoke over Cape Verde inferred from multiwavelength lidar measurements, *Tellus B*, *63*, 677-694, doi: doi:10.1111/j.1600-0889.2011.00549.x.

Toledano, C., M. Wiegner, S. Gross, V. Freudenthaler, J. Gasteiger, D. Müller, T. Müller, A. Schladitz, B. Weinzierl, B. Torres, and N. T. O'Neill (2011), Optical properties of aerosol mixtures derived from sun-sky radiometry during SAMUM-2, *Tellus B*, *63*, 635-648, doi: doi:10.1111/j.1600-0889.2011.00573.x.

Weinzierl, B., D. Sauer, M. Esselborn, A. Petzold, A. Veira, M. Rose, S. Mund, M. Wirth, A. Ansmann, M. Tesche, S. Gross, and V. Freudenthaler (2011), Microphysical and optical properties of dust and tropical biomass burning aerosol layers in the Cape Verde region-an overview of the airborne in situ and lidar measurements during SAMUM-2, *Tellus B*, *63*, 589-618, doi: doi:10.1111/j.1600-0889.2011.00566.x.

Wolke, R., A. M. Sehili, W. Schröder, M. Simmel, and E. Renner (2004), Parameterisation and numerical treatment of aerosol-cloud-chemistry interactions in regional chemistry-transport models, paper presented at 27th NATO/CCMS International Technical Meeting (ITM) on Air Pollution Modelling and Its Application, Banff, Canada, 24-29 October.

**Funding**
- German Research Foundation (DFG), Bonn, Germany

**Cooperation**
- SAMUM consortium (http://www.tropos.de/samum/)
- Deutscher Wetterdienst, Offenbach, Germany

# Hill Cap Cloud Thuringia 2010 (HCCT-2010): A ground based integrated study on aerosol cloud interaction

Dominik van Pinxteren[1], Andreas Tilgner[1], Laurent Poulain[1], Wadinga Fomba[1], Thomas Gnauk[1], Konrad Müller[1], Yoshiteru Iinuma[1], Gerald Spindler[1], Benjamin Fahlbusch[1], Conny Müller[1], Luisa Schöne[1], Peter Bräuer[1], Stephan Mertes[1], Katrin Dieckmann[1], Michael Schäfer[1], Peter Zedler[1], Frank Stratmann[1], Maik Merkel[1], Wu Zhijun[1], Kai Weinhold[1], Wolfram Birmili[1], Alfred Wiedensohler[1], Anja Roth[2], Johannes Schneider[2], Stephan Borrmann[2], Eliza Harris[2], Bärbel Sinha[2], Ingrid George[3], Lisa Whalley[3], Dwayne Heard[3], Markus Müller[4], Barbara D'Anna[4], Christian George[4], Andrea Wéber[5], Werner Haunold[5], Andreas Engel[5], Damien Amedro[6], Coralie Schoemaecker[6], Christa Fittschen[6], Taehyoung Lee[7], Jeff Collett[7], Hartmut Herrmann[1]

[1] Leibniz Institute for Tropospheric Research (IfT), Leipzig, Germany
[2] Particle Chemistry Department, Max Planck Institute for Chemistry, Mainz, Germany
[3] School of Chemistry, University of Leeds, UK
[4] Université Lyon 1, France; CNRS, UMR5256, IRCELYON, Institut de Recherches sur la Catalyse et l'Environnement de Lyon, Villeurbanne, France
[5] Institut für Atmosphäre und Umwelt, Goethe Universität Frankfurt, Germany
[6] University of Lille, UMR CNRS-USTL 8522, Villeneuve d'Ascq, France
[7] Department of Atmospheric Science, Colorado State University, Fort Collins, USA

*In Wolken finden zahlreiche Wechselwirkungen zwischen Gasphase, Partikeln und flüssiger Phase statt. Bodengestützte Feldexperimente an orographischen Wolken erlauben eine Untersuchung dieser Wechselwirkungen in der realen Atmosphäre. Hill Cap Cloud Thuringia 2010 (HCCT-2010) war ein solches Experiment, das im September/Oktober 2010 an der Schmücke im Thüringer Wald durchgeführt wurde. Gasphase, Partikel und Wolkentropfen wurden an drei Messpunkten im Luv, auf dem Gipfel und im Lee der Schmücke umfassend chemisch und physikalisch charakterisiert. Während der sechswöchigen Kampagne wurde während insgesamt 370 Stunden eine Wolke an der Gipfelstation registriert. Anhand meteorologischer Analysen wurden 51 Wolkenstunden ermittelt, während derer durch vergleichende Betrachtung der 3 Messstationen ein Einfluss der Wolke auf das lokale Aerosol untersucht werden kann. Der umfangreiche Datensatz wird momentan detailliert ausgewertet und dient als Grundlage für eine mikrophysikalische und chemische Modellierung einzelner Zeitabschnitte. Dieser Beitrag zeigt erste Ergebnisse.*

## Introduction

Clouds have a strong impact on physical and chemical processes in the atmosphere. Studying the interaction of aerosol and clouds under natural conditions is challenging, due to the height, as well as the spatial and temporal variability of clouds. Lagrangian-type field experiments, where a hill cap cloud is used as a natural flow-through reactor were successfully performed in the past to investigate different aspects of physical and chemical aerosol cloud interaction [*Bower et al.*, 2000; *Fuzzi*, 1994; *Fuzzi*, 1997; *Gallagher*, 1999; *Herrmann*, 2005].

In September/October 2010, the international cloud experiment "Hill Cap Cloud Thuringia 2010" (HCCT-2010) was performed at the Schmücke, which is part of a large mountain ridge in Thuringia, Germany. The location was essentially the same as during the previous FEBUKO experiments in 2001 and 2002 [*Herrmann*, 2005]. HCCT-2010 aimed at a better understanding of (i) the chemistry and microphysics within a cloud, (ii) chemical and physical modifications of aerosol particles by their passage through a cloud, (iii) the effects of clouds on the phase partitioning of oxygenated volatile organic compounds (OVOCs), and (iv) the effects of clouds on the budget of the main radical oxidants OH and $HO_2$.

## Campaign description

To address novel issues in our understanding of aerosol cloud interactions, an extended pool of instruments was installed, with a focus on highly time-resolving instruments that were not available during previous studies, e.g. four aerosol mass spectrometers (AMS) and two FAGE instruments (fluorescence assay by gas expansion) for $HO_x$ measurements. In Fig. 1 a scheme of the campaign area is given. Three measurement sites were set up: An upwind site to comprehensively characterize incoming air masses, an in-cloud site on the Schmücke summit to sample the different phases of a cloud, and a downwind site to study possible modifications of the aerosol after the cloud passage. Measurements of particle size distributions and cloud condensation nuclei (CCN) concentrations were performed at both valley sites. The hygroscopic growth of particles was determined upwind only. Vertical distributions of aerosol extinction and cloud

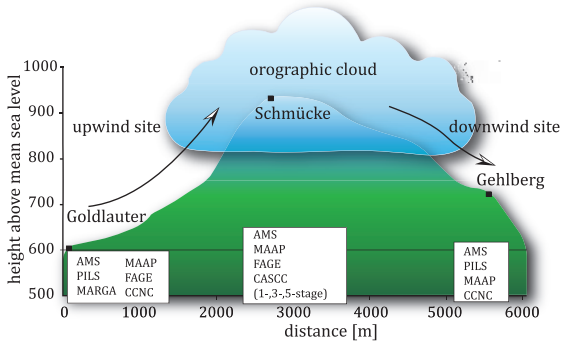


***Fig. 1:*** *Scheme of the campaign area with upwind site Goldlauter, in-cloud site Schmücke summit, and downwind site Gehlberg, including some highlight instrumentation at the sites.*

base were measured by a ceilometer. The gas phase chemical composition at the valley sites was studied by sampling and analyzing trace gases, inorganic acidic gases, organic acids, OVOC, non-methane hydrocarbons (NMHCs), and the reactive species OH and $HO_2$. The chemical particle composition, notably inorganic ions, organic matter (OM), and black carbon (BC) concentrations was obtained from various online instruments. For a detailed analysis of the carbonaceous particle fraction, offline method were applied to determine organic carbon (OC), elemental carbon (EC), and water soluble organic carbon (WSOC), as well as single organic species such as a number of organic acids as typical secondary organic compounds, levoglucosan and further anhydrosugars as biomass burning tracers, and sugars as tracers for biological material. Furthermore, metal concentrations were studied from these samples.

Within the cloud, liquid water content (LWC) and droplet size distributions were measured. Particle size distributions, inorganic ions, OM, and BC of droplet residuals and interstitial particles were determined online behind a counterflow virtual impactor (CVI) after evaporation of the droplet water and an interstitial particle inlet (INT). Offline samplers behind the CVI and INT provided data on OC, EC, WSOC, ions, organic acids, and OVOC. The gas phase radicals OH and $HO_2$ were measured directly within the cloud on a 20 m high tower. On the same tower, cloud water was sampled for chemical analysis in the laboratories of the participating institutes. Several bulk cloud water collectors as well as two size-resolving instruments (3-stage and 5-stage collectors) were applied. Aqueous phase concentrations of inorganic ions, hydrogen peroxide, sulfur(IV), hydroxymethanesulfonic acid, WSOC, organic acids, sugars, anhydrosugars, OVOC, and metal ions, including Fe(II)/Fe(III) were determined from these samples.

HCCT-2010 was successful in that a total of 370 hours of clouds could be captured at the summit station. Certain offline samplers were operated only when meteorological observations predicted favourable flow connectivity between the sites. The criteria included an LWC > 0.1 g $m^{-3}$, wind direction between 200°-250° with wind speed between 2-12 m $s^{-1}$, no fog at the valley sites, no precipitation at any site, and a temperature >0°C. They were fulfilled for a total of 73 hours during 12 so-called “full cloud events” (FCE, all instruments running). The times of these events are given in Tab. 1. After the campaign, these events were classified as described in the following chapter to result in a total of 6 top events (marked green in Tab. 1) with a total of 51 hours of cloud observation. These events are the basis for all data analysis related to the modification of aerosol particles by clouds.

| Rating | FCE /Date |
|---|---|
| 1 | FCE11.3 I 02.10. 14:30 - 20:00 |
| 2 | FCE1.1 I 14.09. 11.00 - 15.09. 02:00 |
| 3 | FCE26.2 I 24.10. 09:15 - 11:45 |
| 4 | FCE26.1 I 24.10. 01:30 - 08:45 |
| 5 | FCE22.1 I 19.10. 21:30 - 20.10. 03:30 |
| 6 | FCE13.3 I 06.10. 12:15 - 07.10. 03:15 |
| 7 | FCE11.2 I 01.10. 22:30 - 2.10. 05:30 |
| 8 | FCE13.1 I 05.10. 19:15 - 06.10. 04:30 |
| 9 | FCE7.1 I 24.09. 23:45 - 25.09. 01:45 |
| 10 | FCE12.1 I 05.10. 11:00 - 13:00 |
| 11 | FCE13.2 I 06.10. 05:15 - 06:15 |
| 12 | FCE20.1 I 15.10. 23:00 - 23:45 |

***Tab. 1:*** *Dates and times of full cloud events during HCCT-2010. Color code indicates the classification of the events as described in the text.*

## Campaign meteorology and flow connectivity

HCCT-2010 was carried out during September and October as the formation of warm orographic clouds was most probable during this season. The evaluation of flow connectivity between the three stations and classification of cloud events was performed in several steps on the basis of extensive meteorological data, including synoptic charts, satellite pictures, locally measured parameters, and calculated flow indicators.

First, an evaluation of large-scale conditions with particular emphasis on the incident flow conditions and on the separation of orographic and non-orographic clouds was performed. Weather charts and calculated backward trajectories were used to determine the horizontal wind pattern and rawinsonde data from a nearby weather

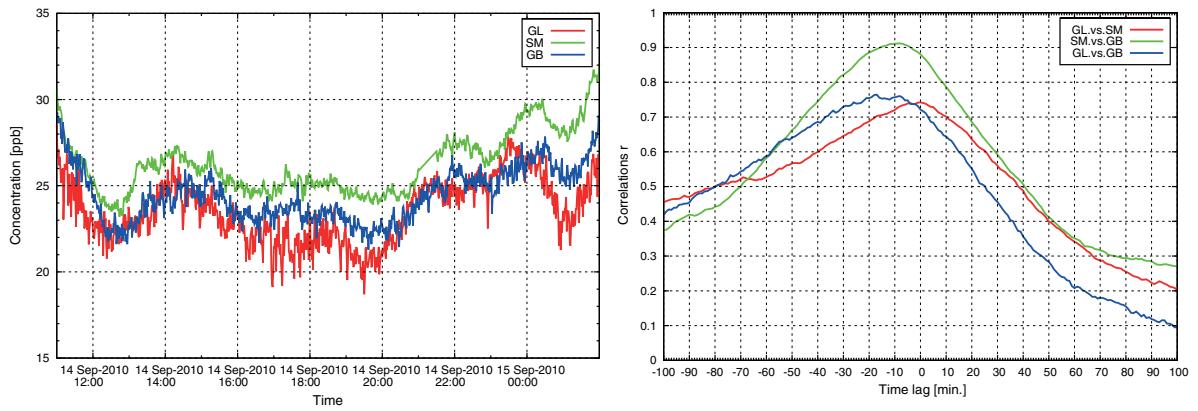


***Fig. 2:*** *Representation of the a) measured ozone concentrations at upwind (GL), summit (SM) and downwind (GB) site and b) the corresponding calculated cross-correlation between the different measurement sites throughout the cloud event FCE1.1.*

station was used for the vertical structure of wind vectors. Synoptic charts were analyzed for frontal processes, synoptic scale advection and air mass classification in the lower troposphere. For the following examination of the cloud orographic character, satellite pictures, rawinsonde data as well as locally measured meteorological and microphysical parameters were evaluated. Especially for the anticyclonic southwest weather-type (SWZAF), stable flow conditions combined with orographic cloudiness were identified. In total, about 30% of the HCCT-2010 cloud event periods were characterized by orographic cloudiness and about 60% by clouds associated to synoptic front systems.

The local flow conditions were analyzed by a cross-correlation analysis of ozone, a chemically inert trace gas on the timescale considered. Figure 2 shows the measured ozone concentrations and the calculated cross-correlations for FCE1.1. The results indicated consistent time profiles and thus a good flow connectivity with an estimated time delay between upwind and downwind site of about 20 minutes. Similar results were found particularly for days with constant southwesterly flow conditions, high wind speeds and less stable stratification.

Additionally to the ozone based flow investigations, the Froude number (Fr) were used to characterize the airflow over the mountain range. The Fr can be calculated from local meteorological data and is known to be a relevant non-dimensional parameter describing the flow regime in mountainous terrain [*Pierrehumbert and Wyman*, 1985]. The obtained results were in general consistent with the ozone analyses.

In order to study air flow conditions experimentally on-site, four tracer experiments were conducted during the campaign. An inertial gas ($SF_6$) was released from a point source at the upwind site and air samples were taken at 8 different locations around the area. In Fig. 3 the results of a tracer experiment on 20 September 2010 are depicted. As can be seen, an intense $SF_6$ plume reached the Schmücke summit about 25 min after the start of the release. Five minutes later, $SF_6$ mixing ratios peaked at the Gehlberg downwind site, although on a much lower level due to dispersion. These results demonstrate a connected flow between the sites under appropriate meteorological conditions.

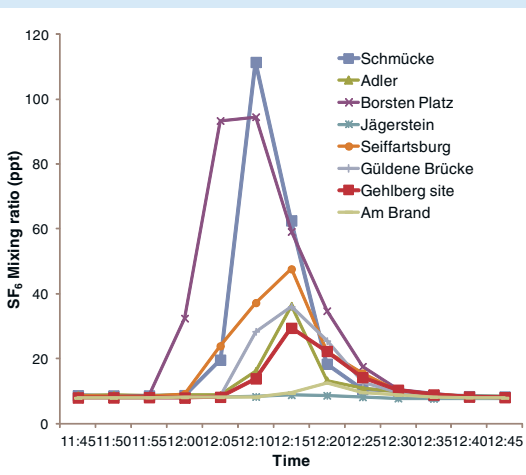


***Fig. 3:*** *Mixing ratios of $SF_6$ for the tracer experiment on 20 September 2010 at different sites around the campaign area, including the Schmücke summit site and the Gehlberg downwind site.*

## Upwind site aerosol characterization

**Trace gas measurements.** The trace gases $O_3$, $NO_x$ (NO and $NO_2$) and $SO_2$ were measured continuously at the upwind site using commercial trace gases analyzers. Additionally, hourly measurements of water soluble acid trace gases and ammonia were realized with a Monitor for Aerosols & Gases in ambient Air (MARGA) on-line analyzer. Mean concentrations during the campaign were 2.7, 0.5, 21.8, and 1.0 ppb, for of $NO_2$, $SO_2$, $O_3$, and $NH_3$, respectively. Elevated concentrations of $SO_2$ up to 6.2 ppb were observed

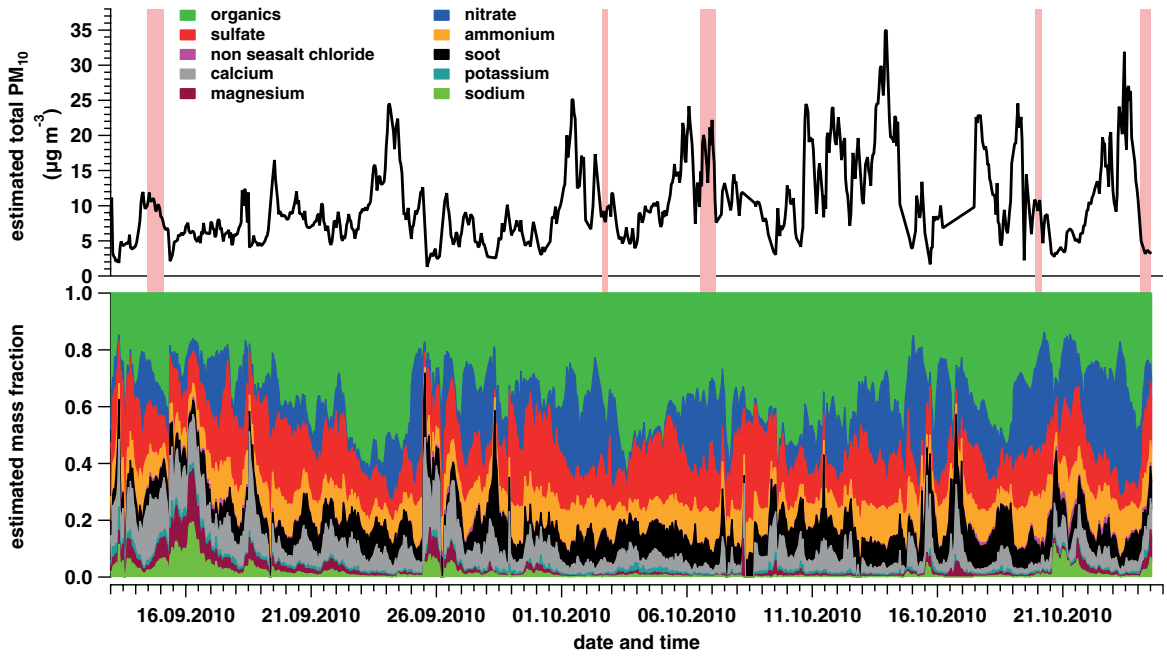


*Fig. 4: Estimation of the total $PM_{10}$ mass concentration during the HCCT-2010 campaign (top) and the corresponding mass fraction of the different aerosol components (bottom) according to the combination of the HR-ToF-AMS, MARGA and MAAP results. The bars in the top panel correspond to different cloud events.*

during few days (11-14 October 2010), indicating air masses strongly influenced by anthropogenic emissions. Comparing the $NH_3$ concentrations with typical fall values at the IfT reseach site Melpitz reveals a lower influence of agricultural emissions at the campaign site.

In addition to the continuous inorganic trace gas measurements, volatile organic carbon (VOC) samples were taken into stainless steel canisters during the cloud events. The analysis of the C2 to C8 non-polar VOC (hydrocarbons) showed a range of total VOC from 15.8 -3.7 ppbv. The percentage of aromatic compounds was between 5 and 14% whilst the n- and i-alkanes reach 50 to 67% and alkenes between 13 and 31% of the VOC. The benzene to toluene ratio varied between 0.6 and 2.7 with a mean of 1.1, what is a hint for air masses that are not freshly polluted from traffic. In general, these ratios are typically for rural areas.

**Chemical particle composition.** Particle chemical composition was characterized at the upwind station using online instrumentation such as a MARGA, an AMS, a Multi-Angle Absorption Photometer (MAAP), and a semi-online Particle-Into-Liquid Sampler (PILS). While MARGA and MAAP were connected to a $PM_{10}$ inlet, both AMS and PILS were measuring $PM_1$. The MARGA (1 h time resolution) provided the composition of the water soluble inorganic particle fraction ($NO_3^-$, $SO_4^{2-}$, $Cl^-$, $Na^+$, $NH_4^+$, $K^+$, $Ca^{2+}$, $Mg^{2+}$ and $Na^+$) as well as information of the gas phase composition (see above). The AMS (5 min time resolution) provided size resolved chemical composition of non-refractory particle components (i.e. soot, crustal material and sea-salts were not detected). A comparison of the nitrate, sulfate and ammonium concentrations measured by MARGA and AMS indicated that these three compounds were mainly present in the submicron fraction of particles during HCCT-2010, except for the first week of the campaign, where a significant coarse mode fraction of nitrate was observed.

Based on the results of AMS, MARGA, and MAAP, total $PM_{10}$ mass was estimated as $9.7 \pm 5.9$ µg $m^{-3}$ (mean ± 1 standard deviation). The chemical composition of upwind particles is shown in Fig. 4 for the whole campaign. They were mainly consisting of organics (36.8% mass fraction), nitrate (16.2%) and sulfate (16.8%). Calcium represents around 7% of the total $PM_{10}$ mass and its mass fraction was strongly increased during periods of low particle concentrations, suggesting a possible local source for this compound. The largest contributions of sodium were measured within maritime influence air masses indicating the presence of sea salts.

**Drop residual and interstitial particle characterization**

At the in-cloud site, the cloud microphysical parameters LWC, effective drop radius ($R_e$), and drop concentration ($N_D$) were measured with a particle volume monitor (PVM) and a forward scattering spectrometer probe (FSSP). The

prevailing clouds exhibited mean values for LWC, $R_e$ and $N_D$ between 150 and 300 mg $m^{-3}$, 5.6 and 7.0 µm, and 350 and 660 $cm^{-3}$, respectively, during the top events.

Two CVI and one interstitial inlet were operated inside the clouds in order to separate and sample cloud drops and non-activated interstitial particles (IP) at a separation size of 5 µm. Downstream of the inlets, physico-chemical properties of cloud drop residues (CDR) and IP were determined by two sets of identical and timely high resolved measurement devices, like condensation particle counter (CPC), particle soot absorption photometer (PSAP), AMS, and scanning mobility particle sizer (SMPS).

The time series of LWC, $R_e$ and different aerosol parameters measured during cloud event FCE11.3 are shown in Fig. 5, where the period of stable south westerly overflow conditions is indicated by the hatched area. In the upper graph the LWC

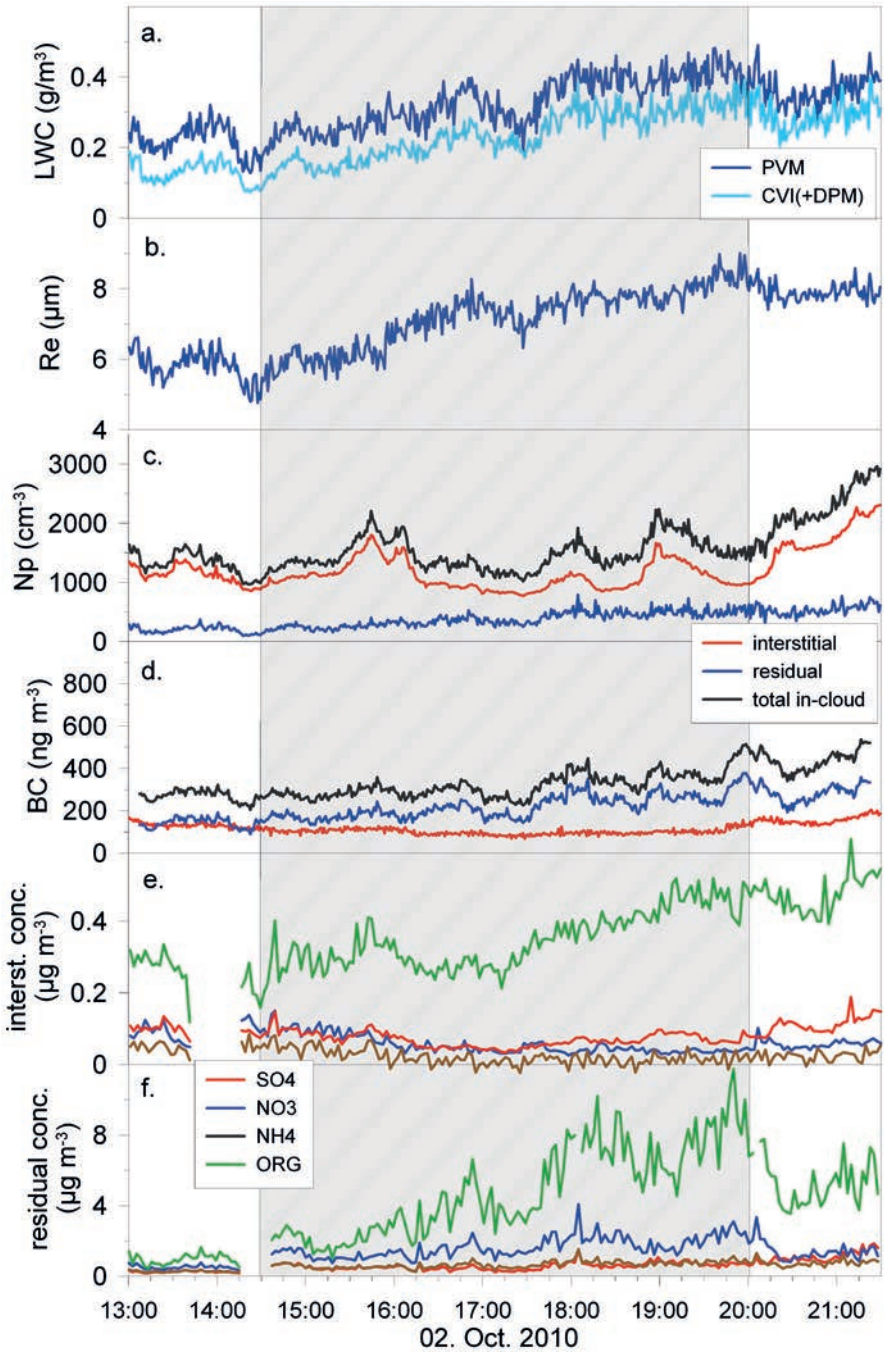


***Fig. 5:*** *Time series of different cloud and aerosol parameters measured inside cloud at the mountain ridge Schmücke site during FCE11.3: a. LWC measured by the PVM (dark blue) and sampled measured by the CVI systems (light blue); b. Effective drop radius; c. number concentration of IP (red), CDR (blue) and their summation (black); d. Black carbon mass concentration of IP (red), CDR (blue), and their summation (black); e. IP mass concentration of sulfate (red), nitrate (blue), ammonium (brown) and organic compounds (green); f. same as e. for the CDR.*

collected by the CVIs and derived from water vapor measurements by a dew point mirror (DPM) is compared to the in-situ LWC determined with the PVM. This comparison reveals that on average 70% of the LWC was sampled by the CVI. This sampling efficiency varied between 66 and 74% for the top cloud events due to differences in wind direction, wind speed and drop size distribution. LWC and $R_e$ increased (Fig. 5a,b) with time, which implies that the cloud base decreased during the measurement period. The CDR number concentration (which is a measure of the drop concentration since one evaporating drop inside the CVI releases one residual particle inside the CVI) slightly increases with LWC, whereas the IP number concentration has a weak anti-correlated trend (Fig. 5c). On average 24 to 34% of the atmospheric particles are detected as drop residues within the top cloud events in this way. With regard to mass concentration of chemical species the dominant part is found in the CDR, which is even observed for BC (Fig. 5d). A mean phase partitioning of 45 to 84% is derived for BC (determined by the two PSAP) within the top cloud events, which implies a substantial aging of the particles before activation or a non-negligible contribution of impaction scavenging of BC particles. The mass concentration of soluble ions in the interstitial and drop phase determined simultaneously by two AMS is shown in Fig. 5e and f, respectively. Both particle reservoirs are dominated by the mass concentration of organic compounds during FCE11.3, but this is not a unique observation for all cloud events. However, 82 to 97% of the organic and inorganic mass concentration are observed in the CDR, but the relation of the phase partitioning changes from event to event and needs further investigation.

Two SMPS behind the CVI and interstitial inlet measured the size distribution of CDR and IP simultaneously. Among the top cloud events, the maximum of the number size distribution varied for the IP from 35 to 75 nm and for the CDR from 120 to 200 nm, caused by different atmospheric particle size distribution, particle chemical composition and supersaturation conditions at cloud base. The 50% activation diameter, calculated from the intersection of IP and CDR number size distributions, typically ranged from 90 to 220 nm. These differences in the cloud formation process observed for the top cloud events will be extensively evaluated by the microphysical and chemical aerosol properties of IP and CDR.

## Chemical cloud water composition

The chemical composition of clouds was studied by different sampling and analytical techniques. Four Caltech Active Strand Cloud Water Collectors (CASCC2) were applied to sample large volumes

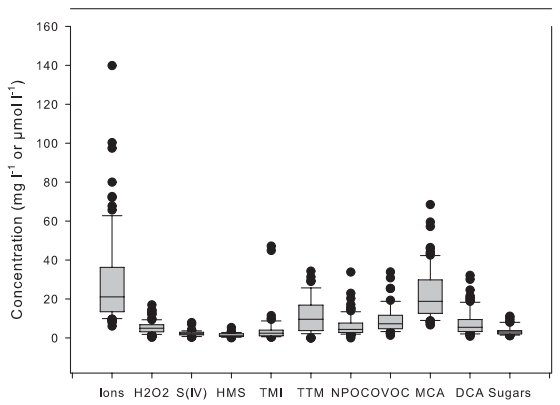


***Fig. 6:*** *Bulk cloud water concentration ranges of the sum of inorganic ions (mg $l^{-1}$), hydrogen peroxide (µmol $l^{-1}$), sulfur(IV) (µmol $l^{-1}$), hydroxymethanesulfonic acid (µmol $l^{-1}$), sum of transition metal ions (µmol $l^{-1}$), sum of total transition metals (µmol $l^{-1}$), non-purgable organic carbon (mg $l^{-1}$), sum of oxygenated volatile organic compounds (µmol $l^{-1}$), sum of monocarboxylic acids (µmol $l^{-1}$), sum of dicarboxylic acids (µmol $l^{-1}$), and sum of monosaccharides (µmol $l^{-1}$). Number of analyzed samples: 88, except for S(IV), TMI, TTM, OVOC, and sugars, where 51 samples were analyzed.*

(up to 640 ml) of bulk cloud water with a 50 percent droplet size cut ($D_{50}$) of 3.5 µm and a one hour time resolution. Additionally, two multistage versions of the CASCC were used: A 3-stage collector with $D_{50}$ of 22, 16, and 4 µm diameter (2 h time resolution), and a 5 stage collector with $D_{50}$ of 30, 25, 15, 10, and 4 µm (4 h time resolution). To complement the liquid cloud water samples, droplet residuals and interstitial particles were sampled downstream of a CVI and INT using filters and two AMS, as detailed above. Many different compounds were analyzed from the bulk cloud water samples, their aqueous phase concentrations are summarized in a boxplot in Fig. 6. Highest concentrations were observed for inorganic ions, determined by ion chromatography (IC). Within this fraction, ammonium, nitrate, and sulfate were the most abundant compounds, with mean concentrations of 5.5, 15, and 5.6 mg $l^{-1}$ (corresponding to 296, 235, and 57 µmol $l^{-1}$), respectively. Elevated concentrations (up to 150 µmol $l^{-1}$) of sodium and chloride were observed within maritime influenced air masses during FCE1.1. Sulfur(IV), i.e. $SO_2$(aq) and $HSO_3^-$, was determined from the cloud water after derivatization by a spectroscopic method and was found in a range between 0 and 8 µmol $l^{-1}$. In the presence of formaldehyde, a fraction of S(IV) is present as hydroxmethanesulfonic acid (HMS), which was determined after stabilization and derivatization in concentrations lied from 0-5.4 µmol $l^{-1}$. S(IV) can be oxidized to S(VI), i.e. sulfate, by different oxidants, including $H_2O_2$, OH radical, $O_3$, and $O_2$ in the presence of transition metal ions (TMI). $H_2O_2$ was analyzed from the cloud water samples after stabilization by fluorescence spectroscopy. Observed concentrations were between 0.3 and

17 µmol $l^{-1}$. Various TMI ($Fe^{2+}$, $Cu^{2+}$, $Zn^{2+}$, $Ni^{2+}$, $Cd^{2+}$, $Co^{2+}$, $Mn^{2+}$ and $Fe^{3+}$) were analyzed by an IC method directly on-site during the campaign. Additionally to the soluble TMI, total trace metal (TMM) concentrations were determined after digestion using total reflection x-ray fluorescence analysis (TXRF). The observed concentrations were about one order of magnitude higher than the TMI concentrations, indicating a large proportion of crustal material in the cloud water. Of the observed soluble iron, the largest fraction was present in the Fe(III) redox state.

Dissolved organic carbon (DOC) was measured as non-purgable organic carbon (NPOC) with a TOC analyzer concentrations between 1.2 and 3.4 mgC $l^{-1}$. Among the organic compound classes determined from the samples, monocarboxylic acids (MCA, mainly formic and acetic acid) had the highest concentrations, followed by the sum of OVOC and dicarboxylic acids (DCA with oxalic acid as most abundant compound). Monosaccharides (levoglucosan and other sugar-derivatives) were present in relatively minor concentrations only (1-11 µmol $l^{-1}$).

Generally, aqueous phase concentrations of cloud water are governed by two main factors: The LWC of the cloud and the chemical composition of the corresponding CCN. By calculating air-equivalent concentrations which take the LWC into account, the budgets of the different compounds found in cloud water will be compared to the concentrations observed at the valley sites in further data analysis.

## CCN activation behavior and modification

The influence of cloud processing on CCN activation behaviour was investigated during the HCCT campaign. Utilizing two CCN Counters (CCNC), CCN size distributions for supersaturations between 0.07 and 0.4% were measured upwind and downwind. Total CCN number concentrations and hygroscopicity parameters κ [*Petters and Kreidenweis*, 2007] were determined and compared for both sites.

In Fig. 7 critical diameters (50% activation diameter, $D_{crit}$) determined during FCE 11.3, 13.3, and 22.1 are shown. It can be seen that $D_{crit}$ were smaller downwind than upwind for supersaturations between 0.07 and 0.2%. After passing through the clouds, particles were more CCN active. The according hygroscopicity parameters κ for the mentioned FCE were found to be higher for downwind particles, indicating that particles became more hygroscopic after the cloud passage. In contrast, during periods with good flow connectivity but no clouds (non cloud events, NCE), $D_{crit}$ and κ featured the same values for both stations. In other words, the processing inside the cloud formed at Mount Schmücke resulted in an

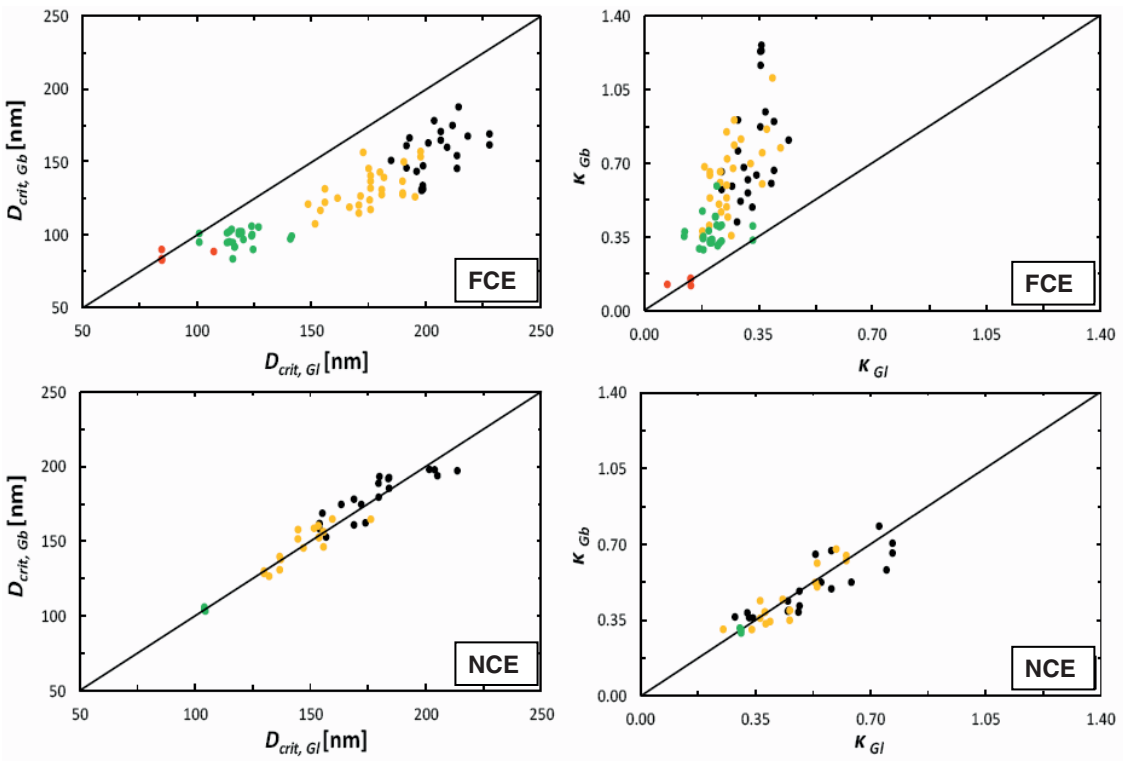


***Fig. 7:*** *$D_{crit}$ and κ during the FCE 11.3, 13.3, and 22.1 (upper panel) and non cloud events (NCE; lower panel). Black dots are $D_{crit}$, respectively κ values, gained from 0.07% supersaturation, yellow dots from 0.1% supersaturation, green dots from 0.2% supersaturation, and red dots from 0.4% supersaturation measurements. Gb indicates the downwind site near the village of Gehlberg, Gl the upwind site near Goldlauter.*

increased hygroscopicity of the residual particles after cloud dissipation, which is likely a result of a modified chemical composition of the particles.

Interestingly, for 0.4% supersaturation, $D_{crit}$ were found to be equal at both valley stations, with values between 71 nm and 107 nm (Fig. 7). This suggests that particles in this size range were not activated to cloud droplets, remained part of the interstitial aerosol, and were consequently not processed in the cloud. Hence, the supersaturation reached within the cloud was lower than 0.4% during the considered FCE. In connection with the findings described above, the supersaturation in the observed clouds can be estimated to be between 0.2 and 0.4%.

## Modification of chemical particle composition

Chemical reactions within the aqueous phase of a cloud can modify the chemical composition of CCN after a cloud passage. In order to study the influence of clouds to the particle chemical composition, the AMS measurements performed at the upwind and downwind stations were compared

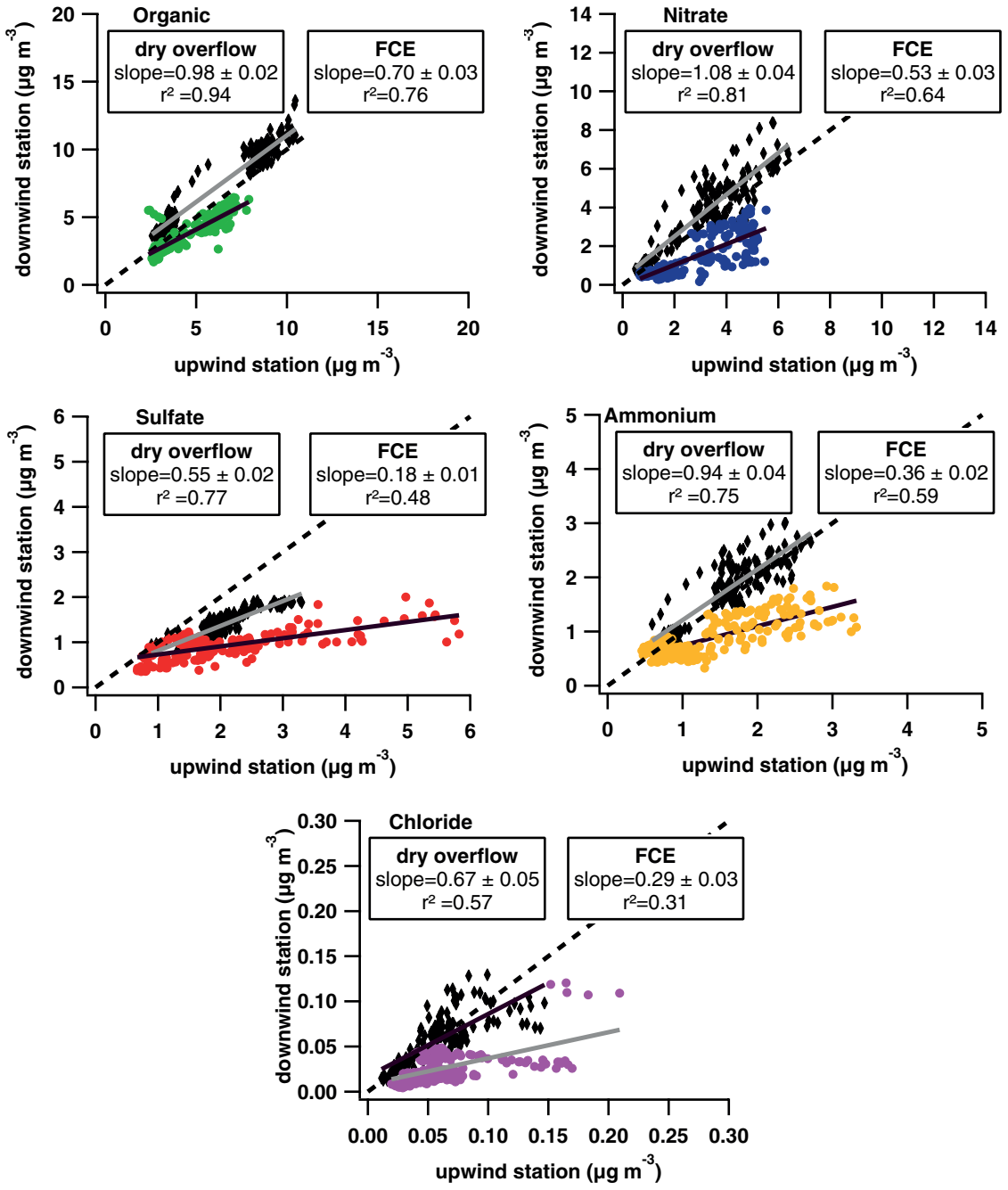


*Fig. 8: Comparison between the particle chemical composition measured by AMS at the upwind and downwind stations during dry-overflow (black diamond) and the Top-FCE (colored circle) periods.*

during cloud events with good connected flow conditions. The main aerosol chemical components detected by AMS at the upwind and downwind station are presented in Fig. 8 for NCE with good flow connectivity and the 6 top FCE (Tab. 1). Except for sulfate, similar concentrations and time series (not shown) were measured at the two valley stations during NCE. The differences can be attributed to the instrumental uncertainties as well as a possible particle loss or dilution effects during the air mass transport between the stations. During the FCE, concentrations at the downwind station were significantly lower than the ones measured at the upwind station. This discrepancy can be attributed to wet deposition processes or entrainment of cleaner air masses. However, the correlation slopes of the each compound during FCE strongly differ from the NCE ones. Besides a size effect, this may suggest a possible influence of the cloud chemistry to the aerosol chemical composition. More investigation will be performed especially to better estimate influence of cloud chemistry to the organic composition. In addition to the concentrations, also relative compositions will be compared and the AMS data from the in-cloud site will be included to the comparisons.

### Multiphase chemistry modeling

After the chemical sample analysis, the parcel model SPACCIM (SPectral Aerosol Cloud Chemistry Interaction Model; [*Wolke et al.*, 2005]) will be applied to investigate the effects of cloud processing during HCCT-2010. The applied model combines a complex microphysical and a detailed multiphase chemistry model with 11381 gas phase and about 2200 aqueous phase reactions. The chemical multiphase mechanism (MCMv3.1 (Master Chemical Mechanism; [*Saunders et al.*, 2003])/CAPRAM3.0i-ext (Chemical Aqueous Phase RAdical Mechanism; [*Tilgner and Herrmann*, 2010])) incorporates a detailed explicit description of the inorganic and organic multiphase chemistry based on time-dependent size-resolved aerosol/cloud spectra. The measured physical and chemical data at the upwind site will provide the basis for the model initialisation.

SPACCIM simulations will be performed for the top cloud events. Model results of the cloud passage simulation will be compared with cloud water composition data at the summit site as well as gas and particle measurements at the downwind site in order to interpret the experimental data and to evaluate the model results. To this end, a detailed analysis will be performed including chemical source and sink studies with special emphasis on radical and non-radical oxidants as well as important organic and inorganic chemical subsystems. For the first time, measured gas phase in-cloud $HO_x$ concentrations during a hill cap cloud experiment will be directly compared to the modelled concentrations. Another objective of the study will be to assess in-cloud oxidations of important C2 and C3 organic compounds such as glyoxal and methylglyoxal. Moreover, the enrichment of organic compounds with smaller Henry solubility in the cloud droplets will also be studied by the model. To this end, an extended phase transfer description will be implemented in SPACCIM to consider e.g. interfacial adsorption at the air–water interface. The application of the refined model might finally allow a better interpretation of the experimental findings.

### Outlook

HCCT-2010 yielded a novel and complex dataset on aerosol cloud interactions. A good number of cloud events with appropriate meteorological conditions for a connected air flow between the three measurement sites was obtained. Many different instruments sampled a wealth of physical and chemical data, which is currently being analyzed under various aspects. The dataset will also be the basis for extensive modeling of certain time periods during the campaign. All experimental and theoretical results will be published in a special issue of Atmospheric Chemistry and Physics, which has recently been opened with the issue editors G. McFiggans, M.C. Facchini, C. George and H. Herrmann.

### References

Bower, B. K. N., T. W. Choularton, M. W. Gallagher, K. M. Beswick, M. J. Flynn, A. G. Allen, B. M. Davison, J. D. James, L. Robertson, R. M. Harrison, C. N. Hewitt, J. N. Cape, G. G. McFadyen, C. Milford, M. A. Sutton, B. G. Martinsson, G. Frank, E. Swietlicki, J. Zhou, O. H. Berg, B. Mentes, G. Papaspiropoulos, H. C. Hansson, C. Leck, M. Kulmala, P. Aalto, M. Vakeva, A. Berner, M. Bizjak, S. Fuzzi, P. Laj, M. C. Facchini, G. Orsi, L. Ricci, M. Nielsen, B. J. Allan, H. Coe, G. McFiggans, J. M. C. Plane, J. L. Collett, K. F. Moore, and D. E. Sherman (2000), ACE-2 HILLCLOUD. An overview of the ACE-2 ground-based cloud experiment, *Tellus*, *52B*(2), 750-778.

Brüggemann, E., T. Gnauk, S. Mertes, K. Acker, R. Auel, W. Wieprecht, D. Möller, J. L. Collett, H. Chang, D. Galgon, R. Chemnitzer, C. Rüd, R. Junek, W. Wiedensohler, and H. Herrmann (2005), Schmücke

hill cap cloud and valley stations aerosol characterisation during FEBUKO (I): Particle size distribution, mass, and main components, *Atmos. Environ.*, *39*(23-24), 4291-4303.

Fuzzi, S. (Ed.) (1994), *J. Atmos. Chem. 19(1-2)*.

Fuzzi, S. (Ed.) (1997), *Atmos. Environ. 31(16)*.

Gallagher, M. W. (Ed.) (1999), *Atmos. Res. 50(3-4)*.

Herrmann, H. (Ed.) (2005), *Atmos. Environ. 39(23-24)*.

Mertes, S., D. Galgon, K. Schwirn, A. Nowak, K. Lehmann, A. Massling, A. Wiedensohler, and W. Wieprecht (2005), Evolution of particle concentration and size distribution observed upwind, inside and downwind hill cap clouds at connected flow conditions during FEBUKO, *Atmos. Environ.*, *39*(23-24), 4233-4245, doi: DOI 10.1016/j.atmosenv.2005.02.009.

Petters, M. D., and S. M. Kreidenweis (2007), A single parameter representation of hygroscopic growth and cloud condensation nucleus activity, *Atmos. Chem. Phys.*, *7*(8), 1961-1971.

Pierrehumbert, R. T., and B. Wyman (1985), Upstream Effects of Mesoscale Mountains, *J. Atmos. Sci.*, *42*(10), 977-1003.

Saunders, S. M., M. E. Jenkin, R. G. Derwent, and M. J. Pilling (2003), Protocol for the development of the Master Chemical Mechanism, MCM v3 (Part A): tropospheric degradation of non-aromatic volatile organic compounds, *Atmos. Chem. Phys.*, *3*, 161-180.

Tilgner, A., and H. Herrmann (2010), Radical-driven carbonyl-to-acid conversion and acid degradation in tropospheric aqueous systems studied by CAPRAM, *Atmos. Environ.*, *44*(40), 5415-5422, doi: 10.1016/j.atmosenv.2010.07.050.

Tilgner, A., Z. Majdik, A. M. Sehili, M. Simmel, R. Wolke, and H. Herrmann (2005), SPACCIM: Simulations of the multiphase chemistry occurring in the FEBUKO hill cap cloud experiments, *Atmos. Environ.*, *39*(23-24), 4389-4401, doi: DOI 10.1016/j.atmosenv.2005.02.028.

van Pinxteren, D., A. Plewka, D. Hofmann, K. Müller, H. Kramberger, B. Svrcina, K. Bächmann, W. Jaeschke, S. Mertes, J. L. Collett, and H. Herrmann (2005), Schmücke hill cap cloud and valley stations aerosol characterisation during FEBUKO (II): Organic compounds, *Atmos. Environ.*, *39*(23-24), 4305-4320.

Wolke, R., A. M. Sehili, M. Simmel, O. Knoth, A. Tilgner, and H. Herrmann (2005), SPACCIM: A parcel model with detailed microphysics and complex multiphase chemistry, *Atmos. Environ.*, *39*(23-24), 4375-4388, doi: DOI 10.1016/j.atmosenv.2005.02.038.

**Funding**
- German Research Foundation (DFG), Bonn, Germany

**Cooperation**
- Max Planck Institute for Chemistry, Mainz, Germany
- University of Leeds, Great Britain
- Université Lyon, IRCELYON, France
- Goethe Universität Frankfurt, Germany
- University of Lille, France
- Colorado State University, USA
- Eidgenössische Technische Hochschule Zürich, Switzerland

# The CARRIBA project: Experiment Overview and Highlights

Holger Siebert[1], Julia Bethke[1], Thomas Conrath[1], Florian Ditas[1], Susan Hartmann[1], Miguel A. Izaguirre[2], Jeannine Katzwinkel[1], Greg Roberts[3], Michael Schäfer[1], Tina Schmeissner[1], Raymond A. Shaw[4], Björn Stevens[5], Frank Stratmann[1], Birgit Wehner[1], Manfred Wendisch[6], Frank Werner[6], Heike Wex[1]

[1] Leibniz Institute for Tropospheric Research (IfT), Leipzig, Germany
[2] University of Miami, USA
[3] Meteo France, Toulouse, France
[4] Technological University of Michigan, USA
[5] Max Planck Institute for Meteorology, Hamburg, Germany
[6] Leipzig Institute for Meteorology, University of Leipzig, Germany

*Im November 2010 und April 2011 wurden über Barbados zwei Messkampagnen mit der Hubschrauberschleppsonde ACTOS in flachen Passatwindwolken durchgeführt. Die Experimente wurden sowohl durch bodengestützte Messungen von physikalischen Aerosoleigenschaften und meteorologischen Parametern als auch von Fernerkundungsmesssystemen des Max-Planck Instituts für Meteorologie, Hamburg an der Ostküste Barbados' unterstützt. Im besonderen Fokus der Untersuchungen standen die Wechselwirkungen von Aerosol und Wolken, kleinskalige Wolkendynamik, Strahlung und Grenzschichtentwicklung. In diesem Beitrag werden neben einer Einführung in die Motivation zu dem Experiment und einem Überblick über die zwei Feldkampagnen die Vielfältigkeit der verschiedenen Untersuchungen an Hand von sechs ausgewählten „Highlights" der Kampagne dar gestellt.*

## Motivation

Shallow cumulus convection is one of the prevalent cloud forming mechanism in the tropics. Since shallow cumulus clouds are very widespread in the trade wind regions, they play an important role in the moisture transport to the free atmosphere [*Tiedtke*, 1989] and also for the Earth's radiation budget [*Albrecht et al.*, 1995]. Furthermore, shallow cumulus convection significantly influences the dynamics of the entire planetary boundary layer (PBL) by intensifying the vertical transport of moisture, momentum, and heat from the surface to higher levels.

As early as in the late 1940's the trade wind regions were in the focus of the scientific cloud community. In a series of pioneering aircraft measurements known as the "Wyman and Woodcock Caribbean Expedition" in April 1946, soundings of wet and dry-bulb temperature in- and outside the clouds were performed. New concepts of cloud dynamics and entrainment were tested based on these measurements [*Stommel*, 1947, 1951]. *Malkus* [1954] recognized the trade wind cumuli as an *"example of the convective process operating under more uniform and relatively less complex conditions than in the case of land cumulus in middle latitudes"*. He published a body of three papers about the structure and dynamics of trade wind cumuli [*Malkus*, 1954, 1956, 1958].

Although the trades were in the focus of several extensive field experiments since then, such as BOMEX ("Barbados Oceanographic and Meteorological EXperiment" in 1968/69, *Davidson* [1968]; *Holland and Rasmusson* [1973]), ATEX ("Atlantic Trade wind EXperiment" in 1969, *Augstein et al.* [1973]), or more recently the RICO campaign ("Rain In Cumulus over the Ocean", *Rauber et al.* [2007]), several aspects are still not understood.

One of the most important open issues is the formation of precipitation. As the lifetime of trade wind cumuli is relatively short - in the range of hours - formation of precipitation should be hampered. Also, if precipitation does form, it is purely without ice phase. Thus trade wind cumulus clouds embody the warm rain problem, namely how such short-lived shallow clouds can at times produce significant amounts of precipitation [e.g., *Squires and Warner*, 1957]. There is a big discrepancy between model results (which usually show no significant amount of precipitation) and observations, which indicate the onset of precipitation sometimes in less than one hour. Already *Langmuir* [1948] pointed out that *"... warm cumulus clouds often developed rain within less than thirty minutes after their formation..."*.

Objects of investigation in this respect are e.g. the influence of turbulence on cloud droplet growth, but also the influences of atmospheric aerosol particles and cloud condensation nuclei (CCN) on the droplet number concentration, the droplet size, and the amount of drizzle forming from a cumulus cloud [e.g., *Heymsfield and McFarquhar*, 2001; *Kaufman et al.*, 2005]. So-called "giant nuclei" play a particular role among the aerosol particles, as they might promote the rapid development of precipitation, a topic which was mentioned and examined already by *Woodcock et al.* [1950, 1953] and is still a topic of ongoing research [e.g., *Rudich*

*et al.*, 2002; *Blyth* et al., 2003]. In general, the role of aerosol in controlling radiative properties of clouds is likely important, as already discussed by e.g. *Twomey* [1977] and *Albrecht* [1989], but it should also be stressed, that aerosol particles may not be the major driver in the development of precipitation. The warm rain problem may mainly be due to an incomplete description of turbulent processes such as entrainment and subsequent mixing.

Overall, it has to be stated that despite significant research efforts in the past, we are still lacking means to predict the behavior of shallow cumulus clouds in terms of their microphysical and radiative properties, the initiation of precipitation, and their influences on large-scale boundary layer dynamics.

Therefore, the CARRIBA-project (Cloud, Aerosol, Radiation and tuRbulence in the trade wInd regime over BArbados) was initiated. The project is embedded in a long-term initiative of the Max Planck Institute for Meteorology in Hamburg, which has operated an observatory at the East coast of Barbados for more than three years. This article provides a general introduction of the CARRIBA-project including specific goals, a measurement overview, and several research highlights from two measurement campaigns in 2010 and 2011. This compilation of different research highlights is not intended to provide detailed results but rather should emphasize the multidisciplinary of the whole project.

## The CARRIBA Project: Open Questions and Methods

The scientific goals of CARRIBA can be divided into two major parts: i) the influence of aerosol particles on trade wind cumuli - including their anthropogenic perturbations (e.g., biomass burning) - and their influences on the microphysical and radiative cloud properties in particular in the early stage of cloud development, and ii) the dynamic/thermodynamic processes of shallow cumulus convection including entrainment, turbulent mixing, and a general description of the underlying turbulent flow field in the cloudy PBL, which is important for transport processes into the cloud, and coalescence of cloud droplets and, therefore, the warm rain process.

In order to tackle these two topics, the helicopter-borne measurement payloads ACTOS (Airborne Cloud Turbulence Observation System) and SMART-Helios (Spectral Modular Airborne Radiation measurements sysTem) were deployed for two one-month periods in November 2010 and April 2011 on Barbados with 32 2h-research flights altogether. The airborne measurements were supported by ground-based aerosol and meteorological observations at the East coast of Barbados (see Fig. 1).


***Fig. 1:*** *Map of Barbados with the helipad in the South (close to the airport) and Ragged Point at the East coast with the ground-based station of IfT close to the MPI observatory at Deebles Point. The red line shows the flight pattern of April 10th with operation from the helipad.*

The ACTOS and SMART-Helios payloads are autonomous systems, which are carried in combination as external cargo by a helicopter. The SMART-HELIOS measures radiances and irradiances for the visible and near-infrared spectral ranges and is attached about 20 m below the helicopter and mainly remains above the clouds during measurement flights. ACTOS is attached by means of a second 140 m long rope below SMART-Helios and can be dipped into the clouds to measure the meteorological standard parameters such as the three-dimensional wind vector, temperature, static pressure, and humidity with decimeter resolution. A sophisticated navigation unit based on GPS and inertial sensors yields the full set of attitude and position parameters. Furthermore, ACTOS is equipped with sensors to measure the aerosol number size distribution and concentration of the interstitial aerosol particles, the cloud droplets, and the liquid water content (*LWC*) in clouds. For the first time, a small and lightweight cloud condensation nuclei (CCN) counter was included. A comprehensive description of the two systems can be found in *Siebert et al.* 2006 and *Henrich et al.*, 2010.

For the two CARRIBA campaigns the helicopter was operated from a helipad close to the international airport at the South coast of Barbados. This allowed the helicopter to avoid flying over densely populated areas at low levels and to go directly over sea after take-off. In Fig. 1, the flight track is plotted for April 10th, which is typical for most of the measurement flights. All flights start with a 10km-long horizontal leg in about 50 m above sea level (asl) followed by a vertical

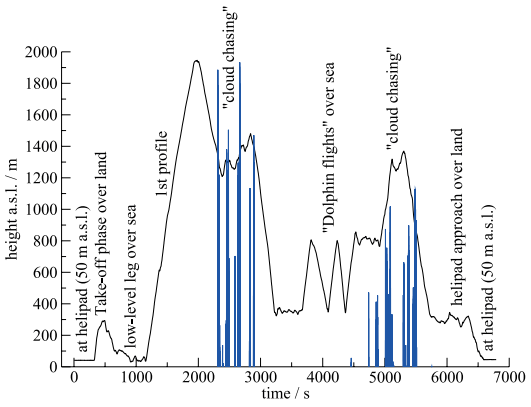


***Fig. 2:*** *Time series of the measurement height over sea level (asl) for April 10th. The blue lines indicate the LWC (arbitrary units) and serve as a marker for cloud passages. Typical flight sections are labeled.*

profile up to 2 – 2.5 km without cloud contact. Both data sets are taken over the sea East of Ragged Point in order to compare with the ground-based measurements. After profiling, the flight pattern was decided by the on-board scientist depending on local cloud conditions in the measurement area over sea or the island. Typically, first cloud fields were sampled followed by a more detailed investigation of the marine boundary layer (MBL) structure by performing dolphin flights around the interfacial layer at top of the well-mixed MBL. The height profile for the flight of April 10th is presented in Fig. 2. The height is given above sea level (asl) and the helipad is about 50 m asl. The blue lines indicate cloud contact of ACTOS in terms of the *LWC* (in arbitrary units).

Ground based measurements were done on Ragged Point, at one of the eastern most points of Barbados, where a measurement station has already been operated for several decades [*Li-Jones & Prospero*, 1998]. A 17 m tall mast exists at this station, situated right at the cliffs falling off to the ocean. On top of that mast, measurements of meteorological parameters and aerosol filter measurements are done continuously. During CARRIBA 2010 and 2011, we used an aerosol inlet installed on top of the mast from which we could additionally measure total particle number concentrations (N) and size distributions (both for the size range of 20 nm to 500 nm) and number concentrations of cloud condensation nuclei (CCN) at different super-saturations. From the latter, information of the particle hygroscopicity can be derived.

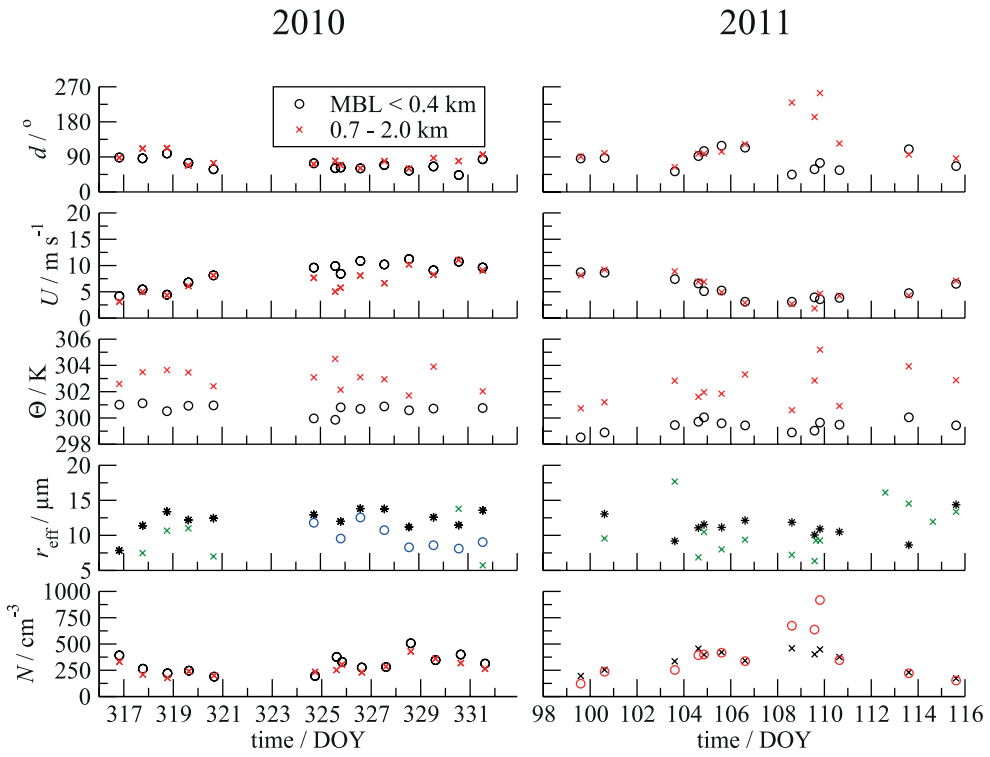


***Fig. 3:*** *Time series of parameters measured with ACTOS averaged over individual flights. The presented values are for the MBL defined as the height between sea level and 400 m (black circles) and for cloud-free regions in a height range between 0.7 and 2.0 km (red stars). In particular for the MBL, only measurements over sea are considered to exclude land effects (d: wind direction; u: horizontal wind speed; Θ: potential temperature, $r_{eff}$: effective radius of cloud droplets; N: particle number concentration (normalized to standard conditions)). The values for $r_{eff}$ are valid for clouds sampled below 2 km and derived from the LWC/PSA ratio (black stars), from the droplet size distribution (blue circles), and as a retrieval from radiation measurements with SMART-Helios (green symbols).*

## Ground Based Aerosol Measurements and Synoptics

Barbados is the eastern most island in the arc of islands that separates the Atlantic from the Caribbean. The climate is characterized by the steady trade winds blowing in from the east. Besides local ship and aircraft emissions there are no anthropogenic aerosol sources upwind the island for several thousands of kilometers. Figure 3 shows values for a selection of parameters measured at individual ACTOS flights during the two campaigns. Data are given as time series and for two different altitude ranges. Presented are the parameters wind direction *d*, horizontal wind speed *u*, potential temperature Θ, effective radius of cloud droplets $r_{eff}$ and particle number concentration *N* (normalized to standard conditions). During most times, *d*, *u* and also *N* were similar in the two heights ranges that are depicted in Fig. 3. *u* mostly varied between 5 to 10 m $s^{-1}$, while *d* was predominantly from the sector between 45° and 90°. Only during a time period in April 2011, when the trades were weak, *d* was more variable. Θ was higher in the cloud layer, as to be expected, and was about 2 K larger in November 2010 than in April 2011, and varied by less than 3 K within each of the campaigns, indicating again the stable weather conditions prevailing in the tropics. Values for $r_{eff}$ derived from three different instruments differ somewhat, an issue that will have to be examined in more detail in the future. *N* varied, as will be described in more detail below, from about 100 to 500 $cm^{-3}$, exept for a time period in April 2011, when flights inside of clouds originating from fires on the island were performed.

The aerosol properties measured at Ragged Point were correlated with 10-day-trajectories arriving at Ragged Point at heights of 500 m. For times when the trajectories had passed over continental biomass burning or desert regions, the measured amount of insoluble material (which can be either soot or dust), derived from the filter measurements, and also the measured particle number concentration, were both comparably large (see Fig. 4).

Three distinctly different types of aerosol were found. There were situations with comparably high *N* (> 200 $cm^{-3}$), during which size distributions were as shown in panel A in Fig. 4, and during which the trajectories indicated a continental influence. During times without this continental influence, the Hoppel-minimum that divides particles that had been activated into a cloud droplet from the smaller ones [*Hoppel et al.*, 1986], usually could be seen at sizes of about 70 to 80 nm, as shown in panel B and C in Fig. 4. On some days (panel C), particularly many particles were found for sizes below the Hoppel-minimum. The air masses during these times were very clean – conditions that likely had favored new particle generation from the gas phase in the corresponding air mass.

Particle hygroscopicity (i.e., κ, *Petters & Kreidenweis*, [2007]) was determined from CCN counter measurements and was found to be 0.62 on average. This is close to the values reported

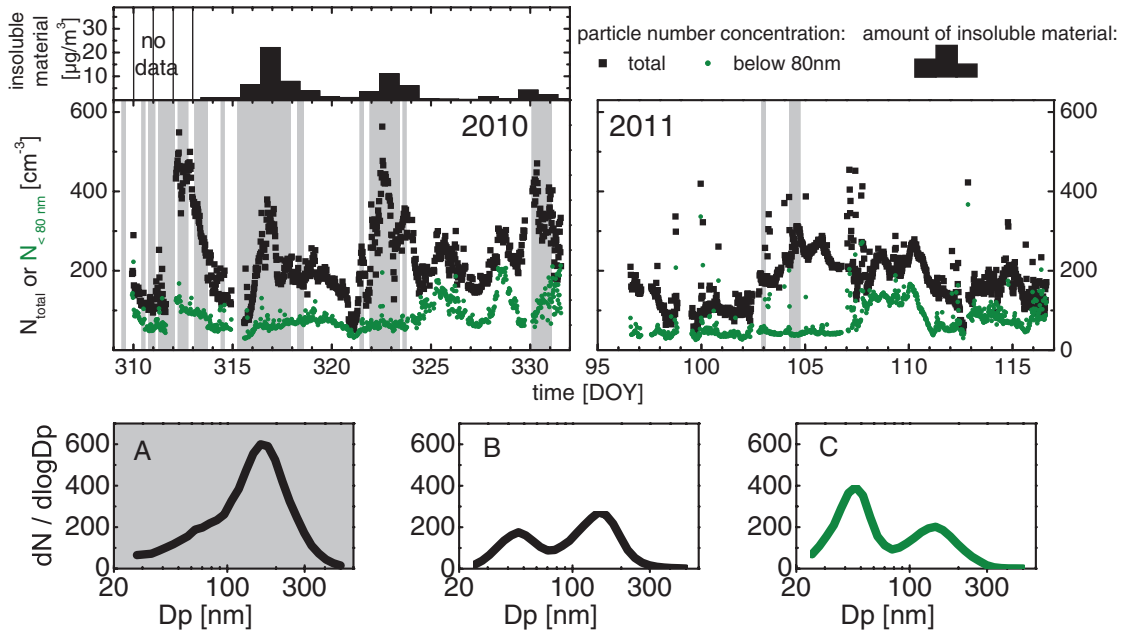


*Fig. 4: Upper panels: time series of the amount of insoluble material found on the daily filter samples (only available for 2010) and particle number concentration (both, total and for sizes < 80 nm). Grey background denotes times during which 10-day-trajecoties had passed over continental biomass burning or desert regions. Lower panels (A, B and C): size distributions exemplary for the three different aerosol types (see text).*

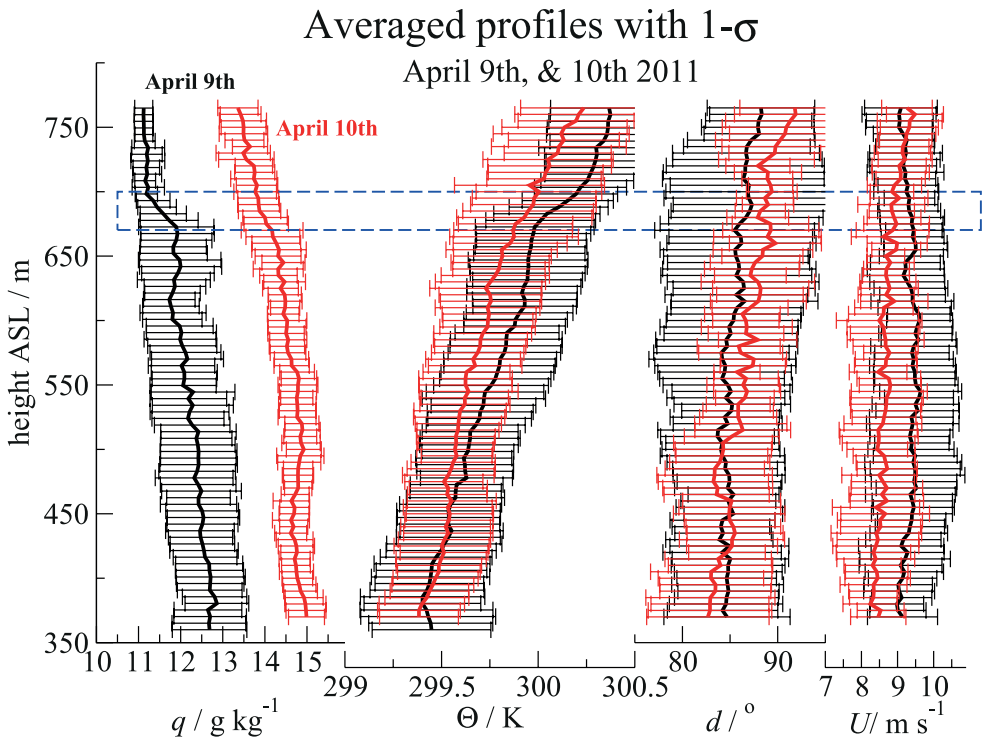


***Fig. 5:*** *Mean vertical profiles around the interfacial layer in the height range between 350 and 770 m asl. The black curves are for April 9th (no clouds in the measurement area) and the red curves are for April 10th with cumulus clouds. Shown is the water vapor mixing ratio q, potential temperature Θ, wind direction d, and wind speed u, respectively. The thick lines represent the mean value; error bars indicate 1-σ. The profile of April 9th is based on 12 individual profiles whereas for April 10th the average is over 8 profiles.*

in literature for North Atlantic aerosol as derived from a model (0.59, *Pringle et al.*, [2010]) or for ammonium sulfate (0.61, *Petters & Kreidenweis*, [2007]). The κ-value, together with the particle size at the Hoppel-minimum, can be used to infer that the maximum super-saturation in the trade wind cumulus clouds was around 0.2 to 0.3%. CCN can be derived from measured number size distributions by integration over the distribution from the activation diameter onward. When this was done e.g. for a super saturation of 0.26%, these calculated CCN correlated very well with measured ones ($R^2$ of 0.97). A good correlation was found between CCN measured on ground and those measured on ACTOS ($R^2$ of 0.89). This shows, together with the above mentioned agreements between the ground based aerosol characterization and the trajectories arriving at 500 m, that the ground based data measured during CARRIBA 2010 and 2011 can be taken as being representative for the aerosol that was present in the MBL.

## The Typical Structure of the Marine Boundary Layer

The typical vertical structure of the cloudy trade wind region is characterized by a 600 to 800 m thick humid and well-mixed MBL over the ocean. Above this sub-cloud layer a thin transition layer is situated where the thermodynamic parameters exhibit a significant jump. Above this transition layer, a conditionally unstable cloud layer exists. This layer typically does not exceed 2 km and is topped by the inversion, which separates the cloud from the dry and potentially warmer air of the free atmosphere. In Fig. 5, we present averaged profiles around the transition layer in a height range between 360 and 760 m asl for two different subsequent days without clouds in the measurement area (April 9th, 2011) and with shallow cumulus convection (April 10th, 2011). The error bars denote the standard deviation σ of the different profiles. The profile for April 9th consists of 12 individual profiles and for April 10th eight profiles are considered – all of them over the sea. For the specific humidity *q*, the values are nearly constant in the well-mixed MBL below 670 m (April 9th) and 640 m (April 10th). Above the MBL on both days a slight decrease can be observed indicating the mean height of the so-called transition layer. The transition layer is more pronounced for the cloud-free day. In general, on April 10th the MBL was significantly moister by about 2.5 g $kg^{-1}$, which explains the onset of cumulus convection on April 10th in contrast to cloud-free conditions on April 09th. There is little difference between the two days for the other parameters such as Θ, *d*, and *u*. The stratification is slightly conditionally unstable with a mean gradient of 0.2 K 100 $m^{-1}$, the transition

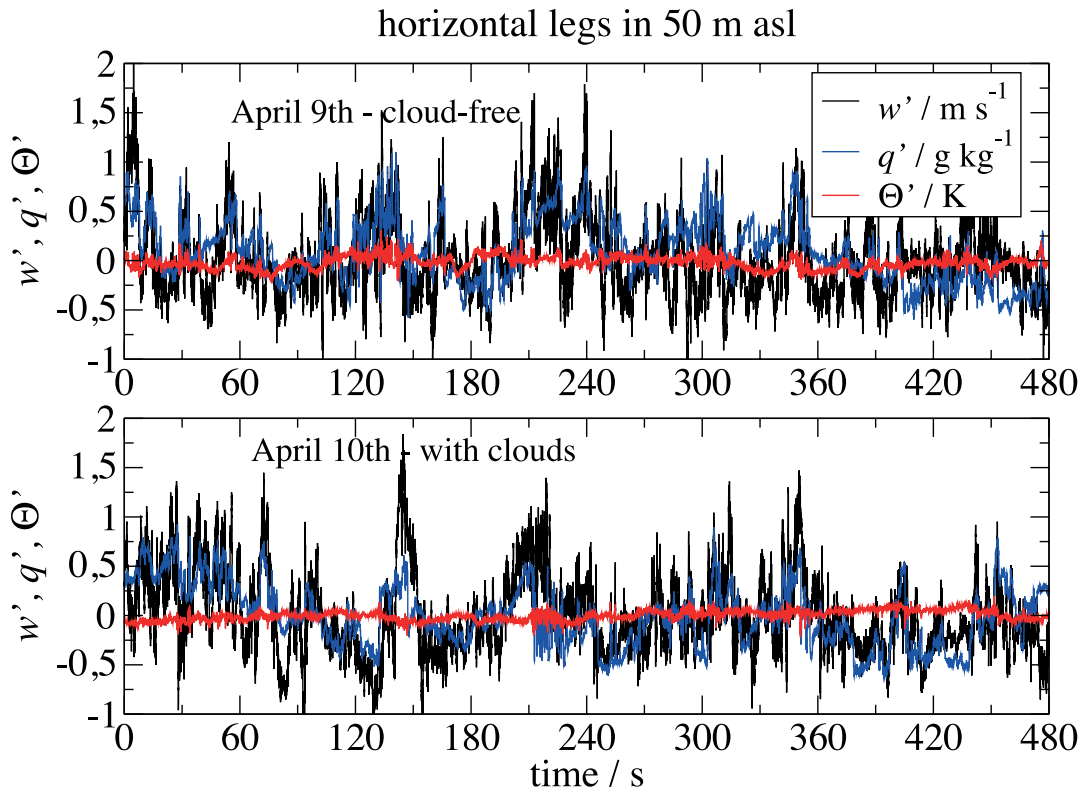


***Fig. 6:*** *Time series of fluctuations of vertical wind velocity w', water vapor mixing ratio q' and potential temperature Θ' for April 9th (top) and 10th (bottom). From the fluctuations, turbulent fluxes of latent heat (L) and sensible heat (H) were estimated: H = 7 W m-2 and L = 165 W m-2 (April 9th) and H = -2 W m-2 and L = 175 W m-2 (April 10th), respectively. The data was sampled during a 10km-long leg in 50 m asl.*

layer is less pronounced in the temperature but still obvious. A fresh breeze with $u$ in the range of 8 to 9 m s$^{-1}$ from easterly directions prevailed on both days.

In Fig. 6, the time series of fluctuations of $w$, $q$, and Θ (denoted as $w'$, $q'$, and Θ') are plotted. The fluctuations are defined by linear detrending the original time series. The data were taken during 10 km-long low-level legs shortly after take-off in about 50 m asl. Qualitatively, the time series looks quite similar. The vertical velocity and humidity show a high correlation with strong fluctuations and temperature fluctuations are comparable weak. From these data turbulent vertical fluxes of latent heat $L = \rho\, L_v \langle w'q' \rangle$ and sensible heat $H = c_p \langle \Theta' w' \rangle$ are derived where <...> denotes temporal averaging. For April 9th we estimate $H$ = 7 W m$^{-2}$ and $L$ = 165 W m$^{-2}$ with a statistical error of about 15%. The next day with cumulus convection yields $H$ = -2 W m$^{-2}$ and $L$ = 175 W m$^{-2}$. It has to be pointed out that for a more robust estimate of the fluxes the legs are too short due to the intermittent character of the time series. However, the estimated values are quite comparable to the published values for the RICO LES study [*van Zaanten et al.*, 2011] for similar MBL conditions. The slightly increased latent heat flux on April 10th is consistent with a moister MBL, which is obviously the reason for the onset of cumulus convection.

## Typical Cloud Microphysics Properties in the Trades

During CARRIBA cloud microphysical properties of shallow cumulus clouds were measured. Cloud droplet number size distributions were derived from a Phase Doppler Interferometer (PDI). As a case study we present data from November 20th, 2010. Figure 7 shows the time series of droplet counts and size distributions for two different cloud types. At the beginning, ACTOS flew through a rather stratiform cloud layer, which is most likely an outflow from a deep convective cloud. This stratiform layer shows the typical narrow droplet number size distribution in the range of rather small cloud droplet sizes (see Fig. 7, left plot of lower panel). A peak can be seen at a diameter of around 18 – 20 µm. Afterwards, ACTOS traversed some typical trade wind clouds. Consequently, the droplet number size distribution became broader (see Fig. 7, right side of lower panel). The development of a tail towards large drop sizes indicates that these clouds contain a significant amount of droplets larger than 50 µm and even a few droplets in the size range of drizzle (larger than 100 µm). Compared to the stratiform cloud the peak in the distribution shifted towards larger sizes of about 30 µm in diameter as well.

The occurrence of those very large droplets in the convective clouds might be explained

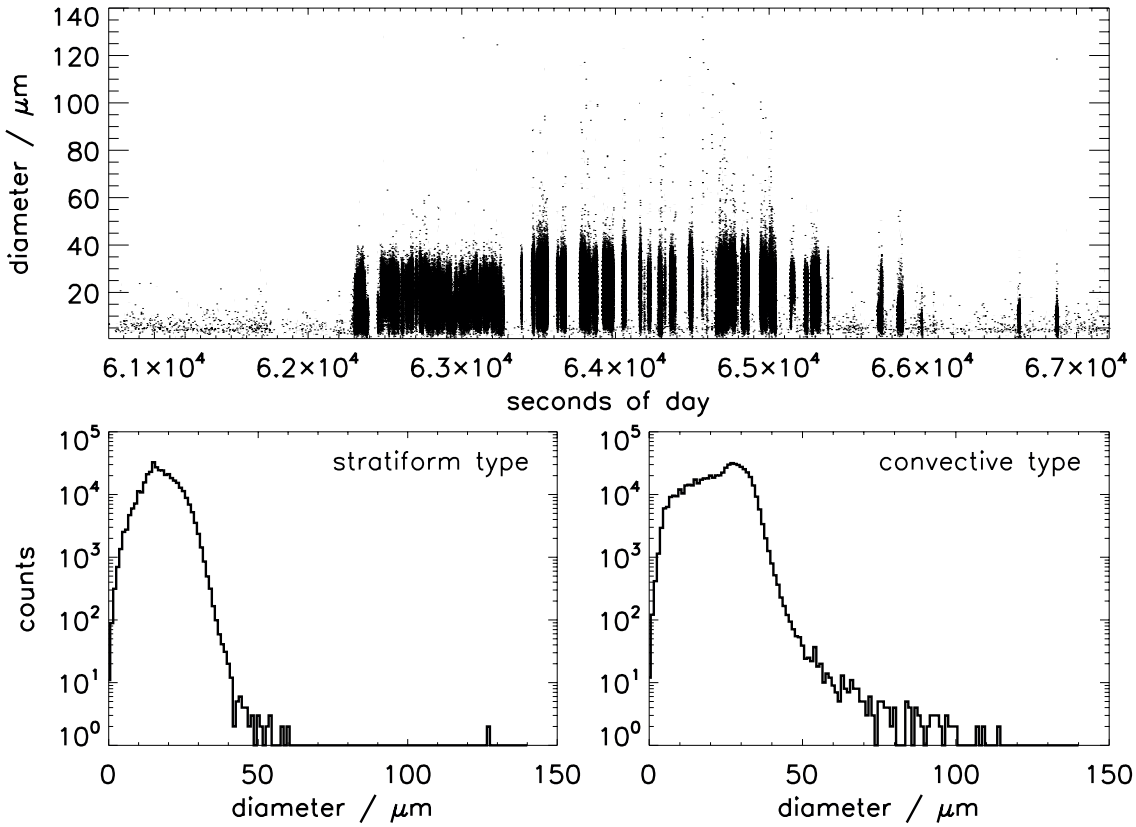


*Fig. 7: Time series of droplet diameters (upper panel), droplet number size distributions of the stratiform cloud type (lower panel, left side) and the convective cloud type (lower panel, right side).*

by a further observation made during the measurement flights. As can be seen in the upper panel of Fig. 7, the PDI detected droplets not only during cloud passages, but also in cloud free air of the MBL. These particles are expected to be dissolved sea salt particles, which might serve as so-called "giant nuclei". Their measured maximum size ranged from 10 to 20 µm. These giant nuclei are supposed to cause the production of larger droplets in the drizzle mode and might play a key role in explaining the warm rain initiation [*Woodcock* 1950, 1953; *Feingold et al.* 1999].

In Fig. 8, the particle number concentration of giant nuclei is plotted together with *RH* (relative humidity) as a function of height for the first profile from sea level up to 2.5 km under cloud-free conditions. It becomes obvious that those particles have a rather small number concentration of about 1 to 2 $cm^{-3}$, which is a typical number concentration for giant nuclei [*Woodcock*, 1950; *Feingold et al.*, 1999]. A few events with increased number concentrations of up to 6 or even 9 $cm^{-3}$ could be observed, which needs further investigation. Most of such giant nuclei observations were found in a height range between 0 and 500 m above sea level, that is, in the well-mixed MBL. In 600 to 900 m altitude the number of events for which giant nuclei are observed, is significantly reduced. This might be due to two different effects: First, as the giant nuclei are produced at the sea surface, they need to be transported upwards in the atmosphere, and their concentrations away from the source can be expected to decrease. Second, the size of giant nuclei in the atmosphere will change constantly, as they will always grow or shrink towards their equilibrium diameter at the current *RH* of the surrounding air. Therefore, it is likely that at lower

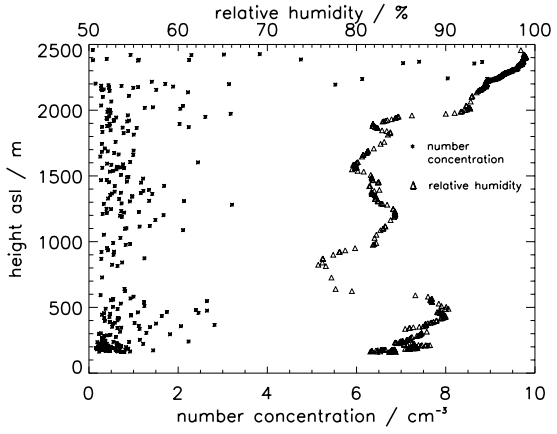


*Fig. 8: Number concentration of giant nuclei particles per cubic centimeter (asterisk) and relative humidity (triangle) plotted against the measurement altitude above sea level. Data displayed here were solely taken outside of clouds. Each data point is an average over one second.*

*RH* less and less giant nuclei can be detected by the PDI instrument, which has a lower detection limit of 1 µm. In Fig. 8 it can be seen that the *RH* in heights between 500 and 2000 m was lower than in the well mixed MBL or in higher regions. This can explain why the number of detected giant nuclei is comparably low at these heights. At the maximum altitude of the profile, the giant nuclei number concentration rises up again to values of 9 $cm^{-3}$. Since the PDI instrument cannot distinguish between cloud droplets and giant nuclei, it might also be possible, that these are already a few detected cloud droplets, since ACTOS was reaching cloudy areas at that time.

## Cloud Mixing and Entrainment

Typical trade wind cumuli are characterized by their fluffy appearance indicating a high degree of dilution. Due to their limited vertical extend, entrainment of sub-saturated environmental air is very effective and results in thoroughly mixing of the entire cloud. Therefore, turbulence at cloud edges plays an important role for the dynamics and evolution of clouds. The evaporative cooling due to entrainment results in negative buoyant air, which is transported downwards at the cloud edges leading to significant vertical wind shear, which in turn enhances the turbulence and consequently the entrainment process at cloud edges. In order to quantify the degree of dilution, in this section the *LWC* normalized with its adiabatic value is used as a simple measure.

First, we discuss the mean constitution of a typical active trade wind cumulus. Figure 9 shows an average over 12 cumuli sampled during November 2010, where the vertical wind velocity inside the cloud is on average greater than 2 m $s^{-1}$. To accomplish the averaging, the sampling time was normalized with $t$ = 0 defining the cloud entrance and the cloud outlet is at $t$ = 1. Figure 9 shows the *LWC*, $w$, absolute humidity $a$, Θ, and local energy dissipation rate $\varepsilon_\tau$ plotted as a function of the normalized time $t$. The average cloud is characterized by *LWC* = 0.5 g $m^{-3}$ , $w$ = 2.5 m $s^{-1}$, $a$ = 15 g $m^{-3}$ , Θ = 304.3 K, and $\varepsilon_\tau = 3 \times 10^{-2}$ $m^2$ $s^{-3}$.

The cloud edges are characterized by a rapid decrease of *LWC* and slight downdrafts of 0.5 m $s^{-1}$ (see also *Heus and Jonker* [2008] and *Jonas* [1990] for example). The regions of the downdrafts typically have a width of 0.25 of the cloud diameter. Also the absolute humidity and the $\varepsilon_\tau$ show a slight transition region from cloud value to an environmental value. However, these regions are smaller than the downdraft regions and have typically only an extension of 0.1 of the cloud diameter. The temperature seems to decrease at cloud edges without showing a clear transition region.

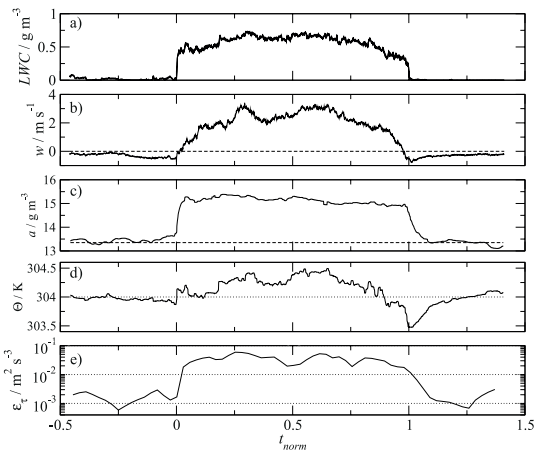


***Fig. 9:*** *The averaged picture of 12 cloud penetrations through active trade wind cumuli over Barbados is presented. The following data are shown: (a) liquid water content LWC, (b) vertical wind velocity w, (c) absolute humidity a, (d) potential temperature Θ and (e) energy dissipation rate $\varepsilon_\tau$. The x-axis is normalized concerning the cloud layer defining the cloud entrance by t = 0 and the cloud outlet by t = 1.*

In a next step we analyze the correlation between $w$ and the dimensionless *LWC* (normalized by its adiabatic value). This was done by *Bethke* [2011] for cloud penetrations with *LWC* > 0.05 g $m^{-3}$ based on seven measurement flights during CARRIBA 2010. As expected from Fig. 9, the most diluted cloud parts were found in regions with downdrafts ($w$ < 0 m $s^{-1}$) at cloud edges. A linear relationship between $w$ and *LWC* was found for all flights but with different regression slopes (see left panel of Fig. 10). The right panel of Fig. 10 shows the regression slope as a function of median cloud penetration height. Typically, this height was about 100 m below cloud top and, therefore, the median penetration height can be interpreted as a rough measure for the vertical cloud depth (assuming a nearly constant cloud base height, which is usally the case for shallow marine clouds). The error bars indicate the 5 and 95% percentile of the height distribution and are a measure for the cloud top height variability. There is a clear correlation between cloud depth and the regression slope. This is consistent with the picture that deeper clouds produce higher updraughts in general. The same degree of dilution can be found in regions with higher vertical velocity compared to shallower clouds. Future LES studies with the high-resolution model PALM [*Raasch and Schröter*, 2001] will help to understand this relationship in more detail, to analyze the possible influence of flight strategy, and to derive robust parameterizations for numerical models.

## Cloud Aerosol Interaction

Aerosol particles serve as condensation nuclei, and therefore play an important role in the activation

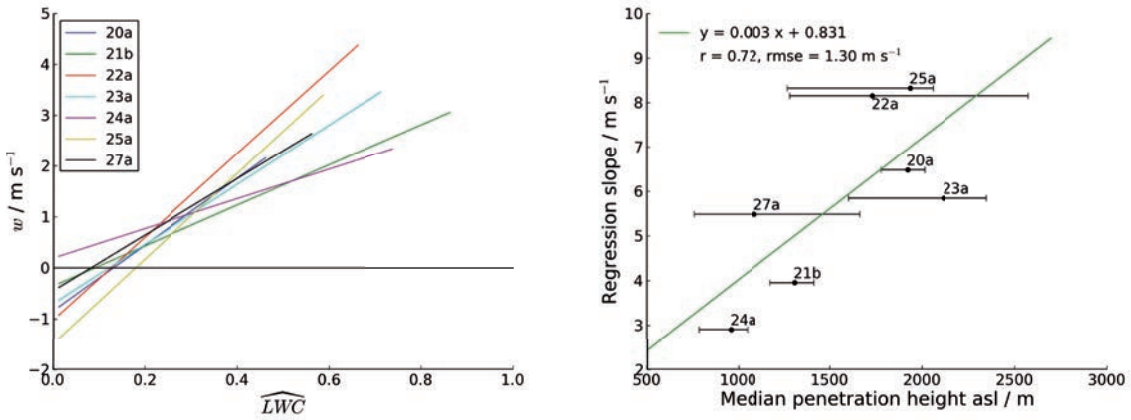


***Fig. 10:*** *Regression lines of vertical velocity w and normalized LWC for seven different measurement flights in November 2010 (left panel). In the right panel, the regression slope is plotted as a function of the median measurement height asl. Since measurements with ACTOS are performed close to cloud top, the median is a rough measure of cloud top. The error bars are the 5% and 95% percentile of the measurement height distribution and, therefore, a measure of cloud top variability.*

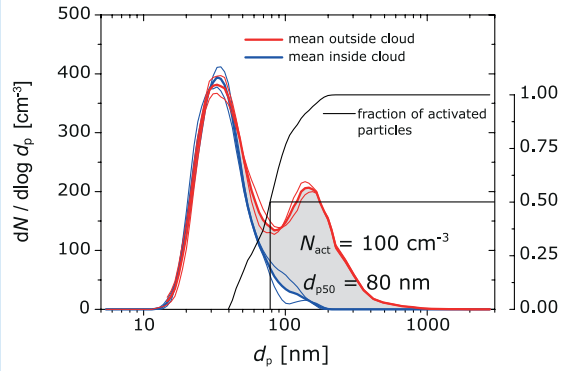


***Fig. 11:*** *Left ordinate: aerosol number size distributions inside (blue) and outside clouds (red), right ordinate: fraction of activated particles (η). Shaded area refers to the number of activated particles ($N_{act}$).*

process of cloud droplets. In the following paragraph we compare physical properties of interstitial aerosol inside and outside of trade wind cumuli to derive the activation diameter, critical super-saturation *S* and number of activated particles as described in *Ditas et al.* [2011].

Figure 11 shows aerosol number size distributions (*NSDs*) inside and outside of trade wind cumuli at 1500 m asl. The total aerosol number concentration (*N*) in cloud-free air was about 270 cm$^{-3}$. The *NSDs* sampled in cloud-free air (red lines) show a bimodal distribution with a clear minimum at $d_p$ = 85 nm. This Hoppel-minimum [*Hoppel et al.*, 1986] gives information about the average *S* the air mass was exposed to during former cloud contacts. Using Köhler theory [*Köhler*, 1936] the critical super-saturation necessary to activate particles in the size range of the minimum is *S* = 0.25% (assuming an ammonium sulfate particle with an insoluble core and 70% soluble material).

The *NSDs* inside clouds feature a mono-modal distribution. The accumulation mode (particles between 80 nm < $d_p$ < 1000 nm) vanishes due to activation to cloud droplets. The activated fraction η defined by

$$\eta(D_p) = 1 - \frac{\overline{NSD}_{incloud}(D_p)}{\overline{NSD}_{cloud-free}(D_p)}$$

shows a steep increase for particles larger than $d_p$ = 40 nm and approaches unity for particles larger than $d_p$ = 150 nm. For η = 0.5 we define a 50% - activation diameter $d_{p50}$ = 80 nm, which requires *S* = 0.3% (same chemistry as above). The smallest activated particles are in the size range of $d_p$ = 40 nm, corresponding to *S* = 0.75%. The shaded area in Fig. 11 refers to the number of activated particles $N_{act}$ = 100 cm$^{-3}$. Measurements of cloud condensation nuclei concentration at S = 0.3% in cloud free air agree well with these findings.

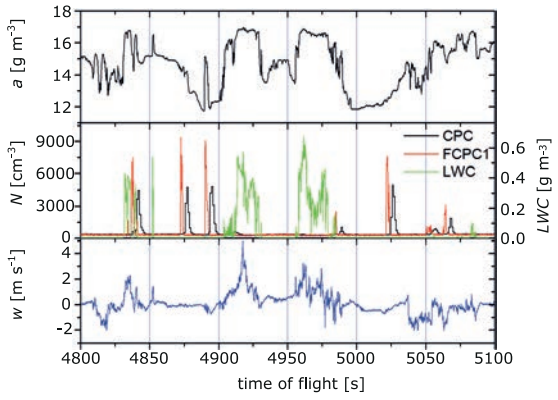


***Fig. 12:*** *Time series of absolute humidity (a, black line), total number concentration N measured with CPC1 (black line) and FCPC (red line), vertical wind velocity (w, blue line) and liquid water content LWC (right ordinate, green line).*

Under appropriate circumstances cloud edges may provide favorable conditions for new particle formation [e.g., *Perry and Hobbs*, 1994]. Figure 12 shows time series of absolute humidity (*a*), *N* recorded by a commercial Condensational Particle Counter (CPC) and a new fast CPC build at IfT (FCPC1, see *Wehner et al.*, [2011]), *w*, and *LWC*. Due to different inlet lines and response times of CPC and FCPC there is an offset between the two signals. Episodes with non-zero *LWC* mark cloud regions. These regions are characterized by high values of absolute humidity of $a$ = 17 g m$^{-3}$ and strong fluctuations in *w*. In the vicinity of these clouds both time series of *N* feature peaks exceeding the background concentration of $N$ = 300 cm$^{-3}$ by more than one order of magnitude, which are very likely caused by new particle formation. Measurements of $CO_2$ do not follow this behavior, which excludes anthropogenic pollution as origin. Further evidence arrives from measured aerosol number size distributions with a clearly enhanced concentration of small particles (not shown here). The peaks in *N* exhibit remarkable short durations of a few seconds, indicating a horizontal extent less than 100 m (taking into account the forward motion of the platform). Such new particle formation events were observed during 80% of the measurement flights of both campaigns. Former airborne studies did not show a comparable cumulation of particle bursts in the MBL, possibly due to the lower spatial resolution in the order of 100 m.

## Radiation Measurements with SMART-Helios

The reflectivity measurements performed by the SMART-HELIOS instrument are used to derive cloud properties (effective droplet radius $r_{eff}$, cloud optical thickness τ, and *LWC*) by means of a new retrieval method, which effectively corrects for the influence of cirrus above the cumuli.

If the cirrus is not accounted for in the classic Nakajima-King retrieval [*Nakajima and King*, 1990], the effective radius $r_{eff}$ is overestimated by up to 25%, assuming a constant cirrus with τ = 0.5 at 550 nm. The new algorithm exploits gradients of the radiance spectrum at multiple wavelengths and allows for retrievals under thin (τ < 1), overcast cirrus conditions. In addition, the retrieval error can be reduced by about 50%, compared to the Nakajima-King retrieval.

The difference between the Nakajima-King retrieval and the new approach is used to estimate the cloud optical thickness of the cirrus. The retrieval results are shown in Fig. 13 for a low-level cumulus cloud scene from the measurement flight on April 22nd, 2011. The in-situ ACTOS measurements of *LWC* (lower panel) and $r_{eff}$ (third panel) are shown in black lines, while the red circles indicate the retrieval results from the Nakajima-King method and the blue circles the results from the new approach.

The strong overestimation of $r_{eff}$ from the Nakajima-King retrieval is caused by the observed overlying thin cirrus field during that day. Retrieving $r_{eff}$ with the new method yields values much closer

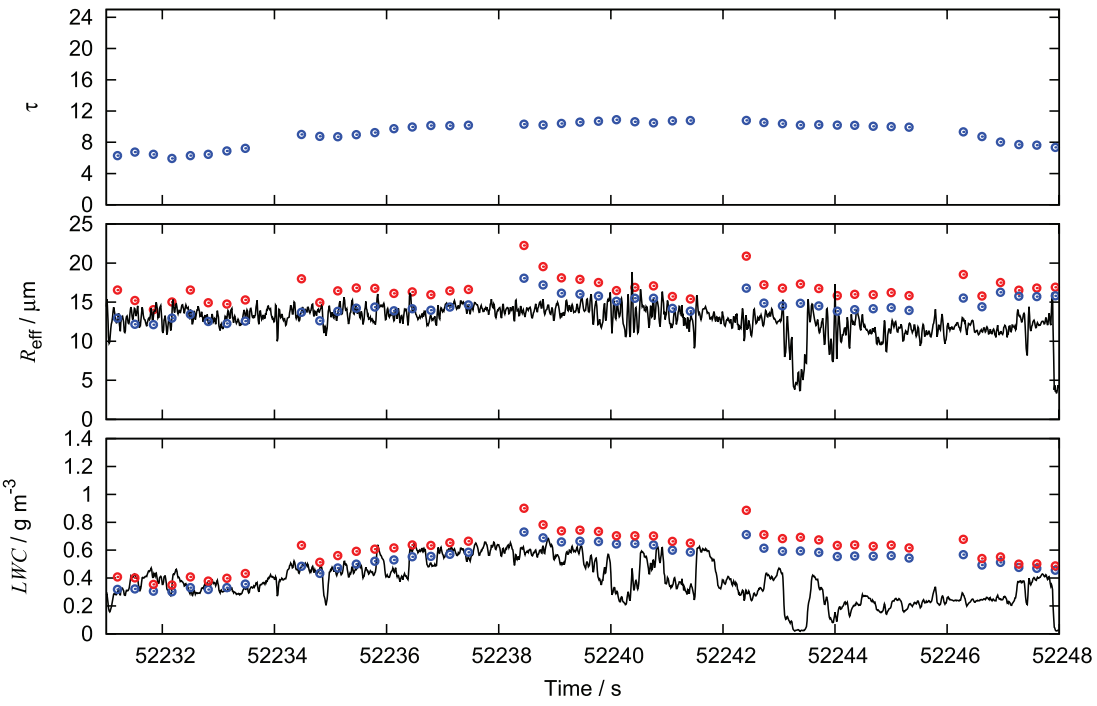


***Fig. 13:*** *Time series of liquid water content LWC, effective droplet radius $r_{eff}$ and cloud optical thickness τ for a low level cumulus cloud scene on April 22nd, 2011. In-situ measurements from the PVM on ACTOS are illustrated by solid lines; the retrieval results by means of the Nakajima-King method and the new retrieval approach are shown in red and blue circles, respectively.*

to the in-situ measurements and the difference of around 20% between the two approaches indicates a $\tau$ of the cirrus of about 0.2 - 0.5.

The retrieval of $\tau$ (second panel) yields values between 5 and 12. Since the sensitivity of the $\tau$ retrieval regarding overlying cirrus is not very pronounced, only the results from the new approach are shown. This example shows that the retrieval of cumulus cloud microphysical properties with a cirrus above the cumulus is possible. These measurements will be used for comparison with satellite retrievals and in-situ measurements.

## Summary

In the present overview, the CARRIBA project, based on two intensive field campaigns in November 2010 and April 2011, was introduced. After motivating the major goals of this project and providing some background on the measurements over Barbados, we presented several highlights of this campaign, dealing with a multitude of different scientific topics, in order to illustrate the multidisciplinary approach of this project and to give an overview of the ongoing work at IfT and partner institutes.

## Acknowledgements

The two campaigns were not possible without the great support of our two experienced pilots Milos Kapetanovic and Alwin Vollmer who were responsible for the safe helicopter flights. Local logistics was greatly supported by Paul Archer (Horizon Helicopters) and David Farrell (CIMH). ACTOS and SMART-HELIOS would never fly without the technical support from Dieter Schell and Christoph Klaus (enviscope company). We thank Stephan Henne from EMPA for providing the trajectories. Finally, we thank Lutz Hirsch, Friedhelm Jansen, and Louise Nuijens (MPI-M in Hamburg) for the nice cooperation and help during this exciting project.

## References

Albrecht, B. A. (1989), Aerosols, cloud microphysics and fractional cloudiness, *Science, 245*, 1227 – 1230.

Albrecht, B. A., C. S. Bretherton, D. Johnson, W. H. Scubert, and A. S. Frisch (1995), The atlantic stratocumulus transition experiment – ASTEX, *Bull. Amer. Meteor. Soc., 76*, 889–904.

Augstein, E., H. Riehl, F. Ostapoff, and V. Wagner (1973), Mass and energy transports in an undisturbed atlantic trade-wind flow, *Mon. Wea. Rev., 101*, 101 – 111.

Bethke, J. (2011), Liquid water content measurements in trade wind cumuli, Master's Thesis, Leipzig.

Blyth, A. M., S. Lasher-Trapp, W. A. Cooper, C. A. Knight, and J. Latham (2003), The role of giant and ultragiant nuclei in the formation of early radar echoes in warm cumulus clouds, *J. Atmos. Sci., 60*, 2557–2572.

Davidson, B. (1968), The Barbados oceanographic and meteorological experiment, *Bull. Amer. Meteor. Soc., 49*(9), 928–934.

Ditas, F., R. A. Shaw, H. Siebert, M. Simmel, B. Wehner, and A. Wiedensohler (2011), Aerosols-cloud microphysics-thermodynamics-turbulence: evaluating supersaturation in a marine stratocumulus cloud, *Atmos. Chem. Phys. Discuss., 11*, 29777-29805, doi:10.5194/acpd-11-29777-2011.

Feingold, G., W. R. Cotton, S. M. Kreidenweis, and J. T. Davis (1999), The impact of giant cloud condensation nuclei on drizzle formation instratocumulus: Implications for cloud radiative properties, *J. Atmos. Sci., 56*, 4100-4117.

Henrich, F., H. Siebert, E. Jäkel, R. A. Shaw, and M. Wendisch (2010), Collocated measurements of boundary layer cloud microphysical and radiative properties: A feasibility study, *J. Geophys. Res., 115*, D24214, doi:10.1029/2010JD013930.

Heus, T., and H. J. J. Jonker (2008), Subsiding shells around shallow cumulus clouds, *J. Atmos. Sci., 65*, 1003-1018.

Heymsfield, A. J., and G. M. McFarquhar (2001), Microphysics of indoex clean and polluted trade cumulus clouds, *J. Geophys. Res., 106*, 28653–82673.

Holland, J. Z., and E. M. Rasmusson (1973), Measurements of the atmospheric mass, energy, and momentum budget over a 500-kilometer square of tropical ocean, *Mon. Wea. Rev., 101*(1), 44–55.

Hoppel, W. A., G. M. Frick, and R. E. Larson (1986), Effect of nonprecipitating clouds on the aerosol size distribution in the marine boundary layer, *Geophys. Res. Lett., 13*(2), 125–128, doi:10.1029/GL013i002p00125.

Jonas, P. R. (1990), Observations of cumulus cloud entrainment, *Atmos. Res., 25*, 105-127.

Kaufman, Y., I. Koren, L. A. Remer, D. Tanre, P. Ginoux, and S. Fan (2005), Dust transport and deposition observed from the Terra-Moderate Resolution Imaging Spectroradiometer (modis) spacecraft over the Atlantic Ocean, *J. Geophys. Res., 110*, D10S12, doi:10.1029/2003JD004436.

Köhler, H. (1936), The nucleus in and the growth of hygroscopic droplets, *Trans. Faraday Soc., 32*, 1152–1161.
Langmuir, I. (1948), The production of rain by a chain reaction in cumulus clouds at temperature above freezing, *J. Meteor., 5*, 175 – 192.
Li-Jones, X., and J. M. Prospero (1998), Variations in the size distribution of non-sea-salt sulfate aerosol in the marine boundary layer at Barbados: Impact of African dust, *J. Geophys. Res.-Atmos., 103*(D13), 16073-16084.
Malkus, J. S. (1954), Some results of a trade-cumulus cloud investigation, *J. Meteor., 11*, 220 – 237.
Malkus, J. S. (1956), On the maintenance of the trade winds, *Tellus, 8*, 335 – 350.
Malkus, J. S. (1958), On the structure of the trade wind moist layer, *Pap. Phys. Oceanogr. Meteor., 12*, 1 – 47.
Nakajima, T., and M. King (1990), Determination of the optical thickness and effective particle radius of clouds from reflected solar radiation measurements. Part I: Theory, *J. Atmos. Sci., 47*, 1878-1893.
Perry, K. D., and P. V. Hobbs (1994), Further evidence for particle nucleation in clear air adjacent to marine cumulus clouds, *J. Geophys. Res., 99*(D11), 22,803–22,818, doi:10.1029/94JD01926.
Petters, M. D., and S. M. Kreidenweis (2007), A single parameter representation of hygroscopic growth and cloud condensation nucleus activity, *Atmos. Chem. Phys., 7*, 1961-1971.
Pringle, K. J., H. Tost, A. Pozzer, U. Pöschl, and J. Lelieveld (2010), Global distribution of the effective aerosol hygroscopicity parameter for CCN activation, *Atmos. Chem. Phys., 10*, 5241-5255.
Raasch, S. and M. Schröter (2001), A large-eddy simulation model performing on massively parallel computers, *Meteorol. Z., 10*, 363-372. doi: 10.1127/0941-2948/2001/0010-0363.
Rauber, R. M., and coauthors (2007), Rain in shallow cumulus over the ocean, *Bull. Amer. Meteor. Soc., 88*, 1912 – 1928.
Rudich, Y., O. Khersonsky, and D. Rosenfeld (2002), Treating clouds with a grain of salt, *Geophys. Res. Lett., 29*, doi:2010.1029/2002GL016055.
Siebert, H., H. Franke, K. Lehmann, R. Maser, E. W. Saw, R. Shaw, D. Schell, and M. Wendisch (2006), Probing fine-scale dynamics and microphysics of clouds with helicopter-borne measurements, *Bull. Amer. Meteor. Soc., 87*, 1727-1738.
Squires, P., and J. Warner (1957), Some measurement in the orographic cloud of the island of Hawaii and of trade wind cumuli, *Tellus, 9*, 475–494.
Stommel, H. (1947), Entrainment of air into a cumulus cloud, *J. Meteor., 4*, 91–94.
Stommel, H. (1951), Entrainment of air into a cumulus cloud II, *J. Meteor., 8*, 127 – 129.
Tiedtke, M. (1989), A comprehensive mass flux scheme for cumulus parameterization in large-scale models, *Mon. Wea. Rev., 117*, 1779–1800.
Twomey, S. (1977), The influence of pollution on the shortwave albedo of clouds, *J. Atmos. Sci., 34*, 1149–1152.
Van Zaanten, M. C., B. Stevens, L. Nuijens, A. P. Siebesma, A. Ackerman, F. Burnet, A. Cheng, F. Couvreux, H. Jiang, M. Khairoutdinov, Y. Kogan, D. C. Lewellen, D. Mechem, K. Nakamura, A. Noda, B. J. Shipway, J. Slawinska, S. Wang, and A. Wyszogrodzki (2011), Controls on precipitation and cloudiness in simulations of trade-wind cumulus as observed during RICO, *J. Adv. Model. Earth Syst.*, *3*, M06001, doi:10.1029/2011MS000056.
Wehner, B., H. Siebert, M. Hermann, F. Ditas, and A. Wiedensohler (2011), Characterisation of a new Fast CPC and its application for atmospheric particle measurements, *Atmos. Meas. Tech., 4*, 823-833, doi:10.5194/amt-4-823-2011.
Woodcock, A. H., C. F. Kientzler, A. B. Arons, and D. C. Blanchard (1953), Giant condensation nuclei from bursting bubbles, *Nature, 172*, 1144–1145.
Woodcock, A. H. (1950), Condensation nuclei and precipitation, *J. Meteor., 7*, 161-162.

**Funding**
- German Research Foundation (DFG), Bonn, Germany

**Cooperation**
- Leipzig Institute for Meteorology, Leipzig, Germany
- Technological University of Michigan, USA
- Max Planck Institute for Meteorology, Hamburg, Germany
- Caribbean Institute for Meteorology and Hydrology, Barbados, West Indies
- University of Miami, USA
- Meteo France, Toulouse, France
- University of Warsaw, Poland

# Volcanic aerosol plumes over Europe: Ash and fine mode separation and volcanic effects on heterogeneous ice nucleation

Patric Seifert[1], Albert Ansmann[1], Matthias Tesche[2], Ulla Wandinger[1], Ina Mattis[3], Johannis Bühl[1], Anja Hiebsch[1], Thomas Kanitz[1], Jörg Schmidt[1]

[1] Leibniz Institute for Tropospheric Research (IfT), Leipzig, Germany
[2] Department of Applied Environmental Science, Stockholm University, Stockholm, Sweden
[3] Deutscher Wetterdienst, Hohenpeißenberg, Germany

*Zwischen dem 16. April und 17. Mai 2011 durchgeführte Lidarmessungen der optischen Eigenschaften von Vulkanaerosol des Eyjafjallajökull in Island wurden genutzt, um die Massenkonzentration getrennt für Asche und den aschefreien Anteil (z.Bsp. Sulfataerosol) zu bestimmen und den Einfluss von Vulkanaerosol auf die heterogene Eisbildung in dünnen Wolkenschichten zu untersuchen. Mittels eines kombinierten Lidar-Sonnenphotometer-Ansatzes wurden zuerst die optischen Aerosoleigenschaften anhand der gemessenen Partikeldepolarisationsverhältnisse in pure Asche und aschefreie Bestandteile separiert, um anschließend anhand von mit Sonnenphotometer bestimmten Extinktions-zu-Masse-Verhältnissen deren Massenkonzentration zu berechnen. Asche-Massenkonzentrationen von bis zu 1500 µg/m³ wurden gemessen.*

*Eine statistische Untersuchung der heterogenen Gefriertemperatur von 90 in Vulkanasche eingebetteten Wolken belegte zudem die guten Eisbildungsfähigkeiten von Vulkanasche. In 100% aller Wolken mit Wolkenoberkantentemperaturen von unterhalb -15°C wurde Eisbildung beobachtet.*

## Introduction

The advection of the plume of the Icelandic Eyjafjallajökull volcano towards central Europe in April and May 2010 provided the unprecedented opportunity to study the transport and the optical and microphysical properties of volcanic aerosol based on measurements with the technical infrastructure available in Europe. At IfT Leipzig, Lidar and Sun photometer observations of the volcanic aerosol performed in the framework of the European Aerosol Research Lidar Network (EARLINET) were used to relate the optical properties of the volcanic aerosol to the particle mass concentration separately for the ash and non-ash (i.e., sulfates) fraction and to investigate the effect of the volcanic ash on heterogeneous freezing processes in clouds. Knowledge of the ash mass concentration is a basic requirement for air traffic regulations and for the validation of ash dispersion models whereas the effect of volcanic ash on cloud glaciation may influence cloud evolution and formation of precipitation.

## Instrumentation and Methodology

**Determination of ash and non-ash mass concentration.** The presented method to derive the ash and non-ash mass concentration relies on lidar measurements of the particle backscatter coefficient and particle linear depolarization ratio and on the spectrally resolved aerosol optical depth (AOD) and sky radiances obtained from Aerosol Robotic Network (AERONET) Sun photometer observations. For the study lidar and Sun photometer data of the period of the Eyjafjallajökull volcanic eruption from 16 April to 20 May 2010 of the European Aerosol Research Lidar Network (EARLINET) stations Cabauw, the Netherlands, and Hamburg, Leipzig, and Munich, Germany were analyzed.

The determination of the particle mass concentration is a three-step procedure as described in *Ansmann et al.* [2011]. In the first step the particle depolarization ratio is used to separate the total backscatter and extinction coefficient of the volcanic aerosol into contributions of weakly depolarizing non-ash and strongly depolarizing ash particles, respectively. The separation is performed according to Equation (14) of *Tesche et al.* [2009] by applying a particle depolarization ratio of 0.35-0.37 [*Ansmann et al.*, 2010] for pure ash and assuming a particle depolarization ratio of 0.01 for the non-ash fraction.

In the second step Sun photometer measurements are analyzed to determine the ratio of particle volume concentration to AOD separately for the fine mode and the coarse mode. For a given mass density of the coarse- and fine-mode aerosol, respectively, the volume-to-extinction conversion factors can be transformed into mass-to-extinction conversion factors.

The third step is based on the fundamental assumption that the photometer-derived coarse mode and fine mode corresponds to the lidar-derived ash and non-ash fractions, respectively. In that case, profiles of the aerosol mass concentration of each fraction can be obtained by applying the respective coarse- and fine-mode mass-to-extinction conversion factors to the corresponding measured profiles of the particle extinction coefficient.

**Observations of heterogeneous ice formation.** For the investigation of the effect of volcanic ash on heterogeneous ice formation temperatures in clouds, polarization lidar measurements from Leipzig and Munich were analyzed to separate pure liquid water clouds from ice-containing clouds [*Seifert et al.*, 2011]. Information about cloud top temperature, which is usually the minimum temperature in a cloud layer, was obtained from radiosonde profiles or model data. Cloud layers were identified from the slope of the measured signal profiles as described in *Seifert et al.* [2010] and a single cloud layer is distinguished from neighboring layers when they are separated by 5 min in time and 500 m vertically. The phase-state of a cloud layer can easily be determined from the depolarization ratio profile, which is zero throughout the cloud in the case of backscattering by spherical liquid water droplets. Cloud layers that produce depolarization are counted as ice-containing clouds. Only ash-influenced cloud layers that were surrounded by depolarizing volcanic ash were used for further analysis.

## Results

**Ash and non-ash mass concentrations.** Figure 1 shows the determination of the particle linear depolarization ratio (Fig. 1b), the total and ash-related particle backscatter coefficient (Fig. 1c), and the ash and fine-mode particle mass concentration (Fig. 1d) for a lidar measurement performed at Leipzig on 19 April 2010 from 14:35 to 15:36 UTC (1a). A dense volcanic layer (red in Fig. 1a) extending from 2 to 3 km height is located just above the ash-free and thus non-depolarizing (Fig. 1b) planetary boundary layer. Another ash layer (yellow in Fig. 1a) occurred in the free troposphere from 4 to 6 km height. Ash mass concentrations of up to 230 µg $m^{-3}$ were measured in the lower ash layer. Even at 4.5 km height ash mass concentrations reached values of close to 50 µg $m^{-3}$.

The highest ash mass concentrations were determined on the day of arrival of the volcanic plume on 16 April 2010 when values were of the order of 1000 µg $m^{-3}$.

After 19 April 2010 two further major volcanic plumes were observed over central Europe. On 21 April an ash plume was observed between 4 and 8 km height above Leipzig. On that day peak values of ash mass concentration were of the order of 35 µg $m^{-3}$. On 17 May 2011 a volcanic layer was observed above Cabauw between 2.5 and 6 km height, which contained ash mass concentrations that were of the order of 400 µg $m^{-3}$.

**Ice formation in ash-influenced clouds.** From the lidar measurements at Munich and Leipzig 90 ash-influenced cloud layers were identified that showed cloud top temperatures between -40 and 0°C. The cloud data set was separated into cloud

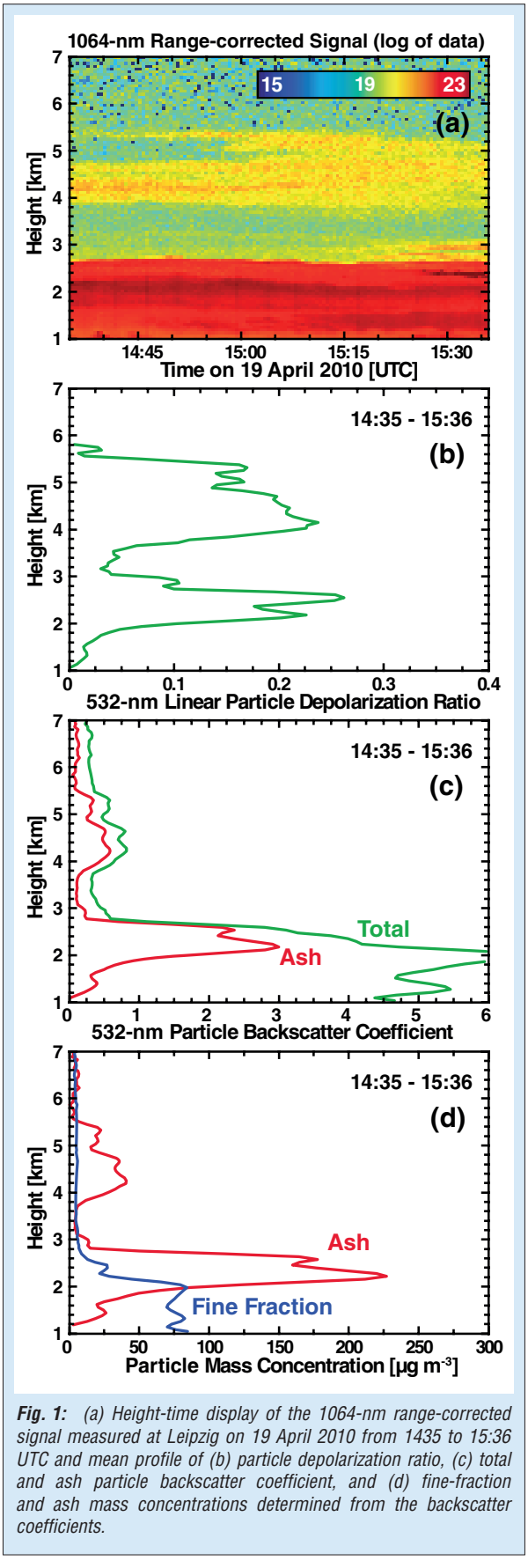


*Fig. 1: (a) Height-time display of the 1064-nm range-corrected signal measured at Leipzig on 19 April 2010 from 1435 to 15:36 UTC and mean profile of (b) particle depolarization ratio, (c) total and ash particle backscatter coefficient, and (d) fine-fraction and ash mass concentrations determined from the backscatter coefficients.*

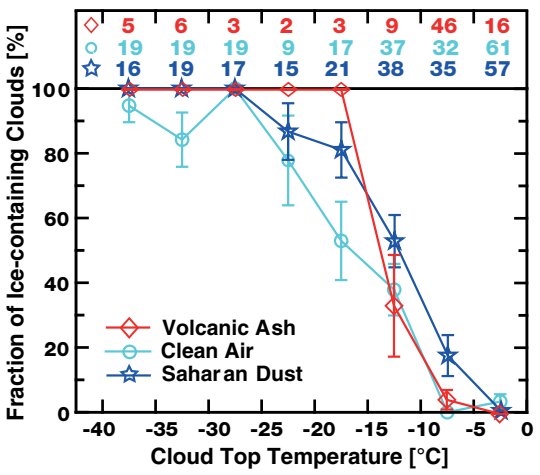


*Fig. 2: Comparison of the frequency of occurrence of ice–containing clouds as a function of cloud top temperature (5 K intervals) for clouds which formed in volcanic air (red diamonds), in clean air (bright blue circles) and in Saharan dust layers (dark blue stars). The clear air and Saharan dust statistics are based on 11–year observations at Leipzig [Seifert et al., 2010]. Error bars are based on Eq. 1 of Seifert et al. [2010].*

top temperature intervals of 5 K for each of which the fraction of ice containing clouds was calculated. Figure 2 shows the fraction of ice-containing clouds as a function of cloud top temperature for ash-influenced clouds (red curve). For comparison respective functions are shown for clean (light blue curve) and Saharan-dust-influenced clouds (dark blue curve), which were reported by *Seifert et al.* [2010]. A steep increase of the curve from almost 0% to 100% within a comparably narrow temperature range of less than 10 K is found in the case of the volcanically influenced clouds. In contrast to the volcanic aerosol curve, the desert dust curve is broader, ice nucleation starts at higher temperature, but the 100% value is not reached before –25°C (as is the case for clean conditions). The behavior of the volcanic curve is in agreement with laboratory studies [*Fornea et al.*, 2009] in which first activation was found from about –10°C for contact freezing and from –17°C to –20°C for immersion freezing.

## Conclusions

A technique to derive height-resolved profiles of ash and non-ash particle mass concentrations from combined polarization lidar and Sun photometer measurements was successfully developed and applied to observations of the Eyjafjallajökull volcanic plume in April and May 2010. In the case of a future volcanic eruption the technique will enable immediate estimates of the ash mass concentrations as it was already done during the eruption of the Grimsvötn volcano in May 2011.

The investigation of the effect of volcanic ash on heterogeneous ice formation shows that the observations confirm existing laboratory studies. In an ash-rich environment ice formation starts at higher temperatures as under clean or dust-laden conditions.

## References

Ansmann, A., et al. (2011), Ash and fine-mode particle mass profiles from EARLINET-AERONET observations over central Europe after the eruptions of the Eyjafjallajökull volcano in 2010, *J. Geophys. Res.*, 116, D00U02, doi:10.1029/2010JD015567.

Ansmann, A., et al. (2010), The 16 April 2010 major volcanic ash plume over central Europe: EARLINET lidar and AERONET photometer observations at Leipzig and Munich, Germany, *Geophys. Res. Lett.*, 37, L13810, doi:10.1029/2010GL043809.

Fornea, A. P., S. D. Brooks, J. B. Dooley, and A. Saha (2009), Heterogeneous freezing of ice on atmospheric aerosols containing ash, soot, and soil, *J. Geophys. Res.*, 114, D13201, doi:10.1029/2009JD011958.

Seifert, P., et al. (2011), Ice formation in ash-influenced clouds after the eruption of the Eyjafjallajökull volcano in April 2010, *J. Geophys. Res.*, 116, D00U04, doi:10.1029/2011JD015702.

Tesche, M., A. Ansmann, D. Müller, D. Althausen, R. Engelmann, V. Freudenthaler, and S. Groß (2009), Vertically resolved separation of dust and smoke over Cape Verde using multiwavelength Raman and polarization lidars during Saharan Mineral Dust Experiment 2008, *J. Geophys. Res.*, 114, D13202, doi:10.1029/2009JD011862.

**Funding**
- EARLINET is funded by the European Commission under grant RICA-025991

**Cooperation**
- Ludwig-Maximilians-Universität, Munich, Germany
- Royal Netherlands Meteorological Institute, De Bilt, Netherlands
- Max Planck Institute for Meteorology, Hamburg, Germany

# Simulations of the 2010 Eyjafjallajökull volcanic ash dispersal over Europe using COSMO-MUSCAT

Bernd Heinold[1,2], Ralf Wolke[1], Ina Tegen[1]

[1] Leibniz Institute for Tropospheric Research (IfT), Leipzig, Germany
[2] Now at School of Earth & Environment, University of Leeds, United Kingdom

*Im April und Mai 2010 ereignete sich der Ausbruch des Isländischen Vulkans Eyjafjallajökull. Zuverlässige Prognosen der Ascheausbreitung bilden die Grundlage für Entscheidungen im Krisenfall. Die Vorhersagequalität wird wesentlich durch die Eingabeparameter bestimmt. Heute erlauben umfangreiche Beobachtungsdaten eine Evaluierung der Modellergebnisse und eine Verbesserung der Vorhersagemodelle. Hierzu wurden Ausbreitungsrechnungen mit einem regionalen Transportmodellsystem durchgeführt. Der Modellinitialisierung dienten unter anderem MISR Satellitendaten zur Bestimmung der Höhe der Vulkanaschewolke sowie Flugzeugmessungen zur Größenverteilung der Aschepartikel. Es zeigt sich, dass das MISR Produkt eine Alternative zu komplexen Modellen für Injektionshöhen darstellt, die genaue Informationen zur Eruptionsdynamik benötigen. Die Simulationen zeigen, welche Emissionshöhen zur tatsächlichen raumzeitlichen Verteilung der Vulkanasche über Europa beigetragen haben.*

## Introduction

The ash plume of the Icelandic volcano Eyjafjallajökull in April and May 2010 severely disrupted air traffic in Europe, but also notably attracted the interest of atmospheric researchers. Based on ash dispersal forecasts by the Volcanic Ash Advisory Centre (VAAC), London [*Jones et al.,* 2007] and hastily established safety limits, large parts of the European air space were closed, as volcanic ash is considered to be harmful for aircraft engines. However, quantitative forecasts of ash concentration are problematic due to unknown emission parameters (mass eruption rate, injection height, vertically resolved ash release, particle size distribution). Meanwhile, many data are available from various different observations that allow evaluation of the model results and will lead to improved forecasts during possible future events.

We present simulations of the Eyjafjallajökull ash plume by a regional aerosol-transport model. The impact of different injection heights on the volcanic ash dispersion is tested.

## Method

The model system COSMO-MUSCAT (COSMO: Consortium for Small-scale Modeling; MUSCAT: MultiScale Chemistry Aerosol Transport) is used to simulate the volcanic ash transport over the European domain at a horizontal resolution of 28 km [*Heinold et al.,* 2011]. COSMO is the operational forecast model of the Deutscher Wetterdienst. It is online coupled with the chemistry transport model MUSCAT developed at the IfT.

Volcanic emissions are treated as vertical line source above the crater (63.63°N, 19.62°W, 1666 m asl). For initialization we use early estimates of primary PM10 emissions, which were obtained from field observations within the first 72 hours and were distributed by The Norwegian Meteorological Institute. The model allows for a size-resolved description of the ash transport. The initial size spectrum was obtained by adapting to in-situ measurements taken during a research flight by the Deutsches Zentrum für Luft- und Raumfahrt (DLR) [*Schumann et al.,* 2011] within the volcanic ash layer over Germany. London VAAC reports on plume top heights as well as statistics on the vertical extent of the Eyjafjallajökull plume provided by NASA's Multi-angle Imaging SpectroRadiometer (MISR) plume height project [*Scollo et al.,* 2010] allowed to set up maximum injection heights and to apply vertically resolved emission rates.

The uncertainties in the modeled ash distribution due to the choice of injection heights are studied with additional independent tracers, each released in three model layers below ("Low"), within ("Medium") and above ("High") the standard emission height ("MISR").

## Results

On April 14, 2010 the eruption of Eyjafjallajökull volcano started to send a vast ash plume into the troposphere. On the first day the plume height reached more than 9 km, decreasing during the following days [*Gudmunsson et al.,* 2010]. A high-pressure system over Iceland and later Scandinavia favored the ash transport towards Central Europe. Within 1–2 days, the plume crossed large parts of Europe, reaching Germany at 2–7 km height. In central Europe, aerosol optical depths (AODs) up to 1 were observed [*Ansmann et al.,* 2010].

A detailed description of the Eyjafjallajökull simulations together with a comprehensive model evaluation is given by *Heinold et al.* [2012]. A map of AODs in Fig. 1a illustrates the volcanic ash

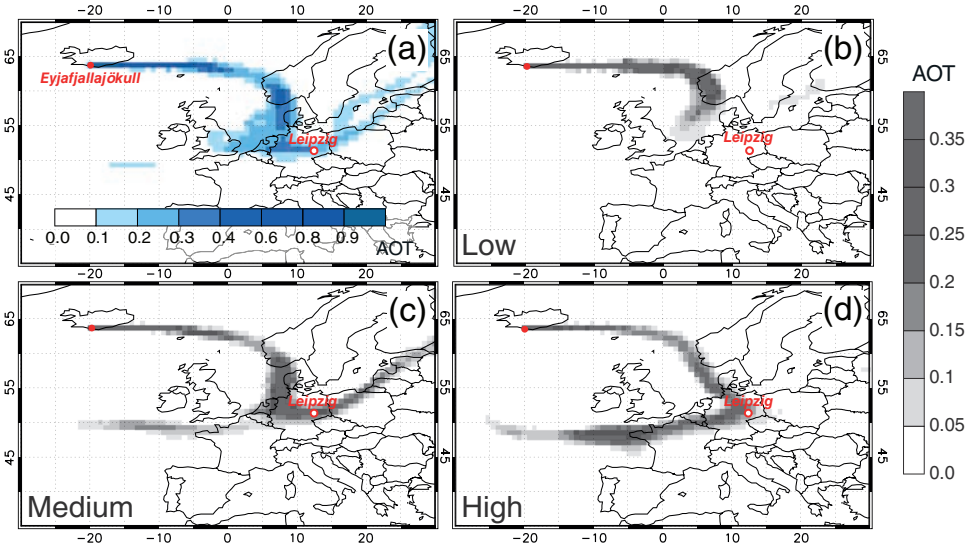


*Fig. 1: Maps of modeled aerosol optical thickness (550 nm) of the Eyjafjallajökull ash plume on April 16, 2010. Shown is the volcanic ash dispersal as computed with COSMO-MUSCAT using (a) MISR plume height retrievals and (b–d) different control injection heights [Heinold et al., 2011]. The ash particle mixture shows similar light absorption properties like Saharan dust [Ansmann et al., 2010]. Thus, optical parameters calculated from Mie theory using dust refractive indices from Sokolik and Toon [1999] were used for the optical thickness computation.*

dispersal over Europe on 16 April as simulated with the standard emission height range ("MISR"). The sensitivity of aerosol transport to different release heights is investigated using additional tracers. Tracking their dispersion indicates to which extent each injection height contributes to the observed ash plume. The lower part of the ash plume quickly subsides and reaches only the North Sea (Fig. 1b). The middle part is transported across Europe and towards the Atlantic Ocean (Fig. 1c). Volcanic ash, which is emitted above the plume top height from London VAAC reports, mainly moves clockwise around the high east of the British Isles and is advected over the Atlantic Ocean (Fig. 1d).

Figure 2 shows the vertical distribution of volcanic ash over Leipzig on 16 April. The backscatter coefficient profile from lidar measurements reveals the presence of ash particles at 4.5–6 km height. The observed values reached up to 6 $Mm^{-1}$ $sr^{-1}$. Another dense ash layer was centered at 3 km. As surface microphysical measurements at Melpitz (Fig. 3) suggest, ash particles also contributed to the boundary layer aerosol in the lowest 1.5 km. The model matches the vertical profile of volcanic ash very well, except from the fine layer structure in the free troposphere. A second peak of up to 3 $Mm^{-1}$ $sr^{-1}$ is simulated below 1 km height indicating that ash particles were mixed down to the surface. Comparing lidar data to model results with different injection heights shows that volcanic aerosol released below the standard injection height does not arrive at Leipzig (Fig. 2). The observed plume height is slightly underestimated in the "Medium" case. The plume is placed too high at 7–8 km for the highest emission heights. Apparently, a combination of the

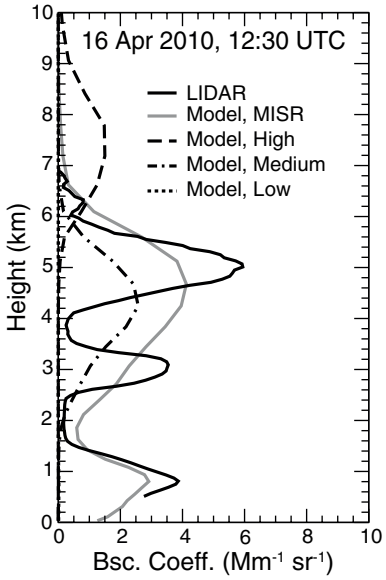


*Fig. 2: Vertical profiles of the particle backscatter coefficient (532 nm) over Leipzig on April 16, 2010. Comparison of modeled profiles with lidar data (averaged from 12:21–12:41 UTC). The dashed/dotted lines denote model results with different injection heights [Heinold et al., 2011]. Model-derived backscatter coefficients were calculated using dust optical properties, including a lidar ratio of 55 sr [Ansmann et al., 2010].*

injection heights of the "Medium" and "High" case represents the actual spatial-temporal evolution of the Eyjafjallajökull ash plume. This finding confirms the assumptions made in the "MISR" standard case.

## Conclusions

The spread of the Eyjafjallajökull volcano ash plume in April and May 2010 was simulated by the regional

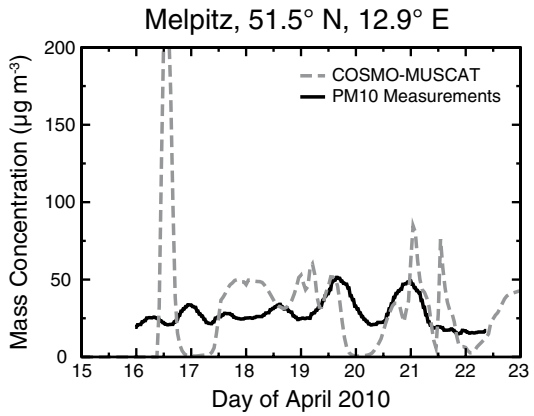


***Fig. 3:*** *Time series of observed and modeled surface concentration of PM10 at Melpitz on April 15–23, 2010 [Heinold et al., 2011]. Source of experimental data: IfT [Schäfer et al., 2011].*

model system COSMO-MUSCAT. Special focus was on the injection height as a key input parameter. Its impact on the dispersion and evolution was studied with additional independent ash emitted at specific control levels, which allows to assess the relative contribution of each layer to the spatial distribution after transport. Taking into account the remaining uncertainties in the other input parameters as well, COSMO-MUSCAT performed well in simulating the 2010 Icelandic volcanic ash plume. In particular the good agreement between modeled vertical profiles of volcanic ash and lidar observations indicates that using the MISR stereo-height retrievals to characterize atmospheric ash input provide an alternative to complex injection height models in case of lacking information on eruption dynamics.

## References


Ansmann, A., M. Tesche, S. Groß, V. Freudenthaler, P. Seifert, A. Hiebsch, J. Schmidt, U. Wandinger, I. Mattis, and M. Wiegener (2010), The 16 April 2010 major volcanic ash plume over central Europe: EARLINET lidar and AERONET photometer observations at Leipzig and Munich, Germany, *Geophys. Res. Lett.*, 37, L13810, doi: 10.1029/2010GL043809.

Gudmunsson, M. T., R. Pedersen, K. Vogfjörd, B. Thorbjarnardottir, S. Jakobsdottir, and M. J. Roberts (2010), Eruptions of the Eyjafjallajökull volcano, Iceland, *EOS*, 91(21), 190–191.

Heinold, B., I. Tegen, R. Wolke, A. Ansmann, I. Mattis, A. Minikin, U. Schumann, and B. Weinzierl (2011), Simulations of the 2010 Eyjafjallajökull volcanic ash dispersal over Europe using COSMO-MUSCAT, *Atmos. Environ.*, in press, doi: 10.1016/j.atmosenv.2011.05.021.

Jones, A., D. Johnson, M. Hort, and B. Devenish (2007), The UK Met Office's Next-Generation Atmospheric Dispersion Model, NAME III, in *Air Pollution Modeling and Its Application XVII*, edited by C. Borrego and A. L. Norman, pp. 580-589, Springer.

Schäfer, K., W. Thomas, A. Peters, L. Ries, F. Obleitner, J. Schnelle-Kreis, W. Birmili, J. Diemer, W. Fricke, W. Junkermann, M. Pitz, S. Emeis, R. Forkel, P. Suppan, H. Flentje, H. E. Wichmann, S. Gilge, F. Meinhardt, R. Zimmermann, K. Weinhold, J. Soentgen, C. Münkel, C. Freuer, and J. Cyrys (2011), Influences of the 2010 Eyjafjallajökull volcanic plume on air quality in the northern Alpine region, *Atmos. Chem. Phys.*, 11, 9083-9132, doi: 10.5194/acpd-11-9083-2011.

Schumann, U., B. Weinzierl, O. Reitebuch, H. Schlager, A. Minikin, C. Forster, R. Baumann, T. Sailer, K. Graf, H. Mannstein, C. Voigt, S. Rahm, R. Simmet, M. Scheibe, M. Lichtenstern, P. Stock, H. Rüba, D. Schäuble, A. Tafferner, M. Rautenhaus, T. Gerz, H. Ziereis, M. Krautstrunk, C. Mallaun, J.-F. Gayet, K. Lieke, K. Kandler, M. Ebert, S. Weinbruch, A. Stohl, J. Gasteiger, S. Groß, V. Freudenthaler, M. Wiegner, A. Ansmann, M. Tesche., H. Olafsson, and K. Sturm (2011), Airborne observations of the Eyjafjalla volcano ash cloud over Europe during air space closure in April and May 2010, *Atmos. Chem. Phys.*, 11, 2245-2279, doi: 10.5194/acp-11-2245-2011.

Scollo, S., A. Folch, M. Coltelli, and R. V. J. (2010), Three-dimensional volcanic aerosol dispersal: A comparison between Multiangle Imaging Spectroradiometer (MISR) data and numerical simulations, *J. Geophys. Res.*, 115, D24210, doi: 10.1029/2009JD013162.

Sokolik, I. N., and O. B. Toon (1999), Incorporation of mineralogical composition into models of the radiative properties of mineral aerosol from UV to IR wavelengths, *J. Geophys. Res.*, 104, 9423-9444.


**Cooperation**
- Deutsches Zentrum für Luft- und Raumfahrt (DLR), Oberpfaffenhofen, Germany
- Deutscher Wetterdienst (DWD), Offenbach, Germany
- The Federal Environmental Agency (UBA), Dessau, Germany
- GUAN Network (http://wiki.tropos.de/index.php/GUAN)

# Immersion freezing of biological particles investigated at LACIS

Susan Hartmann[1], Tina Šantl Temkiv[2,3], Stefanie Augustin[1], Ulrich Gosewinkel Karlson[2], Heike Wex[1], Tina Clauss[1], Jens Voigtländer[1], Dennis Niedermeier[1], Michael Raddatz[1], Maher M. Sahyoun[2,4], Frank Stratmann[1]

[1] Leibniz Institute for Tropospheric Research (IfT), Leipzig, Germany
[2] Aarhus University, Department of Environmental Science, Roskilde, Denmark
[3] Aarhus University, Department of Bioscience, Microbiology Section, Aarhus, Denmark
[4] Danish Meteorological Institute, Copenhagen, Denmark

*Biologische Partikel, insbesondere Bakterien, gehören gegenwärtig zu den effektivsten Eiskeimen, die in der Atmosphäre bzw. in Niederschlagsproben gefunden werden. Daher wurde in der hier vorgestellten, und am Leipzig Aerosol Cloud Interaction Simulator (LACIS) durchgeführten Studie, das Immersionsgefrierverhalten größenselektierter biologischer Partikel (SNOMAX® und Außenmembranvesikel) untersucht. SNOMAX® als Bakterienreferenzsubstanz ist unterhalb von -5°C eisaktiv mit maximalen Eisfraktionen in der Größenordnung von einigen 10%, während die für die Außenmembranvesikel bestimmten Eisfraktionen nahe dem Detektionslimit, und damit im Prozentbereich und darunter, liegen. Somit wird klar gezeigt, dass der Bakterienstamm Pseudomonas-syringae, unter ähnlichen Bedingungen wie in Mischphasenwolken vorhanden, als Eiskeim im Immersionsgefriermodus fungiert. Hingegen ist die Eiskeimfähigkeit der untersuchten Außenmembranvesikeln eher unbedeutend.*

## Introduction

Atmospheric observations indicate that heterogeneous ice nucleation in mixed-phase clouds can already occur at temperatures higher than -20°C [*Ansmann et al.*, 2009; *Seifert et al.*, 2010]. In contrast, laboratory studies showed that mineral dust and soot particles, which are two of the major components of ice crystal residues [e.g., *Pratt et al.*, 2009], function as ice nuclei (IN) at lower temperatures. One possible explanation for the observed temperature differences is the presence of biological particles (e.g., bacteria) acting as ice IN already at temperatures above –10°C.

Ice nucleation active bacteria, being ubiquitous in the atmosphere, are currently the most efficient IN known [e.g., *Möhler et al.*, 2008]. Investigating the freezing behavior of Pseudomonas-syringae bacteria, *Maki et al.* [1974] found freezing temperatures of about -2°C. Bacteria possess membrane proteins able to mimic the structure of an ice nucleus. The proteins act as a template for ice cluster formation reducing the energy barrier required for critical ice cluster formation. Furthermore, it has been confirmed that some ice nucleating active bacterial strains have the ability to produce outer membrane vesicles (OMV), which might contain ice nucleating active proteins [*Phelps et al.*, 1986] and act as IN as well.

Nevertheless, the dominating freezing mechanism, the properties inducing ice nucleation, and the relative importance of bacteria in the atmosphere are still unclear.

To study the relevance of bacteria and OMV as atmospheric IN, we analyzed the ice nucleation behaviour of SNOMAX®, as surrogate for Pseudomonas-syringae, and outer membrane vesicles shed from ice nucleating active bacteria collected from rain samples. Investigations were performed at the Leipzig Aerosol Cloud Interaction Simulator (LACIS) [*Stratmann et al.*, 2004; *Hartmann et al.*, 2011] with special focus being given to the immersion freezing mode.

## Material and Measurement Method

SNOMAX® (SMI Snow Makers AG, Steffisburg, Switzerland) consists of deadened Pseudomonas-syringae bacteria grown under ideal conditions to maximize their IN ability. Therefore, SNOMAX® is considered as convenient surrogate for ice nucleation active bacteria.

An outer membrane vesicle is a strangulated part of a bacteria cell with membrane material surrounding its interior. OMV released from two bacterial strains extracted from rain samples (collected 30 m above ground level in Roskilde, Denmark in February and October of 2009) were analyzed. The extraction and the cultivation of the bacteria cells as well as the production of the OMV were conducted by our collaborators from the University Aarhus [*Temkiv et al.*, 2011]. Figure 1 shows exemplarily TEM images of outer membrane vesicles (left) and a cell shedding OMV (right).

For producing IN, dry SNOMAX® pellets (essentially the fragments of Pseudomonas-syringae) were suspended in double deionized water, while the OMV were suspended in a 0.1% sodium chloride solution in order to avoid destruction of the OMV structure. The respective suspensions were atomized and dried, resulting in

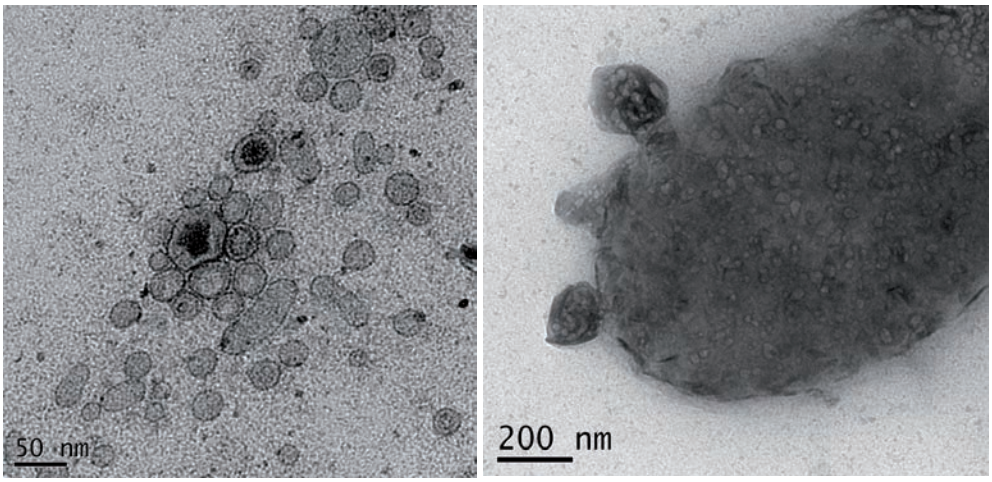


*Fig. 1: TEM images of outer membrane vesicles (left) and a cell shedding OMV (right).*

either SNOMAX® particles or OMV particles coated with sodium chloride and pure sodium chloride particles.

Subsequently, the particles were size selected and then fed into LACIS which was operated in immersion freezing mode [*Hartmann et al.*, 2011]. LACIS facilitates the investigation of well-characterized, size-selected particles with only one particle being immersed in each droplet. Additionally, a Cloud Condensation Nucleus counter (CCN) was used to determine the concentration of the OMV containing particles based on their activation behaviour being different from that of the pure sodium chloride particles. Results of the performed immersion freezing measurements are ice fractions, i.e. the number of ice particles divided by the sum of ice particles and droplets. Differentiation between droplets and ice particles takes place via the evaluation of the polarization state of the light scattered by the droplets and ice particles. The used instrument (TOPS-ICE) has been developed at the IfT.

## Results and Discussion

The immersion freezing behaviour of the SNOMAX® and OMV particles was analyzed as function of temperature in the range from -3°C to -38°C and is illustrated in Fig. 2 (left panel). For SNOMAX®, 650 nm and 800 nm large particles were chosen. The ice fraction curves are very steep, almost linear for temperature values between -3°C and -10°C. For lower temperatures they level off to constant values of about 0.2 and 0.4 for the 650 nm and 800 nm particles, respectively. This suggests that only 20% of 650 nm and 40% of SNOMAX® particles are ice active.

Considering the linear ranges of the ice fraction curves and assuming spherical particles and an ice nucleation time of 1 s, the effective heterogeneous

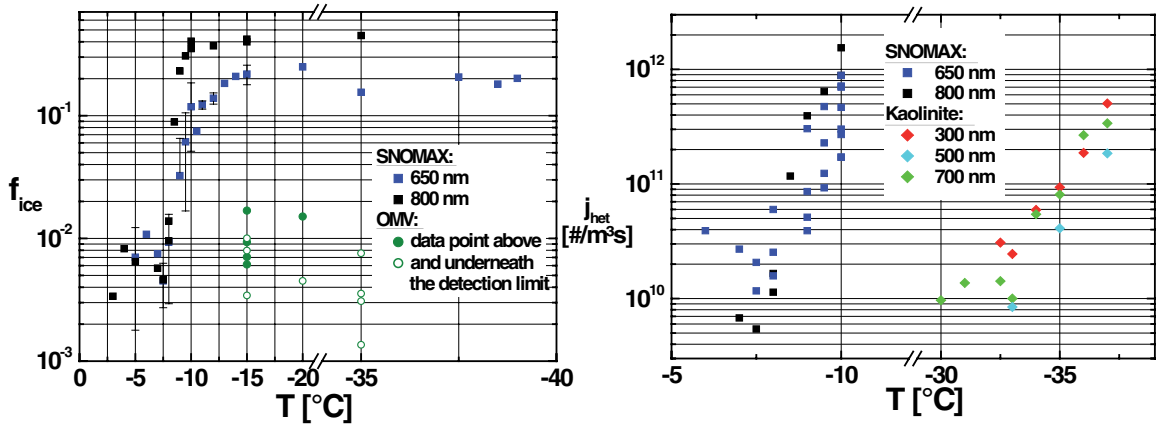


*Fig. 2: Ice fractions $f_{ice}$ for 650 nm and 800 nm SNOMAX® and OMV particles (size varying between 50 nm and 160 nm, filled symbols: data point above, open symbol: data point underneath the detection limit) as function of temperature (left panel). Derived effective heterogeneous ice nucleation rate coefficient $j_{het}$ for SNOMAX® and koalinite particles vs. temperature are given in the right panel.*

ice nucleation rate coefficients $j_{het}$ can be calculated and are shown in Fig. 2 (right panel). In comparison to mineral dust, e.g. kaolinite, the $j_{het}$ of SNOMAX® varies from about $10^{10}$ at -7°C to $10^{12}$ at -10°C. This corresponds to the same order of magnitude as for kaolinite particles but already at 22 K higher temperature. This confirms the higher ice nucleating potential of SNOMAX® particles.

The ice fractions observed for the OMV containing particles where close to the detection limit of the TOPS-ICE instrument, i.e., in the order of 1% and lower. This indicates that only a small fraction of the OMV particles nucleate ice. However, considering the small size of the OMV particles (ranging between 50 nm and 160 nm as shown in *Temkiv et al.* [2011]) it might be possible that compared to SNOMAX®, the significantly reduced IN ability is mainly due to size effects.

**Outlook**

Ice nucleating active biological particles are multifarious and ubiquitous in the atmosphere. Besides bacteria and bacterial vesicles, other biological particles possibly inducing ice nucleation are pollen. Very recently, it was found that even water which had been in contact with pollen grains, and then been separated from the pollen bodies, can be as ice active as the pollen grains themselves [*Pummer et al.*, 2011]. Investigation of this interesting effect will complement the biological ice nucleation experiments at LACIS via analysis of the immersion freezing behaviour of the macromolecules contained pollen washing water.

**References**


Ansmann, A., et al. (2009), Evolution of the ice phase in tropical altocumulus: SAMUM lidar observations over Cape Verde, *J. Geophys. Res.-Atmos.*, *114*, 20.

Hartmann, S., et al. (2011), Homogeneous and heterogeneous ice nucleation at LACIS: operating principle and theoretical studies, *Atmos. Chem. Phys.*, *11*(4), 1753-1767.

Maki, L. R., et al. (1974), Ice nucleation induced by Pseudomonas-syringae, *Appl. Microbiol.*, *28*(3), 456-459.

Möhler, O., et al. (2008), Heterogeneous ice nucleation activity of bacteria: new laboratory experiments at simulated cloud conditions, *Biogeosciences*, *5*(5), 1425-1435.

Phelps, P., et al. (1986), Release of cell-free ice nuclei by erwina-herbicola, *J. Bacteriol.*, *167*(2), 496-502.

Pratt, K. A., et al. (2009), In situ detection of biological particles in cloud ice-crystals, *Nat. Geosci.*, *2*(6), 397-400.

Pummer, B. G., et al. (2011), Birch and conifer pollen are efficient atmospheric ice nuclei, *Atmos. Chem. Phys. Discuss.*, *11*, 27219–27241.

Seifert, P., et al. (2010), Saharan dust and heterogeneous ice formation: Eleven years of cloud observations at a central European EARLINET site, *J. Geophys. Res.-Atmos.*, *115*, 13.

Stratmann, F., et al. (2004), Laboratory studies and numerical simulations of cloud droplet formation under realistic supersaturation conditions, *J. Atmos. Ocean. Tech.*, *21*(6), 876-887.

Temkiv, T. Š., et al. (2011) Bacteria in Clouds. PhD dissertation, Graduate School of Science and Technolopgy, Aarhus University, Denmark.


**Cooperation**

- Leibniz Institute for Tropospheric Research/Physic Department, Leipzig, Germany
- Aarhus University/Department of Environmental Science, Roskilde, Denmark
- Aarhus University/Department of Bioscience, Microbiology Section, Aarhus, Denmark
- Danish Meteorological Institute, Copenhagen, Denmark

# Evidence for a clear aerosol impact on heterogeneous ice formation: Southern versus northern hemisphere

Thomas Kanitz, Patric Seifert, Albert Ansmann, Ronny Engelmann, Dietrich Althausen

*Hemisphärische Unterschiede in der heterogenen Eisbildungstemperatur in freien troposphärischen Wolken wurden mittels Lidarmessungen im Rahmen des OCEANET-Projektes untersucht. Die Messungen wurden an Bord des Forschungsschiffes Polarstern, in Punta Arenas (53°S), Chile und Stellenbosch (34°S), Südafrika durchgeführt. Der Datensatz umfasst je Station einen Zeitraum von 4 Monaten und wurde zusammen mit den Langzeit-Messungen der EARLINET Station IfT Leipzig (51°N) für eine Studie zur heterogenen Eisnukleation in Wolken unter verschiedenen Aerosolbedingungen in der nördlichen und südlichen Hemisphäre benutzt. Deutliche Unterschiede in der Eisnukleation in Abhängigkeit der Temperatur wurden zwischen Leipzig und Punta Arenas festgestellt. In einem Temperaturbereich von -15°C bis -20°C wurden in 70% der untersuchten Wolken über Leipzig Eiskristalle gefunden, am Standort Punta Arenas hingegen in weniger als 20%. Unter der Annahme vergleichbarer Meteorologie in nördlichen und südlichen mittleren Breiten ist dieses Ergebnis ein Zeichen für den Effekt unterschiedlicher Aerosolbedingungen auf die heterogene Eisnukleation in den beiden Hemisphären.*

## Introduction

Aerosol particles are required to initiate ice formation in the atmosphere at temperatures down to –37°C. Besides aerosol properties, ambient meteorological conditions as well as cloud properties control at which temperature the nucleation of first ice crystals in supercooled water clouds is initiated. There is no doubt that aerosol particles serving as cloud condensation nuclei (CCN) or ice nuclei (IN) influence these cloud processes. However, large uncertainties in global climate models exist about the aerosol effect on the formation of ice crystals in different clean to heavily polluted areas around the globe. Lidar cloud observations were performed during three cruises of the German research vessel (RV) Polarstern, from Germany to Chile in October-November 2009 (ANT-XXVI/1), and back to Germany in April-May 2010 (ANT-XXVI/4), and during a cruise to South Africa in October-November 2010 (ANT-XXVII/1). Figure 1 (left) shows the installation of the lidar within the OCEANET-container that was deployed at the upperdeck, starboard of Polarstern (Fig. 1 right). Further, we used the opportunity to deploy the lidar


***Fig. 1:*** *(left) Mounting the lidar within the OCEANET-container at the pier of Punta Arenas. (right) The OCEANET-container was deployed at the upperdeck, starboard of the research vessel Polarstern.*

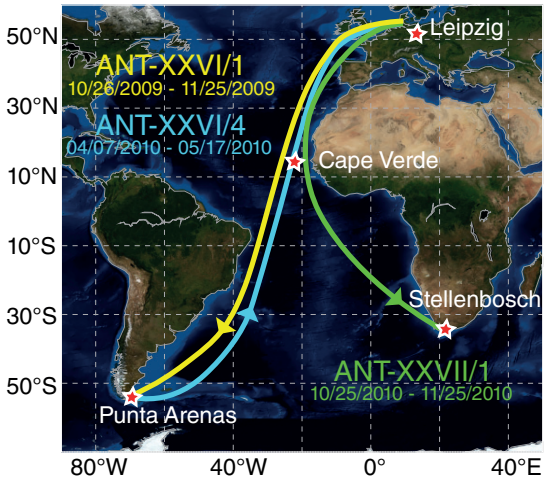


***Fig. 2:*** *RV Polarstern cruises to Punta Arenas (autumn 2009, ANT-XXVI/1), back to Bremerhaven (spring 2010, ANT-XXVI/4), and to Cape Town (autumn 2010, ANT-XXVII/1), and lidar field sites Punta Arenas, and Stellenbosch, at which cloud observations used in this study were performed.*

at Punta Arenas and Stellenbosch to extend our lidar studies toward the southern hemisphere while the RV Polarstern moved on to Antarctica. Figure 2 provides an overview of the three cruises of the RV Polarstern and the locations of the lidar sites in the southern hemisphere. Also locations of previous IfT lidar-based cloud observations at Cape Verde (14.7°N), and Leipzig are indicated in Fig. 2 that complete the cloud data set of this study and gives the chance to compare cloud observations from polluted to almost unpolluted atmospheric conditions.

## Instrumentation and Methodology

In this study we applied a methodology that was developed at IfT within the last 4 years [*Ansmann et al.*, 2008, 2009; *Seifert et al.*, 2010]. The portable

multi-wavelength Raman and polarization lidar system Polly$^{XT}$ [*Althausen et al.*, 2009] was used to perform automated and remotely controlled cloud observations. The vertical extent of a single cloud layer was determined by means of the obtained signal profiles. A cloud layer was defined as one single cloud layer, when it was separated from adjacent ones by 500 m in the vertical or by 5 minutes in time. The cloud phase was defined from volume linear depolarization ratio profiles. The ratio is zero for spherical liquid-water droplets and larger than zero for non-spherical ice-crystals. Ice formation is initiated in the coldest part of the cloud layer, which is typically the cloud top. The temperature information was obtained from radiosondes or from model assimilation data.

## Results

Figure 3 shows the fraction of ice-containing clouds related to all observed cloud layers for eight classes (5 K intervals) of cloud top temperature between 0°C and –40°C. Curves are shown for Leipzig and Punta Arenas, and for comparison, also for Stellenbosch, the RV Polarstern cruises, and Cape Verde (January-February 2008 observations [*Ansmann et al.*, 2009]). The strongest increase in the ice-containing cloud fraction with decreasing temperature, expressing most efficient heterogeneous ice nucleation, is observed over Leipzig. The weakest increase is found for Punta Arenas. Less than 10%, <20%, about 30% – 40% and around 70% of the cloud layers with cloud top temperatures from –15°C to –20°C, showed ice formation over Cape Verde, Punta Arenas, Stellenbosch/Polarstern, and Leipzig, respectively. More than 90% of the cloud layers contained ice over Leipzig and Stellenbosch at temperatures from –25°C to –30°C, whereas this 90% level was not reached at Punta Arenas before cloud top temperatures were below –35°C. At Cape Verde, a westerly air flow from remote tropical oceanic regions prevails with an apparently low IN number concentration so that heterogeneous ice formation is weak at least for temperatures down to –25°C. The RV Polarstern data set includes all clouds observed during the three journeys and thus represents almost mean conditions of heterogeneous ice nucleation for the tropics and midlatitudes. At Stellenbosch, aerosol conditions are controlled by local African particle sources [*Kanitz et al.*, 2011].

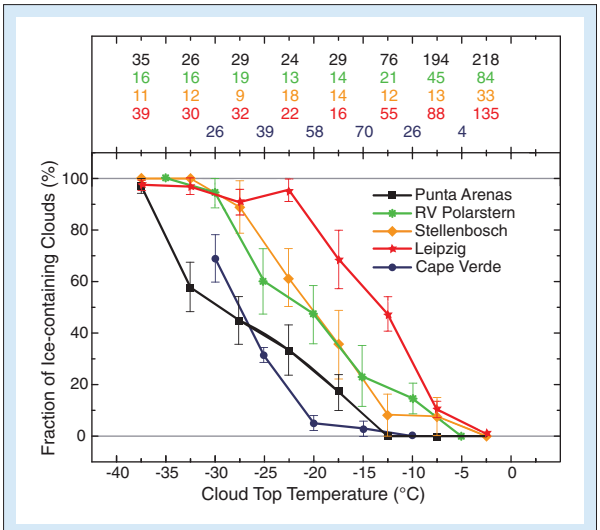


***Fig. 3:*** *Fraction of ice-containing clouds over Punta Arenas (black, December 2010 – January 2011), RV Polarstern (green), Stellenbosch (orange), Leipzig (red), and Cape Verde (blue) as a function of cloud top temperature (for 5 K intervals). Error bars indicate the statistical uncertainty [Seifert et al., 2010]. The total number of clouds within each temperature interval are given at the top (Cape Verde from Ansmann et al. [2009]).*

The strong contrast found in the cloud observations over Leipzig and Punta Arenas is obviously related to the different aerosol conditions. The free troposphere over Leipzig is determined by anthropogenic pollution, desert dust, release of forest fire, and other biomass burning smoke [*Müller et al.*, 2005, *Mattis et al.*, 2008]. Instead, at high southern latitudes over remote oceanic areas (>50°S), continental aerosol particles are widely absent and marine conditions prevail. This clearly points to higher concentrations of favorable IN in the northern midlatitudes than in the southern midlatitudes and to powerful role of atmospheric aerosol particles in the formation of ice phase in former pure-water clouds as well as the formation of precipitation [*Kanitz et al.*, 2011].

## Conclusions

By contrasting liquid-water and ice-containing cloud data sets observed with polarization lidar at several places in the northern and southern hemisphere and aboard the RV Polarstern a clear north-to-south decrease in the efficiency of heterogeneous ice nucleation was found. This decrease is well correlated with the abundance of continental aerosol particles that are known to be favorable IN and whose concentration in the free troposphere decreases when going from northern to southern hemispheric sites or to maritime sites close to the Oceans. The study documents the significant role of aerosol particles for the glaciation of shallow cloud layers in the northern hemisphere.

## Acknowledgements

We thank the RV Polarstern team, the Alfred Wegener Institute for Polar and Marine Research (Bremerhaven, Germany), the Leibniz Institute for Marine Research of the University Kiel (IFM-GEOMAR, Kiel, and the Helmholtz-Centre Geesthacht (Geesthacht, Germany) for the

cooperation at the cruises ANT-XXVI/1, ANT-XXVI/4, and ANT-XXVII/1. Many thanks also to the University of Magallanes (Punta Arenas,Chile), and to the University of Stellenbosch (Stellenbosch, South Africa) for the support during our measurements in the southern hemisphere.

## References

Althausen, D., R. Engelmann, H. Baars, B. Heese, A. Ansmann, D. Müller, and M. Komppula (2009), Portable Raman lidar Polly$^{XT}$ for automated profiling of aerosol backscatter, extinction, and depolarization., J. Atmos. Oceanic Technol., 26, 2366-2378, doi:10.1175/2009JTECHA1304.1.

Ansmann, A., et al. (2008), Influence of Saharan dust on cloud glaciation in southern Morocco during the Saharan Mineral Dust Experiment, J. Geophys. Res., 113, D04210, doi:10.1029/2007JD008785.

Ansmann, A., M. Tesche, P. Seifert, D. Althausen, R. Engelmann, J. Fruntke, U. Wandinger, I. Mattis, and D. Müller (2009), Evolution of the ice phase in tropical altocumulus: SAMUM lidar observations over Cape Verde, J. Geophys. Res., 114, D17208, doi:10.1029/2008JD011659.

Mattis, I., D. Müller, A.Ansmann, U. Wandinger, J. Preißler, P. Seifert, and M. Tesche (2008), Ten years of multiwavelength Raman lidar observations of free tropospheric aerosol layers over central Europe: Geometrical properties and annual cycle, J. Geophys. Res., 113, D20202, doi: 10.1029/2007JD009639.

Müller, D., I. Mattis, U. Wandinger, A. Ansmann, D. Althausen, and A. Stohl (2005), Raman lidar observations of aged siberian and canadian forest fire smoke in the free troposphere over germany in 2003: Microphysical particle characterization, J. Geophys. Res, 110, D17201, doi:10.1029/2004JD005756.

Kanitz, T., , P. Seifert, A. Ansmann, R. Engelmann, D. Althausen, C. Casiccia, and E. G. Rohwer (2011), Contrasting the impact of aerosols at northern and southern midlatitudes on heterogeneous ice formation, *Geophys. Res. Lett.*, 38, L17802, doi:10.1029/2011GL048532.

Seifert, P., A. Ansmann, I. Mattis, U. Wandinger, M. Tesche, R. Engelmann, D. Müller, C. Pérez, and K. Haustein (2010), Saharan dust and heterogeneous ice formation: Eleven years of cloud observations at a central European EARLINET site, *J. Geophys. Res.*, 115, D20201, doi:10.1029/2009JD013222.

**Funding**
- Wilhelm Gottfried Leibniz Association (OCEANET project in the framework of PAKT)

**Cooperation**
- Leibniz Insitute for Marine Research of the University Kiel (IFM-GEOMAR), Kiel, Germany
- Helmholtz Centre Geesthacht, Geesthacht, Germany
- Alfred-Wegner-Institute, Bremerhaven, Germany
- University of Magallanes, Ozone and RUV Laboratory, Punta Arenas, Chile
- University of Stellenbosch, Physics Department, Laser Research Institute, Stellenbosch, South Africa

# Heterogeneous ice nucleation: Reconciling stochastic and singular freezing behavior

Dennis Niedermeier[1], Raymond A. Shaw[2], Susan Hartmann[1], Heike Wex[1], Tina Claus[1], Jens Voigtländer[1], Frank Stratmann[1]

[1] Leibniz Institute for Tropospheric Research (IfT), Leipzig, Germany
[2] Department of Physics, Michigan Technological University, Houghton, Michigan, USA

*Heterogene Eisnukleation ist ein wichtiger Prozess für die Bildung von Eiskristallen in der Atmosphäre. Er wird in der Literatur wahlweise als stochastisch, d.h. analog zur homogenen Eisnukleation, als zeitabhängiger, oder singular, d.h. als zeitunabhängiger Prozess beschrieben. Im Folgenden wird ein idealisiertes, konzeptionelles Modell vorgestellt, das auf einem rein stochastischen Ansatz beruht. Unter Verwendung dieses Modells wurde gezeigt, dass die heterogene Eisnukleation fundamental ein stochastischer Prozess ist. Unterscheiden sich jedoch die Eis bildenden Partikel hinsichtlich ihrer Oberflächeneigenschaften stark voneinander, können heterogene Eisnukleationsprozesse ein singulares Verhalten aufweisen.*

## Introduction

Heterogeneous ice nucleation, a primary pathway for ice formation in the atmosphere, has been described alternatively as being stochastic, in direct analogy with homogeneous nucleation, or singular, with ice nuclei initiating freezing at deterministic temperatures. The stochastic hypothesis is exemplified by the work of e.g., *Bigg* [1953a, b] and *Carte* [1959] and characterizes heterogeneous ice nucleation as a time dependent process.

The singular hypothesis was developed by *Levine* [1950] and *Langham and Mason* [1958], among others. It assumes that ice embryos form at certain sites on the IN surface at a specific, i.e., deterministic temperature $T_s$ [*Langham and Mason*, 1958; *Vali*, 2008]. Being cooled to $T_s$, specific active sites will initiate instantaneous ice formation, i.e., the ice nucleation process is assumed to be non-random and time-independent.

## Description of the Soccer-ball model

To explore this apparent contradiction, we introduce a conceptual model describing the freezing behavior of an idealized population of ice nucleating particles. Our conceptual model is fundamentally based on the stochastic view of nucleation: That is, nucleation is viewed as always occurring as a result of random fluctuations of water molecules leading, eventually, to a critical ice embryo which is able to grow spontaneously. We explore the stochastic-singular transition in the context of a highly idealized model that possesses the following essential features: A large number $N_0$ (statistical ensemble) of spherical 'ice nucleus' particles of identical size (particle diameter of 300 nm) is considered, each immersed in a water droplet. The population of particle-containing water droplets is assumed to be exposed to uniform thermodynamic conditions. The surface of each particle is imagined to be divided into a number $n_{site}$ of surface sites with each site having well-defined properties (e.g., interfacial free energy). The word site is used to denote a surface two-dimensional 'patch' of finite extent and the image of a spherical particle covered by a finite number of patches leads to the colloquial name 'Soccer-ball' model. For simplicity, $n_{site}$ is identical for all particles and the sites are assumed to be of the same size, $s_{site} = S_p / n_{site}$, where $S_p$ is the total particle surface area. Ice embryo formation can be described by classical nucleation theory. Each surface site *i* is characterized by a fixed, but randomly chosen water contact angle $\theta$. For simplicity, the contact angle distribution function $P(\theta)$ is assumed to be the integral over the Gaussian (error function) characterized through mean $\mu_\theta$ and standard deviation $\sigma_\theta$.

## Model results and discussion

Model results showing the time dependence of the freezing process are presented in Fig. 1, in which the logarithm of the unfrozen fraction is plotted as a function of time t. Here, the effect of variable surface properties over the particle population is considered by setting $\sigma_\theta$ = 0.001, 0.010, 0.100 and 0.500. We do so for different numbers of particle surface sites by setting $n_{site}$ to 1, 10 and 100. All populations are assumed to feature the same mean contact angle (here, $\mu_\theta$ = 1.0 rad was chosen). The model results are presented for different absolute temperatures (details are given in *Niedermeier et al.* [2011]).

For $\sigma_\theta$ = 0.001 rad (Fig. 1a), we observe a straight line for all three $n_{site}$ values. That means freezing appears as purely stochastic, despite the small variability of the contact angles across the particle population. For $\sigma_\theta$ = 0.01 rad (Fig. 1b), the curve

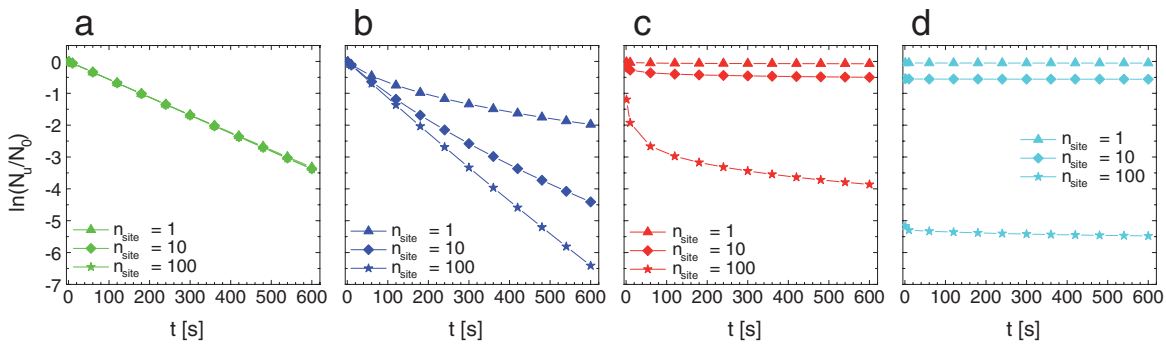


***Fig. 1:*** *Logarithm of the unfrozen fraction (ln $N_u/N_0$) versus the nucleation time t for different fixed absolute temperatures T showing the effect of variable surface properties across the particle populations for different $n_{site}$ values. Different colors represent different $\sigma_\theta$ values, different symbols represent different $n_{site}$ values: a) $\sigma_\theta$ = 0.001 rad and T = -20°C, b) $\sigma_\theta$ = 0.01 rad and T = -20°C, c) $\sigma_\theta$ = 0.1 rad and T = -15°C and d) $\sigma_\theta$ = 0.5 rad and T = -1°C.*

slopes start to change. For $n_{site}$ = 1, a decrease in the slope, i.e., a weaker time dependence of the nucleation process with increasing time can be observed. However, with increasing number of sites on the particle surfaces this effect weakens, returning to an almost constant slope for $n_{site}$ = 100. Considering even wider ranges of contact angles $\sigma_\theta$ = 0.1 rad (Fig. 1c) and $\sigma_\theta$ = 0.5 rad (Fig. 1d), the flattening out of the frozen fraction versus time curves becomes even more pronounced. For $\sigma_\theta$ = 0.5 rad, after an initial jump, the frozen droplet fraction stays more or less constant, i.e., the freezing process appears to be of a purely singular nature. A similar behavior to that shown in Fig. 1c and Fig. 1d was observed by *Yankofsky et al.* [1981] who were investigating the freezing time dependence of droplets containing cells from INA bacteria. In summary, Fig. 1 displays the transition from a stochastic to an apparently singular behavior of the heterogeneous ice nucleation process. This transition is due to a wider distribution of contact angles, and consequently mean nucleation times, or more generally speaking, ice nucleation related surface properties across the particle population.

## Conclusion and Outlook

Based on classical nucleation theory alone, a population of particles can exhibit behavior over a continuous range, from purely stochastic to nearly singular. The emergence of singular or nearly singular behavior arises from the existence of sites possessing widely differing nucleation rates, with each individual site exhibiting purely stochastic behavior. Therefore, an idealized population of particles with a statistical distribution of nucleation properties, characterized by a relatively wide distribution of surface free energies, and subject to purely stochastic freezing behavior, can manifest what traditionally has been interpreted as singular behavior: weak time dependence of freezing probability, and wide freezing temperature distributions (not shown here). Fundamentally, in the conceptual model described here, the freezing process is stochastic, so there is always a time dependence. It just may be that the time dependence occurs with a characteristic time scale much smaller than or much larger than the time scales resolved in a hypothetical experiment.

But of course the results taken alone do not verify the model. Evaluation of the basic, fundamental features of the model (i.e., inherent stochastic nature of ice nucleation operating over a finite number of patches) challenges current experimental methods because it requires determining the freezing probability versus both time and temperature.

Furthermore, when parameterizing heterogeneous ice nucleation for e.g. atmospheric modeling applications and depending on the heterogeneity of the IN considered, it might be a satisfactory approximation to assume a singular behavior. However, parcel model simulations assuming a transition from stochastic to apparently singular behavior lead to significant differences in ice formation predictions for mixed-phase clouds [*Ervens and Feingold*, 2011]. Therefore, the heterogeneity of the IN and the resulting time scales should be carefully considered for atmospheric applications. The developed Soccer-ball model will continue to valuably contribute to these considerations.

## References

Bigg, E. (1953a), The supercooling of water, *Proc. Phys. Soc. B*, 66, 688–694.

Bigg, E. (1953b), The formation of atmospheric ice crystals by the freezing of droplets, *Quart. J. Royal Meteorol. Soc.*, 79(342), 510–519.

Carte, A. (1959), Probability of freezing. *Proc. Phys. Soc. B*, 73, 324.

Ervens, B. and G. Feingold (2011): The dependence of the active site distribution of heterogeneous IN on the phase partitioning in mixed-phase clouds, paper presented at AGU Fall Meeting, American Geophysical Union, San Francisco, CA, USA, 12/04 – 12/09/2011.

Langham, E. J. and B. J. Mason (1958), The heterogeneous and homogeneous nucleation of supercooled water, *Proc. Roy. Soc., A*, 247, 493-505.

Levine, J. (1950): Statistical explanation of spontaneous freezing of water droplets, *NACA Tech. Notes*, No. 2234.

Niedermeier, D., R. A. Shaw, S. Hartmann, H. Wex, T. Clauss, J. Voigtländer, and F. Stratmann (2011): Heterogeneous ice nucleation: exploring the transition from stochastic to singular freezing behavior, *Atmos. Chem. Phys.*, 11, 8767-8775, doi:10.5194/acp-11-8767-2011.

Yankofsky, S. A., Z. Levin, T. Bertold, and N. Sandlerman (1981), Some basic characteristics of bacterial freezing nuclei, *J. Appl. Meteorol.*, 20(9), 1013-1019.

Vali, G. (2008), Repeatability and randomness in heterogeneous freezing nucleation, *Atmos. Chem. Phys.*, 8, 5017–5031, doi:10.5194/acp-8-5017-2008.

**Cooperation**
- Department of Physics, Michigan Technological University, Houghton, Michigan, USA

# The role of temperature inversions for the particulate patter (PM) episode in January 2010

Wolfram Birmili[1], Stephan Nordmann[1], Kay Weinhold[1], Laura Tomsche[1], Alfred Wiedensohler[1], Birgit Heese[1], Gerald Spindler[1], Ralf Wolke[1], Holger Wille[2]

[1] Leibniz Institute for Tropospheric Research (IfT), Leipzig, Germany
[2] Jenoptik, Verteidigung & Zivile Systeme Geschäftsbereich Sensorik, Jena, Germany

*Winterliche Smog-Episoden erschweren die Einhaltung gesetzlicher Grenzwerte für Feinstaub ($PM_{10}$). Im Januar 2010 wurden in Mitteleuropa während anhaltender Inversionswetterlagen Rekordwerte in der Feinstaubkonzentration verzeichnet. In Sachsen erreichte die $PM_{10}$-Konzentration 250 µg/m³, die Rußmassenkonzentration 15 µg/m³. Bodenmessungen und Modellsimulationen zeigten eine Ausdehnung der Feinstaubschicht von mehreren hundert km in der Horizontalen an, Ceilometerprofile hingegen eine scharfe Begrenzung in der Vertikalen bei 400 m. Die Hauptquellgebiete der Feinstaubbelastung in Sachsen werden in Osteuropa vermutet. Es gibt aber auch deutliche Anzeichen, dass die lokalen Emissionen bei einer derartigen Inversionswetterlage die Situation verschärften. Eine statistische Betrachtung des Zeitraums 1999-2010 zeigte, dass die Zahl der PM-Grenzwertüberschreitungen in Sachsen klimatisch an tiefe Temperaturen gekoppelt war.*

## Introduction

Epidemiological studies suggest adverse health effects, including respiratory and cardiovascular disease, by enhanced levels of tropospheric particles (particulate matter - PM) [*Rückerl et al.*, 2011]. To alleviate these health effects, EU council directives prescribe limit values for the annual average concentrations of $PM_{10}$ and $PM_{2.5}$[1] (40 µg/m³ and 25 µg/m³, respectively), as well a maximum of 35 exceedances for the daily average value of $PM_{10}$ (50 µg/m³) per year. Since the introduction of these limit values, however, many member states have found it difficult particularly to meet the criterion of the daily average $PM_{10}$ value [*Harrison et al.*, 2008]. As the reported PM emissions, especially from the industrial sector, are falling, it remains unclear why the number of limit value exceedances is not declining as well. There are hypotheses that PM emission reductions in the industrial sector might be offset by an increase in traffic emissions, and by so-far underrated sources such as domestic wood and coal combustion. On the other hand, pollution episodes are greatly controlled by meteorological factors. The climatological variability of regional background PM is crucial to explain the exceedances of the daily limit value [*Engler et al.*, 2011]. Near-surface temperature inversions are a further critical factor leading to high PM levels near the ground. This article examines the circumstances of a high PM concentration episode in Germany in January 2010 and puts the episode into a multi-annual context.

[1] $PM_x$ denotes the total mass concentration of ambient particles with aerodynamic diameter < x nm.

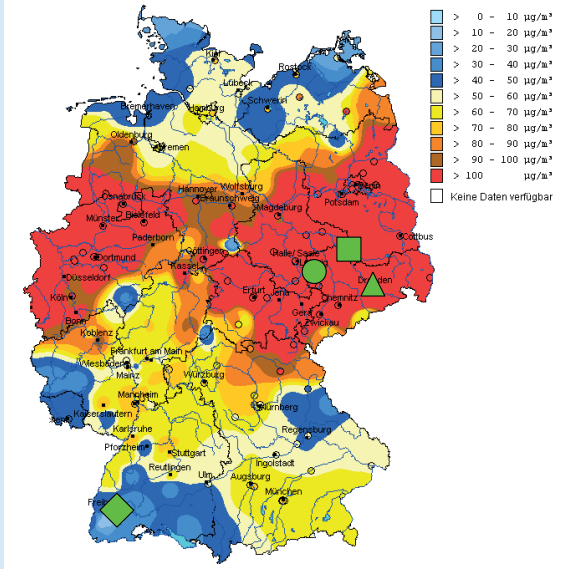


***Fig. 1:*** *Spatial distribution of $PM_{10}$ mass concentrations in Germany on January 26, 2010. Symbols indicate the measurement sites Melpitz (square), Leipzig (circle), Dresden (triangle), Schauinsland (diamond). Data source source: Umweltbundesamt, Dessau.*

## Results

The winter of 2009/2010 was characterized by a steady persistence of the negative phase of the North-Atlantic Oscillation [*Cattiaux et al.*, 2010], which caused several severe cold spells over Central Europe. On January 26, 2010, these weather conditions led to extreme $PM_{10}$ concentrations across Germany (Fig. 1). Easterly winds had advected a significant background during the previous days. With ambient temperatures dropping below -10°C, the concentrations of $PM_{10}$ and black carbon rose to maximum values of

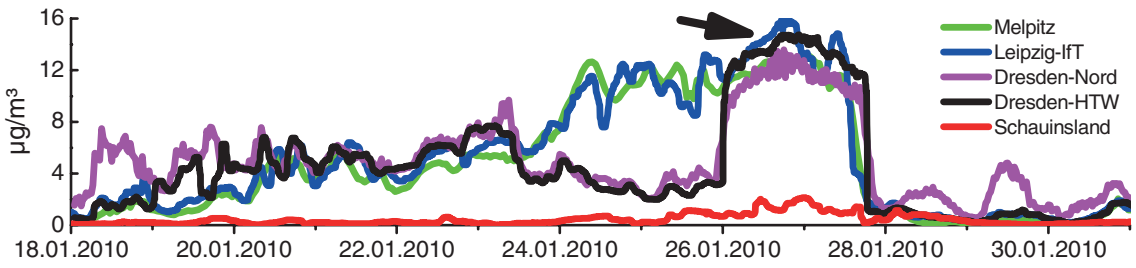


***Fig. 2:*** *Time evolution of the black carbon mass concentration (BC), obtained from multi angle absorption photometry (MAAP) during late January 2010. The arrow marks the period with maximum PM and BC concentrations in Saxony.*

250 and 15 µg/ m³, respectively (Fig. 2). These concentrations were a multiple of those at an unaffected site in South Germany (Schauinsland), and reflect the impact of combustion sources. Radiosoundings confirmed a temperature inversion of around 15 K in the lowest 400 m of the troposphere. Ceilometer measurements revealed a sharp-edged aerosol layer of around 500 m in depth (Fig. 3). The profiling measurements illustrate the small mixing volume available for dispersion.

Simulations of the episode with the COSMO-MUSCAT model (Renner and Wolke, 2010) confirmed the wide extension of a relatively shallow layer of high PM concentrations in Central Europe. However, the simulated PM concentrations were substantially lower than the observations. Two deficiencies of the model are likely to contribute to this misestimation: 1) underestimation of the real emissions, especially during cold periods, 2) inaccurate parameterization of shallow boundary layers for strong thermal inversions.

## Climatological context

We examined the statistical connection between low temperatures and high PM values for the government observation site Radebeul-Wahnsdorf (near Dresden) since 1999. Fig. 4a shows no obvious trend in the annual number of exceedances of the daily limit value. The highest number of exceedances occurred in 2003, 2006, 2009 and 2010. A look at the number of daily minimum temperatures below -7.7°C revealed exactly the four same years as containing the “coldest” winter periods (Fig. 4b). This points to a climatological connection between low ambient temperatures, temperature inversions, and enhanced regional PM concentrations.

## Conclusions

The episode from January 2010 demonstrates that enhanced PM concentrations during winter-time inversion situations still pose a problem for

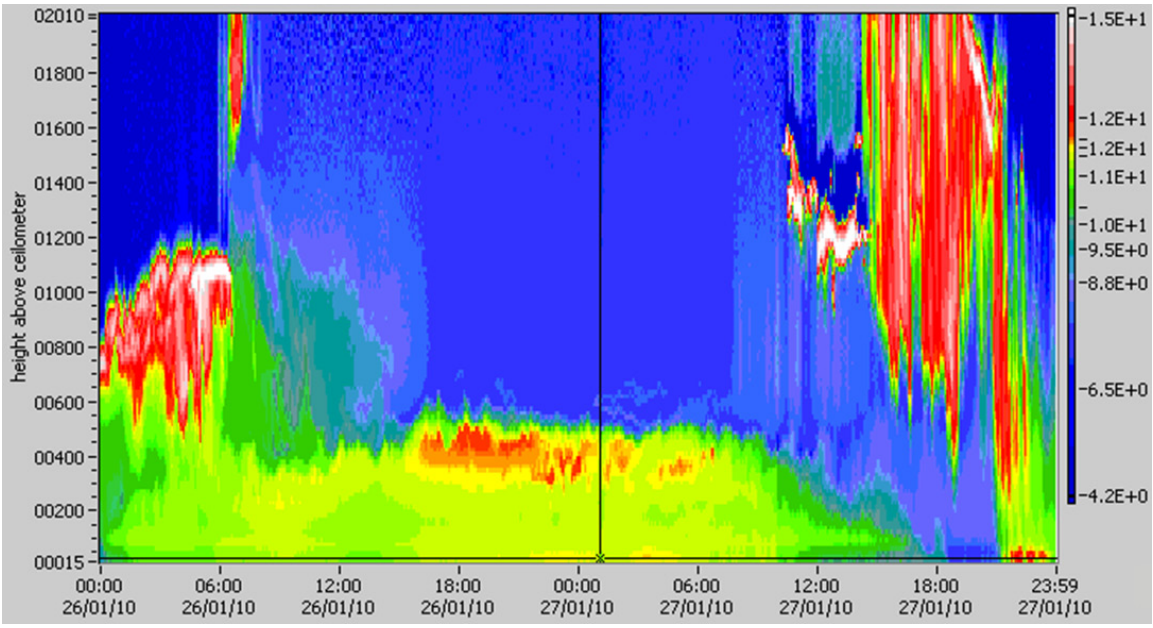


***Fig. 3:*** *Atmospheric backscattering profile of a Jenoptik CHX15k instrument on January 26 and 27, 2010 in Dresden. In the centre of the graph, a sharp-edged aerosol layer of 500 m height can be seen.*

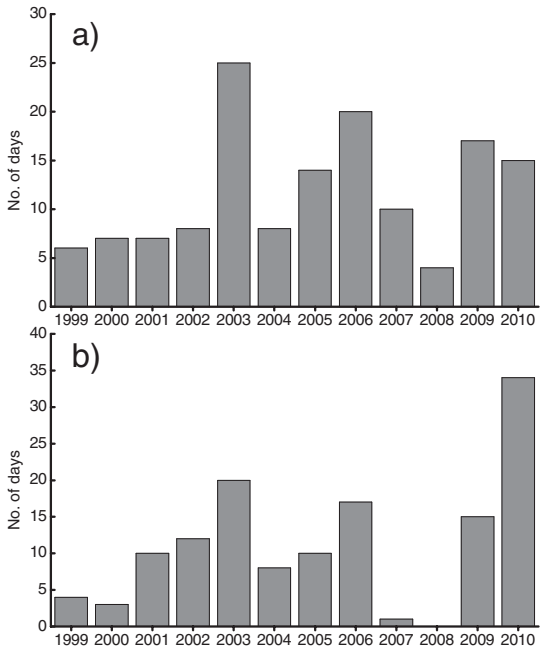


***Fig. 4:*** *Connection between $PM_{10}$ and low temperatures at the government monitoring station Radebeul-Wahnsdorf: a) annual number of exceedances of the daily limit value of $PM_{10}$ (50 µg/m³). b) Annual number of days with temperatures below -7.7 °C.*

air quality legislation and human health. The combination of easterly winds, low temperatures and the temperature inversion proved instrumental in generating the high PM concentrations over several days. Near-future research will focus on the identification of the source areas of these particles and the regional and local dispersion mechanisms.

## References

Engler, C., W. Birmili, G. Spindler, and A. Wiedensohler (2011), Analysis of exceedances in the daily $PM_{10}$ mass concentration (50 µg $m^{-3}$) at a roadside station in Leipzig, Germany, *Atmos. Chem. Phys. Discuss.*, *11*, 15831–15873.

Cattiaux, J., R. Vautard, C. Cassou, P. Yiou, V. Masson-Delmotte, and F. Codron (2010), Winter 2010 in Europe: A cold extreme in a warming climate, *Geophys. Res. Lett.*, *37*, L20704.

Harrison, R.M., J. Stedman, and D. Derwent (2008), Why are $PM_{10}$ concentrations in Europe not falling? *Atmos. Environ*., *42*, 603–606.

Renner, E. and R. Wolke (2010), Modelling the formation and atmospheric transport of secondary inorganic aerosols with special attention to regions with high ammonia emissions. *Atmos Environn, 44,* 1904-1912.

Rückerl, R., A. Schneider, S. Breitner, J. Cyrys and A. Peters (2011), Health effects of particulate air pollution: A review of epidemiological evidence, *Inhal. Toxicol.*, *23*, 555–592.

**Funding**

- The Leibniz Association (PAKT), grant title: “Feinstaubbelastung in städtischen Ballungsgebieten am Beispiel von Dresden und Leipzig”

**Cooperation**

- Federal Environment Agency (UBA), Dessau
- Saxon State Office for Environment, Agriculture and Geology (LfULG), Dresden

# Ten years of aerosol measurements in the upper troposphere by CARIBIC

Markus Hermann[1], Jost Heintzenberg[1], Annica Ekman[2], Andreas Weigel[1], Alfred Wiedensohler[1]

[1] Leibniz Institute for Tropospheric Research (IfT), Leipzig, Germany
[2] Department of Meteorology, Stockholm University, Sweden

*Im Rahmen des CARIBIC Projekts (www.caribic.de) werden seit 1997 einmal pro Monat Messflüge mit einem Messgerätecontainer auf einem Passagierflugzeug durchgeführt. Dabei werden Spurengas- und Aerosolpartikelkonzentrationen in Flughöhen von 8-13 km gemessen. Diese Region, die obere Troposphäre und unterste Stratosphäre (UT/LMS), ist äußerst wichtig im Klimasystem. Das IfT ist in CARIBIC für die Messung der physikalischen Aerosolparameter verantwortlich und hilft das Projekt zu koordinieren. Die gewonnen Daten wurden 2010/11 dazu genutzt erstmals „globale" Verteilungen des UT/LMS Aerosols zu erzeugen und einen Vergleich mit einem globalen Klimamodell durchzuführen. Dabei stellten sich einige Unterschiede zwischen den gemessenen und den modellierten Verteilungen heraus, was auf Unzulänglichkeiten im Modell hindeutet.*

## Introduction

The limited knowledge on aerosol particles in the Earth's atmosphere still causes one of the largest uncertainties concerning climate change [*IPCC*, 2007]. Whereas aerosol measurements at the surface have made progress in recent years, measurements of particles in the free troposphere are still rare. This lack of knowledge is mainly related to technical and financial issues, as e.g. satellite instruments cannot detect ultrafine particles (< 100 nm) and research aircraft flights are too expensive for regular measurements. To partly close this observation gap, the Civil Aircraft for the Regular Investigation of the atmosphere Based on an Instrument Container (CARIBIC) project was initiated in 1994 ([*Brenninkmeijer et al.*, 1999; 2007], www.caribic.de). In CARIBIC, an air-freight container equipped with trace gas and aerosol measurement instruments (Fig. 1) is flown once per month for two to four intercontinental flights onboard a passenger aircraft. Starting 1997 onboard a B767 of Lufttransport Unternehmen (LTU), CARIBIC is hosted since 2004 onboard a Lufthansa (LH) A340. By using a commercial aircraft platform, the costs could be reduced by a factor of about twelve compared to research aircraft.


***Fig. 1:*** *CARIBIC container in the forward cargo compartment of the LH A340-600.*

## Data set

In 2010/11, IfT was operating three CARIBIC instrument units, yielding the number concentration of nucleation (4-12 nm, $N_{4\text{-}12}$) and Aitken plus accumulation mode particles (> 12 nm, $N_{12}$) as well as the size distribution of the accumulation mode (0.12-1.2 µm). The majority of data is obtained at cruise altitude (8-13 km) in the upper troposphere and lowermost stratosphere (UT/LMS), a region most sensitive to, but also important for climate change. Until the end of 2011, 271 successful long-distance flights were carried out by CARIBIC (~2600 h). In the past, this world-wide unique data set was mainly used for process studies. In 2010/11, the CARIBIC aerosol data were also used to compose the first near-global maps for the submicrometer aerosol in the UT/LMS [*Heintzenberg et al.*, 2011] and to compare the data for the first time with results from a global climate model [*Ekman et al.*, 2012].

## First near-global UT/LMS aerosol maps

CARIBIC measurement flights are restricted to the flight corridors of civil aircraft and thus cover only 14% of the globe, when classified into 15°x15° geocells. However, the large-scale dynamics of the UT/LMS suggests extrapolating the measured aerosol concentrations along trajectories to increase this coverage. Therefore, two-day forward and backward trajectories were calculated along the CARIBIC flight tracks. These trajectories where combined with satellite images from the International Satellite Cloud Climatology

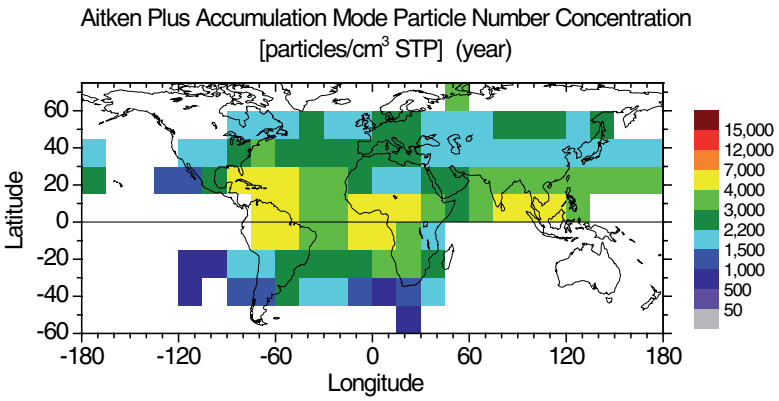


***Fig. 2:*** *Annual map of the Aitken plus accumulation mode (> 12 nm) median particle number concentration (measured and extrapolated values) in 8-13 km altitude.*

Project (ISCCP) in order to detect a cloud contact of the sampled air. An exponential aging function was implemented in the extrapolation algorithm to account for the aging of the aerosol with time. To reduce uncertainties, extrapolation of the particle concentration was finished when either a cloud contact occurred or the two-day limit was reached. Before applying the extrapolation algorithm to the CARIBIC data set, it was validated by comparing measured CARIBIC concentrations with extrapolated CARIBIC concentrations from different flights as well as with measurements from two research campaigns (PEMT-A/B, TRACE-P). The agreement between extrapolated and measured data was surprisingly good and best agreement was achieved with particle lifetimes longer than the maximum length of used trajectories, i.e. two days. Applying the extrapolation algorithm to the CARIBIC data yielded a new data set where the data coverage could be increased to ca. 36% of the globe. From this data set global 15°x15° maps, cross sections and vertical profiles were generated, showing the large-scale distribution of submicrometer aerosol particles in the UT/LMS for the first time. The derived maps reveal regions of high particle number concentrations with frequent new particle formation, in the tropical regions over Africa, South America, the Caribbean, and Southeast Asia (Fig. 2). These regions coincide with those of frequent deep convective clouds. These distributions can now be used for global aerosol model validation.

## First CARIBIC/global climate model data comparison

In recent years, several model studies indicated a significant influence of new particle formation on climate. Freshly formed particles can grow by condensation/coagulation to sizes where they can act as cloud condensation nuclei (CCN). The number of available CCN can have an influence on cloud properties, like cloud albedo and cloud lifetime, and thus on climate. To asses these model results, it is important to check if the models predict the particle formation (magnitude and spatiotemporal distribution) correctly. Therefore, the CARIBIC aerosol data were used in a comparison study with the global climate model MIT-CAM3. Modeled and observed global $N_{4\text{-}12}$ and $N_{12}$ medians agree fairly well (within a factor of two) indicating that the relatively simplified binary $H_2SO_4$-$H_2O$ nucleation parameterization applied in the model produces reasonable results in the UT/LMS. However, a comparison of the spatiotemporal distributions displays a number of discrepancies between model results and CARIBIC data: The vertical transport of carbonaceous aerosols appears to be overestimated by the model. The reason for this overestimation is most likely the constant supersaturation threshold applied in the model for the activation of aerosol particles to cloud droplets. At mid-latitudes, $N_{4\text{-}12}$ is overestimated by

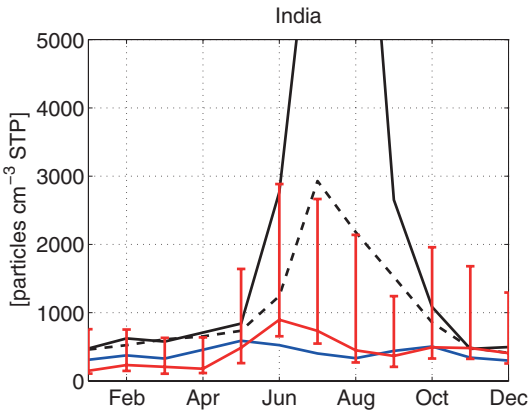


***Fig. 3:*** *Annual cycle of measured (red) and modeled (blue/black, three different simulations) median nucleation mode particle number concentrations for 8-13 km altitude over the Arabian Sea, South Asia, and Bay of Bengal. Error bars denote 25- and 75-percentiles.*

the model which may be due to a too slow growth of the newly formed particles to the Aitken mode and/or due to an insufficient vertical mixing in the UT/LMS region. For the $N_{4\text{-}12}$ particles, the seasonal variability in the modeled concentration is also in poor agreement with CARIBIC data (Fig. 3). This may partly be a result of the annually constant $SO_2$ emissions applied in the model or the lack of condensable organic compounds that may help growth of newly formed clusters in the UT/LMS.

**CARIBIC Future**

The CARIBIC data set, number of users, and scientific impact is continuously growing. Therefore, CARIBIC became part of the In-service Aircraft for a Global Observing System (IAGOS) European Research Infrastructure (ERI), in order to secure operation for the next 10-20 years (www.iagos.org).

**References**

Brenninkmeijer, C. A. M., P. J. Crutzen, H. Fischer, H. Güsten, W. Hans, G. Heinrich, J. Heintzenberg, M. Hermann, T. Immelmann, D. Kersting, M. Maiss, M. Nolle, A. Pitscheider, H. Pohlkamp, D. Scharffe, K. Specht, and A. Wiedensohler (1999), CARIBIC - civil aircraft for global measurements of trace gases and aerosols in the tropopause region, *J. Atmos. Oceanic Technol.*, *16*, 1373-1383.

Brenninkmeijer, C. A. M., P. Crutzen, F. Boumard, T. Dauer, B. Dix, R. Ebinghaus, D. Filippi, H. Fischer, H. Franke, U. Frieß, J. Heintzenberg, F. Helleis, M. Hermann, H. H. Kock, C. Koeppel, J. Lelieveld, M. Leuenberger, B. G. Martinsson, S. Miemczyk, H. P. Moret, H. N. Nguyen, P. Nyfeler, D. Oram, D. O'Sullivan, S. Penkett, U. Platt, M. Pupek, M. Ramonet, B. Randa, M. Reichelt, T. S. Rhee, J. Rohwer, K. Rosenfeld, D. Scharffe, H. Schlager, U. Schumann, F. Slemr, D. Sprung, P. Stock, R. Thaler, F. Valentino, P. van Velthoven, A. Waibel, A. Wandel, K. Waschitschek, A. Wiedensohler, I. Xueref-Remy, A. Zahn, U. Zech, and H. Ziereis (2007), Civil Aircraft for the regular investigation of the atmosphere based on an instrumented container: The new CARIBIC system, *Atmos. Chem. Phys.*, *7*, 4953-4976.

Ekman, A. M. L., M. Hermann, P. Groß, J. Heintzenberg, D.-C. Kim, and C. Wang (2012), Sub-micrometer aerosol particles in the upper troposphere/lowermost stratosphere as measured by CARIBIC and modeled using the MIT-CAM3 global climate model. Accepted by *J. Geophys. Res.*

Heintzenberg, J., M. Hermann, A. Weigelt, A. Clarke, V. Kapustin, B. Anderson, K. Thornhill, P. van Velthoven, A. Zahn, and C. Brenninkmeijer (2011), Near-global aerosol mapping in the upper troposphere and lowermost stratosphere with data from the CARIBIC project, *Tellus B*, 63, 875–890, DOI: 10.1111/j.1600-0889.2011.00578.x.

IPCC (2007), *Climate Change 2007: The Physical Science Basis*, 996 pp., Cambridge University Press, Cambridge.

**Funding**
- European Commission (EC), Brussels, Belgium
- Federal Ministry of Education and Research (BMBF), Bonn, Germany
- German Research Foundation (DFG), Bonn, Germany

**Cooperation**
- Max Planck Institute for Chemistry (MPI-C), Mainz, Germany
- Karlsruhe Institute of Technology (KIT), Karlsruhe, Germany
- Forschungszentrum Jülich (FZJ), Jülich, Germany
- German Aerospace Center (DLR), Oberpfaffenhofen, Germany
- University of Lund, Lund, Sweden
- University of Stockholm, Stockholm, Sweden
- Royal Netherlands Meteorological Institute (KNMI), De Bilt, Netherlands

# LACROS: Leipzig Aerosol and Cloud Remote Observations System

Ulla Wandinger, Patric Seifert, Ronny Engelmann, Dietrich Althausen, Birgit Heese, Jörg Schmidt, Johannes Bühl, Annett Skupin, Albert Ansmann, Andreas Macke

*Aktuelle Schwerpunkte der Atmosphärenforschung betreffen Fragen zur Niederschlagsbildung und der Aerosol-Wolken-Interaktion einschließlich deren Auswirkungen auf den Strahlungshaushalt der Atmosphäre. Die Erfassung zugehöriger Prozesse erfordert neue Messstrategien, die auf dem Informationsgewinn durch die Anwendung verschiedenster Messsysteme basieren. Einhergehend mit dieser Anforderung wurde am IfT Leipzig die mobile Beobachtungsstation "Leipzig Aerosol and Cloud Remote Observations System" LACROS konzipiert. LACROS vereint aktive und passive Fernerkundungsinstrumente, die die höhenaufgelöste Beobachtung von Aerosol- und Wolkeneigenschaften in der gesamten Troposphäre ermöglichen. Kern von LACROS sind das 35-GHz- Wolkenradar MIRA-35 sowie ein Mehrwellenlängen-Polarisations-Raman-Lidar. Schwerpunkte zukünftiger Studien liegen in der Untersuchung von heterogenen Eisbildungsprozessen sowie der Entwicklung und Verifizierung von Algorithmen zur Bestimmung von wolkenmikrophysikalischen Eigenschaften. LACROS ist bereits fest für die für 2013 angesetzten Kampagnen „High Definition Clouds and Precipitation for advancing Climate Prediction" (HD(CP)²) sowie das „Saharan Aerosol Long-range Transport and Aerosol-Cloud-Interaction Experiment" (SALTRACE) eingeplant.*

## Introduction

During the last decade active remote sensing of aerosol-cloud interaction processes with lidar gained increasing relevance at IfT Leipzig. One of the main conclusions of these studies is that heterogeneous ice formation at temperatures between –40 and 0°C is considerably driven by the amount and type of aerosol particles that act as ice nuclei [*Kanitz et al.*, 2011]. However, aerosol-cloud interaction studies solely based on lidar techniques are restricted to scenarios with optically thin cloud layers. Optically thick clouds cannot be penetrated by the laser beam of the lidar. Hence, lidar alone is not capable of documenting aerosol-cloud interaction processes in their full extent. The large number of unsolved questions concerning the interaction between aerosol particles and clouds and corresponding indirect effects on precipitation and radiative transfer demand new measurement strategies to resolve the atmospheric processes involved. In this regard, obtaining synergistic information about cloud and aerosol properties from multi-instrument observations is a key approach to overcome the current lack of knowledge. Motivated by these needs, the novel mobile multi-instrument platform Leipzig Aerosol and Cloud Remote Observations System – LACROS – has been set up at IfT.

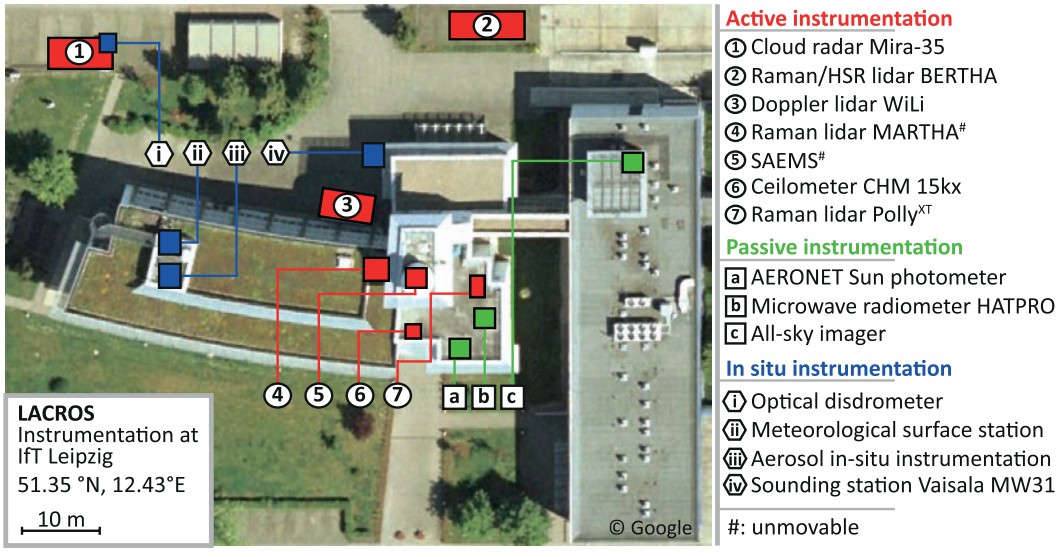


***Fig. 1:*** *Instrumentation of LACROS at IfT. Besides MARTHA (4) and SAEMS (5) all instruments are mobile or at least available in a mobile version.*

## Instrumentation

LACROS comprises a unique set of active and passive remote-sensing instruments, which are to a large extent containerized and available for application in field campaigns. The instruments of LACROS are shown in Fig. 1. In 2011, the 35-GHz cloud radar MIRA-35 and the microwave radiometer HATPRO have been integrated. The active-remote-sensing branch now spans the wavelength range from the UV to microwave radiation, which is covered with multiwavelength-Raman-polarization lidar (Multiwavelength Atmospheric Raman lidar for Temperature, Humidity, and Aerosol profiling – MARTHA, Backscatter Extinction lidar-Ratio Temperature Humidity profiling Apparatus – BERTHA, POrtabLe Lidar sYstem – Polly$^{XT}$), high-spectral-resolution lidar (BERTHA), a ceilometer CHM 15kx, the Doppler Wind Lidar (WiLi), and the cloud radar. The Spectral Aerosol Extinction Measurement System (SAEMS) provides spectrally resolved extinction coefficients of aerosols under ambient conditions at about 30 m above ground. Passive instrumentation, which helps to interpret the active remote measurements, consists of an Aerosol Robotic Network (AERONET) Sun photometer, the microwave radiometer HATPRO that includes also two infrared radiometers, pyranometer for radiative flux measurements, and an all-sky imager. Meteorological surface data and radiosonde measurements are available as well. For the determination of precipitation properties an optical disdrometer records the velocity and size distribution of falling hydrometeors in the size range from 0.1 to 10 mm at 4 m above ground.

## Fields of Application

The available lidar systems measure the optical and microphysical properties of aerosols and thin clouds, vertical winds within aerosol layers and at cloud base, as well as temperature and humidity profiles. The integration of the cloud radar into LACROS overcomes the limitation of the lidar systems to observe only cloud-free and thin-cloud (cirrus, altocumulus) scenarios. It enables extensive insights into the microphysical and dynamical processes of thick stratiform and convective clouds, and thus the investigation of droplet activation and precipitation formation in convective cloud systems. This achievement will facilitate novel links between atmospheric measurements, laboratory studies, and modeling activities. The future application of LACROS concentrates on three main subjects:

(1) Investigation of heterogeneous ice-formation processes by exploiting co-located remote-sensing observations of aerosol and cloud radiative and microphysical properties.

(2) Instrument validation and development of algorithms and new measurement techniques for cloud and aerosol microphysics retrieval in the frame of the Aerosols, Clouds, and Trace gases Research InfraStructure Network (ACTRIS). Here, activities will concentrate on the development of the dual-field-of-view lidar technique to derive cloud droplet size information and on retrievals of aerosol microphysical properties from combined lidar and Sun photometer measurements. In this context, the CLOUDNET algorithms [*Illingworth*, 2007] have been implemented at IfT. CLOUDNET already provides a framework for the determination of cloud microphysics from remote-sensing observations, but further extensions are needed to improve reliability and availability.

(3) Deployment during field campaigns in key regions of atmospheric research. LACROS is

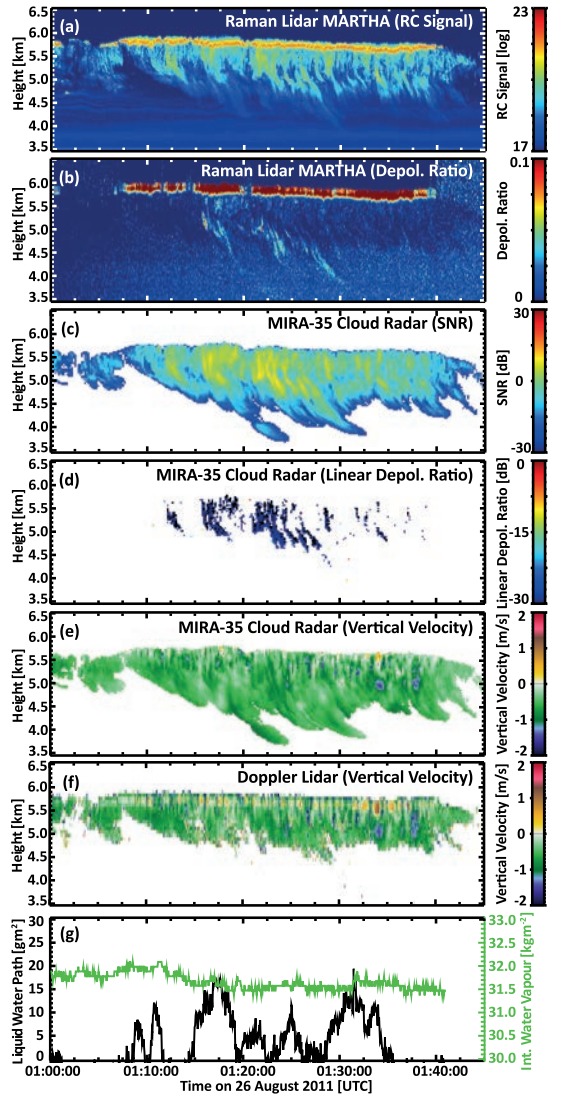


*Fig. 2: Combined LACROS observation of an ice-precipitating altocumulus layer on 26 August 2011. Shown are measurements of MARTHA (a,b), MIRA-35 (c-e), WiLi (f), and HATPRO (g); RC Signal – range-corrected signal, SNR – signal-to-noise ratio.*

already scheduled for the deployment in field campaigns at Barbados and in Jülich, Germany, which will both take place in 2013.

## Measurement Example

Figure 2 provides insight into the measurement capabilities of LACROS. Shown is the observation of an ice-precipitating altocumulus layer that occurred at heights from 4.5 to 6 km between 0100 and 0140 UTC on 26 August 2011. The measurements were performed with the Raman lidar MARTHA (a,b), cloud radar MIRA-35 (c-e), Doppler lidar WiLi (f), and microwave radiometer HATPRO (g). The lidar measurements of the 1064-nm range-corrected signal (a) and the 532-nm depolarization ratio (b) indicate that the cloud layer was topped with an optically thick, about 200 m deep liquid-water layer. Beneath the liquid-water layer, ice crystals were precipitating. The amount of liquid water present in the liquid-water layer is derived from measurements of HATPRO (g, black line). The total amount of water vapor available in the atmospheric column is provided as well (g, green line). No liquid-water layer is indicated in the cloud radar measurements (c-e), because the radar is much more sensitive to the larger ice crystals due to the long wavelength of 0.8 cm of the emitted signal. This also explains the differences in the observed vertical velocities between MIRA-35 (e) and the Doppler lidar (f). In the liquid layer, WiLi is sensitive to the motion of the numerous small water droplets whereas MIRA-35 already detects the fall velocity of the larger ice crystals. Below the liquid layer, the vertical velocities measured with both systems are similar. Further analysis of the measurement would reveal the lidar-derived optical and microphysical properties of the aerosol particles present at cloud level from which the number of cloud condensation nuclei and ice nuclei could be estimated. Spectral information from the radar signal and velocity data would yield information about the size distribution of the scattering hydrometeors.

## References

Kanitz, T., P. Seifert, A. Ansmann, R. Engelmann, D. Althausen, C. Casiccia, and E. G. Rohwer (2011), Contrasting the impact of aerosols at northern and southern midlatitudes on heterogeneous ice formation, *Geophys. Res. Lett.*, 38, L17802 , doi:10.1029/2011GL048532.

Illingworth, A. J., R. J. Hogan, E. J. O'Connor, D. Bouniol, M. E. Brooks, J. Delanoë, D. P. Donovan, J. D. Eastment, N. Gaussiat, J. W. F. Goddard, M. Haeffelin, H. Klein Baltink, O. A. Krasnov, J. Pelon, J.-M. Piriou, A. Protat, H. W. J. Russchenberg, A. Seifert, A. M. Tompkins, G.-J. van Zadelhoff, F. Vinit, U. Willen, D. R. Wilson, and C. L. Wrench (2007), Cloudnet, *Bull. Am. Meteorol. Soc.*, 88, 883-898, doi:10.1175/BAMS-88-6-883.

**Funding**

- The implementation of the cloud radar and microwave radiometer was funded by the Bundesministerium für Bildung und Forschung under grant number 01LP10011A

# Functionalized carboxylic acids in particles: Seasonal trends and possible sources

Dominik van Pinxteren, Monique Teich, Hartmut Herrmann

*Carbonsäuren, die neben der Carboxylgruppe noch mindestens eine weitere funktionale Gruppe (z.B. eine Hydroxy-, Oxo- oder Nitrogruppe) tragen, wurden bisher noch wenig bis kaum untersucht. Als stabile Produkte atmosphärenchemischer Oxidationsprozesse kann ihre Bestimmung jedoch interessante Einblicke in die Chemie der Atmosphäre erlauben. Im Rahmen des DFG Projektes FUCAPAC wurde daher eine Methode entwickelt, mit der diese in sehr niedrigen Konzentrationen vorliegenden Verbindungen in wässrigen Partikelextrakten bestimmt werden können. Die Auswertung eines ganzjährigen Datensatzes der $PM_{10}$ Konzentrationen von 28 verschiedenen Carbonsäuren zeigt unterschiedliche jahreszeitliche Trend und erlaubt verschiedenen Vorschläge für Quellen und Bildungswege dieser Verbindungen.*

## Introduction

Tropospheric particles contain a huge variety of water soluble organic compounds [*Saxena and Hildemann*, 1996]. Among them, short-chain dicarboxylic acids (e.g. oxalic acid) are known to be one of the most abundant compound classes. Their relatively high concentrations led to a large body of field data within the past decades. Much less is known, however, for longer-chain carboxylic acids (C5-C10) which have been identified in great number within atmospheric particles [*van Pinxteren and Herrmann*, 2007]. Among these, many acids with an additional functional group (e.g. hydroxy-, oxo-, carboxyl-, or nitro-group) were included. Such functionalized carboxylic acids are likely products of oxidation processes and their determination could help to better understand the chemical processes taking place in the atmosphere.

Therefore, one year of $PM_{10}$ filter samples from the rural IfT research site Melpitz was analyzed for functionalized carboxylic acids within the DFG project FUCAPAC.

## Experimental

A sample preparation method was developed for sample clean-up and enrichment. It is based on a relatively new technique termed "hollow fibre liquid phase microextraction". A water insoluble liquid membrane is immobilized within the pores of a short piece (12 cm) of a hollow fibre, which is then filled with an alkaline acceptor solution and dipped into the acidified sample (donor phase). During an extraction time of 2 hours, the free carboxylic acids partition into the liquid membrane and from there into the acceptor phase, where they are being trapped as carboxylates due to the high pH. Several parameters of the extraction were optimized to result in a method which yields high enrichment (up to a factor of 120) and relatively clean extracts. The method was applied to a total of 256 24h $PM_{10}$ samples from Melpitz and 28 acids were quantified from the extracts by capillary electrophoresis -

| Compound | min | mean | max |
|---|---|---|---|
| **Oxidized monocarboxylic acids** | | | |
| 4-oxopentanoic acid | 0,4 | 2,7 | 19,2 |
| 6-oxoheptanoic acid | 0,6 | 1,1 | 4,9 |
| 7-oxooctanoic acid | 0,3 | 0,8 | 8,6 |
| 8-hydroxyoctanoic acid | 0,2 | 0,6 | 3 |
| **Aromatic monocarboxylic acids** | | | |
| benzoic acid | 0,02 | 0,3 | 4,6 |
| cinnamic acid | 0,001 | 0,2 | 3,5 |
| 2-hydroxybenzoic acid | 0,1 | 0,5 | 6,9 |
| 3-hydroxybenzoic acid | 0,002 | 0,7 | 9,1 |
| 4-hydroxybenzoic acid | 0,003 | 1,1 | 18,7 |
| **Aromatic dicarboxylic acids** | | | |
| phthalic acid | 0,1 | 3,8 | 39,6 |
| terephthalic acid | 0,03 | 2 | 38 |
| 4-methylphthalic acid | 0,003 | 1,3 | 13,4 |
| homophthalic acid | 0,01 | 0,6 | 4,6 |
| **Nitrated aromatic monocarboxylic acids** | | | |
| 2-hydroxy-3-nitrobenzoic acid | 0,003 | 0,4 | 5,7 |
| 2-hydroxy-4-nitrobenzoic acid | 0,000 | 0,06 | 0,6 |
| 2-hydroxy-5-nitrobenzoic acid | 0,01 | 0,4 | 3,5 |
| **Aliphatic dicarboxylic acids** | | | |
| glutaric acid | 0,01 | 4 | 19 |
| adipic acid | 1 | 7,8 | 57 |
| pimelic acid | 0,3 | 1,6 | 10,9 |
| suberic acid | 0,5 | 1,9 | 16,4 |
| azelaic acid | 0,7 | 3,6 | 33 |
| sebabic acid | 0,2 | 0,6 | 6 |
| **Oxidized dicarboxylic acids** | | | |
| citramalic acid | 0,2 | 4,4 | 10,5 |
| 2-isopropylmalic acid | 0,06 | 1,5 | 8,4 |
| 3-hydroxy-3-methylglutaric acid | 0,1 | 1,7 | 9,1 |
| 4-oxopimelic acid | 0,2 | 6,1 | 34,1 |
| 5-oxoazelaic acid | 0,02 | 4,7 | 25,8 |
| 4-oxosebabic acid | 0,03 | 1,4 | 10 |

***Tab. 1:*** *Minimum, maximum, and mean concentrations in ng $m^{-3}$ for all determined carboxylic acids.*

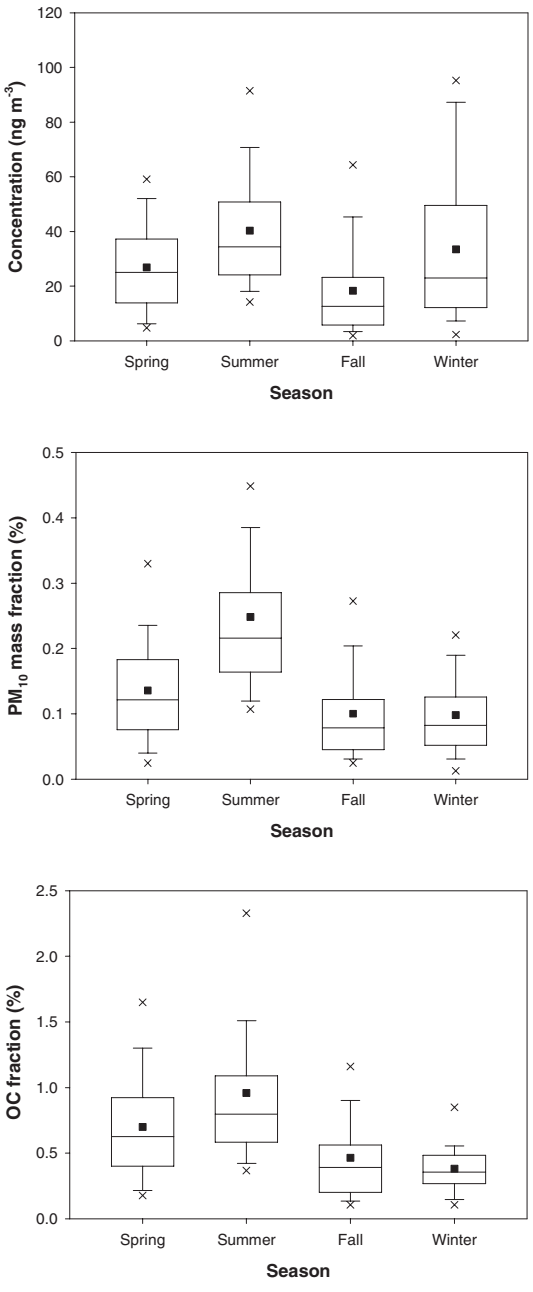


***Fig. 1:*** *Box-whisker plots of concentration, $PM_{10}$ mass fraction and OC fraction of the sum of all determined acids for different seasons. The boxes indicate the 25, 50, and 75% quantiles, the whiskers the 10 and 90% quantiles, the crosses the 5 and 95% quantiles, and the black square marks the mean value.*

mass spectrometry using the method of standard addition.

## Results

In Tab. 1 all determined carboxylic acids are given with their observed concentration range and mean concentration. As can be seen, typical concentrations lie in the low ng $m^{-3}$ range, maximum values, however, can reach up to several tens of ng $m^{-3}$. The concentration of the sum of all acids explained between 0.003 and 1.1% of total $PM_{10}$ mass (mean 0.15%) and between 0.01 and 4.5% of $PM_{10}$ organic carbon (OC, mean 0.6%).

The seasonal trends of concentration, $PM_{10}$ mass fraction, and OC fraction are shown in Fig. 1 as box-whisker plots for the sum of all acids. As can be seen, the concentration shows two maxima, one during summer and another one during winter. This likely indicates different sources of the carboxylic acids: Photochemistry in summer and primary emissions in winter. Both the $PM_{10}$ mass contribution as well as the OC fraction clearly peak in summer with the "darker" seasons showing much lower values. This highlights the importance of secondary organic material during spring and summer.

In Fig. 2, examples of typical seasonal trends for four single acids are given. For the two aromatic acids 4-hydroxybenzoic acid and 2-hydroxy-3-nitrobenzoic acid a clear winter maximum can be observed. It is thus likely that these acids are emitted from primary sources. Hydroxybenzoic acids were for example detected in biomass combustion aerosol [*Iinuma et al.*, 2007], which is an important emission source in winter. The nitrated salicylic acids are detected in atmospheric particles for the first time within this work. Besides primary emission, possibly from combustion processes as well, they could also be formed by secondary reactions. For nitrophenols it is known that their most important formation mechanism is the nitration of phenol, leading predominantly to 2-nitrophenol and 4-nitrophenol due to the ortho/para-directing effect of the hydroxyl-group [*Harrison et al.*, 2005]. Similarly, 2-hydroxybenzoic acid could be the precursor for the three 2-hydroxy-nitrobenzoic acid isomers that were detected. As the carboxylic group has a meta-directing effect, 2-hydroxy-3-nitrobenzoic acid and 2-hydroxy-5-nitrobenzoic acid would be expected as the main products of the nitration reaction. Indeed, these two compounds were detected in many more samples than the 2-hydroxy-4-nitrobenzoic acid isomer (ca. 250 vs. 50) and their mean annual concentration is about one order of magnitude higher (Tab. 1). These findings support the idea that the nitro-compounds are at least in part formed from the respective hydroxybenzoic acid in the atmosphere.

The two aliphatic acids azelaic acid (C9 dicarboxylic acid) and 5-oxoazelaic acid shown in Fig. 2 both have summer concentration maxima, with the latter one showing a very pronounced concentration increase during summer. This indicates the importance of secondary sources for these compounds. Azelaic acid is known to be a product of the oxidation of oleic acid, an unsaturated fatty acid emitted by plants and algae [*Stephanou and Stratigakis*, 1993]. Interestingly, the mean concentration of 5-oxoazelaic acid is

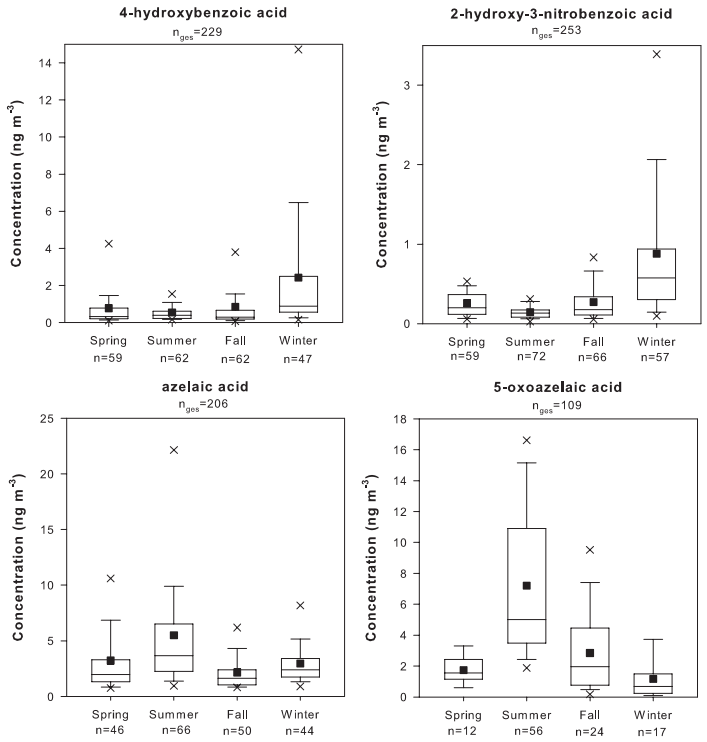


***Fig. 2:*** *Box-whisker plots of the concentrations of two aromatic and two aliphatic carboxylic acids for different seasons. The number of data points above the detection limit is indicated. The boxes indicate the 25, 50, and 75% quantiles, the whiskers the 10 and 90% quantiles, the crosses the 5 and 95% quantiles, and the black square marks the mean value.*

higher than that of azelaic acid during summer, while it is similar or lower during the other seasons. An oxidation of dicarboxylic acids to their oxo-derivatives has been suggested in the literature [*Römpp et al.*, 2006], which could likely lead to the observed concentration trend.

## References

Harrison, M. A. J., S. Barra, D. Borghesi, D. Vione, C. Arsene, and R. L. Olariu (2005), Nitrated phenols in the atmosphere: a review, *Atmos. Environ.*, *39*(2), 231-248.

Iinuma, Y., E. Brüggemann, T. Gnauk, K. Muller, M. O. Andreae, G. Helas, R. Parmar, and H. Herrmann (2007), Source characterization of biomass burning particles: The combustion of selected European conifers, African hardwood, savanna grass, and German and Indonesian peat, *J. Geophys. Res. - Atmos.*, *112*(D8), D08209, Doi 10.1029/2006jd007120.

Römpp, A., R. Winterhalter, and G. K. Moortgat (2006), Oxodicarboxylic acids in atmospheric aerosol particles, *Atmos. Environ.*, *40*(35), 6846-6862.

Saxena, P., and L. M. Hildemann (1996), Water-soluble organics in atmospheric particles: A critical review of the literature and application of thermodynamics to identify candidate compounds, *J. Atmos. Chem.*, *24*(1), 57-109.

Stephanou, E. G., and N. Stratigakis (1993), Oxocarboxylic and α,ω-dicarboxylic acids: Photooxidation products of biogenic unsaturated fatty acids present in urban aerosols, *Environ. Sci. Technol.*, *27*(7), 1403-1407.

van Pinxteren, D., and H. Herrmann (2007), Determination of functionalised carboxylic acids in atmospheric particles and cloud water using capillary electrophoresis/mass spectrometry, *J. Chromatogr. A*, *1171*(1-2), 112-123, Doi 10.1016/j.chroma.2007.09.021.

**Funding**
- German Research Foundation (DFG), Bonn, Germany

# Tropospheric multiphase amine chemistry: Laboratory studies and modeling

Christian Weller, Andreas Tilgner, Hartmut Herrmann

*Bei der Verwendung von Aminwäsche zur $CO_2$-Abscheidung aus Rauchgas von Kraftwerken kann es zur Emission von geringen Mengen der eingesetzten Amine kommen. In der vorliegenden Studie wurden der chemische Abbau und die Umwandlung verschiedener Amine und deren mögliche Folgeprodukte umfassend durch Laborexperimente und anschließende troposphärische Multiphasenchemiemodellierung charakterisiert. OH-Radikalreaktionen sind die hauptsächliche Umwandlungsroute für Amine unter der Bildung von Amiden während Nitrosamine nur in sehr geringem Ausmaß in der Troposphäre gebildet werden.*

## Introduction

Amine based solvent technology is an option to realize $CO_2$ capture from the exhaust of power plants. Amines may potentially be released in trace amounts during the carbon capture and storage (CCS) process. Gassnova, representing the Norwegian Government, has initiated an extensive investigation program with the objective of developing a set of methods and procedures for evaluating health and environmental impacts of amine solvents. To investigate the tropospheric chemical fate of amines from $CO_2$ capturing processes and their oxidation products in the present study, aqueous phase reactivity experiments with different amines and their corresponding nitrosamines and multiphase modelling were performed. The modeling work was specifically designed to resemble conditions present at a planned power plant with $CO_2$ capture in the area close to Bergen, Norway.

## Laboratory investigations of amine degradation and conversion reactions

Aqueous phase reactivity experiments with the amines dimethylamine (DMA), diethanolamine (DEA), pyrrolidine (PYL) and their corresponding nitrosamines have been performed. Quantum yields for nitrosamine photolysis at 313 and 366 nm have been obtained from experiments and range between 0.32 and 0.43 with no significant influence of pH and wavelength in the range studied. $NO_3$ radical reaction rate constants for DMA, DEA and PYL are on the order of ~$10^5$ $M^{-1}s^{-1}$ and ~$10^8$ $M^{-1}s^{-1}$ for nitrosodimethylamine (NDMA), nitrosodiethanolamine (NDEA) and nitrosopyrrolidine (NPYL). Rate constants for nitrosamines show a weak dependence on temperature (Fig. 1). Ozone is unreactive towards amines and nitrosamines. Furthermore, aqueous nitrosamine formation has been investigated. Measured nitrosation rate constants range from $10^{-3}$ to $10^{-1}$ $M^{-1}s^{-1}$ with mean values on the order of $10^{-2}$ $M^{-1}s^{-1}$. Therefore, an upper limit of

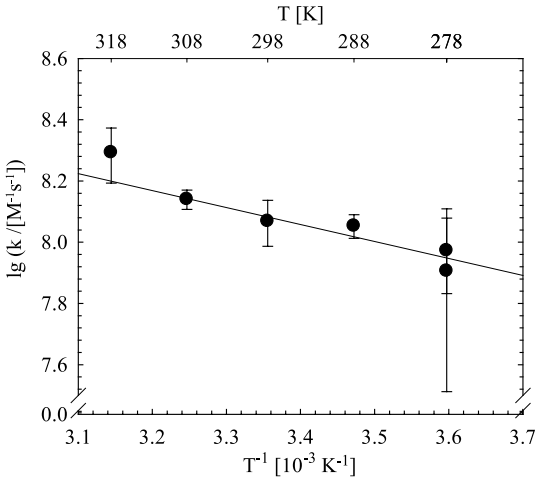


***Fig. 1:*** *Plot of temperature dependent rate constants of NDMA with $NO_3$ radical (Arrhenius plot).*

$k_{2nd\ nitrosation}$ = 0.1 $M^{-1}s^{-1}$ has been used for the multiphase modeling for all investigated amines. No experimental evidence for an overall third order nitrosation reaction was found and thus a second order reaction between $NO_2^-$/HONO and the amines was assumed.

## Multiphase chemical modeling of amines and their degradation products

A complex chemical reaction module describing the multiphase chemistry of amines and their oxidation products has been developed. The full amine mechanism module contains in total 71 gas phase reactions and 220 aqueous phase reactions, 39 equilibrium reactions and 42 phase transfers. The amine reaction module was coupled to a complex state of the art multiphase chemistry mechanism, RACM-MIM2ext/CAPRAM3.0i [*Tilgner and Herrmann*, 2010], and finally applied within the SPectral Aerosol Cloud Chemistry Interaction Model (SPACCIM) model framework [*Wolke et al.*, 2005]. SPACCIM simulations have been performed for summer and winter conditions, different environmental

trajectories and different initial amine concentration levels, investigating the chemical fate of amines and their oxidation products in the tropospheric multiphase system including the potential to form environmental harmful compounds such as nitrosamines and amides.

The model calculations show that amines can be oxidized readily by OH radicals in both the gas and the aqueous phase during daytime summer conditions. The importance of either phase depends strongly on the partitioning of the different amines. The model results show that for DMA the gaseous oxidation is much more important than for monoethanolamine (MEA) and DEA, which are mostly present in the aqueous phase under the simulated conditions (illustrated by Fig. 2). Moreover, the model simulations have revealed that the oxidation of amines is quite restricted under low photochemical winter conditions leading to quite long lifetimes under those conditions. For this reason, the parcel model studies implicated that the deposition of quite soluble amines and the corresponding input into other environmental compartments might be a relevant process. This should be studied in detail by the foreseen regional dispersion model applications.

Furthermore, the model simulations have clearly revealed that the formation of nitrosamines by aqueous reactions with $HONO/NO_2^-$ should not be a relevant process under typical tropospheric conditions. Gaseous formation of N-nitroso amines has been shown to be more important leading to, however, very low gaseous N-nitroso amine concentrations below 0.2 ppt (Fig. 3). In contrast to the N-nitroso amines, the model simulation have shown much higher concentrations for amides, which can be effectively formed and oxidized particularly under daytime cloud conditions. Model runs with aqueous amine chemistry have predicted usually much lower amide levels than model runs without aqueous phase amine chemistry. However, clouds represent not just an important sink for amides, the model calculations have also revealed that often produced imines might be rapidly degraded in tropospheric clouds leading to the formation of smaller amine compounds.

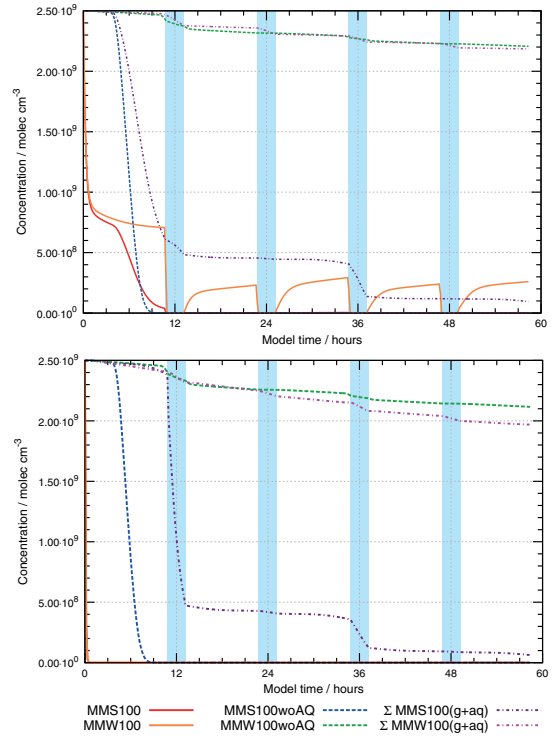


***Fig. 2:*** *Simulated dimethylamine (DMA, top) and diethanolamine (DEA, bottom) time concentration profiles.*

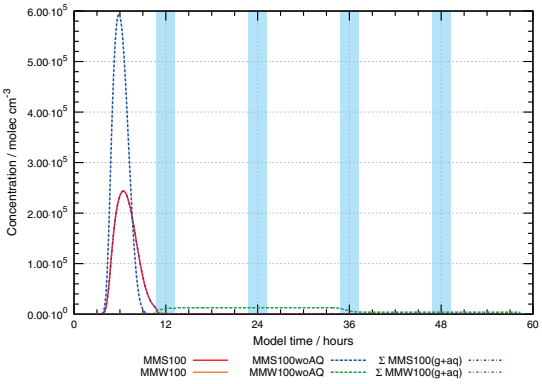


***Fig. 3:*** *Simulated nitrosodimethylamine (NDMA) concentration time profiles.*

The chemical sink and source studies have revealed that both cloud droplets and deliquescent particles are important for the multiphase amine chemistry. Furthermore, the detailed flux studies have shown that in the most cases the OH radical represents the main aqueous radical oxidant. However, in some case also the Cl and $NO_3$ radical pathways can contribute to a substantial amount to the degradation of amines and their further oxidized products such as amides.

In conclusion, the model runs have shown the importance of the aqueous phase to be an important compartment for the multiphase processing of amines and their reactions products as well as the need to develop and consider a reduced multiphase amine scheme for future regional scale dispersion model applications.

## References

Tilgner, A., and H. Herrmann (2010), Radical-driven carbonyl-to-acid conversion and acid degradation in tropospheric aqueous systems studied by CAPRAM, Atmos. Environ., 44(40), 5415-5422.

Wolke, R., A. M. Sehili, M. Simmel, O. Knoth, A. Tilgner, and H. Herrmann (2005), SPACCIM: A parcel model with detailed microphysics and complex multiphase chemistry, Atmos. Environ., 39(23-24), 4375-4388.

**Funding**
- Gassnova, Norwegian state enterprise for carbon capture and storage, Porsgrunn, Norway

**Cooperation**
- UiO, University of Oslo, Oslo, Norway
- Tel-Tek, Research institute, Porsgrunn, Norway

# CAPRAM mechanism extension and coupling to MCMv3.1

Peter Bräuer, Andreas Tilgner, Roland Schrödner, Ralf Wolke, Hartmut Herrmann

*Zur umfassenden Beschreibung der Oxidation von organischen Verbindungen in der Troposphäre wurde ein Multiphasenchemiemechanismus entwickelt. Dazu wurde der bereits bestehende Gasphasenmechanismus MCM an den Flüssigphasenmechanismus CAPRAM 3.0i gekoppelt. Die Flüssigphasenchemie wurde mit Hilfe eines automatisierten Mechanismusgenerators erweitert, der in Zusammenarbeit mit dem LISA in Paris, Frankreich entwickelt wurde. Bei der Auswertung der Ergebnisse aus anschließenden Modellrechnungen mit dem Trajektorienmodell SPACCIM wurden Konzentrationsprofile ausgewertet sowie umfangreiche zeitaufgelöste Studien zu den Quell- und Senkenflüssen troposphärisch relevanter Verbindungen durchgeführt.*

## Introduction

Volatile organic compounds (VOCs) are ubiquitous in the tropospheric multiphase system. With large biogenic and anthropogenic sources they play an important role in atmospheric research. In the progressive oxidation process a multitude of intermediates with changing physical properties are formed that can partition into the tropospheric aqueous phase, i.e. deliquescent particles and cloud droplets. Their further oxidation in the aqueous phase will not only alter the chemical composition of deliquescent particles and cloud droplets, but upon phase transfer also the gas phase composition. Hence, it is important to precisely describe the fate of VOCs in either compartment. However, comprehensive oxidation schemes exist mainly for the gas phase. In the aqueous phase, the most comprehensive chemistry mechanism, the Chemical Aqueous Phase RAdical Mechanism [CAPRAM 3.0i, see *Tilgner and Herrmann*, 2010], is complete only for organic compounds with up to two carbon atoms (C2 compounds) while chemistry up to the oxidation of C4 compounds is only partly implemented.

## CAPRAM mechanism development

The focus of the CAPRAM mechanism development is on a near-explicit description of the oxidation of organics in the tropospheric aqueous phase. However, one always has to consider the link to the gas phase and a description of the oxidation in an equally adequate manner in that compartment. With the latest developments of CAPRAM 3.0i the coupled gas phase mechanism RACM-MIM2ext [*Tilgner and Herrmann*, 2010] did not meet these needs anymore with only 281 reactions and many lumped species compared to the fully explicit aqueous phase mechanism with 777 reactions. Therefore, CAPRAM 3.0i has been linked to the Master Chemical Mechanism [MCM, see *Saunders et al.*, 2003] with 11381 reactions. The coupling and the necessary modifications to the SPectral Aerosol Cloud Chemistry Interaction Model [SPACCIM; see *Wolke et al.*, 2005] used for the simulations were performed in close cooperation with the modeling department.

However, the main focus is on the further development of the aqueous oxidation scheme. Yet, with a rising complexity of the mechanism and a growing number of reactions, a manual creation of oxidation schemes is almost impossible and automation methods become necessary. Therefore, a mechanism generator has been developed, which fully automatically generates large explicit oxidation schemes of any organic compound. The work was performed in close cooperation with the Laboratoire inter-universitaire des Systèmes Atmosphériques (LISA). There, such a generator has already been developed for the gas phase. The Generator for Explicit Chemistry and Kinetics of Organics in the Atmosphere [GECKO-A, *Aumont et al.*, 2005] has been modified to be used for the aqueous phase as well. A protocol has been developed for the automated creation of aqueous phase oxidation schemes. The protocol is based on a comprehensive experimental database and evaluated prediction methods. The prediction of rate constants was mainly done by structure-activity relationships (SARs).

## SPACCIM model studies

Model studies have been performed with the parcel model SPACCIM and the recently created multiphase chemical mechanism MCMv3.1 and an extended CAPRAM mechanism. A standard meteorological scenario with non-permanent clouds under remote continental and urban conditions [see *Tilgner and Herrmann*, 2010] was chosen for the model runs.

In a first attempt, the C3 chemistry in CAPRAM 3.0i has been extended. Therefore, the phase transfer of aliphatic alcohol, carbonyl, and carboxyl compounds present in MCMv3.1, yet missing in CAPRAM 3.0i have been implemented. Missing experimental data were estimated with

the structure-activity relationship GROMHE [*Raventos-Duran et al.*, 2010]. In the aqueous phase GECKO-A was applied, which produced 145 new species and 225 new reactions of which 26 species undergo phase transfer. The influence of the new C3 scheme on the concentration profiles of important organic and inorganic species was investigated. In addition, detailed time-resolved flux analyses have been performed to study important subsystems together with the production and destruction pathways of key compounds.

One chemical subsystem investigated was the malonic acid production. In Fig. 1 modeled aqueous phase concentration profiles are plotted for simulations with (black line) and without (red line) the C3 extension. While malonic acid oxidation occurs throughout the whole model run, it is produced mostly during cloud periods. Daytime production is more efficiently than night-time production. The new scheme raises the concentration in the aqueous phase as more malonic acid is produced during cloud periods. Although the production of malonic acid increases during the model run, which can be seen by stronger peaks after cloud periods with increasing simulation time, the concentration does still not reflect the values from field measurements. Figure 2 shows the concentration profiles for two selected precursors of malonic acid in the gas phase. 3-oxo propanoic acid (red line) had already been implemented in the aqueous phase in CAPRAM 3.0i as the only precursor of malonic acid. While in the old run (dashed line) its oxidation to malonic acid is stronger than its production during cloud periods and thus concentrations are lowered after cloud periods, this is different in the new run (solid line). With the implementation of several precursors taken up from the gas phase, production dominates during cloud periods raising the $CHOCH_2COOH$ concentrations after cloud periods. This is also the cause for the higher gas

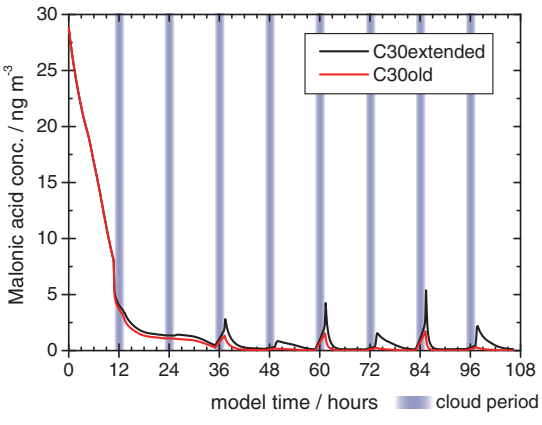


***Fig. 1:*** *Modeled aqueous phase concentrations of the sum of malonic acid, malonate mono- and dianion for the model runs with (C30extended) and without (C30old) C3 extension.*

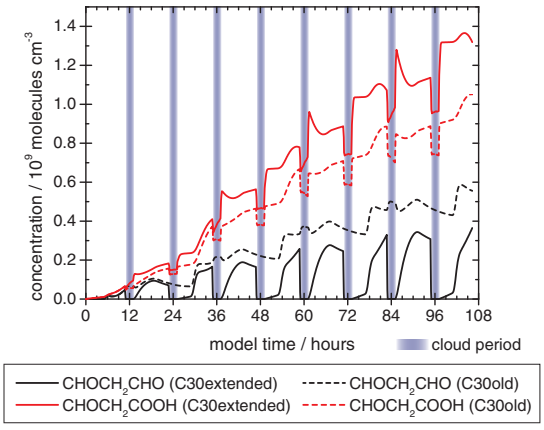


***Fig. 2:*** *Modeled gas phase concentrations of selected malonic acid precursors, molondial (black lines) and 3-oxo propanoic acid (red lines), for the model runs with (solid lines) and without (dashed lines) C3 extension under remote conditions.*

concentrations of 3-oxo propanoic acid in the new run then in the old run as this acid degases from deliquescent particles after cloud evaporation. Malondial as an example of an added species in the new aqueous C3 oxidation scheme shows a different behavior. With the uptake now implemented, it partitions into the aqueous phase during cloud periods and hence concentrations are lowered in the gas phase (see black lines in Fig. 2). Due to its oxidation, concentrations stay low after cloud and have to recover again. Therefore, concentrations of the old run are always exceeding those of the new run.

## Conclusions and outlook

The model runs with the new extended C3 oxidation scheme have shown concentration profiles of key species that were closer to measurements from the field. However, there are still unresolved questions. Therefore, there is a need to expand the oxidation scheme to higher compound classes. This leads however to new species in the aqueous phase that can partition into the gas phase, but are not already part of MCM. Thus, a further development of the gas phase mechanism MCM would be desirable. Further expansions in the aqueous phase could include the oxidation of e.g. esters and ethers. Besides further extension of the mechanism, it is planned to apply the advanced multiphase mechanism in simulations comparing model results with chamber experiments from the "LEipziger AerosolKammer" (LEAK) as well as modeling case studies from field experiments, e.g. the Hill Cloud Cap Thuringia 2010 (HCCT-2010).

## References

Aumont, B., S. Szopa, and S. Madronich (2005), Modelling the evolution of organic carbon during its gas-phase tropospheric oxidation: development of an explicit model based on a self generating approach, *Atmos. Chem. Phys.*, *5, 9*, 2497-2517.

Raventos-Duran, T., M. Camredon, R. Valorso, and B. Aumont (2010), Structure-activity relationships to estimate the effective Henry's law coefficients of organics of atmospheric interest, *Atmospheric Chemistry and Physics - Discussions (ACPD)*, *10, 2*, 4617-4647.

Saunders, S. M., M. E. Jenkin, R. G. Derwent, and M. J. Pilling (2003), Protocol for the development of the Master Chemical Mechanism, MCM v3 (Part A): tropospheric degradation of non-aromatic volatile organic compounds, *Atmospheric Chemistry Physics*, *3, 1*, 161-180.

Tilgner, A., and H. Herrmann (2010), Radical-driven carbonyl-to-acid conversion and acid degradation in tropospheric aqueous system studied by CAPRAM, *Atmos. Environ.*, *44 (49)*, 5415-5422.

Wolke, R. A., A. M. Sehili, M. Simmel, O. Knotz, A. tilgner, and H. Herrmann (2005), A parcel model with detailed microphysics and complex multiphase chemistry, *Atmos. Environ.*, *39 (23-24)*, 4375-4388.

**Funding**
- German Research Foundation (DFG), Bonn, Germany

**Cooperation**
- Laboratoire inter-universitaire des Systèmes Atmosphériques (LISA), Paris, France

# Heterogeneous nucleation of water and sulfuric acid in the presence of mineral dust

Olaf Hellmuth[1], Jürn W. P. Schmelzer[2], Alexander K. Shchekin[3], Alexander S. Abyzov[4]

[1] Leibniz Institute for Tropospheric Research (IfT), Leipzig, Germany
[2] University Rostock, Institute of Physics, Rostock, Germany, and Bogoliubov Laboratory of Theoretical Physics, Dubna, Russia
[3] St. Petersburg State University, Department of Statistical Physics, St. Petersburg, Russia
[4] Kharkov Institute of Physics and Technology, Kharkov, Ukraine

*Im Rahmen der klassischen Nukleationstheorie wurden konzeptionelle Untersuchungen zur Sulfatbildung auf der Oberfläche von atmosphärischen Mineralstaubpartikeln durch heterogene Nukleation durchgeführt. Es erfolgten Sensitivitätstests zum Einfluss verschiedener Mechanismen des Embryowachstums auf die Nukleationsrate in einem heteromolekularen System. Unter atmosphärenrelevanten Bedingungen führt das Embryowachstum durch Oberflächendiffusion von adsorbierten Gasmolekülen im Vergleich zum Wachstum durch direkte Gasdeposition auf den Embryo zu einer Erhöhung der Nukleationsrate um mehrere Größenordnungen. Das Ergebnis zeigt, dass heterogene Nukleation von atmosphärischen Gasgemischen auf Oberflächen unlöslicher Partikel ein effektiver Weg zur Bildung von Sulfatbeschichtungen („sulfate coating") auf Mineralstaubpartikeln ist. Diese Effekte können insbesondere in Bezug auf strahlungsoptische und mikrochemische Aerosoleigenschaften nicht a priori vernachlässigt werden. Zur Berücksichtigung in atmosphärischen Modellen wurde ein entsprechendes FORTRAN-Programm für die heterogene Nukleationsrate entwickelt.*

## Introduction

Heterogeneous heteromolecular nucleation of water vapor and sulfuric acid ($H_2SO_4$) vapor has long been neglected as a possible coating pathway for mineral dust particles because of the thermodynamic energy barrier limiting this process. However, as heterogeneous nucleation on preexisting particles requires much lower supersaturation than homogeneous nucleation, it might be a plausible dust-coating mechanism. The onset of heterogeneous nucleation strongly depends on the characteristics of the mineral dust surface (shape, composition). The spatiotemporal variability of these surface characteristics is reconcilable with the observation that only few mineral dust particles exhibit soluble coating.

Here, we focus on the impact of the kinetic prefactor on the heterogeneous nucleation rate.

## Method

Classical nucleation theory (CNT) is one of the most widely employed formalisms to describe phase transitions, such as atmospheric new particle formation. This theory postulates that a metastable phase relaxes to the thermodynamically favored phase by growth of a small fragment of the stable phase, initially formed by a fluctuation within the metastable phase. Contact with most substances leads to a reduction of the free-energy barrier to nucleation (surface catalysis), where some substances reduce that barrier more than others. Nucleation of an embryo of the new phase on the surface of a pre-existing particle (hereafter called a core) is subject of the classical heterogeneous nucleation theory (CHNT). CHNT is based on the same physico-chemical principles as CNT, i.e., molecular clusters are treated as liquid droplets with bulk liquid values for density and surface tension (capillary approximation). When the interaction of a droplet with a substrate surface is taken into account, only one macroscopic parameter, namely the contact angle between the nucleating droplet and the surface, is needed.

We consider a three-phases nucleation system consisting of new embryos (embryonic phase $\alpha$), which are heterogeneously formed from a condensing vapor (primordial or mother phase $\beta$) on pre-existing particles or cores (substrate phase $\gamma$) (see Fig. 1). The condensing vapor is assumed to consist of $H_2O$ and $H_2SO_4$ monomers. Sulfuric acid has the tendency to form hydrates, i.e., small clusters of $H_2SO_4$ and $H_2O$ molecules in the vapor phase. Hydration, considered in the model, leads to the rearrangement of molecules into three groups: (a) nonhydrated-free $H_2O$ molecules; (b) nonhydrated-free $H_2SO_4$ molecules, and $H_2SO_4 \bullet (hH_2O)$ hydrates consisting of one $H_2SO_4$ molecule and $h$ $H_2O$ molecules. For simplicity we assume that the preexisting particles have a spherical convex shape with uniform radius $R_n$, mass density $\rho_n$, and mass concentration $c_{dust}$ (see nucleation geometry in Fig. 1). The heterogeneous nucleation rate $J^{(het)}$ is proportional to a Boltzmann-type function of the Gibbs number (representing the thermodynamic energy barrier to form a critical embryo of the new phase on the

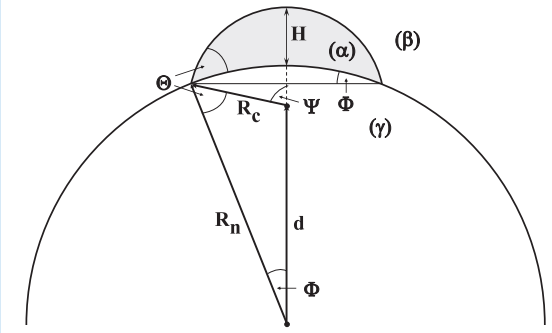


***Fig. 1:*** *Geometry of a lens-like embryo (phase α) nucleated on a spherical surface of a solid core (phase γ) from a binary vapor (phase β). Here, $R_n$ denotes the radius of the core, $R_c$ the radius of the critical embryo, and θ the contact angle. The remaining symbols define auxiliary lengths and angles for the determination of the nucleation geometry.*

preexisting surface). The proportionality constant (or kinetic prefactor) in the determination of $J^{(het)}$ is the product of the concentration of active nucleation sites (in units of $m^{-3}$) in the bulk of the ambient phase, the impinging rate (in units of $s^{-1}$) and the dimensionless heterogeneous Zeldovich factor. In order to determine the impinging rate, we considered three different mechanisms: (i) adsorption-induced impingement (ads); (ii) surface-diffusion induced impingement (diff); (iii) collision-induced impingement (coll).

A comprehensive review of previous phenomenological and modeling studies on this issue and a detailed description of both the kinetic and thermodynamic parts of the nucleation rate model used here are given in *Hellmuth et al.* [2008].

## Results of nucleation rate calculations

For our example we used the following parameters as model input: temperature $T$=293 K; relative humidity $RH$=50%; sulfuric acid vapor concentration $N_2$=$10^7$-$10^{10}$ $cm^{-3}$; contact angle Θ=70°; radius of the mineral dust particle $R_n$=200 nm; mass density of the mineral dust particle $\rho_n$=2650 kg $m^{-3}$; mineral dust mass concentration $c_{dust}$=20 µg $m^{-3}$.

The results of the calculations can be summarized as follows [for figures see *Hellmuth et al.*, 2008]:

- *Catalyzing effect:* The presence of a curved substrate has a very strong impact on the critical formation work. In the present case, the surface catalyzing effect lowers the critical formation work down to approximately 25% of its reference value for homogeneous nucleation, leading to the known strong enhancement of nucleation.
- *Hydration:* At fixed ambient $H_2SO_4$ vapor (SAV) concentration, hydration leads to a dilution of the binary embryo and (via decrease of the Raoult effect) to an increase of the critical cluster radius and the critical formation work. Consequently, the critical SAV supersaturation for nucleation to occur increases. This result is in line with the known fact that hydration strongly disfavors nucleation.
- *Impinging rate:* The average impinging rate increases with increasing SAV vapor concentration and is very sensitive against the choice of the impingement mechanism. Surface diffusion-induced impingement is by approximately 10 orders of magnitude higher than adsorption-induced impingement, and appears to very effectively enhance the heterogeneous nucleation rate. At typical atmospheric SAV concentrations of $N_2$≈$10^7$ $cm^{-3}$ adsorption- and collision-induced impingement yields nucleation rates, which are well below a limiting value of 1 embryo $cm^{-3}s^{-1}$ (accepted as a threshold value for significant nucleation). Unlike this, surface-diffusion induced impingement yields nucleation rates, which are by several orders of magnitude above this nucleation rate threshold (Fig. 2). To the best of our knowledge, this effect has not been considered previously in atmospheric heterogeneous vapor-to-liquid nucleation models.
- *Critical cluster composition:* According to the nucleation theorem, the steepness $p$ of the function

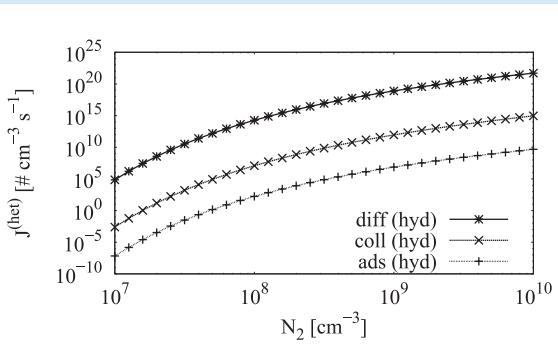


***Fig. 2:*** *Dependence of the heterogeneous heteromolecular nucleation rate, $J^{(het)}$, on the total number concentration of $H_2SO_4$ monomers, $N_2$, with consideration of sulfuric acid hydration.*

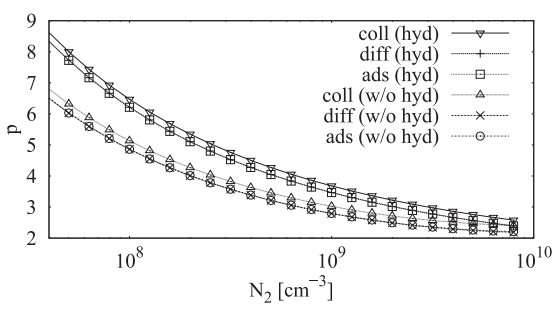


***Fig. 3:*** *Dependence of the steepness p of the function $J^{(het)}$~$(N_2)^p$ on the total number concentration of $H_2SO_4$ monomers, $N_2$. According to the nucleation theorem, the exponent p is identified with the number of $H_2SO_4$ molecules in the critical cluster.*

$J^{(het)} \sim (N_2)^p$ gives the number of $H_2SO_4$ molecules in the critical cluster. Here, $p$ approaches a value of two for large SAV concentrations ($p \approx 2$-2.5 at $N_2 \approx 10^{10}$ cm$^{-3}$), indicating a kinetic limitation of the nucleation process at high sulfuric acid supersaturation. At low SAV concentrations, the existence of a thermodynamic energy barrier is reflected in relatively high values of the exponent ($p \approx 7$-9 at $N_2 = 5 \cdot 10^7$ cm$^{-3}$) (Fig. 3).

## Conclusions

Heterogeneous nucleation of water/sulfuric acid vapor appears to be very sensitive to both the consideration of hydration and the choice of the impingement mechanism. Surface-induced impingement enables effective new particle formation at ambient atmospheric acidity levels. However, it's potential to explain patchy coating of mineral dust and other particles and its contribution to both the atmospheric sulfur mass and radiation budgets deserve further studies. This includes dedicated nucleation chamber experiments to evaluate surface-diffusion mediated heterogeneous nucleation.

## References

Hellmuth, O., J. W. P. Schmelzer, A. K. Shchekin and A. S. Abyzov (2008), Atmospheric New Particle Formation by Heterogeneous Nucleation Revisited: Comments on Phenomenology and Genesis. In: Schmelzer, J. W. P., G. Röpke and V. B. Priezzhev (eds.), Nucleation Theory and Applications. JINR Joint Institute for Nuclear Research, BLTP Bogoliubov Laboratory of Theoretical Physics, JINR Dubna 2008, ISBN 978-5-9530-0199-1.

**Cooperation**
- University Rostock, Institute of Physics, Rostock, Germany
- BLTP Bogoliubov Laboratory of Theoretical Physics, Dubna, Russia
- St. Petersburg State University, Department of Statistical Physics, St. Petersburg, Russia
- Kharkov Institute of Physics and Technology, Kharkov, Ukraine

# Detection of odor sources and high concentrations of pollutants in the Ore Mountains by modeling of the air mass paths

Michael Jähn, Ralf Wolke, Beate Sändig, Eberhard Renner

*Geruchsbelastung ist seit Jahrzehnten ein bekanntes Problem in den grenznahen Gebieten des Erzgebirges und des Vogtlandes. Als Verursacher gelten die in großer Anzahl vorhandenen Industrieanlagen in Nordböhmen. Besonders in den Herbst- und Wintermonaten treten im Zusammenhang mit Hochdruck- und Inversionswetterlagen Belastungen auf. Dem eher rückläufigen Trend an Beschwerden, welcher auf die Modernisierung und teilweiser Stilllegung von Anlagen zurückzuführen ist, steht eine deutlich erhöhte Anzahl an Beschwerden im Jahr 2011 gegenüber, als im Herbst aufgrund einer langanhaltenden Hochdrucklage überdurchschnittlich viele Geruchsmeldungen der Bevölkerung registriert wurden. Dennoch werden die Grenzwerte für Luftschadstoffe in den seltensten Fällen überschritten. Mithilfe des Trajektorienmodells TRAJEK, welches Reanalysedaten des Lokalmodells COSMO (Consortium for Small-Scale Modelling) vom Deutschen Wetterdienst (DWD) nutzt, können die Zugbahnen der Luftmassen simuliert werden. Dabei werden Rückwärtstrajektorien der belasteten Orte sowie Vorwärtstrajektorien der vermuteten Quellen berechnet. Darüber hinaus wird mit dem Modellsystem COSMO-MUSCAT (Multi-Scale Chemistry Aerosol Transport) die Ausbreitung von Spurenstoffen simuliert, wobei die vorhandenen Strömungsstrukturen sowie die Abluftfahnen der Emittenten sichtbar gemacht werden können.*

## Introduction

Each year the inhabitants of the Ore Mountains and the Vogtland are complaining about unpleasant odors. Frequent occurrences of these odors are recorded during high-pressure weather situations particularly when horizontal pressure gradients are weak. Potential odor sources are Czech industrial facilities in North Bohemia (altogether about 150 factories, refineries, chemical plants etc.). In case of an "odor event", the human-perceived stench is not necessarily detected at the emission source, because of chemical conversion and mixing processes that take place after the emission. These odors are assumed to correlate with certain health problems, which many people are experiencing in the affected regions. This has been an issue for decades, even though nowadays the limits for air pollutants are not exceeded in most cases, because many facilities have been remanufactured. However, accidents and averages are possible at any time and can cause high amounts of emissions. Due to the special orographic situation in the Ore Mountains, very stable pollutant clouds can develop at corresponding weather conditions. Hence, more than one polluter can be responsible for the odors [*Sächsisches Staatsministerium für Umwelt und Landwirtschaft*, 2011].

In 2010, on 26 days of the year a total number of 60 complaints were registered. This corresponds to the approximate expected annual value. More than half of these registrations occured on November 10, 2010. On this day an accident was reported in a pressure gas plant in Vřesová. In 2011, the amount of complaints was six times higher than in the year before. Until November 9, 2011, on 87 days of the year over 360 complaints were registered. The main reasons for this were long lasting high-pressure weather situations with very low wind speeds in October and November 2011.

## Methods and numerical models

Mesoscale tracer transport and trajectory modeling is used to clarify the origin of the odors arriving at the Ore mountains. The quality of modeled results strongly depends on the initial data. The three-dimensional, non-hydrostatical local model COSMO (Consortium for Small-Scale Modeling) of the Deutscher Wetterdienst (DWD) provides the required reanalysis data at 2.8 km horizontal grid resolution [*Steppeler et al.*, 2003; *Schättler et al.*, 2008].

For detecting the emission sources, a multi-stage modeling is necessary. First, backward trajectories based on the cities in which complaints were reported are calculated. This is realized with the trajectory model TRAJEK, in which the time integral of the wind speed is solved via a 2$^{nd}$ order Euler-Cauchy-method. The interpolation of the data fields is realized by a 3$^{rd}$-order-in-space and 1$^{st}$-order-in-time Lagrange method. With the information given by backward trajectories, forward trajectories for potential sources can be computed. For visualization of the output data the geographical information system GRASS is used [*GRASS*, 2008]. Additionally to the air mass paths, the computations of the transport and the chemical conversion for atmospheric trace substances are performed by the Multi-Scale Chemistry Aerosol Transport (MUSCAT) model [*Knoth and Wolke*, 1998; *Renner and Wolke*, 2010].

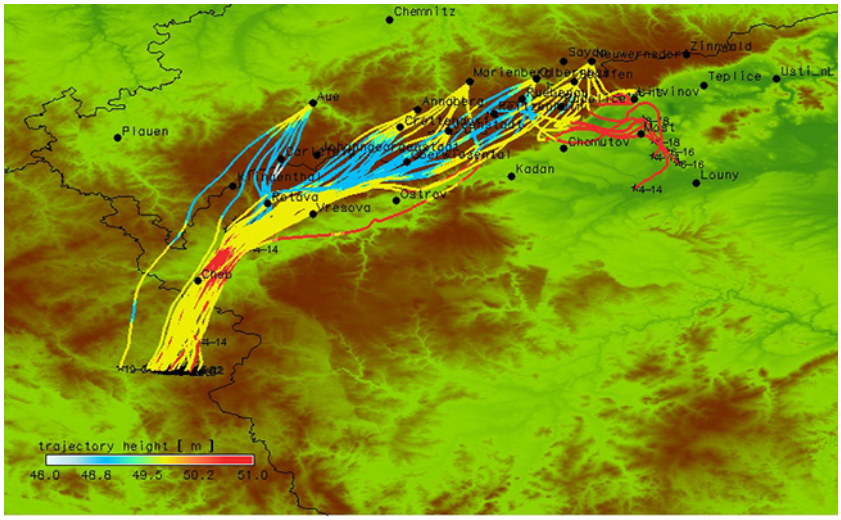


*Fig. 1: Backward trajectories (50 m height) for Neuwernsdorf, Olbernhau, Marienberg, Annaberg, Jöhstadt, Seiffen, Crottendorf and Aue at November 10, 2010, 12-24 CET.*

## Case study

On November 10, 2010 an accident occurred in the pressure gas plant in Vřesová. The breakdown of a compressor made the emission of odor substances inevitable. This defect was repaired at about 14:30 CET. Figure 1 shows backward trajectories for selected cities in the Ore Mountains between 12 and 24 CET. The air masses reach the target location at 50 m above ground, and all trajectories are computed for 10 hours. For the whole region a southwesterly air current is present, where the trajectory paths are passing the known pollution source Vřesová. Trajectories in other heights (50-200 m) show a similar behavior. To analyze the situation with the aid of forward trajectories, not only Vřesová itself is taken as an initial point, but also surrounding points within a radius of 5 and 10 km, respectively (Fig. 2, all trajectories starting at 11 CET). The trajectory paths of the southerly located initial points remain in the North Bohemian Basin, whereas the other air masses stream across the Ore Mountains toward the southern part of Saxony. Furthermore, the tracer analysis

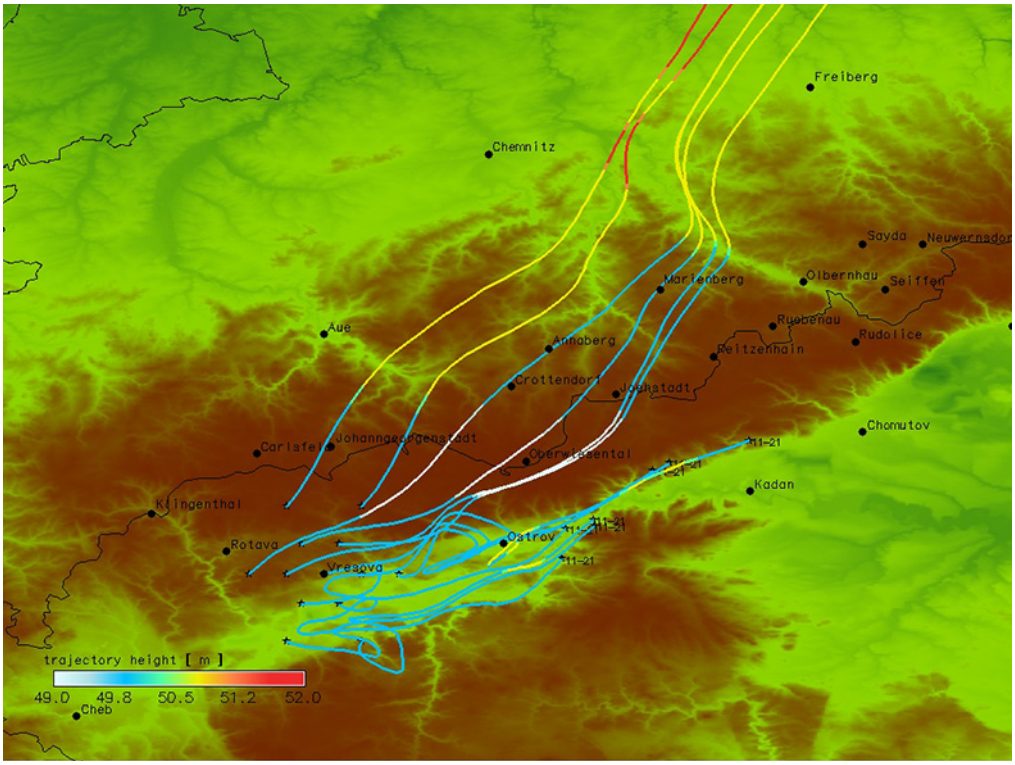


*Fig. 2: Forward trajectories (50 m height) for Vřesová and surrounding area at November 10, 2010, 11 CET.*

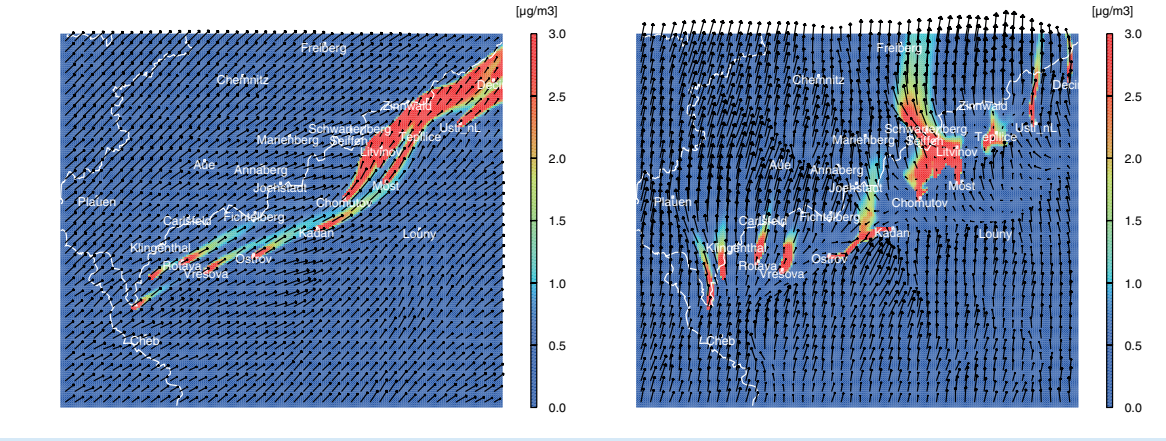


***Fig. 3:*** *Time course of the tracer dispersion at ground level at November 10, 2010, 10:30 (left) and 18:30 CET (right).*

in Fig. 3 shows the development of the flow conditions. During the day air masses flow along the Ore Mountains due to westerly winds. Toward evening the wind changes and the pent-up air can be transported in a northward direction. These flow patterns are in accordance with the results of the trajectory analysis.

## Conclusions

Using a trajectory model in combination with passive tracer analysis turns out to be a useful tool for the detection of emission sources that cause odors in the Ore Mountains and Vogtland regions. With further information, e.g. knowledge of time and location of a chemical plant accident, a more sophisticated investigation is possible. Nevertheless an unambiguous polluter cannot be identified in every case. The air masses often accumulate in front of the Ore Mountains in the North Bohemian Basin. After dissolving of an inversion or an increase of wind speed the emitted mixture of chemical substances can overflow the mountain crest. This situation was frequently observed during October and November 2011 when a high amount of complaints were registered.

## References

GRASS (2008), Geographic Resources Analysis Support System (GRASS) Software. Open Source Geospatial Foundation Project, http://grass.osgeo.org.

Knoth, O., and R. Wolke (1998), An explicit-implicit numerical approach for atmospheric chemistry-transport modelling, *Atmos. Environ.*, *32*, 1785-1797.

Renner, E., and R. Wolke (2010), Modelling the formation and atmospheric transport of secondary inorganic aerosols with special attention to regions with high ammonia emissions, *Atmos. Environ.*, *44*(15), 1904-1912.

Sächsisches Staatsministerium für Umwelt und Landwirtschaft (2011), Geruchsbelastung im Erzgebirge und Vogtland, http://www.umwelt.sachsen.de/umwelt/luft/3647.htm.

Schättler, U., G. Doms, and C. Schraff (2008), A Description of the Nonhydrostatic Regional COSMO-Model. Part VII: User's Guide. Documentation, Consortium for Small-Scale Modelling, 1-28.

Steppeler, J., G. Doms, U. Schättler, H. W. Bitzer, A. Gassmann, U. Damrath, and G. Gregoric (2003), Meso-gamma scale forecasts using the nonhydrostatic model LM, *Meteorol. Atmos. Phys*, *82*, 75-96.

**Funding**
- Sächsisches Landesamt für Umwelt, Landwirtschaft und Geologie, Dresden, Germany

**Cooperation**
- Sächsisches Landesamt für Umwelt, Landwirtschaft und Geologie, Dresden, Germany
- Deutscher Wetterdienst, Offenbach, Germany

# Generation of turbulent inlet boundary conditions for Large-Eddy Simulation

Marcel König, Oswald Knoth

*Large-Eddy Simulationen (LES) benötigen turbulente Einströmbedingungen, um realitätsnahe turbulente Ergebnisse zu erzielen. Diese Ergebnisse variieren stark mit der Wahl der turbulenten Einströmbedingung und vor allem deren turbulenter Intensität. Bei Anwendung periodischer Randbedingungen kann das Einströmproblem umgangen werden. In komplexer Geometrie sind periodische Randbedingungen jedoch nicht praktikabel. Es wird ein Turbulenz-generierender Ansatz zur Modifikation der Einströmbedingungen für LES vorgestellt. Bei diesem Ansatz werden in Umkehrung zur Fourier Analyse die turbulenten Fluktuationen am Einströmrand mit Hilfe von trigonometrischen Funktionen auf den mittleren Wind aufgeprägt. Mit Hilfe von Amplitude, Wellenzahl und Frequenz kann man die Statistik des zu generierenden turbulenten Windfeldes beeinflussen. Diese statistischen Informationen können aus gemessenen meteorologischen Datensätzen oder Simulationen mit gröberer Auflösung bestimmt werden. Der Turbulenz-generierende Algorithmus wurde in das Strömungsmodel All Scale Atmospheric Model (ASAM) implementiert und für Gebäude umströmende Simulationen angewandt.*

## Introduction

In recent years, increased focus has been directed towards modeling of micro-scale flows in urban areas, which are very important for the assessment of possible health damage caused by air pollution [*Arnfield et al.,* 2003; *Souch and Grimmond,* 2006]. Additional attention has focused on the development of models to predict the dispersion of toxic materials in the urban environment [*Gifford and Hanna,* 1973]. Considering the urban impact on meteorological flow fields is very important for the accuracy of the dispersion plume results.

Significant advancement in computational capabilities has led to the application of direct numerical simulations (DNS) and LES for increasingly complex flows. Most DNS or LES of turbulent flows have used periodic boundary conditions, for which the computational domain is assumed to be one repeated unit of the whole urban geometry [*Xie and Castro,* 2009; *Keating and Piomelli,* 2004]. However, simulations of spatially inhomogeneous flow over complex geometry cannot use periodic boundaries and thus require turbulent conditions at the inflow boundary.

To obtain spatially high resolution regional weather forecasts, nesting procedures are applied, where a series of simulations with increasing resolution on smaller domains is performed. Subgrid scale turbulence information is provided from the coarser simulation, which could be used for setting up the inflow velocity field. The method of synthetic turbulence generation by superposition of sinusoidal modes is proposed for this problem. The procedure will be used to create inflow conditions for flow simulations with building-resolved resolutions (1 m) from a meso-gamma scale (100 m) model output, where the urban roughness is taken into account only in parameterized form. Radiosonde and other measurement data can be modified by this synthetic method to determine inflow values.

In many previous studies white noise was used to produce fluctuations in the simulation. But these small-scale eddies dissipate very quickly. Imported eddies from a separate calculation of dimension equal to or larger than the integral length scale of the flow can also be used. However, for this approach extra simulations and additional storage space are needed. The method of synthetic turbulence generation by superposition of sinusoidal modes presented here is a possibility to overcome these disadvantages.

## Synthetic turbulence generation by superposition of sinusoidal modes

The method of generating inflow turbulence by *Lee et al.* [1992] is used to provide a three-dimensional, turbulent synthetic velocity field at the inflow boundary. Turbulent structures in time series are often analyzed by decomposition onto a basis set of harmonic functions (Fourier Analysis). In reverse, here the velocity fluctuations are created using the superposition of sinusoidal and cosinusoidal modes with random phase and wave coefficients. The synthesized turbulent fluctuations are generated at the two-dimensional inflow plane and added to the mean flow profile. The inflow velocity vector is v = <v> + v' with mean value <v> and a fluctuating part v'. For simplicity, the method will be explained for a two-dimensional flow with main flow in direction $x_1$ and zero mean value in cross flow direction $x_2$. We assume at the inlet boundary ($x_1 = 0$) a fluctuating velocity component $v_1$ in direction $x_1$ as follows:

$$v_1 =< v_1 > + \sum_{n=1}^{N} E_1^n \sin[k_1^n x_2^* + \omega_1^n t + \Delta\phi_1^n] \quad (1)$$

where $x_2^* = 2\pi x_2/L_{Inlet}$ is a spatial cross flow coordinate normalized by the length of inflow boundary in this direction. $k^n_1$ and $\omega^n_1$ are wave numbers and frequencies in $x_1$ direction. In order to produce different turbulent eddies, we use a sum over n, where n is the number of different modes. The whole spectrum of turbulence in the atmosphere consists of eddy sizes from about 1–2 km (boundary layer height) down to the scale of dissipation in the 1 mm size range. For a LES simulation the possible wave numbers and frequencies have a lower limit determined by the grid resolution. The third part in Eq. 1 is a simple phase shift for every mode. The amplitude $E^n_1$ represents the strengths of fluctuation, thus the value of turbulent energy can be tuned for every mode n. *Lee et al.* [1992] use

$$E(\omega) = \omega^4 \exp\left[-2\left(\frac{\omega}{\omega_0}\right)^2\right] \qquad (2)$$

to approximate the amplitude values, where $\omega_0$ is the frequency with maximum energy. By varying these different coefficients using statistics from measurements and some random processes as a function of time, the result will be a synthetic random field that evolves in a manner that can be controlled precisely.

For a divergence-free spatial velocity field, $v_2$ must be synthesized by the same structure as Eq. 1. In an idealized eddy circle the $v_1$' velocity fluctuations reach their maximum where the $v_2$' velocity fluctuations vanish (see Fig. 1). The $v_2$' velocity fluctuation should have a phase shift of $\pi/2$.

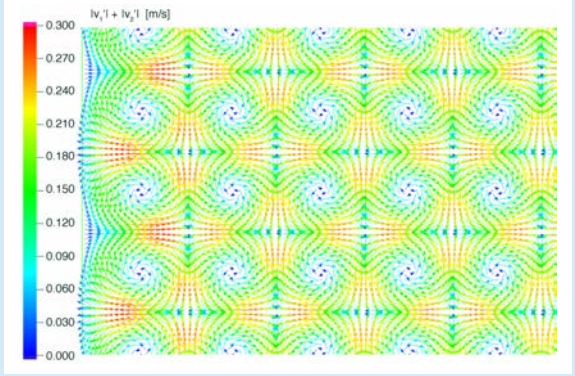


***Fig. 1:*** *The vector plot of a 2D simulation with a simplified inflow setup of one mode (N=1) shows the counter-rotating eddies. Colors indicate the absolute value of horizontal velocity fluctuations.*

## Examples

The turbulence-generating algorithm was implemented into the All Scale Atmospheric Model (ASAM). The synthetic Inflow condition approach is initially tested on a simple 2D domain with in/outflow boundary condition in stream-wise direction and periodic conditions in the cross flow direction. A small section of the modeled domain in Fig. 1 illustrates the horizontal fluctuations that result if only one mode (n=N=1) is used. With this synthetic approach, eddies only form in horizontal directions.

In a further simulation 10 different eddy sizes (N=10) were generated. The range of wave numbers varies from 0.7 to 7.7 and the associated frequencies from 0.03 to 0.3 $s^{-1}$, with the same amplitude in each mode. The mean velocity in main flow direction is $\langle v_1 \rangle = 5$ $ms^{-1}$ and zero crosswise. The sum over these 10 eddy sizes generates a more realistic wind field (Fig. 2). To illustrate its complexity, the distribution of a passive tracer emitted at the center of the inflow boundary is simulated (Fig. 3).

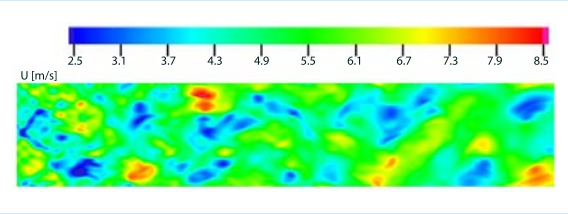


***Fig. 2:*** *2D simulation domain (N=10), colored are the $x_1$ velocity component with fluctuation around 5 $ms^{-1}$ mean flow velocity.*

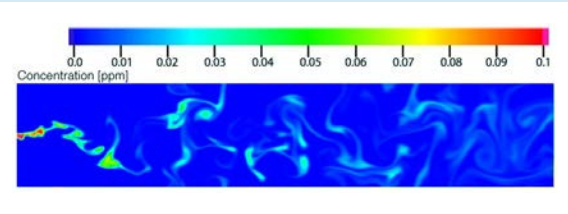


***Fig. 3:*** *2D simulation domain (n=10), colored are the concentrations of an emitted tracer with the source at the center of inflow boundary.*

This new method is adapted to a three-dimensional simulation in an urban like environment. The Mock Urban Setting Test (MUST) experiment is a flow experiment that took place in the desert of Utah/USA in the year 2001. The urban roughness was imitated with 120 shipping containers through which a tracer gas plume is advected. First ASAM simulation results from this experiment are shown in Fig. 4. We use a measured background mean wind profile for $\langle v \rangle$ and add a turbulent behavior. Furthermore we use Eq. 2 with a typical peak value $\omega_0$ for a stable stratified nocturnal boundary layer. The tracer plume showed a turbulent behavior inside the street canyons. In contrast to a fixed boundary condition measured concentration maxima can be simulated more realistically.

## Conclusion

With the new approach of creating turbulent inlet boundary conditions for LES, the inflow conditions can be set up for different model domains and simulations. Furthermore the amount of additional

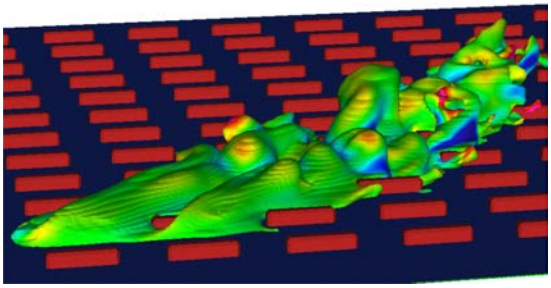

*Fig. 4: 3D simulation of the MUST experiment. A tracer plume colored with the vertical velocity component in an urban-like environment is displayed.*

turbulent fluctuation can be chosen and assigned to specific wave numbers or frequencies appropriate for different situations, for example for simulations of airflow through street canyons.

## References


Arnfield, A. J. (2003), Two decades of urban climate research: a review of turbulence, exchanges of energy and water, and the urban heat island, *International Journal of Climatology*, *23*(1), 1-26.

Gifford, F. A., and S. R. Hanna (1973), Modeling Urban Air-Pollution, *Atmospheric Environment*, *7*(1), 131-136.

Keating, A., and U. Piomelli (2004), Synthetic generation of inflow velocities for large-eddy simulation, in *34th AIAA Fluid Dynamic Conference and Exhibit*, edited, University of Maryland, Portland/ Oregon.

Lee, S., S. K. Lele, and P. Moin (1992), Simulation of spatially evolving turbulence and the applicability of Taylor's hypothesis in compressible flow, *Physics of Fluids A: Fluid Dynamics*, *4*(7), 1521-1530.

Souch, C., and S. Grimmond (2006), Applied climatology: urban climate, *Progress in Physical Geography*, *30*(2), 270-279, doi: 10.1191/0309133306pp484pr.

Xie, Z.-T., and I. P. Castro (2009), Large-eddy simulation for flow and dispersion in urban streets, *Atmospheric Environment*, *43*(13), 2174-2185.



**Funding**

- PAKT für Forschung und Innovation der Leibniz Gemeinschaft (Projekt: Feinstaubbelastung in städtischen Ballungsgebieten am Beispiel von Dresden und Leipzig)

**Cooperation**

- Jülich Supercomputing Centre (JSC) (http://www2.fz-juelich.de/jsc/)

# Numerical simulations of mixing conditions and aerosol dynamics in the CERN CLOUD chamber

Jens Voigtländer[1], Jonathan Duplissy[2], Linda Rondo[3], Andreas Kürten[3], Frank Stratmann[1]

[1] Leibniz Institute for Tropospheric Research (IfT), Leipzig, Germany
[2] CERN, PH Department, Geneva, Switzerland
[3] Institute for Atmospheric and Environmental Science, Goethe-University, Frankfurt/Main, Germany

*Im Rahmen des Cosmics Leaving OUtdoor Droplets (CLOUD) Projektes wird am CERN (Schweiz) die Nukleation von Schwefelsäurepartikeln in Abhängigkeit von ionisierender Strahlung und weiterer chemischer Substanzen wie Ammoniak und Aminen untersucht. Die Experimente finden an der CLOUD-Kammer, einem Edelstahltank mit einem Volumen von 26.1 m³ statt. Voraussetzung für derartige Experimente ist eine gute und definierte Durchmischung des Kammervolumens. Zu diesem Themenkomplex wurden und werden am IfT numerische Simulationen mit einem gekoppelten strömungs- und partikeldynamischen Modell durchgeführt (FLUENT/FPM). Berechnungen des Strömungsfeldes und der Verteilungen von Spurengasen und Partikeln zeigen, dass die Kammer mit nur einem Lüfter nur unzureichend durchmischt wird. Für die Anordnung mit 2-Lüftern ist das Mischungsverhalten besser, der Austausch zwischen oberer und unterer Tankhälfte jedoch gering. Die Simulationen liefern einen wichtigen Beitrag zur Charakterisierung der CLOUD-Kammer, deren fortlaufender Optimierung und zur Interpretation der an der Kammer gewonnenen experimentellen Daten.*

## Introduction

The Cosmics Leaving OUtdoor Droplets (CLOUD) project was established to investigate the effect of galactic cosmic rays on aerosols and clouds by studying the nucleation of sulphuric acid ($H_2SO_4$) particles and its dependence on ionizing radiation and additional other substances such as ammonia. Experiments are carried out at a cylindrical electro-polished stainless steel tank with a volume of 26.1 m³ (Fig. 1), which is located at CERN (Switzerland). The tank was designed to achieve highest standards of cleanliness and temperature stability [*Duplissy et al.*, 2010; *Kirkby et al.*, 2011]. Different inlets and outlets in the chamber wall can be used to connect sampling probes, to introduce trace gases and to evacuate the chamber. Two fans can be installed next to the flanges at the top and the bottom to continuously mix the tank's contents. At the top there is also an UV-illumination system [*Kupc et al.*, 2011], which is used to trigger the OH production via ozone photolysis. The OH radicals then react with $SO_2$ to form $H_2SO_4$. Dependent on precursor concentrations, thermodynamic conditions and beam intensity, $H_2SO_4$ particle nucleation will occur [*Kirkby et al.*, 2011].

A big issue in large volume cloud chambers like the CLOUD chamber at CERN is to attain spatial homogeneity regarding the prevailing thermodynamic conditions, gas concentrations and particle properties. Achieving homogeneity inside the tank becomes even more challenging, if several parameters are changed during the experiments (e.g., via UV-illumination, particle nucleation, trace

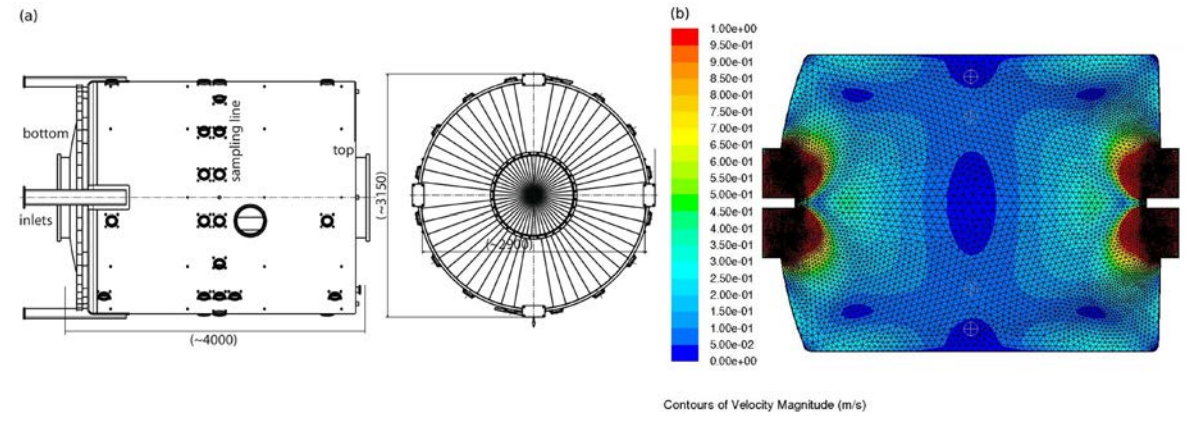


***Fig. 1:*** *Schematic diagram of the CLOUD chamber (a), an electropolished stainless steel cloud tank with 26.1 m³ (diameter ~3.0 m, height ~4.0 m). At the mid-height, the holes for the sampling probes (sampling line) are visible. The tank was simulated using the CLOUD-FPM model. The numerical grid together with an example of the calculated velocity profile is shown on the right panel (b).*

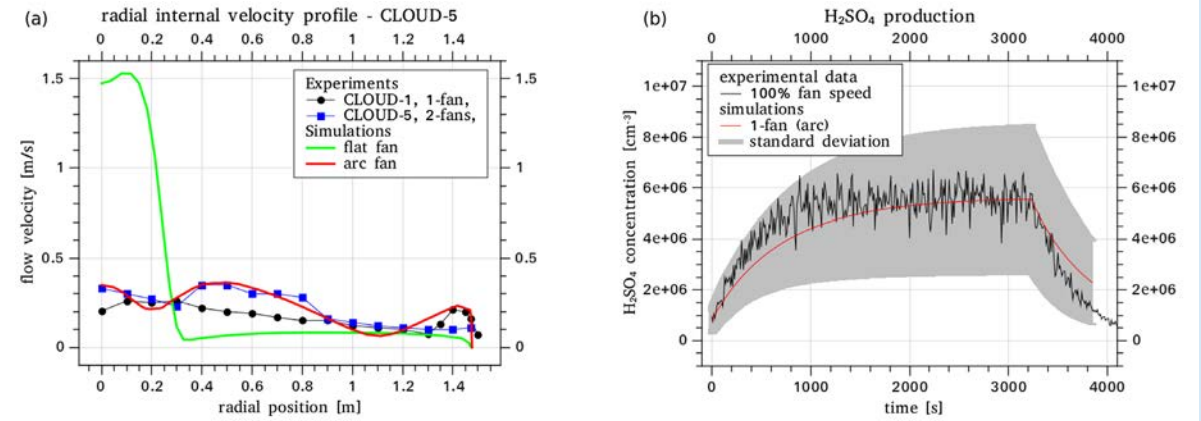


***Fig. 2:*** *Measured internal air velocity 50 cm above the fan (black and blue dots) compared to simulation results (a). The flow direction was not measured. Different shapes of the zero thickness pressure jump layer (representing the mixing fan) result in different velocity profiles. A flat fan configuration results in a velocity profile significantly different from experimental data (green line). To match the experimental data, arc shaped layers are necessary (red line). For adjusted fan shape the model fit experimental $H_2SO_4$ lifetime data within calculated standard deviations (b).*

gas input, wall cooling). To ensure homogeneity, mixing fans are usually applied in such experiments. To check the mixing state, measurements are made at several selected points of the chamber. However, it is not possible to check all parameters continuously, and therefore numerical simulations were performed to investigate the mixing state of the CLOUD chamber [*Voigtländer et al.*, 2011].

## Numerical model

Simulations were carried out using the commercially available computational fluid dynamics (CFD) code FLUENT (ANSYS Inc., Canonsburg, PA, USA) together with the Fine Particle Model (FPM, Particle Dynamics GmbH, Leipzig, Germany). The FLUENT model allows the simulation of a wide range of small scale fluid dynamics problems, while the FPM was developed at IfT as a general purpose particle dynamics model. Both models together form the so-called CLOUD-FPM, a model being capable of handling the coupled fluid and particle dynamical processes taking place inside the CLOUD chamber. In CLOUD-FPM, all relevant properties like velocity, temperature, pressure, turbulence parameters, wall losses of the condensable gas phase species and nucleation and growth of ultra-fine aerosol particles are treated explicitly.

One of the key parameters in the numerical simulations of the CLOUD chamber is a proper description of the mixing fans. Similar to a previous study [*Schütze and Stratmann*, 2008] simulations were carried out on a 2-dimensional grid, which does not allow the consideration of rotating fan blades. Instead, the mixing fans were represented by a suitable pressure jump parametrization at a zero thickness fan surface layer. The accuracy of such an approach is highly dependent on the assumed fan blade shape and therefore requires an adjustment to experimental flow field data. With adjusted arc shaped fans the simulations were found to represent the measured internal velocity profile very well (Fig. 2a). To further evaluate the model, calculated time dependent $H_2SO_4$ concentrations considering $H_2SO_4$ production and wall loss were compared to data of so-called $H_2SO_4$ lifetime experiments. The results show that, within calculated volume averaged standard deviations, the model represents the experimental data well (Fig. 2b).

## Simulation results concerning the mixing state

**Volume-to-wall exchange.** Time resolved simulations were carried out to estimate time scales for mixing the tank's contents. In more detail, the response of the system to an instantaneous change of a) the wall temperature by 20 K (291.65 to 271.65 K), and b) the water mass fraction at the wall by 0.015 (from 0.05 to 0.20) was investigated. Simulations were performed for both the one and the two fan configurations. Calculated wall exchange times to reduce the difference between wall and tank's average value to 1/e of the initial value, called 1/e time, were found to be about 220 seconds for the 1-fan and 100 seconds for the 2-fan set up (both arc shape). This means the second fan reduces the mixing time by a factor of more than 2. This holds for both heat and mass transport processes.

**Internal mixing.** To investigate the internal mixing behaviour, a (small) tracer emitting source was placed below the lower fan. After a certain period of time (1 second) the source was turned off and the evolution of the dilution/mixing in the chamber was calculated. The simulations suggest that the tank is, with respect to the concentration of the tracer species, separated into two parts. Each fan provides well mixed conditions in its half of the chamber, but

the exchange between the upper and the lower half of the tank is small. Therefore, internal mixing takes longer (about 5 minutes) than volume-to-surface exchange discussed above (less than 2 minutes). To increase the exchange between the lower and the upper half of the tank larger fan speeds would be necessary and are recommended for future experiments, although this would increase the wall losses as well.

**Particle nucleation and growth.** Time dependent CLOUD-FPM calculations were also carried out to simulate nucleation and growth of $H_2SO_4$ - $H_2O$ particles in the CLOUD tank. To this end, experimental particle nucleation rates given by *Kirkby et al.* [2011] were applied and particle growth of the freshly nucleated particles was described by a simple growth law given by *Seinfeld and Pandis* [1997] assuming equilibrium between vapour and liquid phase for water. In conclusion, the mixing state of the particle number size distribution with freshly nucleated particles was found to be very similar to the mixing state of the gas species. This means, if the tank's gas contents are well mixed, the nano-sized particles are also homogeneously distributed over the whole tank.

## Conclusions

Numerical simulations with the CLOUD-FPM model were performed to investigate the mixing state inside the CLOUD chamber. In agreement with the results of 1-D flow field measurements, the simulations show that the flow velocities in the chamber are quite low for the fan speeds applied in the experiments. Calculated 1/e volume-to-surface exchange times of about 2 minutes indicate that the tank is well mixed for a 2-fan set up. However, with time scales of about 5 minutes internal mixing is only moderate because the exchange between upper and lower half of the chamber being small. These findings hold for both, gaseous species and fresh nucleated particles. In conclusion, a 2-fan configuration should be chosen to provide well mixed conditions inside of such a chamber.

## References


Duplissy, J., M.B. Enghoff, K. L. Aplin, F. Arnold, H. Aufmhoff, M. Avngaard, U. Baltensperger, T. Bondo, R. Bingham, K. Carslaw, J. Curtius, A. David, B. Fastrup, S. Gagné, F. Hahn, R.G. Harrison, B. Kellett, J. Kirkby, M. Kulmala, L. Laakso, A. Laaksonen, E. Lillestol, M. Lockwood, J. Mäkelä, V. Makhmutov, N.D. Marsh, T. Nieminen, A. Onnela, E. Pedersen, J.O.P. Pedersen, J. Polny, U. Reichl, J.H. Seinfeld, M. Sipilä, Y. Stozhkov, F. Stratmann, H. Svensmark, J. Svensmark, R. Veenhof, B. Verheggen, Y. Viisanen, P.E. Wagner, G.Wehrle, E.Weingartner, H.Wex, M.Wilhelmsson, P. M.Winkler (2010), Results from the cern pilot cloud experiment, *Atmos. Chem. Phys., 10*, 1635 - 1647.

Kirkby, J., J. Curtius, J. Almeida, E. Dunne, J. Duplissy, S. Ehrhart, A. Franchin, S. Gagne, L. Ickes, A. Kürten, A. Kupc, A. Metzger, F. Riccobono, L. Rondo, S. Schobesberger, G. Tsagkogeorgas, D. Wimmer, A. Amorim, F. Bianchi, M. Breitenlechner, A. David, J. Dommen, A. Downard, M. Ehn, R.C. Flagan, S. Haider, A. Hansel, D. Hauser, W. Jud, H. Junninen, F. Kreissl, A. Kvashin, A. Laaksonen, K. Lehtipalo, J. Lima, E.R. Lovejoy, V. Makhmutov, S. Mathot, J. Mikkila, P. Minginette, S. Mogo, T. Nieminen, A. Onnela, P. Pereira, T. Petaja, R. Schnitzhofer, J.H. Seinfeld, M. Sipila, Y. Stozhkov, F. Stratmann, A. Tome, J. Vanhanen, Y. Viisanen, A. Vrtala, P.E. Wagner, H. Walther, E. Weingartner, H. Wex, P.M. Winkler, K.S. Carslaw, D.R. Worsnop, U. Baltensperger, M. Kulmala (2011), Role of sulphuric acid, ammonia and galactic cosmic rays in atmospheric aerosol nucleation. *Nature*, *476*, 429–433.

Kupc, A., A. Amorim, J. Curtius, A. Danielczok, J. Duplissy, S. Ehrhart, H. Walther, L. Ickes, J. Kirkby, A. Kürten, J.M. Lima, S. Mathot, P. Minginette, A. Onnela, L. Rondo, P.E. Wagner (2011), A fibre-optic UV-system for $H_2SO_4$ production in aerosol chambers causing minimal thermal effects, *J. Aerosol Sci.*, *42*, 532–543, 2011.

Schütze, M., and F. Stratmann (2008), Numerical simulation of cloud droplet formation in a tank, *Comput. Geosci., 34*, 1034–1043.

Voigtländer, J., J. Duplissy, L. Rondo, A. Kürten, F. Stratmann (2011), Numerical simulations of mixing conditions and aerosol dynamics in the CERN CLOUD chamber, *Atmos. Chem. Phys. Discuss.*, *11*, 20013-20049, *accepted for publication in Atmos. Chem. Phys.* .



**Funding**

- German Federal Ministry of Education and Research (BMWF, project no. 01LK0902B)

# Sea surface microlayer – the interface between ocean and atmosphere

Manuela van Pinxteren, Konrad Müller, Khanneh Wadinga Fomba, Hartmut Herrmann

*Der Export von organischem Material aus den Ozeanen in die Atmosphäre gehört zu den zahlreichen, teilweise noch unverstandenen Austauschprozessen zwischen diesen beiden Kompartimenten. In diesem Zusammenhang spielt der Oberflächenfilm der Ozeane, der sich durch die unterschiedlichen Eigenschaften von Meerwasser und Atmosphäre ausbildet, eine bedeutende Rolle, da er die direkte Schnittstelle zwischen Ozeanen und Atmosphäre bildet. Bisherige Untersuchungen zeigen eine veränderte Zusammensetzung des Oberflächenfilms im Vergleich zum Oberflächenwasser, beispielsweise eine Anreicherung verschiedener, zum Teil oberflächenaktiver organischer Verbindungen. Um ein besseres Verständnis des Transfers von Organika zwischen Ozeanen und Atmosphäre zu erhalten, wurde in verschiedenen Messkampagnen im Jahre 2011 der ozeanische Oberflächenfilm und die atmosphärische Phase über der Ozeanen untersucht.*

## Exchange processes between Ocean and Atmosphere

Marine aerosols contain, besides sea salt, a significant amount of organic material. As the composition of aerosols may influence their behavior towards absorption and reflection of solar radiation, their chemical characterization and the identification of the source of the organic content is an important task [*Chan et al.*, 2005]. Recent investigations suggest that the organic content of marine aerosols, especially of particles in the sub-micron range, is strongly connected to the biological activities of the ocean [*Cavalli et al.*, 2004]. Within the numerous, to date rarely understood, interaction processes between the oceans and the atmosphere, export of organic material from the oceans in the atmosphere is assumed to take place mostly in two ways, (1) via gas transfer (2) via bubble bursting processes (Fig. 1) [*Müller et al.*, 2009]. Therefore, a detailed chemical investigation especially in terms of organic material of the oceanic and atmospheric phase about the ocean is an important task.

In this context, the sea surface microlayer (SML), i.e. the physical boundary layer between air and sea plays an important role. The SML is operationally defined as the first 1000 micrometers of the ocean surface and therefore the direct interface for all gaseous, liquid and particulate mass transfer between the ocean and the atmosphere [*Liss and Duce*, 1997]. Being often enriched with organic and inorganic matter, the SML may play a key role in the export of organic material from the ocean to the atmosphere.

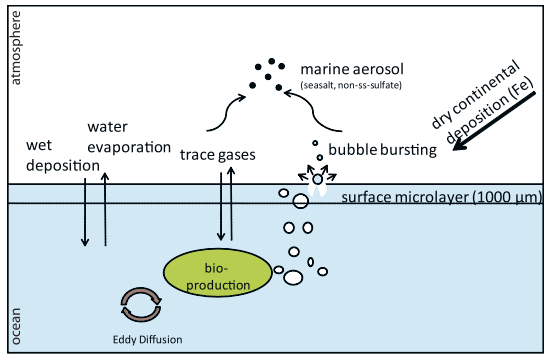


***Fig. 1:*** *Scheme of interaction processes between the oceans and the atmosphere.*

## The sea surface microlayer: chemical analysis and first results

The chemical analysis of the SML is challenging as seawater is quite a complex matrix and the high salt content is often problematic to analytical instruments. Moreover, the organic compounds are present in trace levels and some of them, like aliphatic amines, are very polar and reactive species and therefore difficult to extract from the seawater. Appropriate sample preparation methods with the aim of enrichment of the target analytes and elimination of the matrix, especially the high salt content, are required. Methods involving salt elimination due to a combination of strong cation and weak anion exchange are applied for the enrichment of carbohydrates. Analysis is performed with anion high performance anion-exchange chromatography (HPAEC) with pulsed amperometric detection [*Iinuma et al.*, 2009]. Furthermore, solid phase extraction in combination with liquid chromatography-mass spectrometry (LC-MS) or gas chromatography-mass spectrometry (GC-MS) are applied as analytical methods for a selective and sensitive determination of proteinogenic amino acid and amines in the water samples [*van Pinxteren et al.*, submitted]. Our first results of sea water samples from the southern Baltic Sea suggest that different compound groups within the broad chemical class of nitrogen containing organic compounds and carbohydrates show very different behavior with respect to water

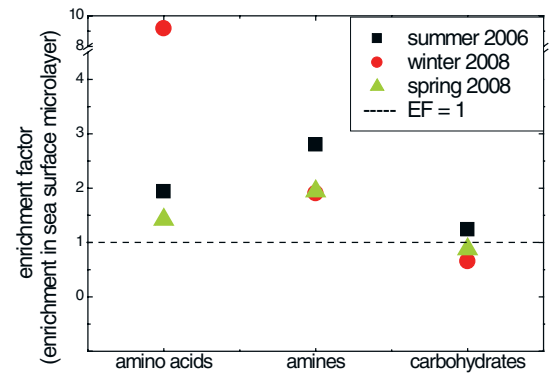


***Fig. 2:*** *Enrichment factors of amines, amino acids and carbohydrates in the SML sampled in 2006 and 2008 in the southern Baltic Sea.*

concentrations and enrichment in the SML (Fig. 2). Generally amines and amino acids tend to be enriched in the sea surface microlayer, whereas for dissolved carbohydrates a trend towards depletion was observed. The characteristics of the different compound classes were found to be in strong correlation to bacterial activity and meteorological conditions [*Stolle et al.*, 2010; *van Pinxteren et al.*, submitted].

**Concerted sampling activities in 2011/2012**

In order to obtain a better understanding of exchange processes between the oceans and the atmosphere, our present activities involve investigations of the oceanic water and furthermore of the atmospheric layer above the oceans. Concerted measurements, which took place within the SOPRAN Project Phase II topic "Ocean export of organic matter" were performed in several field campaigns in 2011 and will be continued in 2012 (Fig. 3). In April / May 2011 and in November 2011 a field campaign at the Cape Verde Atmospheric Observatory CVAO in São Vicente was performed. During these campaign at times of expected high biological activity, marine aerosols smaller than 1 µm ($PM_1$) were collected on top of a 30 m tower at the CVAO station using a high-volume sampler. Moreover, aerosol collection was carried out with a 5-stage-Berner impactor that allows size-segregated sampling of aerosols between 0.05 and 10 µm. The whole size range of aerosols and their organic content can thus be evaluated. Oceanic water was samples near the CVAO station. Bulk water from 1 meter depth was collected using a self-made device consisting of a glass bottle mounted on a telescopic rod. The sampling of the SML was performed with a glass plate that is vertically immersed in the water and slowly removed. The film adheres to the surface of the glass and is removed by framed Teflon wipers (Fig. 4).

Besides the sampling activities at the Cape Verdes, the participation in the Polarstern cruise in spring 2011 allowed the sampling of the oceanic water and marine aerosols in remote marine environment along the North Atlantic and South Atlantic Ocean. Aerosol $PM_1$ sampling was performed with a high volume sampler on board of the ship. This sampling will be performed again during the next cruise in spring 2012 from Punta Arenas (Chile) to Bremerhaven.

Another field campaign took place in Bergen (Norway) in May / June 2011. Bulk water and SML were collected in a Norwegian fjord and $PM_1$


***Fig. 3:*** *Concerted measurement activities performed in 2011 and planned for 2012.*

*Fig. 4: (left) Sampling of the SML using the glass plate technique. (right) Collection of the SML using Teflon Wipers.*

aerosols were collected at the shore. Moreover, mesocosm that were operated at different $CO_2$ partial pressures were sampled to study the behavior of organic compounds at specific acidic conditions.

Detailed chemical analysis of the sea water and the atmospheric particles will be performed within the next weeks and months. A comparison of the contents of organic material in the SML and the atmospheric layer above the oceans will be evaluated to clarify if there is a significant net influx or efflux of specific organic compounds.

## References


Cavalli, F., M. C. Facchini, S. Decesari, M. Mircea, L. Emblico, S. Fuzzi, D. Ceburnis, Y. J. Yoon, C. D. O'Dowd, J. P. Putaud, and A. Dell'Acqua (2004), Advances in characterization of size-resolved organic matter in marine aerosol over the North Atlantic, *Journal of Geophysical Research JGR - Atmospheres*, *109 (D24)*, doi: Artn D24215 Doi 24210.21029/22004jd005137.

Chan, M., M.Y. Choi, N. L. Ng, and C. K. Chan (2005), Hygroscopicity of water-soluble organic compounds in atmospheric aerosols: Amino acids and biomass burning derived organic species, *Environmental Science & Technology*, *39, 6*, 1555-1562, doi: 1510.1021/es049584l.

Iinuma, Y., G. Engling, H. Puxbaum, and H. Herrmann (2009), A highly resolved anion-exchange chromatographic method for determination of saccharidic tracers for biomass combustion and primary bio-particles in atmospheric aerosol, *Atmos. Environ.*, *43, 6*, 1367-1371 doi: 1310.1016/j.atmosenv.2008.1311.1020.

Liss, P. S., and R. A. Duce (1997), The Sea Surface and Global Change.

Müller, C., Y. Iinuma, J. Karstensen, D. van Pinxteren, S. Lehmann, T. Gnauk, and H. Herrmann (2009), Seasonal variation of aliphatic amines in marine sub-mictometer particles at the Cape Verde Islands, *Atmos. Chem. Phys.*, *9, 24*, 9587-9897.

Stolle, C., K. Nagel, M. Labrenz, and K. Juergens (2010), Succession of the sea-surface microlayer in the coastal Baltic Sea under natural and experimentally induced low-wind conditions, *Biogeosci*, *7, 9*, 2975-2988.

Van Pinxteren, M., C. Müller, Y. Iinuma, C. Stolle, and H. Herrmann (submitted), Chemical characterization of dissolved organic compounds from coastal sea surface microlayers (Baltic Sea, Germany), *Environmental Science & Technology*.



**Funding**

- Federal Ministry of Education and Research (BMBF), SOPRAN Phase II

**Cooperation**

- Leibniz-Institute for Baltic Sea Research Warnemuende (IOW)
- Leibniz-Institute of Marine Research (IFM-GEOMAR)
- University of York, Great Britain

# Gas-phase reaction of OH radicals with DMS: Products and particle formation

Torsten Berndt[1], Stefanie Richters[1], Frank Stratmann[1], Roy L. Mauldin III[2], Mikko Sipilä[3]

[1] Leibniz Institute for Tropospheric Research (IfT), Leipzig, Germany
[2] University of Colorado, Boulder, USA
[3] University of Helsinki, Finland

*Dimethylsulfid (DMS) ist die bedeutendste biogene in die Atmosphäre emittierte Schwefelverbindung mit einem Anteil von etwa 60% der natürlichen Emissionen. DMS wird durch Phytoplankton in den Ozeanen produziert. Die atmosphärische Oxidation des DMS wird fast ausschließlich durch das OH-Radikal initiiert.*

*Ziel der experimentellen Arbeiten ist das bessere Verständnis der ablaufenden Gasphasenprozesse beim Abbau des DMS sowie des Prozesses der Partikelneubildung unter atmosphärennahen Bedingungen, [$NO_x$] < $10^{10}$ Moleküle $cm^{-3}$.*

*Die gefundenen DMS Produkte konnten qualitativ unter Verwendung einer modifizierten Version des Master Chemical Mechanism, MCMv3.2. beschrieben werden.*

*Die Experimente zur Partikelneubildung deuten darauf hin, dass Schwefelsäure hauptsächlich (eher als Methansulfonsäure) für diesen Prozess von Bedeutung ist. Es konnten die jeweiligen Säuredimere sowie das gemischte Dimer nachgewiesen werden.*

## Introduction

Dimethylsulfide (DMS; $CH_3SCH_3$) is produced by biological activity of phytoplankton in the ocean´s surface layer. DMS represents the largest natural source of atmospheric sulfur accounting for approximately 60% of natural emissions. The atmospheric degradation of DMS is nearly exclusively initiated by the attack of OH radicals producing among others $SO_2$ and subsequently sulfuric acid particles. The degradation processes, including $SO_2$ with subsequent sulfuric acid formation as well as methane sulfonic acid formation (MSA), are not fully understood so far. It is well established that the primary attack of OH radicals toward DMS proceeds via an addition channel (~30%), path (1), and an H-abstraction channel (~70%), path (2).

$$OH + CH_3SCH_3 \rightarrow CH_3S(OH)CH_3 \quad (1)$$
$$OH + CH_3SCH_3 (+ O_2) \rightarrow CH_3SCH_2O_2 + H_2O \quad (2)$$

The first stable products of the additional channel are dimethyl sulfoxide (DMSO) and dimethyl sulfone ($DMSO_2$). $SO_2$ (and subsequent sulfuric acid) and MSA formation are believed to arise probably from the $CH_3S$ intermediate formed from $CH_3SCH_2O_2$ from the abstraction channel.

At the moment it is highly speculative whether or not DMS products other than sulfuric acid are involved in atmospheric new particle formation processes.

Subject of the present study are investigations regarding the generation of the first stable products and new particle formation in the absence of $NO_x$ ([$NO_x$] < $10^{10}$ molecule $cm^{-3}$) relevant for the remote marine environment. From these results more insight in the atmospheric degradation of DMS and the impact for the nucleation process over the ocean is expected.

The experiments have been carried out in the atmospheric pressure flow-tube *IfT*-LFT (i.d. 8 cm; length 505 cm) at 293 ± 0.5 K. Reactant consumption and product formation were followed by mass spectrometry, CI-API-ToF-MS (chemical ionization - atmospheric pressure ionization - time of flight - MS) and PTR-MS (proton transfer reaction - MS), long-path FT-IR spectroscopy and by trace gas monitors for $O_3$ and $SO_2$.

## Results and Discussion

Figure 1 shows product yields of HCHO and $SO_2$ as well as the signal at 77 amu (attributed to methyl thioformate, MTF) with respect to reacted DMS, $I_{77}/\Delta I_{63}$, as a function of the DMS concentration. OH radicals have been produced by photolysis of $H_2O_2$ using a nearly constant concentration of $H_2O_2$. The formed OH radicals react either with $H_2O_2$ forming $HO_2$ or via the reaction with DMS depending on the ratio [$H_2O_2$]/[DMS]. In case of a large excess of $H_2O_2$ over DMS, efficient $HO_2$ radical formation takes place in parallel to the desired reaction of OH with DMS and the radicals produced in the system (mainly $CH_3SCH_2O_2$ from path (2)) react preferably with $HO_2$. With increasing DMS concentration (and for nearly constant $H_2O_2$) $HO_2$ formation from OH + $H_2O_2$ becomes less favoured, repressing also the probability for the $CH_3SCH_2O_2$ + $HO_2$ reaction. Obviously, the detected HCHO, $SO_2$ and MTF (signal at 77 amu) arise predominantly form the abstraction channel under conditions for which the

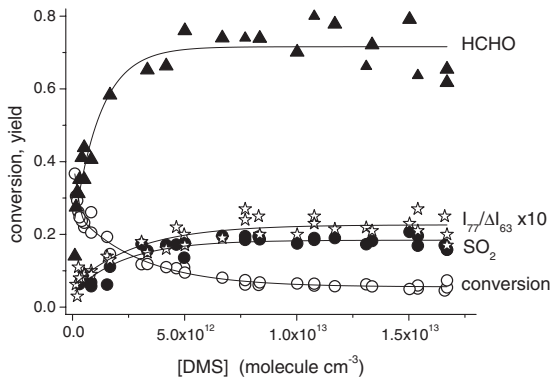


***Fig. 1:*** *DMS conversion and formation yields of HCHO and $SO_2$ and the signal at 77 amu (MTF: methyl thioformate) with respect to reacted DMS at 63 amu ($I_{77}/\Delta I_{63}$) as a function of initial DMS concentration. Initial concentrations: $[H_2O_2]$ = (1.1 - 2.1)·10$^{13}$ molecule cm$^{-3}$, [DMS] = (1.0 - 167)·10$^{11}$ molecule cm$^{-3}$; $H_2O_2$ photolysis for OH radical generation.*

$CH_3SCH_2O_2$ radicals did not react preferably with $HO_2$.

Modelling runs have been performed using the DMS module from the Master Chemical Mechanism, MCMv3.2. In contrast to the original mechanisms, MTF formation via $CH_3SCH_2O_2 + HO_2$ was omitted in order to describe the experimental findings more properly. Generally, the simulation slightly under-predicted the measured yields of HCHO. The $SO_2$ yields observed were roughly in agreement with the modelling results.

In a next set of experiments, for atmospheric relevant $O_3$ concentration, the process of new particle formation was studied including the measurements of potential precursors as sulfuric acid (SA) and methane sulfonic acid (MSA), cf. Fig. 2.

A nearly stable formation yield of ~0.01 for MSA was observed for different reaction conditions. The detected concentrations of SA and MSA depending on the DMS concentration in the reactor were in line with the expectation from the modeling. Beside the acid monomers also the corresponding dimers ($SA_2$ and $MSA_2$) and the mixed dimer (SA·MSA)

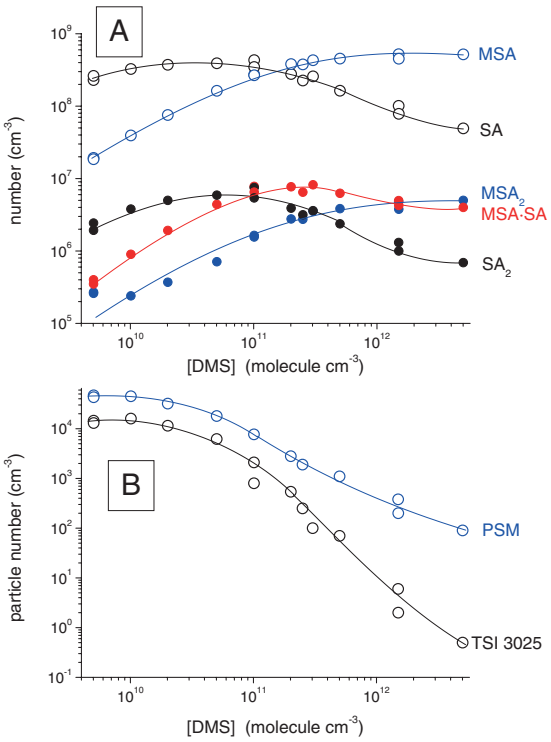


***Fig. 2:*** *Formation of S-containing products and new particle formation as a function of initial DMS concentration. OH radical generation via $O_3$ photolysis at r.h. = 50%; initial concentrations: $[O_3]$ = 4.6·10$^{11}$ molecule cm$^{-3}$, [DMS] = (5.0 - 5000)·10$^9$ molecule cm$^{-3}$. A: sulfuric acid (SA), methane sulfonic acid (MSA), their dimers $SA_2$ and $MSA_2$ as well as the mixed dimer SA·MSA. B: particle measurements by means of a particle size magnifier (PSM) with a 50% cut-off size of about 1.5 nm and from a butanol-based counter (TSI 3025) with a 50% cut-off size of 2.5 - 3.0 nm.*

were observed, $[SA_2]/[SA]$ ~ 0.01, $[MSA_2]/[MSA]$ ~ 0.003-0.005. Simultaneously performed particle measurements with two different particle counters (different counting efficiency for small particles) revealed clearly that the process of new particle formation is strongly connected to SA (and SA related clusters) rather than to MSA. However, contributions of MSA to particle growth cannot be ruled out and will be subject of further investigations

**Cooperation**
- University of Colorado, Boulder, USA
- University Helsinki, Helsinki, Finland

# Ship and satellite observations over ocean for verification of the shortwave cloud radiative effect in climate models

Andreas Macke[1], Timo Hanschmann[1], Hartwig Deneke[2], Rob Roebeling[2]

[1] Leibniz Institute for Tropospheric Research (IfT), Leipzig, Germany
[2] The Royal Netherlands Meteorological Institute (KNMI), Utrecht, Netherlands

*Mit Hilfe von Schiffs- und Satellitenmessungen der Oberflächenstrahlungsbilanz und der Zusammensetzung der Atmosphäre wurde die Genauigkeit untersucht, mit der das Strahlungstransportschema des ECHAM-5 Klimamodelles den solaren Wolkenstrahlungseffekt (engl. Short Wave Cloud Radiative Effect: SWCRE) an der Meeresoberfläche wiedergibt. Die Schiffsmessungen liefern Wolkenbedeckung mittels einer Vollhimmelskamera, Flüssigwasserpfad mittels eines Mikrowellenradiometers, Wolkenunterkantenhöhe durch ein Ceilometer sowie Temperatur- und Feuchtprofile aus Radiosondenaufstiegen. Die Level-2-Produkte des Satellite Application Facility on Climate Monitoring (CM-SAF) Projektes aus den Messungen des Spinning Enhanced Visible and InfraRed Imager (SEVIRI) wurden zur satellitengestützten Charakterisierung des Atmosphärenzustandes genutzt. Generell zeigt sich, dass die Verwendung von Satelliten- statt Schiffsdaten zu keinem Verlust an Genauigkeit führt. Die Kombination beider Datensätze führt aufgrund der Nutzung des satelliten-basierten Effektivradius als zusätzliche Information zu den Schiffsmessungen zu einer Verbesserung.*

## Introduction

Clouds strongly influence the energy budget of the earth's atmosphere. Because of their high degree of temporal and spatial variability, and the complexity of cloud processes, it remains challenging to model and predict the effect of clouds on the energy budget. The International Panel on Climate Change and others [IPCC, *Solomon et al.*, 2007] has identified the representation of clouds in global circulation models (GCMs) as the largest source of uncertainty for predicting future climate change. Especially the cloud radiative effect (CRE), defined as the difference between the net radiative fluxes of the cloudy and cloud-free atmosphere, is often not reproduced satisfactorily. To evaluate this source of uncertainty in GCMs, it is important to identify those situations in which the model can reproduce the CRE well and badly.

Starting with the Meridional Ocean Radiation Experiment MORE (5 cruises; [*Sinitsyn et al.*, 2006; *Macke et al.*, 2007] and continued with the OCEANET project (11 cruises; [*Macke*, 2008]), a comprehensive ship based data set has been established. OCEANET provides measurements of cloud properties and radiative fluxes with high temporal resolution, including a total sky imager (TSI), a microwave radiometer (RPG HATPRO; [*Rose and Czekala*, 2009]), a sun photometer from the MARITIME AEROSOL NETWORK (MAN/AERONET) [*Smirnov et al.*, 2009], a Raman lidar [*Althausen et al.*, 2009] as well as instrumentation for measuring turbulent fluxes such as latent heat and carbon dioxide fluxes on some cruises.

The aim of this study is to establish the utility and level of accuracy of this large and unique collection of data sets for evaluating the representation of cloud properties in GCMs over ocean, and their resulting effect on radiative fluxes. Furthermore, we evaluate to what degree satellite-based estimates of cloud properties can be used as an alternative or complement to these ship-based observations. The majority of clouds observed during the OCEANET cruises are relatively thin liquid water clouds, which still pose significant challenges both to current measurement techniques and our scientific understanding [*Turner et al.*, 2007].

## Data

We use the liquid water path (LWP), temperature, and humidity (T+H) profiles derived from a HATPRO microwave radiometer [*Rose and Czekala*, 2009] for our study. A pyranometer of type CM21 [*Kipp&Zonen*, 2006] is used to measure global radiation. The CM-SAF provides several products on cloud properties and radiative fluxes derived from Meteosat SEVIRI [*Schulz et al.*, 2009]. We have calculated level-2 products with the CM-SAF retrieval algorithms to obtain the cloud properties LWP, cloud optical thickness (COT), and effective radius ($r_e$), [see *Roebeling et al.*, 2006] on the full temporal and spatial resolution of SEVIRI.

## Model

We use the observations to describe the atmosphere in the radiative transfer scheme of the ECHAM-5 climate model [*Roeckner*, 2003]. As in other GCMs, the radiative transfer calculations are based on the assumption of plane parallel clouds, which implies a horizontally homogeneous distribution of cloud water and droplet number concentration within one grid cell. Scattering and absorption by aerosols are considered by using the "Global Aerosol Data Set" [*Koepke et al.*, 1997].

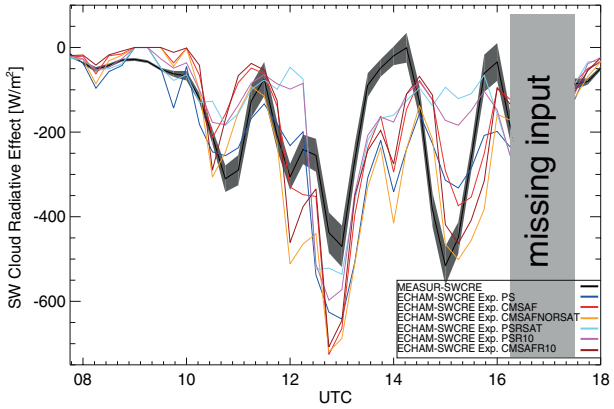


***Fig. 1:*** *Example diurnal cycle of the SWCRE for November the 10th, 2007 with broken cloud conditions and large cloud fraction. Observations are denoted by the black line, the different ECHAM5 results by the colored lines. See text for explanation.*

The used RTM can be run in two vertical resolutions to resolve a range from 1013 hPa to 10 hPa. Our measurements do not provide cloud profiles but rather vertically integrated values. We have chosen to locate the cloud only within a single model layer because most clouds during the selected days have a small vertical extent.

## Closure study

For the radiation closure study we have computed the diurnal cycle of the shortwave cloud radiative effect (SWCRE) and therefore the downward shortwave radiation at the surface with the RTM, and compared it to the ship based SWCRE measurements. We define six experiments for testing the sensitivity of the model to different assumptions about the representation of clouds as input to the RTM, and for understanding the processes and mechanisms leading to deviations between model results and the ship based measurements. In experiment **PS** the atmosphere is completely described by ship based measurements. The ECHAM5 standard profile for the cloud droplet number concentration is used. To examine the effect of an effective radius on the DSR at the surface two more experiments are defined: experiment **PS-RSAT** uses the effective radius estimated by CM-SAF, experiment **PS-R10** assumes a constant effective radius of 10 µm as applied in the ISCCP satellite retrieval ( i.e. *Han et al.* [1994]). In experiment **CMSAF** only satellite products are used to describe the cloud properties. We use the LWP to calculate the mixing ratio of liquid water, and the effective radius to obtain the cloud droplet number concentration. For evaluating the benefit of the effective radius information in combination with CM-SAF LWP on the radiative transfer calculations, we also define the experiment **CMSAF-NORSAT** using the CM-SAF LWP together with the standard profile of cloud droplet number concentrations. Also for the CM-SAF cloud properties we define an experiment using a constant effective radius, experiment **CMSAF-R10**.

Figure 1 show the diurnal cycle of the SWCRE for a day with broken clouds dominated by a large cloud fraction. Figure 2 provides an exemplary impression of the cloud conditions in the afternoon at 2pm of the same day. The black curve in Fig. 1 denotes the ship based measurements and the shaded area around it indicates the variability during each averaging period. The other curves show the model results for the different experiments (blue for experiment PS, light blue for experiment PS-RSAT, magenta for experiment PS-R10, red for experiment CMSAF, orange for experiment CMSAF-NORSAT, and brown for experiment CMSAF-R10). The light grey bar (missing input) indicate time periods with problems with the input data such as rain for the microwave radiometer, sunglint for CM-SAF data, shadowing of the pyranometer etc. This example indicates that the model can generally reproduce the diurnal cycle of the SWCRE. However, there is still a significant spread within the six experiments. The strongest deviations to observations are shown for the experiments without prescribed effective

***Fig. 2:*** *Full sky image taken on 10. 11. 2007, 14:00 UTC on the POLARSTERN cruise ANT-XXIV/1.*

radius. From the analysis of several diurnal cycles we find that using satellite data instead of ship-based atmospheric properties does not result in a loss in accuracy in the modeled CRE. We assume that satellite cloud products are well suited to describe the observed surface radiation fluxes as they result from matching the cloud products to the radiance observed at the satellite. Of course, small-scale radiation variability - as seen by the ship-based observations - cannot be resolved from the coarse satellite products.

Future work will extend the analysis to all ship cruises and will investigate specific cloud regimes and vertical profiles of cloud liquid water and effective radius.

**Reference**


IPCC, 2007: Summary for Policymakers, in *Climate Change 2007: The Physical Science Basis. Contribution of Working Group I to the Fourth Assessment Report of the Intergovernmental Panel on Climate Change*, edited by S. Solomon, D. Qin, M. Manning, Z. Chen, M. Marquis, K. B. Averyt, M. Tignor and H. L. Miller, Cambridge University Press, Cambridge, United Kingdom and New York, NY, USA.

Althausen, D., R. Engelmann, H. Baars, B. Heese, A. Ansmann, D. Müller, and M. Komppula (2009), Portable Raman Lidar Polly(XT) for automated profiling of aerosol backscatter, extinction, and depolarization, *Journal of Atmospheric and Oceanic Technology*, *26*(11), 2366-2378.

Han, Q. Y., W. B. Rossow, and A. A. Lacis (1994), Near-Global Survey of Effective Droplet Radii in Liquid Water Clouds Using Isccp Data, *Journal of Climate*, *7*(4), 465-497.

Kipp&Zonen (2006), Instruction Manual CMP series, *Technical Report Rep.*

Koepke, P., M. Hess, I. Schult, and E. P. Shettle (1997), Global Aerosol Data Set, *243 Rep.*, Max-Planck-Institut für Meteorologie, Hamburg.

Macke, A. E. (2009), The expedition of the research vessel “Polarstern” to the Antarctic in 2008 (ANT-XXIV/4), in *Berichte zur Polar- und Meeresforschung Bd. 591*, edited by A. Macke, p. 64, AWI, Bremerhaven.

Macke, A., L. Kalisch, A. Sinitsyn, and A. Wassmann (2007), More of MORE: the first MORE cruise onboard RV Polarstern, *Flux news*, *4*, 21-22.

Roebeling, R. A., A. J. Feijt, and P. Stammes (2006), Cloud property retrievals for climate monitoring: Implications of differences between Spinning Enhanced Visible and Infrared Imager (SEVIRI) on METEOSAT-8 and Advanced Very High Resolution Radiometer (AVHRR) on NOAA-17, *Journal of Geophysical Research - Atmospheres*, *111*, doi: doi: 10.1029/2005JD006990.

Roeckner, E. (2003), The atmospheric general circulation model ECHAM-5 - Model description, *349 Rep.*, Max-Planck-Institut für Meteorologie, Hamburg.

Rose, T., and H. Czekala (2009), Operational Manual*Rep.*, Radiometer Physics GmbH.

Schulz, J., P. Albert, H. D. Behr, D. Caprion, H. Deneke, S. Dewitte, B. Durr, P. Fuchs, A. Gratzki, P. Hechler, R. Hollmann, S. Johnston, K. G. Karlsson, T. Manninen, R. Muller, M. Reuter, A. Riihela, R. Roebeling, N. Selbach, A. Tetzlaff, W. Thomas, M. Werscheck, E. Wolters, and A. Zelenka (2009), Operational climate monitoring from space: The EUMETSAT Satellite Application Facility on Climate Monitoring (CM-SAF), *Atmospheric Chemistry and Physics*, *9*(5), 1687-1709, doi: doi: 10.1029/2005JD006990.

Sinitsyn, A., S. K. Gulev, A. Macke, J. Kalisch, and A. Sokov (2006), MORE cruises launched WGSF/WCRP, *Flux news*, *1*, 11-13.

Smirnov, A., B. N. Holben, I. Slutsker, D. M. Giles, C. R. McClain, T. F. Eck, S. M. Sakerin, A. Macke, P. Croot, G. Zibordi, P. K. Quinn, J. Sciare, S. Kinne, M. Harvey, T. J. Smyth, S. Piketh, T. Zielinski, A. Proshutinsky, J. I. Goes, N. B. Nelson, P. Larouche, V. F. Radionov, P. Goloub, K. K. Moorthy, R. Matarrese, E. J. Robertson, and F. Jourdin (2009), Maritime Aerosol Network as a component of Aerosol Robotic Network, *Journal of Geophysical Research - Atmospheres*, *114*.

Turner, D. D., A. M. Vogelmann, R. T. Austin, J. C. Barnard, K. Cady-Pereira, J. C. Chiu, S. A. Clough, C. Flynn, M. M. Khaiyer, J. Liljegren, K. Johnson, B. Lin, C. Long, A. Marshak, S. Y. Matrosov, S. A. McFarlane, M. Miller, Q. Min, F. Minnis, W. O’Hirok, Z. Wang, and W. Wiscombe (2007), Thin liquid water clouds - Their importance and our challenge, *Bulletin of the American Meteorological Society*, *88*(2), 177-.



**Funding**

- CM-SAF Visiting Scientist Activity with EUMETSAT (partial)

**Cooperation**

- Max-Planck-Institut für Meteorologie, Hamburg
- Alfred Wegener Institut für Polar- und Meeresforschung, Bremerhaven via RV POLARSTERN cruises ANT-XXIV/1 and ANT-XXIV/4

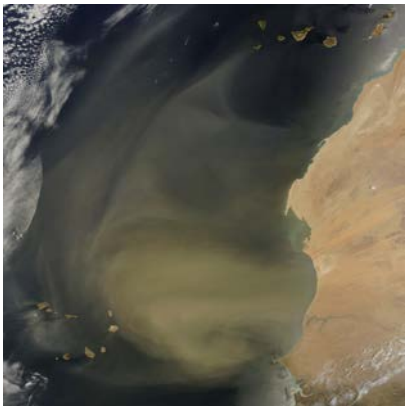

# *Appendices*

## Publication statistics

| | 2010 | 2011 |
|---|---|---|
| **Total number of publications** | **297** | **256** |
| Books (author, editor) | 0 | 0 |
| Book sections | 6 | 4 |
| Conference proceedings | 94* | 27 |
| Publications, peer-reviewed | 82 | 102 |
| Publications, other | 9 | 15 |
| Lectures, invited | 11 | 22 |
| Conference contributions / Lectures, other | 95 | 86 |

*) due to 65 contributions to the International Aerosol Conference in 2010

## Publications

**2010**


**Ansmann, A.**, **Fruntke, J.** and **Engelmann, R.** 2010. Updraft and downdraft characterization with Doppler lidar: Cloud-free versus cumuli-topped mixed layer. Atmos. Chem. Phys., **10**, 7845-7858, doi:10.5194/acp-10-7845-2010.

**Ansmann, A.**, **Tesche, M.**, Gross, S., Freudenthaler, V., **Seifert, P.**, **Hiebsch, A.**, **Schmidt, J.**, **Wandinger, U.**, **Mattis, I.**, **Müller, D.** and Wiegner, M. 2010. The 16 April 2010 major volcanic ash plume over central Europe: EARLINET lidar and AERONET photometer observations at Leipzig and Munich, Germany. Geophys. Res. Lett., **37**, L13810, doi:10.1029/2010gl043809.

Balis, D., Giannakaki, E., **Müller, D.**, Amiridis, V., Kelektsoglou, K., Rapsomanikis, S. and Bais, A. 2010. Estimation of the microphysical aerosol properties over Thessaloniki, Greece, during the SCOUT-O-3 campaign with the synergy of Raman lidar and Sun photometer data. J. Geophys. Res. - Atmos., **115**, D08202, doi:10.1029/2009jd013088.

**Berndt, T.**, Kreipl, A. and Lenski, U. 2010. Epoxidation of 2-Butene from Raffinate 2 Feedstock. Ind. Eng. Chem. Res., **49**, 3957-3960.

**Berndt, T.**, **Stratmann, F.**, Sipilä, M., Vanhanen, J., Petäjä, T., Mikkilä, J., **Grüner, A.**, **Spindler, G.**, Mauldin III, R. L., Curtius, J., Kulmala, M. and **Heintzenberg, J.** 2010. Laboratory study on new particle formation from the reaction OH + $SO_2$: Influence of experimental conditions, $H_2O$ vapour, $NH_3$ and the amine tert-butylamine on the overall process. Atmos. Chem. Phys., **10**, 7101-7116, doi:10.5194/acp-10-7101-2010.

Bierwirth, E., Wendisch, M., Jäkel, E., Ehrlich, A., Schmidt, K. S., Stark, H., Pilewskie, P., Esselborn, M., Gobbi, G. P., Ferrare, R., **Müller, T.** and Clarke, A. 2010. A new method to retrieve the aerosol layer absorption coefficient from airborne flux density and actinic radiation measurements. J. Geophys. Res. - Atmos., **115**, D14211, doi:10.1029/2009jd013636.

**Birmili, W.**, **Göbel, T.**, **Sonntag, A.**, Ries, L., Sohmer, R., Gilge, S., Levin, I. and Stohl, A. 2010. A case of transatlantic aerosol transport detected at the Schneefernerhaus Observatory (2650 m) on the northern edge of the Alps. Meteorol. Z., **19**, 591-600, doi:10.1127/0941-2948/2010/0465.

**Birmili, W.**, **Heinke, K.**, Pitz, M., Matschullat, J., **Wiedensohler, A.**, Cyrys, J., Wichmann, H.-E. and Peters, A. 2010. Particle number size distributions in urban air before and after volatilisation. Atmos. Chem. Phys., **10**, 4643-4660, doi:10.5194/acp-10-4643-2010.

**Birmili, B.**, **Sonntag, A.**, **Tuch, T.** and **Wiedensohler, A.** 2010. *Entwicklung eines mobilen Aerosolstandards*. In: *Schriftenreihe des Landesamtes für Umwelt, Landwirtschaft und Geologie*. Landesamtes für Umwelt, Landwirtschaft und Geologie, Dresden, **Heft 2/2010**, p. 24.

**Birmili, B.**, **Weinhold, K.**, **Nordmann, S.**, **Wiedensohler, A.**, Pitz, M., Cyrys, J., Flentje, H., Nickel, C., Kuhlbusch, T. A. J., Löschau, G., Ries, L. and Wirtz, K. 2010. *Das Messnetz für ultrafeine Partikel in Deutschland (GUAN): Erste Erkenntnisse*. In: *Schriftenreihe der Kommission Reinhaltung der Luft im VDI und DIN*. Bundesministerium für Umwelt, Naturschutz und Reaktorsicherheit, Bonn, p. 12.

Bodenschatz, E., Malinowski, S. P., **Shaw, R. A.** and **Stratmann, F.** 2010. Can we understand clouds

without turbulence? Science, **327**, 970-971, doi:10.1126/science.1185138.

Deguillaume, L., **Tilgner, A.**, **Schrödner, R.**, **Wolke, R.**, Chaumerliac, N. and **Herrmann, H.** 2010. Towards an operational aqueous phase chemistry mechanism for regional chemistry-transport models: CAPRAM-RED and its application to the COSMO-MUSCAT model. J. Atmos. Chem., **64**, 1-35, doi:10.1007/s10874-010-9168-8.

**Deneke, H.** and Roebeling, R. 2010. Downscaling of METEOSAT SEVIRI 0.6 and 0.8 µm channel radiances utilizing the high-resolution visible channel. Atmos. Chem. Phys., **10**, 9761-9772, doi:10.5194/acp-10-9761-2010.

Duplissy, J., Enghoff, M. B., Aplin, K. L., Arnold, F., Aufmhoff, H., Avngaard, M., Baltensperger, U., Bondo, T., Bingham, R., Carslaw, K., Curtius, J., David, A., Fastrup, B., Gagne, S., Hahn, F., Harrison, R. G., Kellett, B., Kirkby, J., Kulmala, M., Laakso, L., Laaksonen, A., Lillestol, E., Lockwood, M., Makela, J., Makhmutov, V., Marsh, N. D., Nieminen, T., Onnela, A., Pedersen, E., Pedersen, J. O. P., Polny, J., Reichl, U., Seinfeld, J. H., Sipilä, M., Stozhkov, Y., **Stratmann, F.**, Svensmark, H., Svensmark, J., Veenhof, R., Verheggen, B., Viisanen, Y., Wagner, P. E., Wehrle, G., Weingartner, E., **Wex, H.**, Wilhelmsson, M. and Winkler, P. M. 2010. Results from the CERN pilot CLOUD experiment. Atmos. Chem. Phys., **10**, 1635-1647.

El Naggar, S. and **Macke, A.** 2010. *The expedition of the research vessel „Polarstern" to the Antarctic in 2009 (ANT-XXVI/1) : ANT-XXVI/1 16 October 2009 - 25 November 2009 Bremerhaven - Punta Arenas*. S. With contribution of the participants: El Naggar and A. Macke (Ed.), In: *Berichte zur Polar- und Meeresforschung = Reports on polar and marine research*. **614**, p. 79.

Fors, E. O., Rissler, J., Massling, A., Svenningsson, B., Andreae, M. O., Dusek, U., Frank, G. P., Hoffer, A., Bilde, M., Kiss, G., Janitsek, S., **Henning, S.**, Facchini, M. C., Decesari, S. and Swietlicki, E. 2010. Hygroscopic properties of Amazonian biomass burning and European background HULIS and investigation of their effects on surface tension with two models linking H-TDMA to CCNC data. Atmos. Chem. Phys., **10**, 5625-5639, doi:10.5194/acp-10-5625-2010.

Gong, Y. G., Hu, M., **Cheng, Y. F.**, Su, H., Yue, D. L., Liu, F., **Wiedensohler, A.**, Wang, Z. B., Kalesse, H., Liu, S., **Wu, Z. J.**, Xiao, K. T., Mi, P. C. and Zhang, Y. H. 2010. Competition of coagulation sink and source rate: New particle formation in the Pearl River Delta of China. Atmos. Environ., **44**, 3278-3285, doi:10.1016/j.atmosenv.2010.05.049.

Hamed, A., **Birmili, W.**, Joutsensaari, J., Mikkonen, S., Asmi, A., **Wehner, B.**, **Spindler, G.**, Jaatinen, A., Uhse, K., **Wiedensohler, A.**, Lehtinen, K. E. J. and Laaksonen, A. 2010. Changes in the production rate of secondary aerosol particles in Central Europe in view of decreasing $SO_2$ emissions between 1996 and 2006. Atmos. Chem. Phys., **10**, 1071-1091.

**Heese, B.**, Flentje, H., **Althausen, D.**, **Ansmann, A.** and Frey, A. 2010. Ceilometer lidar comparison: Backscatter coefficient retrieval and signal-to-noise ratio determination. Atmos. Meas. Tech. (AMT), **3**, 1763-1770, doi:10.5194/amt-3-1763-2010.

Heinle, A., **Macke, A.** and Srivastav, A. 2010. Automatic cloud classification of whole sky images. Atmos. Meas. Tech. (AMT), **3**, 557-567, doi:10.5194/amt-3-557-2010.

**Heintzenberg, J.** and **Birmili, W.** 2010. Aerosols over the Siberian Forest: The ZOTTO project. J. Cryog. Soc. Jpn., **68**, 5-8.

**Henning, S.**, **Wex, H.**, **Hennig, T.**, **Kiselev, A.**, Snider, J., **Rose, D.**, Dusek, U., Frank, G., Pöschl, U., Kristensson, A., Bilde, M., Tillmann, R., Kiendler-Scharr, A., Mentel, T., Walter, S., Schneider, J., **Wennrich, C.** and **Stratmann, F.** 2010. Soluble mass, hygroscopic growth and droplet activation of coated soot particles during LExNo. J. Geophys. Res. - Atmos., **115**, D11206, doi:10.1029/2009JD012626.

Henrich, F., **Siebert, H.**, Jäkel, E., **Shaw, R. A.** and Wendisch, M. 2010. Collocated measurements of boundary layer cloud microphysical and radiative properties: A feasibility study. J. Geophys. Res. - Atmos., **115**, D24214, doi:10.1029/2010jd013930.

Herrmann, E., Brus, D., Hyvarinen, A. P., **Stratmann, F.**, Wilck, M., Lihavainen, H. and Kulmala, M. 2010. A computational fluid dynamics approach to nucleation in the water-sulfuric acid system. J. Phys. Chem. A, **114**, 8033-8042, doi:10.1021/jp103499q, 10.1021/jp103499q.

**Herrmann, H.** 2010. Preface: Physico-chemical aspects of global atmospheric change : Dedicated to Reinhard Zellner on the occasion of his 65th birthday. Z. Phys. Chem., **224**, 943-947, doi:10.1524/zpch.2010.6152.

**Herrmann, H.**, **Hoffmann, D.**, **Schaefer, T.**, **Bräuer, P.** and **Tilgner, A.** 2010. Tropospheric aqueous-phase free-radical chemistry: Radical sources, spectra, reaction kinetics and prediction tools. ChemPhysChem, **11**, 3796-3822, doi:10.1002/cphc.201000533.

Hieronymi, M. and **Macke, A.** 2010. Spatiotemporal underwater light field fluctuations in the open ocean. J. Eur. Opt. Soc.-Rapid, **5**, 10019s, doi:10.2971/jeos.2010.10019s.

**Hoffmann, D.**, **Tilgner, A.**, **Iinuma, Y.** and **Herrmann, H.** 2010. Atmospheric stability of levoglucosan: A detailed laboratory and modeling study. Environ. Sci. Technol., **44**, 694-699, doi:10.1021/es902476f.

Hünerbein, A., **Wandinger, U.** and Berger, F. H. 2010. Die neue Generation von Satellitenmissionen zur vertikal aufgelösten Messung von Wolken und Aerosol. PROMET, **36**, 169-179.

**Iinuma, Y.**, **Böge, O.**, **Gräfe, R.** and **Herrmann, H.** 2010. Methyl-nitrocatechols: Atmospheric tracer compounds for biomass burning secondary organic aerosols. Environ. Sci. Technol., **44**, 8453-8459, doi:10.1021/es102938a.

Kamphus, M., Ettner-Mahl, M., Klimach, T., Drewnick, F., Keller, L., Cziczo, D. J., **Mertes, S.**, Borrmann, S. and Curtius, J. 2010. Chemical composition of ambient aerosol, ice residues and cloud droplet residues in mixed-phase clouds: Single particle analysis during the Cloud and Aerosol Characterization Experiment (CLACE 6). Atmos. Chem. Phys., **10**, 8077-8095, doi:10.5194/acp-10-8077-2010.

Kerminen, V.-M., Petäjä, T., Manninen, H. E., Paasonen, P., Nieminen, T., Sipilä, M., Junninen, H., Ehn, M., Gagné, S., Laakso, L., Riipinen, I., Vehkamäki, H., Kurten, T., Ortega, I. K., Dal Maso, M., Brus, D., Hyvärinen, A., Lihavainen, H., Leppä, J., Lehtinen, K. E. J., Mirme, A., Mirme, S., Hõrrak, U., **Berndt, T.**, **Stratmann, F.**, **Birmili, W.**, **Wiedensohler, A.**, Metzger, A., Dommen, J., Baltensperger, U., Kiendler-Scharr, A., Mentel, T. F., Wildt, J., Winkler, P. M., Wagner, P. E., Petzold, A., Minikin, A., Plass-Dülmer, C., Pöschl, U., Laaksonen, A. and Kulmala, M. 2010. Atmospheric nucleation: Highlights of the EUCAARI project and future directions. Atmos. Chem. Phys., **10**, 10829-10848, doi:10.5194/acp-10-10829-2010.

**Kiselev, A.**, **Wennrich, C.**, **Stratmann, F.**, **Wex, H.**, **Henning, S.**, Mentel, T., Kiendler-Scharr, A., Schneider, J., Walter, S. and Lieberwirth, I. 2010. Morphological characterization of soot aerosol particles during LACIS Experiment in November (LExNo). J. Geophys. Res. - Atmos., **115**, D11204, doi:10.1029/2009JD012635.

Kulmala, M., Riipinen, I., Nieminen, T., Hulkkonen, M., Sogacheva, L., Manninen, H. E., Paasonen, P., Petäjä, T., Dal Maso, M., Aalto, P. P., Viljanen, A., Usoskin, I., Vainio, R., Mirme, S., Mirme, A., Minikin, A., Petzold, A., Hõrrak, U., Plass-Dülmer, C., **Birmili, W.** and Kerminen, V.-M. 2010. Atmospheric data over a solar cycle: No connection between galactic cosmic rays and new particle formation. Atmos. Chem. Phys., **10**, 1885-1898.

Lai, S. C., Baker, A. K., Schuck, T. J., van Velthoven, P., Oram, D. E., Zahn, A., **Hermann, M.**, **Weigelt, A.**, Slemr, F., Brenninkmeijer, C. A. M. and Ziereis, H. 2010. Pollution events observed during CARIBIC flights in the upper troposphere between South China and the Philippines. Atmos. Chem. Phys., **10**, 1649-1660.

**Laurent, B.**, **Tegen, I.**, **Heinold, B.**, **Schepanski, K.** and Weinzierl, B. 2010. A model study of Saharan dust emissions and distributions during the SAMUM-1 campaign. J. Geophys. Res. - Atmos., **115**, D21210, 20 p., doi:10.1029/2009JD012995.

Lee, J. D., McFiggans, G., Allan, J. D., Baker, A. R., Ball, S. M., Benton, A. K., Carpenter, L. J., Commane, R., Finley, B. D., Evans, M., Fuentes, E., Furneaux, K., Goddard, A., Good, N., Hamilton, J. F., Heard, D. E., **Herrmann, H.**, Hollingsworth, A., Hopkins, J. R., Ingham, T., Irwin, M., Jones, C. E., Jones, R. L., Keene, W. C., Lawler, M. J., **Lehmann, S.**, Lewis, A. C., Long, M. S., Mahajan, A., Methven, J., Moller, S. J., **Müller, K.**, **Müller, T.**, **Niedermeier, N.**, O'Doherty, S., Oetjen, H., Plane, J. M. C., Pszenny, A. A. P., Read, K. A., Saiz-Lopez, A., Saltzman, E. S., Sander, R., von Glasow, R., Whalley, L., **Wiedensohler, A.** and Young, D. 2010. Reactive Halogens in the Marine Boundary Layer (RHaMBLe): The tropical North Atlantic experiments. Atmos. Chem. Phys., **10**, 1031-1055.

Lengfeld, K., **Macke, A.**, Feister, U. and Güldner, J. 2010. Parameterization of solar radiation from model and observations. Meteorol. Z., **19**, 25-33, doi:10.1127/0941-2948/2010/0423.

Lieber, M., **Wolke, R.**, **Grützun, V.**, Müller, M. S. and Nagel, W. E. 2010. *A framework for detailed multiphase cloud modeling on HPC systems*. B. Chapman, F. Desprez, G. R. Joubert, A. Lichnewsky, F. Peters, and T. Priol (Ed.), In: *Parallel computing: From multicores and GPU´s to petascale : Proceedings of ParCo09 „Advances in Parallel Computing"*. IOS Press, Amsterdam et al., p. 281-288. (Advances in parallel computing ; 19)

Löschau, G., **Wiedensohler, A.**, **Wehner, B.**, **Birmili, W.** and Gerwig, H. 2010. Measurement of the number concentration of ultrafine particles in ambient air in an air quality monitoring network - Part 2: Results of a traffic-orientated long term measurement. Gefahrst. Reinhalt. L., **70**, 183-187.

**Macke, A.**, Kalisch, J. and Hollmann, R. 2010. Validation of downward surface radiation derived from MSG data by in-situ observations over the Atlantic ocean. Meteorol. Z., **19**, 155-167, doi:10.1127/0941-2948/2010/0433.

Manninen, H. E., Nieminen, T., Asmi, E., Gagné, S., Häkkinen, S., Lehtipalo, K., Aalto, P., Vana, M., Mirme, A., Mirme, S., Hõrrak, U., Plass-Dülmer, C., Stange, G., Kiss, G., Hoffer, A., Töro, N.,

Moerman, M., Henzing, B., de Leeuw, G., Brinkenberg, M., Kouvarakis, G. N., Bougiatioti, A., Mihalopoulos, N., O'Dowd, C., Ceburnis, D., Arneth, A., Svenningsson, B., Swietlicki, E., Tarozzi, L., Decesari, S., Facchini, M. C., **Birmili, W.**, **Sonntag, A.**, **Wiedensohler, A.**, Boulon, J., Sellegri, K., Laj, P., Gysel, M., Bukowiecki, N., Weingartner, E., Wehrle, G., Laaksonen, A., Hamed, A., Joutsensaari, J., Petäjä, T., Kerminen, V.-M. and Kulmala, M. 2010. EUCAARI ion spectrometer measurements at 12 European sites - Analysis of new particle formation events. Atmos. Chem. Phys., **10**, 7907-7927, doi:10.5194/acp-10-7907-2010.

Martin, S. T., Andreae, M. O., **Althausen, D.**, Artaxo, P., **Baars, H**., Borrmann, S., Chen, Q., Farmer, D. K., Guenther, A., Gunthe, S. S., Jimenez, J. L., Karl, T., Longo, K., Manzi, A., Pauliquevis, T., Petters, M. D., Prenni, A. J., Pöschl, U., Rizzo, L. V., Schneider, J., Smith, J. N., Swietlicki, E., Tota, J., Wang, J., **Wiedensohler, A.** and Zorn, S. R. 2010. An overview of the Amazonian Aerosol Characterization Experiment 2008 (AMAZE-08). Atmos. Chem. Phys., **10**, 11415-11438, doi:10.5194/acp-10-11415-2010.

Matsui, H., Koike, M., Kondo, Y., Takegawa, N., Fast, J. D., Pöschl, U., Garland, R. M., Andreae, M. O., **Wiedensohler, A.**, Sugimoto, N. and Zhu, T. 2010. Spatial and temporal variations of aerosols around Beijing in summer 2006: 2. Local and column aerosol optical properties. J. Geophys. Res. - Atmos., **115**, D22207, doi:10.1029/2010jd013895.

**Mattis, I.**, **Seifert, P.**, **Müller, D.**, **Tesche, M.**, **Hiebsch, A.**, **Kanitz, T.**, **Schmidt, J.**, **Finger, F.**, **Wandinger, U.** and **Ansmann, A.** 2010. Volcanic aerosol layers observed with multiwavelength Raman lidar over central Europe in 2008-2009. J. Geophys. Res. - Atmos., **115**, D00L04, doi:10.1029/2009JD013472.

**Müller, C.**, **Iinuma, Y.**, **Müller, K.** and **Herrmann, H.** 2010. Detection of aliphatic amines in the marine environment. Geochim. Cosmochim. Acta, **74**, A735-A735.

**Müller, D.**, **Ansmann, A.**, Freudenthaler, V., Kandler, K., Toledano, C., **Hiebsch, A.**, Gasteiger, J., Esselborn, M., **Tesche, M.**, **Heese, B.**, **Althausen, D.**, Weinzierl, B., Petzold, A. and von Hoyningen-Huene, W. 2010. Mineral dust observed with AERONET Sun photometer, Raman lidar, and in situ instruments during SAMUM 2006: Shape-dependent particle properties. J. Geophys. Res. - Atmos., **115**, D11207, doi:10.1029/2009jd012523.

**Müller, D.**, **Mattis, I.**, Tatarov, B., Noh, Y. M., Shin, D. H., Shin, S. K., Lee, K. H., Kim, Y. J. and Sugimoto, N. 2010. Mineral quartz concentration measurements of mixed mineral dust/urban haze pollution plumes over Korea with multiwavelength aerosol Raman-quartz lidar. Geophys. Res. Lett., **37**, L20810, doi:10.1029/2010gl044633.

**Müller, D.**, Weinzierl, B., Petzold, A., Kandler, K., **Ansmann, A.**, **Müller, T.**, **Tesche, M.**, Freudenthaler, V., Esselborn, M., **Heese, B.**, **Althausen, D.**, **Schladitz, A.**, Otto, S. and Knippertz, P. 2010. Mineral dust observed with AERONET Sun photometer, Raman lidar, and in situ instruments during SAMUM 2006: Shape-independent particle properties. J. Geophys. Res. - Atmos., **115**, D07202, doi:10.1029/2009jd012520.

**Müller, K.**, **Birmili, W.**, **Brüggemann, E.**, **Gnauk, T.**, **Iinuma, Y.**, **Poulain, L.**, **Weinhold, K.**, Löschau, G. and **Herrmann, H.** 2010. Partikuläre Holzheizungsemissionen in einem sächsischen Kurort (Particulate wood combustion emissions in a Saxonian spa town). Gefahrst. Reinhalt. L., **70**, 493-499.

**Müller, K.**, **Lehmann, S.**, **van Pinxteren, D.**, **Gnauk, T.**, **Niedermeier, N.**, **Wiedensohler, A.** and **Herrmann, H.** 2010. Particle characterization at the Cape Verde atmospheric observatory during the 2007 RHaMBLe intensive. Atmos. Chem. Phys., **10**, 2709-2721.

**Niedermeier, D.**, **Hartmann, S.**, **Shaw, R. A.**, Covert, D., Mentel, T. F., Schneider, J., **Poulain, L.**, Reitz, P., Spindler, C., **Clauss, T.**, **Kiselev, A.**, **Hallbauer, E.**, **Wex, H.**, **Mildenberger, K.** and **Stratmann, F.** 2010. Heterogeneous freezing of droplets with immersed mineral dust particles - Measurements and parameterization. Atmos. Chem. Phys., **10**, 3601-3614.

Paasonen, P., Nieminen, T., Asmi, E., Manninen, H. E., Petäjä, T., Plass-Dülmer, C., Flentje, H., **Birmili, W.**, **Wiedensohler, A.**, Hõrrak, U., Metzger, A., Hamed, A., Laaksonen, A., Facchini, M. C. and Kerminen, V.-M. 2010. On the roles of sulphuric acid and low-volatility organic vapours in the initial steps of atmospheric new particle formation. Atmos. Chem. Phys., **10**, 11223-11242, doi:10.5194/acp-10-11223-2010.

Pappalardo, G., **Wandinger, U.**, Mona, L., **Hiebsch, A.**, **Mattis, I.**, Amodeo, A., **Ansmann, A.**, **Seifert, P.**, Linne, H., Apituley, A., Arboledas, L. A., Balis, D., Chaikovsky, A., D'Amico, G., De Tomasi, F., Freudenthaler, V., Giannakaki, E., Giunta, A., Grigorov, I., Iarlori, M., Madonna, F., Mamouri, R. E., Nasti, L., Papayannis, A., Pietruczuk, A., Pujadas, M., Rizi, V., Rocadenbosch, F., Russo, F., Schnell, F., Spinelli, N., Wang, X. and Wiegner, M. 2010. EARLINET correlative measurements for CALIPSO: First intercomparison results. J. Geophys. Res. - Atmos., **115**, D00H19, doi:10.1029/2009jd012147.

**Poulain, L.**, Katrib, Y., Isikli, E., Liu, Y., Wortham, H., Mirabel, P., Le Calvé, S. and Monod, A. 2010. In-

cloud multiphase behaviour of acetone in the troposphere: Gas uptake, Henry's law equilibrium and aqueous phase photooxidation. Chemosphere, **81**, 312-320, doi:10.1016/j.chemosphere.2010.07.032.

**Poulain, L.**, **Wu, Z.**, Petters, M. D., **Wex, H.**, **Hallbauer, E.**, **Wehner, B.**, **Massling, A.**, Kreidenweis, S. M. and **Stratmann, F.** 2010. Towards closing the gap between hygroscopic growth and CCN activation for secondary organic aerosols - Part 3: Influence of the chemical composition on the hygroscopic properties and volatile fractions of aerosols. Atmos. Chem. Phys., **10**, 3775-3785.

Putaud, J.-P., van Dingenen, R., Alastuey, A., Bauer, H., **Birmili, W.**, Cyrys, J., Flentje, H., Fuzzi, S., Gehrig, R., Hansson, H. C., Harrison, R. M., **Herrmann, H.**, Hitzenberger, R., Hüglin, C., Jones, A. M., Kasper-Giebl, A., Kiss, G., Kousa, A., Kuhlbusch, T. A. J., Löschau, G., Maenhaut, W., Molnar, A., Moreno, T., Pekkanen, J., Perrino, C., Pitz, M., Puxbaum, H., Querol, X., Rodriguez, S., Salma, I., Schwarz, J., Smolik, J., Schneider, J., **Spindler, G.**, ten Brink, H., Tursic, J., Viana, M., **Wiedensohler, A.** and Raes, F. 2010. A European aerosol phenomenology – 3: Physical and chemical characteristics of particulate matter from 60 rural, urban, and kerbside sites across Europe. Atmos. Environ., **44**, 1308-1320, doi:10.1016/j.atmosenv.2009.12.011.

Reichardt, J., **Wandinger, U.**, Klein, V., **Mattis, I.**, Hilber, B., Engelbart, D., Begbie, R. and Berger, F. H. 2010. RAMSES - das Wasserdampf-Ramanlidar des Deutschen Wetterdienstes. PROMET, **36**, 161-168.

**Renner, E.** and **Wolke, R.** 2010. Modelling the formation and atmospheric transport of secondary inorganic aerosols with special attention to regions with high ammonia emissions. Atmos. Environ., **44**, 1904-1912.

Ries, L., **Birmili, W.**, Sohmer, R. and Stohl, A. 2010. *Messungen von Fein- und Ultrafeinstaub und nordhemisphärischer Hintergrund an der GAW-Station Zugspitze/Schneefernerhaus*. In: *Forschung im Hochgebirge - Ergebnisse aktueller Projekte am Sonnblick-Observatorium und ein Blick über die Grenzen: Beiträge zum Sonnblick-Symposium 20. und 21. Oktober 2009*. Zentralanstalt für Meteorologie und Geodynamik (ZAMG), Wien, Österreich, p. 115-136.

**Rose, D.**, **Nowak, A.**, **Achtert, P.**, **Wiedensohler, A.**, Hu, M., Shao, M., Zhang, Y., Andreae, M. O. and Pöschl, U. 2010. Cloud condensation nuclei in polluted air and biomass burning smoke near the mega-city Guangzhou, China Part 1: Size-resolved measurements and implications for the modeling of aerosol particle hygroscopicity and CCN activity. Atmos. Chem. Phys., **10**, 3365-3383.

Schmale, J., Schneider, J., Jurkat, T., Voigt, C., Kalesse, H., Rautenhaus, M., Lichtenstern, M., Schlager, H., Ancellet, G., Arnold, F., Gerding, M., **Mattis, I.**, Wendisch, M. and Borrmann, S. 2010. Aerosol layers from the 2008 eruptions of Mount Okmok and Mount Kasatochi: In situ upper troposphere and lower stratosphere measurements of sulfate and organics over Europe. J. Geophys. Res. - Atmos., **115**, D00L07, doi:10.1029/2009jd013628.

**Seifert, P.**, **Ansmann, A.**, **Mattis, I.**, **Wandinger, U.**, **Tesche, M.**, **Engelmann, R.**, **Müller, D.**, Pérez, C. and Haustein, K. 2010. Saharan dust and heterogeneous ice formation: Eleven years of cloud observations at a central European EARLINET site. J. Geophys. Res. - Atmos., **115**, D20201, doi:10.1029/2009JD013222.

**Siebert, H.**, Gerashchenko, S., **Lehmann, K.**, Gylfason, A., Collins, L. R., **Shaw, R. A.** and Warhaft, Z. 2010. Towards understanding the role of turbulence on droplets in clouds: In situ and laboratory measurements. Atmos. Res., **97**, Sp. Iss. SI, 426-437, doi:10.1016/j.atmosres.2010.05.007.

**Siebert, H.**, **Shaw, R. A.** and Warhaft, Z. 2010. Statistics of small-scale velocity fluctuations and internal intermittency in marine stratocumulus clouds. J. Atmos. Sci., **67**, 262-273, doi:10.1175/2009JAS3200.1.

Sipilä, M., **Berndt, T.**, Petäjä, T., Brus, D., Vanhanen, J., **Stratmann, F.**, Patokoski, J., Mauldin III, R. L., Hyvärinen, A. P., Lihavainen, H. and Kulmala, M. 2010. The role of sulphuric acid in atmospheric nucleation. Science, **327**, 1243-1246, doi:10.1126/science.1180315.

Snider, J., **Wex, H.**, **Rose, D.**, Kristensson, A., **Stratmann, F.**, **Hennig, T.**, **Henning, S.**, **Kiselev, A.**, Bilde, M., Burkhardt, M., Dusek, U., Frank, G., Kiendler-Scharr, A., Lieberwirth, I., Mentel, T., Petters, M. D., Pöschl, U. and Tillmann, R. 2010. Intercomparison of cloud condensation nuclei and hygroscopic fraction measurements: Coated soot particles investigated during the LACIS Experiment in November (LExNo). J. Geophys. Res. - Atmos., **115**, D11205, doi:10.1029/2009JD012618.

**Spindler, G.**, **Brüggemann, E.**, **Gnauk, T.**, **Müller, K.** and **Herrmann, H.** 2010. A four-year size-segregated characterization study of particles PM10, PM2.5 and PM1 depending on air mass origin at Melpitz. Atmos. Environ., **44**, 164-173, doi:10.1016/j.atmosenv.2009.10.015.

Spracklen, D. V., Carslaw, K. S., Merikanto, J., Mann, G. W., Reddington, C. L., Pickering, S., Ogren, J. A., Andrews, E., Baltensperger, U., Weingartner, E., Boy, M., Kulmala, M., Laakso, L., Lihavainen, H., Kivekäs, N., Komppula, M., Mihalopoulos, N., Kouvarakis, G., Jennings, S. G., O'Dowd, C., **Birmili, W.**, **Wiedensohler, A.**, Weller, R., Gras, J., Laj, P., Sellegri, K., Bonn, B., Krejci, R., Laaksonen,

A., Hamed, A., Minikin, A., Harrison, R. M., Talbot, R. and Sun, J. 2010. Explaining global surface aerosol number concentrations in terms of primary emissions and particle formation. Atmos. Chem. Phys., **10**, 4775-4793, doi:10.5194/acp-10-4775-2010.

**Stratmann, F.**, Bilde, M., Dusek, U., Frank, G., **Hennig, T.**, **Henning, S.**, Kiendler-Scharr, A., **Kiselev, A.**, Kristensson, A., Lieberwirth, I., Mentel, T., Pöschl, U., **Rose, D.**, Schneider, J., Snider, J., Tillmann, R., Walter, S. and **Wex, H.** 2010. Examination of laboratory-generated coated soot particles: An overview of the LACIS Experiment in November (LExNo) campaign. J. Geophys. Res. - Atmos., **115**, D11203, doi: 10.1029/2009JD012628.

**Stratmann, F.**, Herrmann, E., Petäjä, T. and Kulmala, M. 2010. Modelling Ag-particle activation and growth in a TSI WCPC model 3785. Atmos. Meas. Tech. (AMT), **3**, 273-281.

Su, H., **Rose, D.**, **Cheng, Y. F.**, Gunthe, S. S., **Massling, A.**, **Stock, M.**, **Wiedensohler, A.**, Andreae, M. O. and Pöschl, U. 2010. Hygroscopicity distribution concept for measurement data analysis and modeling of aerosol particle mixing state with regard to hygroscopic growth and CCN activation. Atmos. Chem. Phys., **10**, 7489-7503, doi:10.5194/acp-10-7489-2010.

Sullivan, R. C., Petters, M. D., DeMott, P. J., Kreidenweis, S. M., **Wex, H.**, **Niedermeier, D.**, **Hartmann, S.**, **Clauss, T.**, **Stratmann, F.**, Reitz, P., Schneider, J. and Sierau, B. 2010. Irreversible loss of ice nucleation active sites in mineral dust particles caused by sulphuric acid condensation. Atmos. Chem. Phys., **10**, 11471-11487, doi:10.5194/acp-10-11471-2010.

**Tegen, I.**, Bierwirth, E., **Heinold, B.**, Helmert, J. and Wendisch, M. 2010. Effect of measured surface albedo on modeled Saharan dust radiative forcing. J. Geophys. Res. - Atmos., **115**, D24312, doi:10.1029/2009JD013764.

**Tilgner, A.** and **Herrmann, H.** 2010. Radical-driven carbonyl-to-acid conversion and acid degradation in tropospheric aqueous systems studied by CAPRAM. Atmos. Environ., **44**, 5415-5422, doi:10.1016/j.atmosenv.2010.07.050.

Tillmann, R., Hallquist, M., Jonsson, A. M., Kiendler-Scharr, A., Saathoff, H., **Iinuma, Y.** and Mentel, T. F. 2010. Influence of relative humidity and temperature on the production of pinonaldehyde and OH radicals from the ozonolysis of alpha-pinene. Atmos. Chem. Phys., **10**, 7057-7072, doi:10.5194/acp-10-7057-2010.

**Wandinger, U.**, **Tesche, M.**, **Seifert, P.**, **Ansmann, A.**, **Müller, D.** and **Althausen, D.** 2010. Size matters: Influence of multiple scattering on CALIPSO light-extinction profiling in desert dust. Geophys. Res. Lett., **37**, L10801, doi:10.1029/2010gl042815.

**Wehner, B.**, **Siebert, H.**, **Ansmann, A.**, **Ditas, F.**, **Seifert, P.**, **Stratmann, F.**, **Wiedensohler, A.**, Apituley, A., **Shaw, R. A.**, Manninen, H. E. and Kulmala, M. 2010. Observations of turbulence-induced new particle formation in the residual layer. Atmos. Chem. Phys., **10**, 4319–4330, doi:10.5194/acp-10-4319-2010.

**Weller, C.**, **Hoffmann, D.**, **Schaefer, T.** and **Herrmann, H.** 2010. Temperature and ionic strength dependence of $NO_3$-radical reactions with substituted phenols in aqueous solution. Z. Phys. Chem., **224**, 1261-1287, doi:10.1524/zpch.2010.6151.

Wessels, A., **Birmili, W.**, Albrecht, C., Hellack, B., Jermann, E., Wick, G., Harrison, R. M. and Schins, R. P. F. 2010. Oxidant generation and toxicity of size-fractionated ambient particles in human lung epithelial cells. Environ. Sci. Technol., **44**, 3539-3545, doi:10.1021/es9036226.

**Wex, H.**, Fuentes, E., **Tsagkogeorgas, G.**, **Voigtländer, J.**, **Clauss, T.**, **Kiselev, A.**, Green, D., Coe, H., McFiggans, G. and **Stratmann, F.** 2010. The influence of algal exudate on the hygroscopicity of sea spray particles. Adv. Meteo., **2010**, 11, doi:10.1155/2010/365131.

**Wex, H.**, McFiggans, G., **Henning, S.** and **Stratmann, F.** 2010. Influence of the external mixing state of atmospheric aerosol on derived CCN number concentrations. Geophys. Res. Lett., **37**, L10805, doi:1029/2010GL043337.

Whalley, L. K., Furneaux, K. L., Goddard, A., Lee, J. D., Mahajan, A., Oetjen, H., Read, K. A., **Kaaden, N.**, Carpenter, L. J., Lewis, A. C., Plane, J. M. C., Saltzman, E. S., **Wiedensohler, A.** and Heard, D. E. 2010. The chemistry of OH and HO2 radicals in the boundary layer over the tropical Atlantic Ocean. Atmos. Chem. Phys., **10**, 1555-1576.

**Wolke, R.**, **Schlegel, M.**, **Filaus, E.**, **Knoth, O.** and **Renner, E.** 2010. *Coupled time-integration of chemical and aerosol dynamical processes by using multirate implicit-explicit schemes*. D. G. Steyn and S. T. Rao (Ed.), In: *Air pollution modeling and its application XX : Proceedings of the 30th NATO/SPS International Technical Meeting on Air Pollution Modelling and Its Application (San Francisco, CA, USA, 18-22 May 2009)*. Springer, Dordrecht, p. 475-478. (NATO Science for Peace and Security Series - C : Environmental Security)

Wolters, E., **Deneke, H.**, van den Hurk, B., Meirink, J. F. and Roebeling, R. 2010. Broken and inhomogeneous cloud impact on satellite cloud-phase retrievals J. Geophys. Res. - Atmos., **115**,

D10214, doi:10.1029/2009JD012205.
Yasmeen, F., Vermeylen, R., Szmigielski, R., **Iinuma, Y.**, **Böge, O.**, **Herrmann, H.**, Maenhaut, W. and Claeys, M. 2010. Terpenylic acid and related compounds: Precursors for dimers in secondary organic aerosol from the ozonolysis of alpha- and beta-pinene. Atmos. Chem. Phys., **10**, 9383-9392, doi:10.5194/acp-10-9383-2010.
Yue, D. L., Hu, M., **Wu, Z. J.**, Guo, S., Wen, M. T., **Nowak, A.**, **Wehner, B.**, **Wiedensohler, A.**, Takegawa, N., Kondo, Y., Wang, X. S., Li, Y. P., Zeng, L. M. and Zhang, Y. H. 2010. Variation of particle number size distributions and chemical compositions at the urban and downwind regional sites in the Pearl River Delta during summertime pollution episodes. Atmos. Chem. Phys., **10**, 9431-9439, doi:10.5194/acp-10-9431-2010.
Yue, D. L., Hu, M., Zhang, R. Y., Wang, Z. B., Zheng, J., **Wu, Z. J.**, **Wiedensohler, A.**, He, L. Y., Huang, X. F. and Zhu, T. 2010. The roles of sulfuric acid in new particle formation and growth in the mega-city of Beijing. Atmos. Chem. Phys., **10**, 4953-4960, doi:10.5194/acp-10-4953-2010.

**2011**

**Ansmann, A.**, Petzold, A., Kandler, K., **Tegen, I.**, Wendisch, M., **Müller, D.**, Weinzierl, B., **Müller, T.** and **Heintzenberg, J.** 2011. Saharan Mineral Dust Experiments SAMUM-1 and SAMUM-2: What have we learned? Tellus B, **63**, 403-429, doi:10.1111/j.1600-0889.2011.00555.x.
**Ansmann, A.**, **Tesche, M.**, **Seifert, P.**, Gross, S., Freudenthaler, V., Apituley, A., Wilson, K. M., Serikov, I., Linne, H., **Heinold, B.**, **Hiebsch, A.**, Schnell, F., **Schmidt, J.**, **Mattis, I.**, **Wandinger, U.** and Wiegner, M. 2011. Ash and fine-mode particle mass profiles from EARLINET-AERONET observations over central Europe after the eruptions of the Eyjafjallajokull volcano in 2010. J. Geophys. Res. - Atmos., **116**, D00U02, doi:10.1029/2010JD015567.
Asmi, A., **Wiedensohler, A.**, Laj, P., Fjaeraa, A.-M., Sellegri, K., **Birmili, W.**, Weingartner, E., Baltensperger, U., Zdimal, V., Zikova, N., Putaud, J.-P., Marinoni, A., Tunved, P., Hansson, H.-C., Fiebig, M., Kivekäs, N., Lihavainen, H., Asmi, E., Ulevicius, V., Aalto, P. P., Swietlicki, E., Kristensson, A., Mihalopoulos, N., Kalivitis, N., Kalapov, I., Kiss, G., de Leeuw, G., Henzing, B., Harrison, R. M., Beddows, D., O'Dowd, C., Jennings, S. G., Flentje, H., **Weinhold, K.**, Meinhardt, F., Ries, L. and Kulmala, M. 2011. Number size distributions and seasonality of submicron particles in Europe 2008–2009. Atmos. Chem. Phys., **11**, 5505-5538, doi:10.5194/acp-11-5505-2011.
**Baars, H**., **Ansmann, A.**, **Althausen, D.**, **Engelmann, R.**, Artaxo, P., Pauliquevis, T. and Souza, R. 2011. Further evidence for significant smoke transport from Africa to Amazonia. Geophys. Res. Lett., **38**, L20802, 4 pp., doi:10.1029/2011GL049200.
Baumgardner, D., Brenguier, J.-L., Bucholtz, A., Coe, H., Demott, P., Garrett, T., Gayet, J. F., **Hermann, M.**, Heymsfield, A., Korolev, A., Krämer, M., Petzold, A., Strapp, W., Pilewski, P., Taylor, J., Twohy, C., Wendisch, M., W., B. and Chuang, P. 2011. Airborne instruments to measure atmospheric aerosol particles, clouds and radiation: A cook's tour of mature and emerging technology. Atmos. Res., **102**, 10-29, doi:10.1016/j.atmosres.2011.06.021.
Bhawar, R., Di Girolamo, P., Summa, D., Flamant, C., **Althausen, D.**, Behrendt, A., Kiemle, C., Bosser, P., Cacciani, M., Champollion, C., Di Iorio, T., **Engelmann, R.**, Herold, C., **Müller, D.**, Pal, S., Wirth, M. and Wulfmeyer, V. 2011. The water vapour intercomparison effort in the framework of the convective and orographically-induced precipitation study: Airborne-to-ground-based and airborne-to-airborne lidar systems. Q. J. Roy. Meteor. Soc., **137**, 325-348, doi:10.1002/qj.697.
Breitner, S., Liu, L. Q., Cyrys, J., Bruske, I., Franck, U., Schlink, U., Leitte, A. M., Herbarth, O., **Wiedensohler, A.**, **Wehner, B.**, Hu, M., Pan, X. C., Wichmann, H. E. and Peters, A. 2011. Sub-micrometer particulate air pollution and cardiovascular mortality in Beijing, China. Sci. Total Environ., **409**, 5196-5204, doi:10.1016/j.scitotenv.2011.08.023.
Carpenter, L. J., Fleming, Z. L., Read, K. A., Lee, J. D., Moller, S. J., Hopkins, J., Purvis, R., Lewis, A. C., **Müller, K.**, **Heinold, B.**, **Herrmann, H.**, **Wadinga Fomba, K.**, **van Pinxteren, D.**, **Müller, C.**, **Tegen, I.**, **Wiedensohler, A.**, **Müller, T.**, **Niedermeier, N.**, Achterberg, E. P., Patey, M. D., Kozlova, E. A., Heimann, M., Heard, D. E., Plane, J. M. C., Mahajan, A., Oetjen, H., Ingham, T., Stone, D., Whalley, L., Evans, M., Pilling, M. J., Leigh, R. J., Monks, P. S., Karunaharan, A., Vaughan, S., Tschritter, J., Pöhler, D., Frieß, U., Holla, R., Mendes, M. L., Lopez, H., Faria, B., Manning, A. J. and Wallace, D. W. R. 2011. Seasonal characteristics of tropical marine boundary layer air measured at the Cape Verde Atmospheric Observatory. J. Atmos. Chem., **67**, 87-140, doi:10.1007/s10874-011-9206-1.
Dacre, H. F., Grant, A. L. M., Hogan, R. J., Belcher, S. E., Thomson, D. J., Devenish, B. J., Marenco, F., Hort, M. C., Haywood, J. M., **Ansmann, A.**, **Mattis, I.** and Clarisse, L. 2011. Evaluating the

structure and magnitude of the ash plume during the initial phase of the 2010 Eyjafjallajokull eruption using lidar observations and NAME simulations. J. Geophys. Res. - Atmos., **116**, D00U03, doi:10.1029/2011JD015608.

Deng, Z. Z., Zhao, C. S., Ma, N., Liu, P. F., Ran, L., Xu, W. Y., Chen, J., Liang, Z., Liang, S., Huang, M. Y., Ma, X. C., Zhang, Q., Quan, J. N., Yan, P., **Henning, S.**, **Mildenberger, K.**, **Sommerhage, E.**, Schäfer, M., **Stratmann, F.** and **Wiedensohler, A.** 2011. Size-resolved and bulk activation properties of aerosols in the North China Plain. Atmos. Chem. Phys., **11**, 3835-3846, doi:10.5194/acp-11-3835-2011.

Doyle, J. D., Gaberšek, S., Jiang, Q., Bernardet, L., Brown, J. M., Dörnbrack, A., **Filaus, E.**, Grubišić, V., Kirshbaum, D. J., **Knoth, O.**, Koch, S., Schmidli, J., Stiperski, I., Vosper, S. and Zhong, S. 2011. An intercomparison of T-REX mountain wave simulations and implications for mesoscale predictability. Mon. Wea. Rev., **139**, 2811-2831, doi:10.1175/MWR-D-10-05042.1.

Dusek, U., Frank, G. P., **Massling, A.**, Zeromskiene, K., **Iinuma, Y.**, Schmid, O., Helas, G., **Hennig, T.**, **Wiedensohler, A.** and Andreae, M. O. 2011. Water uptake by biomass burning aerosol at sub- and supersaturated conditions: Closure studies and implications for the role of organics. Atmos. Chem. Phys., **11**, 9519-9532, doi:10.5194/acp-11-9519-2011.

Ebert, M., Worringen, A., Benker, N., **Mertes, S.**, Weingartner, E. and Weinbruch, S. 2011. Chemical composition and mixing-state of ice residuals sampled within mixed phase clouds. Atmos. Chem. Phys., **11**, 1-12, doi:10.5194/acp-11-1-2011.

Emeis, S., Forkel, R., Junkermann, W., Schäfer, K., Flentje, H., Gilge, S., Fricke, W., Wiegner, M., Freudenthaler, V., Groß, S., Ries, L., Meinhardt, F., **Birmili, W.**, Münkel, C., Obleitner, F. and Suppan, P. 2011. Measurement and simulation of the 16/17 April 2010 Eyjafjallajökull volcanic ash layer dispersion in the northern Alpine region. Atmos. Chem. Phys., **11**, 2689-2701, doi:10.5194/acp-11-2689-2011.

**Engelmann, R.**, **Ansmann, A.**, **Horn, S.**, **Seifert, P.**, **Althausen, D.**, **Tesche, M.**, Esselborn, M., **Fruntke, J.**, Lieke, K., Freudenthaler, V. and Gross, S. 2011. Doppler lidar studies of heat island effects on vertical mixing of aerosols during SAMUM-2. Tellus B, **63**, 448-458.

Fountoukis, C., Racherla, P. N., van der Gon, H. A. C. D., Polymeneas, P., Charalampidis, P. E., Pilinis, C., **Wiedensohler, A.**, Dall'Osto, M., O'Dowd, C. and Pandis, S. N. 2011. Evaluation of a three-dimensional chemical transport model (PMCAMx) in the European domain during the EUCAARI May 2008 campaign. Atmos. Chem. Phys., **11**, 10331-10347, doi:10.5194/acp-11-10331-2011.

Franck, U., Odeh, S., **Wiedensohler, A.**, **Wehner, B.** and Herbarth, O. 2011. The effect of particle size on cardiovascular disorders - The smaller the worse. Sci. Total Environ., **409**, 4217-4221, doi:10.1016/j.scitotenv.2011.05.049.

Gagné, S., Lehtipalo, K., Manninen, H. E., Nieminen, T., Schobesberger, S., Franchin, A., Yli-Juuti, T., Boulon, J., **Sonntag, A.**, Mirme, S., Mirme, A., Hõrrak, U., Petäjä, T., Asmi, E. and Kulmala, M. 2011. Intercomparison of air ion spectrometers: An evaluation of results in varying conditions. Atmos. Meas. Tech. (AMT), **4**, 805-822, doi:10.5194/amt-4-805-2011.

Gasteiger, J., Wiegner, M., Gross, S., Freudenthaler, V., Toledano, C., **Tesche, M.** and Kandler, K. 2011. Modelling lidar-relevant optical properties of complex mineral dust aerosols. Tellus B, **63**, 725-741.

Gross, S., Gasteiger, J., Freudenthaler, V., Wiegner, M., Geiss, A., **Schladitz, A.**, Toledano, C., Kandler, K., **Tesche, M.**, **Ansmann, A.** and **Wiedensohler, A.** 2011. Characterization of the planetary boundary layer during SAMUM-2 by means of lidar measurements. Tellus B, **63**, 695-705, doi:10.1111/j.1600-0889.2011.00557.x.

Gross, S., **Tesche, M.**, Freudenthaler, V., Toledano, C., Wiegner, M., **Ansmann, A.**, **Althausen, D.** and Seefeldner, M. 2011. Characterization of Saharan dust, marine aerosols and mixtures of biomass-burning aerosols and dust by means of multi-wavelength depolarization and Raman lidar measurements during SAMUM 2. Tellus B, **63**, 706-724, doi:10.1111/j.1600-0889.2011.00556.x.

Guerrero-Rascado, J. L., **Müller, D.**, Navas-Guzman, F., Perez-Ramirez, D. and Alados-Arboledas, L. 2011. First results of aerosol microphysical properties by 3+2 Raman lidar at EARLINET Granada station. Rom. J. Phys., **56**, 467-475.

Gunthe, S. S., **Rose, D.**, Su, H., Garland, R. M., **Achtert, P.**, **Nowak, A.**, **Wiedensohler, A.**, Kuwata, M., Takegawa, N., Kondo, Y., Hu, M., Shao, M., Zhu, T., Andreae, M. O. and Pöschl, U. 2011. Cloud condensation nuclei (CCN) from fresh and aged air pollution in the megacity region of Beijing. Atmos. Chem. Phys., **11**, 11023-11039, doi:10.5194/acp-11-11023-2011.

Hamburger, T., McMeeking, G., Minikin, A., **Birmili, W.**, Dall'Osto, M., O'Dowd, C., Flentje, H., Henzing, B., Junninen, H., Kristensson, A., de Leeuw, G., Stohl, A., Burkhart, J. F., Coe, H., Krejci, R. and Petzold, A. 2011. Overview of the synoptic and pollution situation over Europe during the EUCAARI-LONGREX field campaign. Atmos. Chem. Phys., **11**, 1065-1082, doi:10.5194/acp-11-1065-2011.

**Hartmann, S.**, **Niedermeier, D.**, **Voigtländer, J.**, **Clauss, T.**, **Shaw, R. A.**, **Wex, H.**, **Kiselev, A.** and **Stratmann, F.** 2011. Homogeneous and heterogeneous ice nucleation at LACIS: Operating principle and theoretical studies. Atmos. Chem. Phys., **11**, 1753-1767, doi:10.5194/acp-11-1753-2011.

**Heinold, B.**, **Tegen, I.**, Bauer, S. and Wendisch, M. 2011. Regional modelling of Saharan dust and biomass-burning smoke Part 2: Direct radiative forcing and atmospheric. Tellus B, **63**, 800-813, doi:10.1111/j.1600-0889.2011.00574.x.

**Heinold, B.**, **Tegen, I.**, Schepanski, K., **Tesche, M.**, Esselborn, M., Freudenthaler, V., Gross, S., Kandler, K., Knippertz, P., **Müller, D.**, **Schladitz, A.**, Toledano, C., Weinzierl, B., **Ansmann, A.**, **Althausen, D.**, **Müller, T.**, Petzold, A. and **Wiedensohler, A.** 2011. Regional modelling of Saharan dust and biomass-burning smoke Part 1: Model description and evaluation. Tellus B, **63**, 781-799, doi:10.1111/j.1600-0889.2011.00570.x.

**Heintzenberg, J.**, **Birmili, W.**, Otto, R., Andreae, M. O., Mayer, J.-C., Chi, X. and Panov, A. 2011. Aerosol particle number size distributions and particulate light absorption at the ZOTTO tall tower (Siberia), 2006-2009. Atmos. Chem. Phys., **11**, 8703-8719, doi:10.5194/acp-11-8703-2011.

**Heintzenberg, J.**, **Hermann, M.**, **Weigelt, A.**, Clarke, A., Kapustin, V., Anderson, B., Thornhill, K., van Velthoven, P., Zahn, A. and Brenninkmeijer, C. 2011. Near-global aerosol mapping in the upper troposphere and lowermost stratosphere with data from the CARIBIC project. Tellus B, **63**, 875-890, DOI: 10.1111/j.1600-0889.2011.00578.x.

**Held, A.**, **Orsini, D. A.**, Vaattovaara, P., Tjernström, M. and Leck, C. 2011. Near-surface profiles of aerosol number concentration and temperature over the Arctic Ocean. Atmos. Meas. Tech. (AMT), **4**, 1603–1616.

Henken, C. C., Schmeits, M. J., **Deneke, H.** and Roebeling, R. A. 2011. Using MSG-SEVIRI cloud physical properties and weather radar observations for the detection of Cb/TCu clouds. J. Appl. Meteorol. Clim., **50**, 1587-1600, doi:10.1175/2011JAMC2601.1.

Herold, C., **Althausen, D.**, **Müller, D.**, **Tesche, M.**, **Seifert, P.**, **Engelmann, R.**, Flamant, C., Bhawar, R. and Di Girolamo, P. 2011. Comparison of Raman lidar observations of water vapor with COSMO-DE forecasts during COPS 2007. Weather Forecast, **26**, 1056-1066.

**Herrmann, H.** 2011. Eyjafjallajokull. Nachr. Chem., **59**, 559-559.

**Jebens, S.**, **Knoth, O.** and Weiner, R. 2011. Partially implicit peer methods for the compressible Euler equations. J. Comput. Phys., **230**, 4955-4974, doi:10.1016/j.jcp.2011.03.015.

**Kahnt, A.**, **Iinuma, Y.**, **Böge, O.**, **Mutzel, A.** and **Herrmann, H.** 2011. Denuder sampling techniques for the determination of gas-phase carbonyl compounds: A comparison and characterisation of in situ and ex situ derivatisation methods. J. Chromatogr. B, **879**, 1402-1411, doi:10.1016/j.jchromb.2011.02.028.

Kandler, K., Lieke, K., Benker, N., Emmel, C., Kupper, M., Müller-Ebert, D., Ebert, M., Scheuvens, D., **Schladitz, A.**, Schütz, L. and Weinbruch, S. 2011. Electron microscopy of particles collected at Praia, Cape Verde, during the Saharan Mineral Dust Experiment: Particle chemistry, shape, mixing state and complex refractive index. Tellus B, **63**, 475-496, doi:10.1111/j.1600-0889.2011.00550.x.

Kandler, K., Schütz, L., Jäckel, S., Lieke, K., Emmel, C., Müller-Ebert, D., Ebert, M., Scheuvens, D., **Schladitz, A.**, Segvic, B., **Wiedensohler, A.** and Weinbruch, S. 2011. Ground-based off-line aerosol measurements at Praia, Cape Verde, during the Saharan Mineral Dust Experiment: Microphysical properties and mineralogy. Tellus B, **63**, 459-474, doi:10.1111/j.1600-0889.2011.00546.x.

**Kanitz, T.**, **Seifert, P.**, **Ansmann, A.**, **Engelmann, R.**, **Althausen, D.**, Casiccia, C. and Rohwer, E. G. 2011. Contrasting the impact of aerosols at northern and southern midlatitudes on heterogeneous ice formation. Geophys. Res. Lett., **38**, L17802, doi:10.1029/2011GL048532.

**Katzwinkel, J.**, **Siebert, H.** and **Shaw, R. A.** 2011. Observation of a self-limiting, shear-induced turbulent inversion layer above marine stratocumulus. Bound.-Lay. Meteorol., doi:10.1007/s10546-011-9683-4.

Kirkby, J., Curtius, J., Almeida, J., Dunne, E., Duplissy, J., Ehrhart, S., Franchin, A., Gagne, S., Ickes, L., Kurten, A., Kupc, A., Metzger, A., Riccobono, F., Rondo, L., Schobesberger, S., **Tsagkogeorgas, G.**, Wimmer, D., Amorim, A., Bianchi, F., Breitenlechner, M., David, A., Dommen, J., Downard, A., Ehn, M., Flagan, R. C., Haider, S., Hansel, A., Hauser, D., Jud, W., Junninen, H., Kreissl, F., Kvashin, A., Laaksonen, A., Lehtipalo, K., Lima, J., Lovejoy, E. R., Makhmutov, V., Mathot, S., Mikkila, J., Minginette, P., Mogo, S., Nieminen, T., Onnela, A., Pereira, P., Petäjä, T., Schnitzhofer, R., Seinfeld, J. H., Sipila, M., Stozhkov, Y., **Stratmann, F.**, Tome, A., Vanhanen, J., Viisanen, Y., Vrtala, A., Wagner, P. E., Walther, H., Weingartner, E., **Wex, H.**, Winkler, P. M., Carslaw, K. S., Worsnop, D. R., Baltensperger, U. and Kulmala, M. 2011. Role of sulphuric acid, ammonia and galactic cosmic rays in atmospheric aerosol nucleation. Nature, **476**, 429-U77, doi:10.1038/nature10343.

Knippertz, P., **Tesche, M.**, **Heinold, B.**, Kandler, K., Toledano, C. and Esselborn, M. 2011. Dust mobilization and aerosol transport from West Africa to Cape Verde - A meteorological overview of

SAMUM-2. Tellus B, **63**, 430-447, doi:10.1111/j.1600-0889.2011.00544.x.

Knote, C., Brunner, D., Vogel, H., Allan, J., Asmi, A., Äijälä, M., Carbone, S., van der Gon, H. D., Jimenez, J. L., Kiendler-Scharr, A., Mohr, C., **Poulain, L.**, Prévôt, A. S., Swietlicki, E. and Vogel, B. 2011. Towards an online-coupled chemistry-climate model: Evaluation of COSMO-ART. Geosci. Model Dev., **4**, 1077-1102.

Koehler, C. H., Trautmann, T., Lindermeir, E., Vreeling, W., Lieke, K., Kandler, K., Weinzierl, B., Gross, S., **Tesche, M.** and Wendisch, M. 2011. Thermal IR radiative properties of mixed mineral dust and biomass aerosol during SAMUM-2. Tellus B, **63**, 751-769, doi:10.1111/j.1600-0889.2011.00563.x.

Kravitz, B., Robock, A., Bourassa, A., Deshler, T., Wu, D. C., **Mattis, I.**, **Finger, F.**, Hoffmann, A., Ritter, C., Bitar, L., Duck, T. J. and Barnes, J. E. 2011. Simulation and observations of stratospheric aerosols from the 2009 Sarychev volcanic eruption. J. Geophys. Res. - Atmos., **116**, D18211, doi:10.1029/2010JD015501.

Kulmala, M., Asmi, A., Lappalainen, H. K., Baltensperger, U., Brenguier, J.-L., Facchini, M. C., Hansson, H.-C., Hov, Ø., O´Dowd, C. D., Pöschl, U., **Wiedensohler, A.**, Boers, R., Boucher, O., de Leeuw, G., van der Gon, H. A. C. D., Feichter, J., Krejci, R., Laj, P., Lihavainen, H., Lohmann, U., McFiggans, G., Mentel, T., Pilinis, C., Riipinen, I., Schulz, M., Stohl, A., Swietlicki, E., Vignati, E., Alves, C., Amann, M., Ammann, M., Arabas, S., Artaxo, P., **Baars, H**., Beddows, D. C. S., Bergström, R., Beukes, J. P., Bilde, M., Burkhart, J. F., Canonaco, F., Clegg, S. L., Coe, H., Crumeyrolle, S., D´Anna, B., Decesari, S., Gilardoni, S., Fischer, M., Fjaeraa, A. M., Fountoukis, C., George, C., Gomes, L., Halloran, P., Hamburger, T., Harrison, R. M., **Herrmann, H.**, Hoffmann, T., Hoose, C., Hu, M., Hyvärinen, A., Horrak, U., **Iinuma, Y.**, Iversen, T., Josipovic, M., Kanakidou, M., Kiendler-Scharr, A., Kirkevag, A., Kiss, G., Klimont, Z., Kolmonen, P., Komppula, M., Kristjansson, J.-E., Laakso, L., Laaksonen, A., Labonnote, L., Lanz, V. A., Lehtinen, K. E. J., Rizzo, L. V., Makkonen, R., Manninen, H. E., McMeeking, G., Merikanto, J., Minikin, A., Mirme, A., Mirme, S., Morgan, W. T., Nemitz, E., O´Donnell, D., Panwar, T. S., Pawlowska, H., Petzold, A., Pienaar, J. J., Pio, C., Plass-Dülmer, C., Prevot, A. S. H., Pryor, S., Reddington, C. L., Roberts, G., Rosenfeld, D., Schwarz, J., Seland, Ø., Sellegri, K., Shen, X. J., Shiraiwa, M., **Siebert, H.**, Sierau, B., Simpson, D., Sun, J. Y., Topping, D., Tunved, P., Vaattovaara, P., Vakkari, V., Veefkind, J. P., Visschedijk, A., Vuollekoski, H., Vuolo, R., **Wehner, B.**, Wildt, J., Woodward, S., Worsnop, D. R., van Zadelhoff, G.-J., Zardini, A. A., Zhang, K., van Zyl, P., Kerminen, V.-M., Carslaw, K. S. and Pandis, S. N. 2011. General overview: European Integrated project on aerosol cloud climate and air quality interactions (EUCAARI) – Integrating aerosol research from nano to global scales Atmos. Chem. Phys., **11**, 13061–13143, doi:10.5194/acp-11-13061-2011.

Lehtipalo, K., Sipilä, M., Junninen, H., Ehn, M., **Berndt, T.**, Kajos, M. K., Worsnop, D. R., Petäjä, T. and Kulmala, M. 2011. Observations of nano-CN in the nocturnal boreal forest. Aerosol Sci. Technol., **45**, 499-509, doi:10.1080/02786826.2010.547537.

Leitte, A. M., Schlink, U., Herbarth, O., **Wiedensohler, A.**, Pan, Y.-C., Hu, M., **Wehner, B.**, Breitner, S., Peters, A., Wichmann, H.-E. and Franck, U. 2011. Associations between size-segregated particle number concentrations and respiratory mortality in Beijing, China. Int. J. Environ. Heal. R., 1-15.

Leitte, A. M., Schlink, U., Richter, M., Herbarth, O., **Wehner, B.**, **Tuch, T.**, **Wiedensohler, A.**, Pan, X.-C., **Wu, Z.**, Hu, M., Yang, M., Liu, L., Breitner, S., Cyrys, J., Peters, A., Wichmann, H.-E. and Franck, U. 2011. Size-segregated particle number concentrations and respiratory emergency room visits in Beijing, China. Environ. Health Persp., **19**, 508-513, doi:10.1289/ehp.1002203.

Liu, L. Q., Breitner, S., Pan, X. C., Franck, U., Leitte, A. M., **Wiedensohler, A.**, von Klot, S., Wichmann, H. E., Peters, A. and Schneider, A. 2011. Associations between air temperature and cardio-respiratory mortality in the urban area of Beijing, China: Aa time-series analysis. Environ. Health, **10**, doi:10.1186/1476-069x-10-51.

Liu, P. F., Zhao, C. S., Gobel, T., **Hallbauer, E.**, **Nowak, A.**, Ran, L., Xu, W. Y., Deng, Z. Z., Ma, N., **Mildenberger, K.**, **Henning, S.**, **Stratmann, F.** and **Wiedensohler, A.** 2011. Hygroscopic properties of aerosol particles at high relative humidity and their diurnal variations in the North China Plain. Atmos. Chem. Phys., **11**, 3479-3494, doi:10.5194/acp-11-3479-2011.

Lonitz, K. and **Horváth, Á.** 2011. Comparison of MISR and Meteosat-9 cloud-motion vectors. J. Geophys. Res. - Atmos., **116**, D24202, doi:10.1029/2011JD016047.

Löschau, G., **Birmili, W.**, **Engler, C.**, **Weinhold, K.**, **Gnauk, T.**, **Brüggemann, E.**, **Müller, K.**, **Herrmann, H.** and **Wiedensohler, A.** 2011. Messung der Anzahl von ultrafeinen Partikeln in der Außenluft in einem Luftgütemessnetz. Gefahrst. Reinhalt. L., **71**, 57-63.

Löschau, G., **Birmili, W.**, **Engler, C.**, **Weinhold, K.**, **Gnauk, T.**, **Brüggemann, E.**, **Müller, K.**, **Herrmann, H.** and **Wiedensohler, A.** 2011. Measurement of the number concentration of ultrafine particles in ambient in an air quality monitoring network - Part 3: Spatial variation of the particle concentration

and main sources in an agglomeration (Messung der Anzahl von ultrafeinen Partikeln in der Außenluft in einem Luftgütemessnetz – Teil 3: Räumliche Variation der Partikelkonzentration sowie Hauptverursacher im Ballungsraum). Gefahrst. Reinhalt. L., **71**, 57-63.

Ma, N., Zhao, C. S., **Nowak, A.**, **Müller, T.**, **Pfeifer, S.**, **Cheng, Y. F.**, Deng, Z. Z., Liu, P. F., Xu, W. Y., Ran, L., Yan, P., **Göbel, T.**, **Hallbauer, E.**, **Mildenberger, K.**, **Henning, S.**, Yu, J., Chen, L. L., Zhou, X. J., **Stratmann, F.** and **Wiedensohler, A.** 2011. Aerosol optical properties in the North China Plain during HaChi campaign: An in-situ optical closure study. Atmos. Chem. Phys., **11**, 5959-5973, doi:10.5194/acp-11-5959-2011.

Marcos, J., Seymour, R., Luhar, M., Durham, W. M., Mitchell, J. G., **Macke, A.** and Stocker, R. 2011. Microbial alignment in flow changes ocean light climate. Proc. Nat. Acad. Sci., **108**, 3860-3864, doi: 10.1073/pnas.1014576108.

**Massling, A.**, **Niedermeier, N.**, **Hennig, T.**, Fors, E. O., Swietlicki, E., Ehn, M., Hämeri, K., Villani, P., Laj, P., Good, N., McFiggans, G. and **Wiedensohler, A.** 2011. Results and recommendations from an intercomparison of six Hygroscopicity-TDMA systems. Atmos. Meas. Tech. (AMT), **4**, 485-497, doi:10.5194/amt-4-485-2011.

Matsui, H., Koike, M., Kondo, Y., Takegawa, N., **Wiedensohler, A.**, Fast, J. D. and Zaveri, R. 2011. Impact of new particle formation on the concentrations of aerosol number and cloud condensation nuclei around Beijing. J. Geophys. Res. - Atmos., **116**, D19208, doi:19210.11029/12011JD016025.

**Meier, J.**, **Tegen, I.**, **Mattis, I.**, **Wolke, R.**, Alados Arboledas, L., Apituley, A., Balis, D., Barnaba, F., Chaikovsky, A., Sicard, M., Pappalardo, G., Pietruczuk, A., Stoyanov, D., Ravetta, F. and Rizi, V. 2011. A regional model of European aerosol transport: Evaluation with sun photometer, lidar and air quality data. Atmos. Environ., **47**, 519-532, doi:10.1016/j.atmosenv.2011.09.029.

Mikkonen, S., Korhonen, H., Romakkaniemi, S., Smith, J. N., Joutsensaari, J., Lehtinen, K. E. J., Hamed, A., Breider, T. J., **Birmili, W.**, **Spindler, G.**, Plass-Dülmer, C., Facchini, M. C. and Laaksonen, A. 2011. Meteorological and trace gas factors affecting the number concentration of atmospheric Aitken ($D_p$ = 50 nm) particles in the continental boundary layer: Parameterization using a multivariate mixed effects model. Geosci. Model Dev., **4**, 1-13, doi:10.5194/gmd-4-1-2011.

Mikkonen, S., Romakkaniemi, S., Smith, J. N., Korhonen, H., Petäjä, T., Plass-Dülmer, C., Boy, M., McMurry, P. H., Lehtinen, K. E. J., Joutsensaari, J., Hamed, A., Mauldin III, R. L., **Birmili, W.**, **Spindler, G.**, Arnold, F., Kulmala, M. and Laaksonen, A. 2011. A statistical proxy for sulphuric acid concentration. Atmos. Chem. Phys., **11**, 11319-11334, doi:10.5194/acp-11-11319-2011.

Möller, D., Feichter, J. and **Herrmann, H.** 2011. *Von Wolken, Nebel und Niederschlag*. R. Zellner and GDCh (Ed.), In: *Chemie über den Wolken ... und darunter*. Wiley-VCH, Weinheim, p. 129-139.

**Müller, C.**, **Fomba, K. W.** and **Herrmann, H.** 2011. *Austauschprozesse zwischen Meeresoberfläche und Atmosphäre - die Bedeutung natürlicher Aerosolpartikel*. J. Lozán, H. Graßl, L. Karbe, and K. Reise (Ed.), In: *Warnsignal Klima: Die Meere - Änderungen & Risiken : Wissenschaftliche Fakten*. Wissenschaftliche Auswertungen ; In Kooperation mit GEO, Hamburg, p. 52-59.

**Müller, D.**, Kolgotin, A., **Mattis, I.**, Petzold, A. and Stohl, A. 2011. Vertical profiles of microphysical particle properties derived from inversion with two-dimensional regularization of multiwavelength Raman lidar data: Experiment. Appl. Optics, **50**, 2069-2079.

**Müller, T.**, Henzing, J. S., de Leeuw, G., **Wiedensohler, A.**, Alastuey, A., Angelov, H., Bizjak, M., Coen, M. C., Engström, J. E., Gruening, C., Hillamo, R., Hoffer, A., Imre, K., Ivanow, P., Jennings, G., Sun, J. Y., Kalivitis, N., Karlsson, H., Komppula, M., Laj, P., Li, S. M., Lunder, C., Marinoni, A., dos Santos, S. M., Moerman, M., **Nowak, A.**, Ogren, J. A., Petzold, A., Pichon, J. M., Rodriquez, S., Sharma, S., Sheridan, P. J., Teinilä, K., **Tuch, T.**, Viana, M., Virkkula, A., Weingartner, E., Wilhelm, R. and Wang, Y. Q. 2011. Characterization and intercomparison of aerosol absorption photometers: Result of two intercomparison workshops. Atmos. Meas. Tech. (AMT), **4**, 245-268, doi:10.5194/amt-4-245-2011.

**Müller, T.**, Laborde, M., Kassell, G. and **Wiedensohler, A.** 2011. Design and performance of a three-wavelength LED-based total scatter and backscatter integrating nephelometer. Atmos. Meas. Tech. (AMT), **4**, 1291-1303, doi:10.5194/amt-4-1291-2011.

**Müller, T.**, **Schladitz, A.**, Kandler, K. and **Wiedensohler, A.** 2011. Spectral particle absorption coefficients, single scattering albedos and imaginary parts of refractive indices from ground based in situ measurements at Cape Verde Island during SAMUM-2. Tellus B, **63**, 573-588, doi:10.1111/j.1600-0889.2011.00572.x.

**Niedermeier, D.**, **Hartmann, S.**, **Clauss, T.**, **Wex, H.**, **Kiselev, A.**, Sullivan, R. C., DeMott, P. J., Petters, M. D., Reitz, P., Schneider, J., Mikhailov, E., Sierau, B., Stetzer, O., Reimann, B., Bundke, U., **Shaw, R. A.**, Buchholz, A., Mentel, T. F. and **Stratmann, F.** 2011. Experimental study of the role of physicochemical surface processing on the IN ability of mineral dust particles. Atmos. Chem. Phys., **11**, 11131-11144, doi:10.5194/acp-11-11131-2011.

**Niedermeier, D.**, **Shaw, R. A.**, **Hartmann, S.**, **Wex, H.**, **Clauss, T.**, **Voigtländer, J.** and **Stratmann, F.** 2011. Heterogeneous ice nucleation: Exploring the transition from stochastic to singular freezing behavior. Atmos. Chem. Phys., **11**, 8767-8775, doi:10.5194/acp-11-8767-2011.

Noh, Y. M., **Müller, D.**, **Mattis, I.**, Lee, H. and Kim, Y. J. 2011. Vertically resolved light-absorption characteristics and the influence of relative humidity on particle properties: Multiwavelength Raman lidar observations of East Asian aerosol types over Korea. J. Geophys. Res. - Atmos., **116**, D06206, doi:10.1029/2010JD014873.

Okin, G. S., Baker, A. R., **Tegen, I.**, Mahowald, N. M., Dentener, F. J., Duce, R. A., Galloway, J. N., Hunter, K., Kanakidou, M., Kubilay, N., Prospero, J. M., Sarin, M., Surapipith, V., Uematsu, M. and Zhu, T. 2011. Impacts of atmospheric nutrient deposition on marine productivity: Roles of nitrogen, phosphorus, and iron. Global Biogeochem. Cy., **25**, GB2022, doi:10.1029/2010GB003858.

Petäjä, T., Sipilä, M., Paasonen, P., Nieminen, T., Kurtén, T., Ortega, I. K., **Stratmann, F.**, Vehkamäki, H., **Berndt, T.** and Kulmala, M. 2011. Experimental observation of strongly bound dimers of sulfuric acid: Application to nucleation in the atmosphere. Phys. Rev. Lett., **106**, 228302 (4), doi:10.1103/PhysRevLett.106.228302.

**Poulain, L.**, **Iinuma, Y.**, **Müller, K.**, **Birmili, W.**, **Weinhold, K.**, **Brüggemann, E.**, **Gnauk, T.**, Hausmann, A., Löschau, G., **Wiedensohler, A.** and **Herrmann, H.** 2011. Diurnal variations of ambient particulate wood burning emissions and their contribution to the concentration of Polycyclic Aromatic Hydrocarbons (PAHs) in Seiffen, Germany. Atmos. Chem. Phys., **11**, 12697-12713, doi:10.5194/acp-11-12697-2011.

**Poulain, L.**, **Spindler, G.**, **Birmili, W.**, Plass-Dülmer, C., **Wiedensohler, A.** and **Herrmann, H.** 2011. Seasonal and diurnal variations of particulate nitrate and organic matter at the IfT research station Melpitz. Atmos. Chem. Phys., **11**, 12579-12599, doi:10.5194/acp-11-12579-2011.

Reddington, C. L., Carslaw, K. S., Spracklen, D. V., Frontoso, M. G., Collins, L., Merikanto, J., Minikin, A., Hamburger, T., Coe, H., Kulmala, M., Aalto, P., Flentje, H., Plass-Dülmer, C., **Birmili, W.**, **Wiedensohler, A.**, **Wehner, B.**, **Tuch, T.**, **Sonntag, A.**, O'Dowd, C. D., Jennings, S. G., Dupuy, R., Baltensperger, U., Weingartner, E., Hansson, H.-C., Tunved, P., Laj, P., Sellegri, K., Boulon, J., Putaud, J.-P., Gruening, C., Swietlicki, E., Roldin, P., Henzing, J. S., Moerman, M., Mihalopoulos, N., Kouvarakis, G., Ždímal, V., Zíková, N., Marinoni, A., Bonasoni, P. and Duchi, R. 2011. Primary versus secondary contributions to particle number concentrations in the European boundary layer. Atmos. Chem. Phys., **11**, 12007-12036, doi:10.5194/acp-11-12007-2011.

Reitz, P., Spindler, C., Mentel, T. F., **Poulain, L.**, **Wex, H.**, **Mildenberger, K.**, **Niedermeier, D.**, **Hartmann, S.**, **Clauss, T.**, **Stratmann, F.**, Sullivan, R. C., DeMott, P. J., Petters, M. D., Sierau, B. and Schneider, J. 2011. Surface modification of mineral dust particles by sulphuric acid processing: Implications for ice nucleation abilities. Atmos. Chem. Phys., **11**, 7839-7858, doi:10.5194/acp-11-7839-2011.

**Rose, D.**, Gunthe, S. S., Su, H., Garland, R. M., Yang, H., **Berghof, M.**, **Cheng, Y. F.**, **Wehner, B.**, **Achtert, P.**, **Nowak, A.**, **Wiedensohler, A.**, Takegawa, N., Kondo, Y., Hu, M., Zhang, Y., Andreae, M. O. and Pöschl, U. 2011. Cloud condensation nuclei in polluted air and biomass burning smoke near the mega-city Guangzhou, China - Part 2: Size-resolved aerosol chemical composition, diurnal cycles, and externally mixed weakly CCN-active soot particles. Atmos. Chem. Phys., **11**, 2817-2836, doi:10.5194/acp-11-2817-2011.

**Sändig, B.** and **Renner, E.** 2011. *The urban impact on the regional climate of Dresden*. D. G. Steyn and S. Trini Castelli (Ed.), In: *Air pollution modeling and its application XXI : Proceedings of the 31th NATO/SPS International Technical Meeting on Air Pollution Modelling and Its Application (Torino, Italy, 27 September - 1 October 2010)*. Springer, Dordrecht, p. 181-185. (NATO Science for Peace and Security Series - C : Environmental Security)

Schäfer, K., Thomas, W., Peters, A., Ries, L., Obleitner, F., Schnelle-Kreis, J., **Birmili, W.**, Diemer, J., Fricke, W., Junkermann, W., Pitz, M., Emeis, S., Forkel, R., Suppan, P., Flentje, H., Wichmann, H. E., Gilge, S., Meinhardt, F., Zimmermann, R., **Weinhold, K.**, Soentgen, J., Münkel, C., Freuer, C. and Cyrys, J. 2011. Influences of the 2010 Eyjafjallajökull volcanic plume on air quality in the northern Alpine region. Atmos. Chem. Phys., **11**, 8555-8575, doi:10.5194/acp-11-8555-2011.

**Schladitz, A.**, **Müller, T.**, **Nordmann, S.**, **Tesche, M.**, Gross, S., Freudenthaler, V., Gasteiger, J. and **Wiedensohler, A.** 2011. In situ aerosol characterization at Cape Verde Part 2: Parametrization of relative humidity- and wavelength-dependent aerosol optical properties. Tellus B, **63**, 549-572, doi:10.1111/j.1600-0889.2011.00568.x.

**Schladitz, A.**, **Müller, T.**, **Nowak, A.**, Kandler, K., Lieke, K., **Massling, A.** and **Wiedensohler, A.** 2011. In situ aerosol characterization at Cape Verde Part 1: Particle number size distributions, hygroscopic growth and state of mixing of the marine and Saharan dust aerosol. Tellus B, **63**, 531-548, doi:10.1111/j.1600-0889.2011.00569.x.

**Schmeissner, T.**, Krejci, R., Ström, J., **Birmili, W.**, **Wiedensohler, A.**, Hochschild, G., Gross, J., Hoffmann, P. and Calderon, S. 2011. Analysis of number size distributions of tropical free tropospheric aerosol particles observed at Pico Espejo (4765 m a.s.l.), Venezuela. Atmos. Chem. Phys., **11**, 3319-3332, doi:10.5194/acp-11-3319-2011.

Schneider, J., Freutel, F., Zorn, S. R., Chen, Q., Farmer, D. K., Jimenez, J. L., Martin, S. T., Artaxo, P., **Wiedensohler, A.** and Borrmann, S. 2011. Mass-spectrometric identification of primary biological particle markers: Indication for low abundance of primary biological material in the pristine submicron aerosol of Amazonia. Atmos. Chem. Phys., **11**, 11415-11429.

Schumann, U., Weinzierl, B., Reitebuch, O., Schlager, H., Minikin, A., Förster, C., Baumann, R., Sailer, T., Graf, K., Mannstein, H., Voigt, C., Rahm, S., Simmet, R., Scheibe, M., Lichtenstern, M., Stock, P., Ruba, H., Schäuble, D., Tafferner, A., Rautenhaus, M., Gerz, T., Ziereis, H., Krautstrunk, M., Mallaun, C., Gayet, J. F., Lieke, K., Kandler, K., Ebert, M., Weinbruch, S., Stohl, A., Gasteiger, J., Gross, S., Freudenthaler, V., Wiegner, M., **Ansmann, A.**, **Tesche, M.**, Olafsson, H. and Sturm, K. 2011. Airborne observations of the Eyjafjalla volcano ash cloud over Europe during air space closure in April and May 2010. Atmos. Chem. Phys., **11**, 2245-2279, doi:10.5194/acp-11-2245-2011.

**Seifert, P.**, **Ansmann, A.**, Gross, S., Freudenthaler, V., **Heinold, B.**, **Hiebsch, A.**, **Mattis, I.**, **Schmidt, J.**, Schnell, F., **Tesche, M.**, **Wandinger, U.** and Wiegner, M. 2011. Ice formation in ash-influenced clouds after the eruption of the Eyjafjallajokull volcano in April 2010. J. Geophys. Res. - Atmos., **116**, D00U04, doi:10.1029/2011JD015702.

**Senf, F.** and Achatz, U. 2011. On the impact of middle-atmosphere thermal tides on the propagation and dissipation of gravity waves. J. Geophys. Res. - Atmos., **116**, D24110 (18 pp.), doi: 10.1029/2011JD015794.

Shen, X. J., Sun, J. Y., Zhang, Y. M., **Wehner, B.**, **Nowak, A.**, **Tuch, T.**, Zhang, X. C., Wang, T. T., Zhou, H. G., Zhang, X. L., Dong, F., **Birmili, W.** and **Wiedensohler, A.** 2011. First long-term study of particle number size distributions and new particle formation events of regional aerosol in the North China Plain. Atmos. Chem. Phys., **11**, 1565-1580, doi:10.5194/acp-11-1565-2011.

Smirnov, A., Holben, B. N., Giles, D. M., Slutsker, I., O´Neill, N. T., Eck, T. F., **Macke, A.**, Croot, P., Courcoux, Y., Sakerin, S. M., Smyth, T. J., Zielinski, T., Zibordi, G., Goes, J. I., Harvey, M. J., Quinn, P. K., Nelson, N. B., Radionov, V. F., Duarte, C. M., Losno, R., Sciare, J., Voss, K. J., Kinne, S., Nalli, N. R., Joseph, E., Krishna Moorthy, K., Covert, D. S., Gulev, S. K., Milinevsky, G., Larouche, P., Belanger, S., Horne, E., Chin, M., Remer, L. A., Kahn, R. A., Reid, J. S., Schulz, M., Heald, C. L., Zhang, J., Lapina, K., Kleidman, R. G., Griesfeller, J., Gaitley, B. J., Tan, Q. and Diehl, T. L. 2011. Maritime aerosol network as a component of AERONET – First results and comparison with global aerosol models and satellite retrievals. Atmos. Meas. Tech. (AMT), **4**, 583-597.

Sorribas, M., de la Morena, B. A., **Wehner, B.**, López, J. F., Prats, N., Mogo, S., **Wiedensohler, A.** and Cachorro, V. E. 2011. On the sub-micron aerosol size distribution in a coastal-rural site at El Arenosillo Station (SW - Spain). Atmos. Chem. Phys., **11**, 11185-11206, doi:10.5194/acp-11-11185-2011.

**Stock, M.**, **Cheng, Y. F.**, **Birmili, W.**, **Massling, A.**, **Wehner, B.**, **Müller, T.**, Leinert, S., Kalivitis, N., Mihalopoulos, N. and **Wiedensohler, A.** 2011. Hygroscopic properties of atmospheric aerosol particles over the Eastern Mediterranean: Implications for regional direct radiative forcing under clean and polluted conditions. Atmos. Chem. Phys., **11**, 4251-4271, doi:10.5194/acp-11-4251-2011.

Tatarov, B., **Müller, D.**, Shin, D. H., Shin, S. K., **Mattis, I.**, **Seifert, P.**, Noh, Y. M., Kim, Y. J. and Sugimoto, N. 2011. Lidar measurements of Raman scattering at ultraviolet wavelength from mineral dust over East Asia. Opt. Express, **19**, 1569-1581, doi:10.1364/OE.19.001569.

**Tesche, M.**, Gross, S., **Ansmann, A.**, **Müller, D.**, **Althausen, D.**, Freudenthaler, V. and Esselborn, M. 2011. Profiling of Saharan dust and biomass-burning smoke with multiwavelength polarization Raman lidar at Cape Verde. Tellus B, **63**, 649-676, doi:10.1111/j.1600-0889.2011.00548.x.

**Tesche, M.**, **Müller, D.**, Gross, S., **Ansmann, A.**, **Althausen, D.**, Freudenthaler, V., Weinzierl, B., Veira, A. and Petzold, A. 2011. Optical and microphysical properties of smoke over Cape Verde inferred from multiwavelength lidar measurements. Tellus B, **63**, 677-694, doi:10.1111/j.1600-0889.2011.00549.x.

Toledano, C., Wiegner, M., Gross, S., Freudenthaler, V., Gasteiger, J., **Müller, D.**, **Müller, T.**, **Schladitz, A.**, Weinzierl, B., Torres, B. and O'Neill, N. T. 2011. Optical properties of aerosol mixtures derived from sun-sky radiometry during SAMUM-2. Tellus B, **63**, 635-648, doi:10.1111/j.1600-0889.2011.00573.x.

Tsyro, S., Aas, W., Soares, J., Sofiev, M., Berge, H. and **Spindler, G.** 2011. Modelling of sea salt concentrations over Europe: Key uncertainties and comparison with observations. Atmos. Chem. Phys., **11**, 10367-10388, doi:10.5194/acp-11-10367-2011.

Uhrner, U., Zallinger, M., von Löwis, S., Vehkamäki, H., **Wehner, B.**, **Stratmann, F.** and **Wiedensohler, A.** 2011. Volatile nanoparticle formation and growth within a diluting diesel car exhaust. J. Air Waste Manage. Assoc., **61**, 399-408, doi:10.3155/1047-3289.61.4.399.

**van Pinxteren, D.**, **Brüggemann, E.**, **Gnauk, T.**, **Müller, K.**, Thiel, C. and **Herrmann, H.** 2011. A GIS based approach to back trajectory analysis for the source apportionment of aerosol constituents and its first application. J. Atmos. Chem., **67**, 1-28, doi:10.1007/s10874-011-9199-9.

Vautard, R., Moran, M. D., Solazzo, E., Gilliam, R. C., Matthias, V., Bianconi, R., Chemel, C., Ferreira, J., Geyer, B., Hansen, A. B., Jericevic, A., Prank, M., Segers, A., Silver, J. D., Werhahn, J., **Wolke, R.**, Rao, S. T. and Galmarini, S. 2011. Evaluation of the meteorological forcing used for the Air Quality Model Evaluation International Initiative (AQMEII) air quality simulations. Atmos. Environ., **47**, doi:10.1016/j.atmosenv.2011.10.065.

Wang, Z. B., Hu, M., Yue, D. L., Zheng, J., Zhang, R. Y., **Wiedensohler, A.**, **Wu, Z. J.**, Nieminen, T. and Boy, M. 2011. Evaluation on the role of sulfuric acid in the mechanisms of new particle formation for Beijing case. Atmos. Chem. Phys., **11**, 12663–12671.

**Wehner, B.**, **Hermann, M.**, **Siebert, H.**, **Ditas, F.** and **Wiedensohler, A.** 2011. Characterisation of a new Fast CPC and its application for atmospheric particle measurements. Atmos. Meas. Tech. (AMT), **4**, 823-833, doi:10.5194/amt-4-823-2011.

Weinzierl, B., Sauer, D., Esselborn, M., Petzold, A., Veira, A., Rose, M., Mund, S., Wirth, M., **Ansmann, A.**, **Tesche, M.**, Gross, S. and Freudenthaler, V. 2011. Microphysical and optical properties of dust and tropical biomass burning aerosol layers in the Cape Verde region-An overview of the airborne in situ and lidar measurements during SAMUM-2. Tellus B, **63**, 589-618, doi:10.1111/j.1600-0889.2011.00566.x.

**Wolke, R.**, **Stoll, J.**, **Smalla, A.**, **Schrödner, R.**, **Knoth, O.** and **Renner, E.** 2011. *The impact of meteorological uncertainties on the prediction of PM in urban areas*. D. G. Steyn and S. Trini Castelli (Ed.), In: *Air pollution modeling and its application XXI : Proceedings of the 31th NATO/ SPS International Technical Meeting on Air Pollution Modelling and Its Application (Torino, Italy, 27 September - 1 October 2010)*. Springer, Dordrecht, p. 473-477. (NATO Science for Peace and Security Series - C : Environmental Security)

**Wu, Z. J.**, Hu, M., Yue, D. L., **Wehner, B.** and **Wiedensohler, A.** 2011. Evolution of particle number size distribution in an urban atmosphere during episodes of heavy pollution and new particle formation. Sci. China Ser. D - Earth Sci., **54**, 1772-1778, doi:10.1007/s11430-011-4227-9.

**Wu, Z. J.**, **Nowak, A.**, **Poulain, L.**, **Herrmann, H.** and **Wiedensohler, A.** 2011. Hygroscopic behavior of atmospherically relevant water-soluble carboxylic salts and their influence on the water uptake of ammonium sulfate. Atmos. Chem. Phys., **11**, 12617-12626, doi:10.5194/acp-11-12617-2011.

Wulfmeyer, V., Behrendt, A., Kottmeier, C., Corsmeier, U., Barthlott, C., Craig, G. C., Hagen, M., **Althausen, D.**, Aoshima, F., Arpagaus, M., Bauer, H.-S., Bennett, L., Blyth, A., Brandau, C., Champollion, C., Crewell, S., Dick, G., Di Girolamo, P., Dorninger, M., Dufournet, Y., Eigenmann, R., **Engelmann, R.**, Flamant, C., Foken, T., Gorgas, T., Grzeschik, M., Handwerker, J., Hauck, C., Höller, H., Junkermann, W., Kalthoff, N., Kiemle, C., Klink, S., König, M., Krauss, L., Long, C. N., Madonna, F., Mobbs, S., Neininger, B., Pal, S., Peters, G., Pigeon, G., Richard, E., Rotach, M. W., Russchenberg, H., Schwitalla, T., Smith, V., Steinacker, R., Trentmann, J., Turner, D. D., van Baelen, J., Vogt, S., Volkert, H., Weckwerth, T., Wernli, H., Wieser, A. and Wirth, M. 2011. The Convective and Orographically-induced Precipitation Study (COPS): The scientific strategy, the field phase, and research highlights. Q. J. Roy. Meteor. Soc., **137**, 3-30, doi: 10.1002/qj.752.

Yue, D. L., Hu, M., Zhang, R. Y., **Wu, Z. J.**, Su, H., Wang, Z. B., Peng, J. F., He, L. Y., Huang, X. F., Gong, Y. G. and **Wiedensohler, A.** 2011. Potential contribution of new particle formation to cloud condensation nuclei in Beijing. Atmos. Environ., **45**, 6070-6077, doi:10.1016/j.atmosenv.2011.07.037.

Zheng, J., Hu, M., Zhang, R., Yue, D., Wang, Z., Guo, S., Li, X., Bohn, B., Shao, M., He, L., Huang, X., **Wiedensohler, A.** and Zhu, T. 2011. Measurements of gaseous H(2)SO(4) by AP-ID-CIMS during CAREBeijing 2008 Campaign. Atmos. Chem. Phys., **11**, 7755-7765, doi:10.5194/acp-11-7755-2011.

## University courses

| Lecturer | Course | WS 2009/ 2010 | SS 2010 | WS 2010/ 2011 | SS 2011 | WS 2011/ 2012 |
|---|---|---|---|---|---|---|
| Althausen, D. | Optical Measurement Techniques | | | x | | |
| Ansmann, A. | Active remote sensing (LIDAR) in environmental and atmospheric research and passive aerosol remote sensing (Photometer, Satellite) | | | x | | |
| Ansmann, A.<br>Birmili, W.<br>Hermann, M.<br>Müller, T.<br>Stratmann, F.<br>Wehner, B.<br>Wiedensohler, A. | Atmospheric Aerosols II | | x | | x | |
| Hellmuth, O. | Visiting Professor, University of Leipzig: Professorship for Theoretical Meteorology, Meteorological Statistics, Numerical Methods of Meteorology | | x | | | |
| Hermann, M.<br>Wendisch, M. | Airborne Physical Measurements: Methods and Instruments | | | x | | x |
| Herrmann, H. | Atmospheric Chemistry I<br>Atmospheric Chemistry II+Exercises<br>Atmospheric Chemistry Seminar<br>Atmospheric Chemistry Lab | x<br><br>x | <br>x<br>x<br>x | x<br><br>x | <br>x<br>x<br>x | x<br><br>x |
| | Visiting Professor, Université Claude Bernard Lyon 1 | | | | | x |
| Macke, A. | Atmospheric Radiation | | | x | | x |
| | Guest lecture: ERCA 2010 European Research Course on Atmospheres, 1. Radiative Transfer - Basics & Examples; 2. Radiation in Clouds and Aerosols, Grenoble, France January - February 2010 | x | | | | |
| | Guest lecture: ERCA 2010 European Research Course on Atmospheres, 1. Radiation in Clouds and Aerosols; 2. Volcanic Ash and its Effect on Air Traffic, Clouds and Climate, Grenoble, France January - February 2011 | | | x | | |
| Macke, A.<br>Ansmann, A.<br>Deneke, H.<br>Wandinger, U. | Satellite Remote Sensing | | x | | x[4)] | |
| Macke, A.<br>Stratmann, F. | Cloud Physics | | x | | x | |

| Lecturer | Course | WS 2009/ 2010 | SS 2010 | WS 2010/ 2011 | SS 2011 | WS 2011/ 2012 |
|---|---|---|---|---|---|---|
| Renner, E. | Modeling of Transport and Chemical Transformation of Air Pollutants | x | | x | | |
| Siebert, H. | Modern Meteorological Instruments II | | x | | x | |
| Tegen, I. | General Circulation G2 | x[2)] | | | | |
| | Guest lecture: 1. Dust Variability; 2. Dust-Climate Interactions, Training Week on WMO SDS-WAS Products, Barcelona, Spain 15.-19.11.2010 | | | x | | |
| van Pinxteren, M. | Analytics and Spectroscopy: Gas Chromatographie | | | | | x |
| Wandinger, U. | Scattering and Atmospheric Optics | | x | | x | |
| Wiedensohler, A. Stratmann, F. Brimili, W. Müller, T. | Atmospheric Aerosols I Lab | x[1)] | | x[3)] | | |

[1)] Lecture was held by A. Wiedensohler and F. Stratmann
[2)] Lecture was held by I. Tegen (substitute for Prof. Metz, Leipzig Insitute of Meteorology)
[3)] Lecture was held by A. Wiedensohler, W. Birmili, T. Müller and F. Stratmann
[4)] Lecture was held by A. Macke and H. Deneke

## Reviews

| Reviews | Number | |
|---|---|---|
| | *2010* | *2011* |
| Journals | 99 | 123 |
| Projects | 21 | 24 |
| Others | 10 | 28 |
| **Total** | **130** | **175** |

## Habilitation, Doctoral theses, Diploma, Master of Science and Bachelor of Science

| Degree*) | Name | Title | Year | Faculty |
|---|---|---|---|---|
| Ph. D. | Arras, C. | A global survey of sporadic e layers based on GPS radio occultations by CHAMP, GRACE and FORMOSAT-3/COSMIC | 2010 | University of Leipzig, Faculty of Physics and Earth Science |
| | Engelmann, R. | Aerosol vertical exchange in the convective planetary boundary layer: Turbulent particle flux measurements with combined wind and aerosol lidar | 2010 | University of Leipzig, Faculty of Physics and Earth Science |
| | Hieronymi, M. | Solar Radiative Transfer into the Ocean: A Study on Underwater Light Fluctuations due to Surface Waves | 2011 | University of Kiel, Faculty for Mathematics and Natural Sciences |
| | Kalisch, J. | Der Einfluss von Wolken auf den Strahlungsantrieb der Erde | 2011 | University of Kiel, Faculty for Mathematics and Natural Sciences |
| | Müller, C. | Chemische Analyse organischer Verbindungen in Oberflächenfilm der Meere und im marinen Aerosol | 2010 | University of Leipzig, Faculty of Chemistry and Mineralogy |
| | Schladitz, A. | Parametrization of relative humidity- and wavelength-dependent optical properties of mixed Saharan dust and marine aerosol | 2011 | University of Leipzig, Faculty of Physics and Earth Science |
| | Seifert, P. | Dust-related ice formation in the troposphere: A statistical analysis based on 11 years of lidar observations of aerosols and clouds over Leipzig | 2010 | University of Leipzig, Faculty of Physics and Earth Science |
| | Tesche, M. | Vertical profiling of aerosol optical properties with multiwavelength aerosol lidar during the Saharan mineral dust experiment | 2011 | University of Leipzig, Faculty of Physics and Earth Science |
| | Voigtländer, J. | Interaction Simulator (LACIS) sowie dessen Einsatz zur Untersuchung des hygroskopischen Wachstums und der Aktivierung laborgenerierter Aerosolpartikel | 2010 | University of Leipzig, Faculty of Physics and Earth Science |
| | Weller, C. | Photochemistry of iron (III) carboxylate complexes in aqueous solution | 2011 | University of Leipzig, Faculty of Chemistry and Mineralogy |
| | Ziese, M. | Entwicklung und Aufbau einer mobilen Version des Leipzig Aerosol Cloud Interaction Simulator (LACIS) sowie dessen Einsatz zur Untersuchung des hygroskopischen Wachstums und der Aktivierung laborgenerierter Aerosolpartikel | 2011 | University of Leipzig, Faculty of Physics and Earth Science |
| Dipl. | Barthel, S. | Modellierung des Lebenszyklus und der Chemie von Seesalzaerosolen in der maritimen Grenzschicht | 2010 | University of Leipzig, Faculty of Physics and Earth Science |

| Degree*) | Name | Title | Year | Faculty |
|---|---|---|---|---|
| Dipl. | Erfurth, M. | Diskretisierung des viskosen Terms der 2-dimensionalen Navier-Stokes-Gleichungen auf logischen Rechteckgittern | 2011 | Leipzig University of Applied Sciences, Faculty of Computer Science, Mathematics and Natural Sciences |
| | Finger, F. | Aerosolschichten in der oberen Troposphäre und unteren Stratosphäre über Mitteleuropa | 2011 | University of Leipzig, Faculty of Physics and Earth Science |
| | Geimecke, C. | Regionale Modellierung direkter und indirekter Effekte des Saharastaubs über Europa | 2010 | University of Leipzig, Faculty of Physics and Earth Science |
| | Göbel, T. | Hygroskopizität anthropogener Aerosole bei hohen Feuchten in der nordchinesischen Tiefebene | 2010 | University of Leipzig, Faculty of Physics and Earth Science |
| | Größ, J. | Partikelneubildung in der atmosphärischen Grenzschicht: Zusammenhang mit mikrometeorologischen Parametern | 2011 | University of Leipzig, Faculty of Physics and Earth Science |
| | Groß, P. | Global Distribution of Submicrometer Aerosol Particles: Comparison Between In Situ Measurements and Global Model Outputs | 2010 | University of Leipzig, Faculty of Physics and Earth Science |
| | Hänel, A. | Untersuchungen zu vertikalen Aeosolprofilen nordöstlich von Peking anhand von Messungen mit dem Raman-Lidar Polly | 2011 | University of Leipzig, Faculty of Physics and Earth Science |
| | Jähn, M. | Die kompressiblen Euler-Gleichungen für die feuchte Atmosphäre | 2011 | University of Leipzig, Faculty of Physics and Earth Sciences |
| | Kamili, K. | Hygroskopische Eigenschaften des urbanen Aerosols einer europäischen Megacity | 2010 | University of Leipzig, Faculty of Physics and Earth Science |
| | Kinder, F. | Hygroscopic properties of atmospheric aerosol particles in Central Europe | 2010 | University of Leipzig, Faculty of Physics and Earth Science |
| | Müller, A. | Mehrwellenlängen-Ramanlidar-Messungen über Leipzig von 2000-2010 | 2011 | University of Leipzig, Faculty of Physics and Earth Science |
| | Opelt, C. | Räumliche Variabilität atmosphärischer Partikelgrößenverteilung im städtischen Ballungsraum Dresden | 2010 | University of Leipzig, Faculty of Physics and Earth Science |
| | Rasch, F. | Verkehrsbedingte Effekte auf die Feinstaubbelastung in der Stadt Leipzig : Eine Analyse von städtischem Feinstaub im Vorfeld der Einführung der Umweltzone Leipzig | 2011 | Freie Universität Berlin, Department of Earth Sciences |

| Degree*) | Name | Title | Year | Faculty |
|---|---|---|---|---|
| Dipl. | Renkosic, N. | Energiebilanz arktischer Bewölkung aus Modell und Beobachtung | 2010 | University of Kiel, Faculty for Mathematics and Natural Sciences |
| | Schäfer, M. | Untersuchung des Aktivierungsverhaltens atmosphärischer Aerosolpartikel in der Nordchinesischen Tiefebene | 2011 | University of Leipzig, Faculty of Physics and Earth Science |
| | Schlimper, S. | Meteorologische und statistische Auswertung von Langzeitmessungen zur Charakterisierung des Aerosols an der Forschungsstation Melpitz | 2010 | University of Leipzig, Faculty of Physics and Earth Science |
| | Schmeißner, T. | Tropical free tropospheric aerosol microphysical properties measured at a high altitude research station in the Venezuelan Andes | 2010 | University of Leipzig, Faculty of Physics and Earth Science |
| | Schöne, L. | Laboruntersuchungen zur möglichen SOA-Bildung infolge der troposphärischen Isoprenoxidation | 2010 | University of Leipzig, Faculty of Physics and Earth Science |
| | Skandera, D. | Untersuchung der vertikalen Aeosolverteilung anhand von Lidarmessverfahren mittels eines Ceilometers am IfT | 2011 | University of Leipzig, Faculty of Physics and Earth Science |
| | Smalla, A. | Hochaufgelöste Chemietransport-Modellierung für den Großraum Dresden mit dem WRF/Chem-Modell | 2010 | University of Leipzig, Faculty of Physics and Earth Science |
| | Sommerhage, E. | Aktivierung atmosphärischer Aerosolpartikel in China | 2010 | University of Münster, Institute of Landscape Ecology |
| | Spörl, U. | Bestimmung des Aerosol-Signals in den SEVIRI-Kanälen anhand von MODIS-Aerosolprodukten über dem Ozean | 2011 | University of Leipzig, Faculty of Physics and Earth Science |
| | Stoll, J. | Kopplung des Wettermodells WRF(ARW) mit dem Chemietransportmodell MUSCAT: Vergleich weiterer meteorologischer Antriebe | 2010 | University of Leipzig, Faculty of Physics and Earth Science |
| | Tessendorf, A. | Strahlungsbilanz arktischer Bewölkung aus Modell und Beobachtung | 2010 | University of Kiel, Faculty for Mathematics and Natural Sciences |
| | Thapaliya, P. | Angepasste Zeitintegrationsverfahren zur numerischen Lösung von Mehrphassenmodellen in der atmospärischen Chemie | 2011 | Leipzig University of Applied Sciences, Faculty of Computer Science, Mathematics and Natural Sciences |

| Degree*) | Name | Title | Year | Faculty |
|---|---|---|---|---|
| Dipl. | Thiem, E. | Physikalische Eigenschaften des atmosphärischen Aerosols am Nordpolarmeer in Alaska | 2010 | University of Leipzig, Faculty of Physics and Earth Science |
| | Vogelsberg, U. | Implementierung eines Bodenmodells in das Atmosphärenmodell ASAM | 2011 | University of Leipzig, Faculty of Physics and Earth Sciences |
| M.Sc. | Bethke, J. | Liquid Water Content Measurements in Trade Wind Cumuli | 2011 | University of Leipzig, Faculty of Physics and Earth Science |
| | Bley, S. | Vergleich zweier Schwellwertalgorithmen zur Wolkendetektion in solaren METEOSAT SEVIRI Bildern und Anwendung auf den hochaufgelösten sichtbaren Kanal | 2011 | University of Leipzig, Faculty of Physics and Earth Science |
| | Schindelka, J. | Mechanistische Untersuchungen zum Abbau von Aceton in der wässrigen Phase | 2010 | University of Leipzig, Faculty of Chemistry and Mineralogy |
| | Teich, M. | Carbonsäuren in atmosphäreischen Partikeln an einer ländlich geprägten Messstation: Saisonale Trends und mögliche Quellen | 2011 | University of Leipzig, Faculty of Chemistry and Mineralogy |
| | Teufert, J. | Modeling the Particle Transmission Efficiency of an Aircraft-Born Aerosol Inlet | 2011 | University of Leipzig, Faculty of Physics and Earth Science |
| B.Sc. | Becher, M. | Klimatologie und Herkunft klimarelevanter Aerosolpartikel über der nordafrikanischen Hochebene | 2010 | University of Leipzig, Faculty of Physics and Earth Science |
| | Herenz, P. | Untersuchung zum Einfluss von (messgerätespezifischen inneren) Temperaturen auf das Aktivierungsverhalten von Aerosolpartikeln | 2011 | University of Leipzig, Faculty of Physics and Earth Science |
| | Klotzsche, S. | Initialisierung tropischer Wirbelstürme | 2011 | University of Leipzig, Faculty of Physics and Earth Sciences |
| | Otto, R. | Characterization and source analysis of atmospheric aerosol particles at ZOTTO, Siberia | 2010 | University of Leipzig, Faculty of Physics and Earth Science |
| | Pfitzenmaier, L. | Einfluss der atmosphärischer Grenzschicht und Luftmassenherkunft auf die Konzentration atmosphärischer Aerosolpartikel an einer Hochgebirgsstation am Beispiel Beo-Moussala, Bulgarien | 2010 | University of Leipzig, Faculty of Physics and Earth Science |
| | Rehn, J. | Die räumliche Verteilung ultrafeiner Partikel auf der städtischen Mikroskala (<100m): Experimentelle Untersuchung mit der Analyse der meteorologischen Transportvorgänge | 2011 | University of Leipzig, Faculty of Physics and Earth Science |

| Degree*) | Name | Title | Year | Faculty |
|---|---|---|---|---|
| B.Sc. | Schierz, P. | Simulation von Wasserströmungen mit freier Oberfläche berechnet mit Grafikprozessoren | 2011 | University of Leipzig, Faculty of Physics and Earth Sciences |
| | Tomsche, L. | Raum-zeitliche Verteilung ultrafeiner Aerosolpartikel in der Rauhigkeitsschicht von Dresden | 2010 | University of Leipzig, Faculty of Physics and Earth Science |
| | Wiesner, A. | Analyse optischer Eigenschaften von urbanem Aerosol während der Feldmessung MEGAPOLI | 2010 | University of Leipzig, Faculty of Physics and Earth Science |
| | Zenker, K. | Analyse feuchter Partikelgrößenverteilung im urbanen Aerosol | 2010 | University of Leipzig, Faculty of Physics and Earth Science |

*) Habil.: Habilitation, Ph. D.: Doctoral theses, Dipl.: Diploma, M.Sc.: Master of Science, B.Sc.: Bachelor of Science

## Guest scientists

| Name | Period of stay | Institution |
|---|---|---|
| Giannakaki, E. | 01.03. - 31.03.10 | Aristotle University of Thessaloniki, Greece |
| Panov, A. | 11.03. - 26.03.10 | V. N. Sukachev Institute of Forest, Russian Academy of Science, Russia |
| Ma, N. | 06.04. - 20.04.10 | Peking University, Beijing, China |
| Shaw, R. A. | 28.04. - 04.05.10 | Technological University Michigan, USA |
| Shen, X. | 01.05. - 16.05.10 | Chinese Academy of Meteorological Science, Beijing, China |
| Reitz, P. | 12.05. - 22.05.10 | Max Planck Institute for Chemistry, Mainz, Germany |
| Chen, Z. | 06.06. - 28.06.10 | Chinese Academy of Sciences Hefei, China |
| Guerrero-Rescado, J. | 15.07. - 23.07.10 | Centro de Geofísica de Évora, Portugal |
| Wagner, F. | 15.07. - 23.07.10 | Centro de Geofísica de Évora, Portugal |
| Preißler, J. | 15.07. - 23.07.10 | Centro de Geofísica de Évora, Portugal |
| Pisani, G. | 15.07. - 24.07.10 | University of Naples, Italy |
| Giannakaki, E. | 17.07. - 23.07.10 | Aristotle University of Thessaloniki, Greece |
| Gligorovski, S. | 18.07. - 14.08.10 | Universités d'Aix-Marseille, Equipe Instrumentation et Réactivité Atmosphérique, Laboratoire Chimie Provence, France |
| Prescod, D. | 06.09. - 10.09.10 | Caribbean Institute for Meteorology and Hydrology, Barbados |
| Navas-Guzman, F. | 15.09. - 30.09.10 | Centro Andaluz de Medio Ambiente (CEAMA), Universidad de Granada, Spain |
| Kristensen, T. | 01.10. - 31.12.10 | University of Copenhagen, Department of Chemistry, Denmark |

| Name | Period of stay | Institution |
|---|---|---|
| Malinka, A. | 21.10. - 28.10.10 | National Academy of Sciences of Belarus, Minsk, Belarus |
| Izaguirre, M. A. | 31.10. - 07.11.10 | University of Miami, USA |
| Roberts, G. | 05.11. - 23.11.10 | Meteo France, Toulouse, France |
| Sassen, K. | 02.01. - 07.01.11 | University of Alaska, Fairbanks, USA |
| Morozov, I. | 30.01. - 30.03.11 | Semenov Institute of Chemical Physics RAS, Moscow, Russia |
| Mouchel-Vallon, C. | 07.03. - 26.03.11 | Laboratoire Inter-universitaire des Systèmes Atmospheriques, Paris, France |
| Izaguirre, M. | 28.03. - 05.04.11 | University of Miami, USA |
| Andrade, M. | 02.05. - 13.05.11 | Universidad Mayor de San Andres, La Paz, Bolivia |
| Böhlke, C. | 19.05. - 17.06.11 | FH Düsseldorf, Germany |
| Shen, X. | 21.05. - 02.07.11 | Chinese Academy of Meteorological Sciences Beijing, China |
| Ma, N. | 01.06. - 30.08.11 | Peking University, Beijing, China |
| Shaw, R. A. | 06.06 - 10-06.11 | Technological University Michigan, USA |
| Wiedemann, K. | 26.06. - 12.07.11 | University of São Paulo, Brazil |
| Toh, Y. Y. | 29.06. - 13.07.11 | Malaysian Meteorological Department, Petaling Jaya, Malaysia |
| Temkiv, T. Š. | 11.08. - 22.08.11 | Aarhus University, Roskilde, Denmark |
| Sahyoun, M. M. | 11.08. - 22.08.11 | Danish Meteorological Institute, Copenhagen, Denmark |
| Stolzenburg, M. | 08.09. - 02.10.11 | University of Minnesota, USA |
| Sipilä, M. | 25.10. - 02.11.11 | University of Helsinki, Finland |
| Mauldin, L. | 29.10. - 19.11.11 | NOAA - National Oceanic and Atmospheric Administration, Boulder, USA |
| O'Connor, E. | 14.11. - 18.11.11 | University of Reading, Great Britain and Finish Meteorological Institute, Helsinki, Finland |
| Komppula, M. | 21.11. - 25.11.11 | Finnish Meteorologcal Institute, Kuopio, Finland |
| Jokinen, T. | 21.11. - 09.12.11 | University of Helsinki, Finland |

## Visits of IfT scientists at other research institutions

| Name | Period of stay | Institution |
|---|---|---|
| Hiebsch, A. | 15.03. - 19.03.10 | Consiglio Nazionale delle Ricerche Istituto di Metodologie per l'Analisi Ambientale I.M.A.A. - C.N.R., Potenza, Italy |
| Wandinger, U. | 15.03. - 19.03.10 | Consiglio Nazionale delle Ricerche Istituto di Metodologie per l'Analisi Ambientale I.M.A.A. - C.N.R., Potenza, Italy |
| Althausen, D. | 16.03. - 23.03.10 | Chinese Meteorological Agency, Beijing,<br>Anhui Institute of Optics and fine Mechanics, Chinese Academay of Sciences, Hefei,<br>and Sun Yat-sen University, Guangzhou, China |
| Heese, B. | 16.03. - 23.03.10 | Chinese Meteorological Agency, Beijing,<br>Anhui Institute of Optics and fine Mechanics, Chinese Academay of Sciences, Hefei,<br>and Sun Yat-sen University, Guangzhou, China |
| Engelmann, R. | 06.04. - 22.4.10 | North-West University, Potchefstroom, South Africa; CSIR - National Laser Centre, Pretoria, South Africa; Laser Research Institute,Stellenbosch University, South Africa |
| Mattis, I. | 14.06. - 19.06.10 | Grupo de Física de la Atmósfera, Centro Andaluz de Medio Ambiente (CEAMA), Universidad de Granada, Spain |
| Bräuer, P. | 20.06. - 09.07.10 | LISA, Université Paris XII, France |
| Mattis, I. | 19.07. - 30.07.10 | Consiglio Nazionale delle Ricerche Istituto di Metodologie per l'Analisi Ambientale I.M.A.A. - C.N.R., Potenza, Italya |
| Engelmann, R. | 23.08. - 27.08.10 | Department of Applied Environmental Science (ITM), Stockholm University, Sweden |
| Katzwinkel, J. | 02.09. - 10.09.10 | International School: Fluctuations and Turbulence in the Microphysics and Dynamics of Clouds, Porquerolles, France |
| Katzwinkel, J. | 11.09. - 18.09.10 | EUFAR TETRAD School: Training and Education for Turbulence, Research via Airborne Data, Hyères, France |
| Mattis, I. | 04.10. - 11.10.10 | Meteorologisches Observatorium Lindenberg, Germany |
| Tegen, I. | 25.10. - 29.10.10 | University of Leeds, School of Earth and Environment, United Kingdom |
| Althausen, D. | 07.03. - 18.03.11 | Sun Yat-sen University, Guangzhou, China |
| Seifert, P. | 27.04. - 12.05.11 | Department of Environmental Science and Engineering Gwangju Institute of Science and Technology (GIST), Gwangju, Republic of Korea |
| Herrmann, H. | 20.06 - 24.07.11 | IRCELYON and Université Claude Bernard Lyon 1, Lyon, France |
| Althausen, D. | 18.10. - 24.11.11 | Sun Yat-sen University, Guangzhou, China |
| Heese, B. | 18.10. - 24.11.11 | Sun Yat-sen University, Guangzhou, China |
| Hünerbein, A. | 07.11. - 14.11. 11 | NOAA/CIMSS University of Wisconsin, Madison, USA |

## Meetings

| Meeting | Date | national/ international | Number of participants |
|---|---|---|---|
| EGU: Clouds, Aerosols and Radiation (General Session), Vienna | 02.05. - 07.05.10 | international | 120 |
| SAMUM Special Issue Workshop, Leipzig | 25.05. - 26.05.10 | national | 33 |
| Vulkanasche-Workshop, Leipzig | 08.09.10 | national | 32 |
| Meteorologentagung DACH 2010: Fernerkundung, Bonn | 20.09. - 24.09.10 | international | 80 |
| OCEANET-Workshop, Bremen | 04.10. - 05.10.10 | national | 20 |
| IfT-Klausur, Nimbschen | 02.12. - 03.12.10 | national | 100 |
| IfT meets UFZ, Leipzig | 02.03.11 | national | 150 |
| Workshop „Ultrafeine Partikel in der Stadt“, Leipzig | 15.03. - 16.03.11 | national | 31 |
| 1st HCCT-2010 data meeting, Leipzig | 28.03. - 29.03.11 | international | 20 |
| EGU: Clouds, Aerosols and Radiation (General Session), Vienna | 03.04. - 08.04.11 | international | 120 |
| Satellite Remote Sensing Workshop, Leipzig | 10.05. - 11.05.11 | international | 20 |
| SALTRACE Preparation Workshop, Leipzig | 14.06.2011 | national | 30 |
| CPC-Workshop, Leipzig | 19.09. - 23.09.11 | international | 23 |
| CARIBIC Science Workshop, Seeheim | 04.10. - 07.10.11 | international | 40 |
| 1st Central European Aerosol Workshop, Leipzig | 19.12. - 20.12.11 | international | 20 |

## International and national field campaigns

| Field Campaign | Project partner |
|---|---|
| **ALPACA 2009-2010**<br>*Aerosol Lidar measurements at Punta Arenas in the frame of Chilean* - German cooperation<br>Punta Arenas, Chile<br>IfT: Physics Dept. | Universidad de Magallanes, Punta Arenas, Chile |
| **CARRIBA 2010**<br>*Cloud, Aerosol, Radiation, and tuRbulence in the trade wInd regime over BArbados*<br>IfT: Physics Dept. | Leipzig Institute for Meteorology, Leipzig, Germany; Max Planck Institute for Meteorology, Hamburg, Germany |
| **CARRIBA 2011**<br>*Cloud, Aerosol, Radiation, and tuRbulence in the trade wInd regime over BArbados*<br>IfT: Physics Dept. | Leipzig Institute for Meteorology, Leipzig, Germany; Max Planck Institute for Meteorology, Hamburg, Germany; Michigan Technological University, Houghton, USA |
| **CARIBIC**<br>28/46 global measurement flights in 2010/2011<br>IfT: Physics Dept. | CARIBIC consortium |

| Field Campaign | Project partner |
|---|---|
| **CLOUD 2010**<br>*Cosmics Leaving OUtdoor Droplets*<br>CERN, Switzerland<br>IfT: Physics Dept. | Austria, Finland, Germany, Portugal, Russia, Switzerland, UK, USA |
| **CLOUD 2011**<br>*Cosmics Leaving OUtdoor Droplets*<br>CERN, Switzerland<br>IfT: Physics Dept. | Austria, Finland, Germany, Portugal, Russia, Switzerland, UK, USA |
| **EARLINET** (permanent experiment)<br>*European Aerosol Research Lidar Network*<br>Leipzig, Germany<br>IfT: Physics Dept. | EARLINET Consortium |
| **EUCAARI**<br>*European Integrated Project on Aerosol, Cloud, Climate and Air Quality Interactions*<br>Melpitz, Germany<br>IfT: Physics and Chemistry Depts. | Finland, France, Germany, Switzerland, The Netherlands, United Kingdom, Sweden, Hungary, Norway, Greece |
| **EUCAARI-China 2009-2010**<br>*European Integrated Project on Aerosol, Cloud, Climate and Air Quality Interactions*<br>Shangdianzi, China<br>IfT: Physics Dept. | Chinese Academy of Meteorological Sciences, China |
| **EUCAARI-South Africa 2009-2010**<br>*European Integrated Project on Aerosol, Cloud, Climate and Air Quality Interactions*<br>Elandsfontein, South Africa<br>IfT: Physics Dept. | Finnish Meteorological Institute, Helsinki, Finland; North-West University, Potchefstroom, South Africa; South African Weather Service, South Africa |
| **EUSAAR**<br>*European Super-Sites for Atmospheric Research*<br>IfT: Physics and Chemistry Depts. | EUSAAR Consortium: Czech Republic, South Africa, India, Denmark, UEA, Brazil, Israel, Poland, Portugal, Estonia, China |
| Feinstaubbelastung in städtischen Ballungsgebieten am Beispiel von Dresden und Leipzig<br>IfT: Physics Dept. | Dresden University of Technology, Institute for traffic planning and road traffic, Dresden, Germany; Federal Environment Agency, Berlin-Dahlen, Germany; Humboldt University Berlin, Department of Geography, Berlin, Germany |
| **GOPHER 2010-2011**<br>*leipziG stellenbOsch cooPeration close to the Hottentotten naturE Reserve*<br>Stellenbosch, South Africa<br>IfT: Physics Dept. | Laser Research Institute, Faculty of Science, Stellenbosch University, South Africa |
| **GUAN**<br>*German Ultrafine Aerosol Network*<br>IfT: Physics and Chemistry Depts. | Umweltbundesamt Langen, Germany; German Research Center for Environmental Health, Munich, Germany; Saxon State Ministry of the Environment and Agriculture, Dresden, Germany; Institute of Energy and Environmental Technology e.V. (IUTA), Duisburg, Germany; DWD Hohenpeißenberg, Germany; ISSEP, Liège, Belgium |

| Field Campaign | Project partner |
|---|---|
| **HCCT 2010**<br>*Hill Cap Cloud Thuringia 2010*<br>Schmücke, Thuringia<br>IfT: Chemistry, Physics and Modeling Depts. | Germany, United Kingdom, France, USA |
| **IMPACT**<br>IfT: Physics Dept. | The Netherlands |
| **LACIS Campaign Examination of coated and uncoated ATD and SO2-Particles**<br>LACIS, IfT Leipzig, Germany<br>IfT: Physics Dept. | Johannes Gutenberg University Mainz, Germany |
| **LACIS Campaign Bioparticles**<br>LACIS, IfT Leipzig, Germany<br>IfT: Physics Dept. | Aarhus University, Roskilde, Denmark; Danish Meteorological Institute, Copenhagen, Denmark |
| **Lagrangian Turbulence of Cloud Droplets**<br>Umweltforschungsstation Zugspitze, Germany<br>IfT: Physics Dept. | Michigan Technology University, Houghton, Michigan, USA; Max Planck Institute for Dynamics and Self-Organization, Göttingen, Germany; University of Warsaw, Poland |
| **LEAK Campaign BMU Feinstaub 2**<br>LEAK IfT Leipzig, Germany<br>IfT: Chemistry and Physics Dept. | Deutsches BiomasseForschungsZentrum, Leipzig, Germany; TU Hamburg-Harburg, Germany; Universität Konstanz, Germany |
| **MEGACITIES-2 2010**<br>Zhongshan, China<br>IfT: Physics Dept. | University of Leipzig, Germany; Peking University, China; Anhui Institute of Optics and Fine Mechanics, Chinese Academy of Sciences, Hefei, China |
| **MEGACITIES-3 2011**<br>Guangzhou, China<br>IfT: Physics Dept. | University of Leipzig, Germany; University of Bielefeld, Germany; Sun Yat-sen University, Guangzhou, China; Taiwan National Tsing Hua University, Taiwan; Montana University, USA |
| **MEGAPOLI**<br>*Megacities: Emissions, urban, regional and global atmospheric pollution and climate effects, and integrated tools for assessment and mitigation*<br>Paris, France<br>IfT: Physics Dept. | MEGAPOLI Consortium |
| **OCEANET**<br>*Autonome Messplattformen zur Bestimmung des Stoff- und Energieaustauschs zwischen Ozean und Atmosphäre*<br>IFM-GEOMAR: Polarstern and IfT: Physics Dept. | Leibniz-Institut für Meereswissenschaften IFM-GEOMAR, Kiel, Germany; GKSS-Forschungszentrum, Geesthacht, Germany; Alfred-Wegener-Institut für Polar- und Meeresforschung AWI, Potsdam, Germany; Universität Bremen, Germany |
| **PRADACS**<br>*Puerto Rico African Dust And Cloud Study*<br>East Peak, Puerto Rico<br>IfT: Physics Dept. | Max Planck Institute for Chemistry, Mainz, Germany; University of Puerto Rico, San Juan, Puerto Rico; Colorado State University, Fort Collins, Colorado, USA; ETH Zurich, Zurich, Switzerland; University of Mexico, Mexico City, Mexico |

| Field Campaign | Project partner |
|---|---|
| **ROLI10**<br>*Romanian Lidar Intercomparison 2010*<br>Cluj, Romania<br>IfT: Physics Dept. | EARLINET Consortium |
| **SOPRAN**<br>*Surface Ocean Processes in the Anthropocene*<br>Cape Verde<br>IfT: Physics, Chemistry and Modeling Depts. | Germany, United Kingdom, Cape Verde |
| **SPALI10**<br>*SPAnish Lidar Intercomparison 2010*<br>Madrid, Spain<br>IfT: Physics Dept. | EARLINET Consortium |
| Strömungsfeldmessungen an der AIDA-Kammer<br>Karlsruhe, Germany<br>IfT: Physics Dept. | Institute of Technology, Karlsruhe, Germany |

## Memberships

| Name | Board | Year |
|---|---|---|
| Birmili, W. | Editorial Board Member "Atmospheric Chemistry and Physics" | 2010/2011 |
| | Member of the advisory board of "Boreal Environmental Research" | 2010/2011 |
| Gnauk, T. | VDI/DIN KRdL-AG Messen von Partikeln in der Außenluft | 2010 |
| Hellmuth, O. | Membership in the International Association for the Properties of Water and Steam (IAPWS), Working Group Thermophysical Properties of Water and Steam (TPWS) | 2011 |
| Hermann, M. | Wissenschaftlicher Lenkungsausschuss (WLA) HALO | 2010/2011 |
| Herrmann, H. | Vorsitz des Arbeitskreises „Atmosphärenchemie" in der GDCh-Fachgruppe „Umweltchemie und Ökotoxikologie (AKAC)" | 2010/2011 |
| | DECHEMA/GDCh/Bunsengesellschaft; Gemeinschaftsausschuss „Chemie der Atmosphäre" | 2010/2011 |
| | „DECHEMA/GDCh/KRdL Expertengruppe Feinstaub" - Mitglied der Lenkungsgruppe | 2010/2011 |
| | Mitglied des wissenschaftlichen Beirats der „Kommission zur Reinhaltung der Luft" (KRdL) des Vereins Deutscher Ingenieure (VDI) | 2010/2011 |
| | Fellow of International Union of Pure and Applied Chemistry | 2010/2011 |
| | Editorial Board Member "Atmospheric Measurement Techniques" | 2011 |
| | Editorial Board Member "Atmospheric Pollution Research" | 2010/2011 |
| Iinuma, Y. | Chair der Working Group "Aerosol Chemistry within the EAA (European Aerosol Assembly)" | 2010/2011 |
| | Editorial Board Member "Atmospheric Measurement Techniques" | 2011 |

| Name | Board | Year |
|---|---|---|
| Macke, A. | Member Advisory Board „Meteorologische Zeitschrift“ | 2010/2011 |
| | Associate Editor “Atmospheric Research” | 2010/2011 |
| | Chairman of „Zweigverein Hamburg der Deutschen Meteorologischen Gesellschaft | 2010 |
| | Member of „Wissenschaftlicher Beirat des Deutschen Wetterdienstes“ | 2010/2011 |
| | Editorial Board Member “Atmospheric Measurement Techniques” | 2010/2011 |
| | Member of „Redaktionsausschuss promet“ | 2010/2011 |
| | Member of the International Radiation Comission | 2010/2011 |
| | Member of „Wissenschaftlicher Beirat des Forschungsprogrammes KLIWAS“ | 2010/2011 |
| | Member of the HALO Science Steering Comitee | 2010/2011 |
| | Member of „HALO Kuratorium“ | 2011 |
| | Member of „EU-Lenkungsgruppe“ der Wissenschaftsgemeinschaft Leibniz | 2011 |
| Renner, E. | DECHEMA/GVC-Arbeitsausschuss „Schadstoffausbreitung“ | 2010/2011 |
| | Scientific Committee of the NATO/CCMS ITM conference series, German member | 2010/2011 |
| Siebert, H. | WG4 leader and Management Comity in “COST ACTION MP0806-Particles in Turbulence” | 2010 |
| Stratmann, F. | Work Package (WP) Leader EU-Projekt EUROCHAMP 2 | 2010 |
| | Member of the EUROCHAMP 2 User Selection Panel (USP) | 2010 |
| | Member of International Conference on Clouds and Precipitation (ICCP) Board | 2010/2011 |
| Stratmann, F. | Member of the International Conference on Clouds and Precipitation (ICCP) 2012 local organizing committee | 2010/2011 |
| Tegen, I. | GESAMP (Group of Experts on the Scientific Aspects of Marine Environmental Protection), Member of Working Group 38, The Atmospheric Input of Chemicals to the Ocean | 2010/2011 |
| | “SDS-WAS (WMO Sand and Dust Storm Warning Advisory and Assessment System), Member of Steering Committee” | 2010/2011 |
| | ADOM (Atmospheric Dynamics during the last glacial cycle: Observation and Modeling) Co-Chair Eolian Records – Atmospheric Dynamics Working Group of PAGES (Past Global Changes, IGBP) | 2010/2011 |
| | Associate Editor, Journal of Geophysical Research, Atmospheres | 2010/2011 |
| Wandinger, U. | Topical Editor “Applied Optics” | 2010 |
| | Member of the ESA-JAXA EarthCARE Joint Mission Advisory Group | 2010/2011 |
| | Member of the EARLINET Council | 2010/2011 |
| | Member Scientific Steering Committee and Work Package Leader EU Project ACTRIS | 2011 |

| Name | Board | Year |
|---|---|---|
| Wehner, B. | Mitglied des GAeF-Vorstands (Gesellschaft für Aerosolforschung) | 2010/2011 |
| | „Vorsitzende des Zweigvereins Leipzig der DMG (Deutsche Meteorologische Gesellschaft)“ | 2010/2011 |
| | Co-Chair der Working Group “Atmospheric Aerosols” within the EAA (European Aerosol Assembly) | 2010/2011 |
| Wex, H. | Member of the International Conference on Clouds and Precipitation (ICCP) 2012 local organizing committee | 2010/2011 |
| Wiedensohler, A. | “Scientific Advisory Group” for aerosols within the “Global Atmosphere Watch”-program of the Meteorological Organization“ | 2010/2011 |
| | VDI-Ausschuss „Partikelzählung in der Atmosphäre“ | 2010/2011 |
| | Member Scientific Steering Committee (SSC) and Work Package (WP) Leader EU Project ACTRIS | 2011 |
| | Member SSC EU-Projekt EUSAAR | 2010/2011 |
| | Guest Professor “Peking University”, Department of Environmental Science, China | 2010/2011 |
| | Leiter Weltkalibrierzentrum für Aerosolphysik im Rahmen von WMO-GAW | 2010/2011 |
| | Editorial Board Member “Atmospheric Chemistry and Physics” | 2010/2011 |
| | Editorial Board Member “Atmospheric Measurement Techniques” | 2010/2011 |

## Cooperations

### International Cooperations

| Research project | Cooperation partners |
|---|---|
| **ACTOS**<br>*Airborne Cloud Turbulence Observation System - Interaction between turbulent mixing processes and cloud micro-physical characteristics in stratiform boundary layer clouds* | Michigan Technological University, Department of Physics, Houghton, USA |
| **ACTRIS**<br>*Aerosols, Clouds, and Trace gases Research InfraStructure Network* | >50 partners |
| **AERONET**<br>*Aerosol Robotic Network* | National Aeronautics and Space Administration (NASA), USA |
| **AIE**<br>*Atmospheric Environmental Impacts of Aerosol in East Asia* | 30 partners |
| **ALPACA**<br>*Aerosol Lidar measurements at Punta Arenas in the frame of Chilean - German cooperation* | Universidad de Magallanes, Punta Arenas, Chile |
| Anthropogenic influence of Asian aerosol on tropical cirrus clouds | National Center for Atmospheric Research (NCAR), Boulder, Colorado, USA |

| Research project | Cooperation partners |
|---|---|
| **AQMEII**<br>*Air Quality Model Evaluation International Initiative* | Austria, Australia, Belgium, Canada, Switzerland, Cyprus, Germany, Denmark, Finland, France, Greece, Italy, Luxembourg, Malta, The Netherlands, Norway, Poland, Portugal, Sweden, United Kingdom, USA |
| **ATMOCHEM**<br>*Modeling the multiphase evolution of organic carbon in the troposphere: Development of an expert system based on a self generating approach* | LISA - Laboratoire Interuniversitaire des Systèmes Atmosphériques, Université Paris, France |
| Atmospheric Nucleation | Universities of Helsinki and Kuopio, Finland |
| **CARIBIC/IAGOS**<br>*Civil Aircraft for Remote Sensing and In situ measurement in Tropospheric and Lower Stratosphere based on the Instrumentation Container Concept* | Germany, United Kingdom, France, The Netherlands, Switzerland, Sweden |
| **CARRIBA**<br>*Cloud, Aerosol, Radiation, and tuRbulence in the trade wInd regime over BArbados* | Caribbean Institute for Meteorology and Hydrology, Barbados, Meteo France, France; University of Leipzig, Germany; Max Planck Institute for Meteorology, Germany; Leipzig Institute for Meteorology (LIM), University of Leipzig |
| **Central European Air Quality Cooperation** -<br>*Harmonization of aerosol sampling and measurement; exchange of measurement data; comparison of PM transport models* | Poland, Czech Republic |
| **CLOUD – ITN**<br>*Cosmics leaving OUtdoor Droplets - International Training Network* | Germany, Switzerland, Finland, Austria, United Kingdom |
| **CLOUD**<br>*Cosmics Leaving OUtdoor Droplets* | Germany, Switzerland, Finland, Austria, Portugal, Russia, United Kingdom |
| Comparison of regional dust models | France, United Kingdom, Spain, Israel, Italy |
| Cooperation partners involved in research projects at the IfT Research Station Melpitz | Norway, United Kingdom, Italy, Switzerland, Czech Republic, Hungary, Ireland, Finland, Austria, Sweden, Bulgaria, Belgium, France, Greece, The Netherlands, Spain, Denmark, Latvia, Poland, Portugal |
| COST “Particles in Turbulence” | European consortium |
| **COST**<br>*Chemistry transport model intercomparison* | Germany, The Netherlands, Finland, France |
| Development and evaluation of methods for the quantification of trace compounds produced by biomass burning | Academy of Science of Taipei, Taiwan |
| **DFG-COPS**<br>*Convective and Orographically-induced Precipitation Study* | Germany, France, The Netherlands, United Kingdom, Italy, Switzerland, USA |
| **EARLINET**<br>*European Aerosol Research Network* | Germany, Italy, Greece, Switzerland, Sweden, Spain, Portugal, Poland, Republic of Belarus, United Kingdom, France, Bulgaria |

| Research project | Cooperation partners |
|---|---|
| **EARLINET-ASOS**<br>*European Aerosol Research Lidar Network-Advanced Sustainable Observation System* | Italy, Germany, Spain, Greece, Switzerland, Sweden, Poland, Republic of Belarus, France, Bulgaria, Romania, Norway, The Netherlands |
| **ESA-ADM**<br>*European Space Agency, Atmospheric Dynamics Mission* | European Space Research and Technology Center (ESTEC), The Netherlands |
| **ESA-CALIPSO**<br>*EARLINET's Spaceborne-lidar-related Activity During the CALIPSO Mission* | European Space Research and Technology Center (ESTEC), The Netherlands; EARLINET Consortium |
| **ESA-EarthCARE**<br>*European Space Agency, Earth Clouds, Aerosol and Radiation Explorer* | European Space Research and Technology Center (ESTEC), The Netherlands; Japan Aerospace Exploration Agency |
| **EUCAARI**<br>*European Integrated Project on Aerosol, Cloud, Climate and Air Quality Interactions* | Norway, Germany, Finland, France, Switzerland, The Netherlands, United Kingdom, Italy, Sweden, Hungary, Ireland, Greece, Czech Republic, Denmark, India, Brazil, South Africa, India, Estonia, Austria, Poland, Portugal, China |
| **EUFAR**<br>*European Fleet for Airborne Research in the Field of Environment and Geo Science* | Germany, United Kingdom, France, Ireland, Sweden |
| **EUROCHAMP-II**<br>*Integration of European Simulation Chambers for Investigating Atmospheric Processes* | Denmark, Germany, Italy, Spain, United Kingdom, Ireland, France, Switzerland, Sweden |
| **EUSAAR**<br>*European Supersites for Atmospheric Aerosol Research* | United Kingdom, The Netherlands, Finland, Switzerland, Norway, France, Greece, Spain, Bulgaria, Ireland, Lithuania, Germany, Italy, Sweden, Czech Republic |
| **HaChi**<br>*The regional aerosol in eastern China and its cloud microphysical and optical properties at high relative humidities* | China, Germany |
| **HCCT 2010**<br>*Hill Cap Cloud Thuringia 2010* | Germany, United Kingdom, France, USA, Switzerland |
| **IAGOS**<br>*Integration of routine Aircraft measurements into a Global Observing System* | Germany, United Kingdom, France |
| **ICAROHS**<br>*Observational Requirements for Multi-wavelength HSRL Systems* | European Space Research and Technology Center (ESTEC), The Netherlands; German Aerospace Center (DLR), Oberpfaffenhofen, Germany; Royal Netherlands Meteorological Institute (KNMI), de Bilt, The Netherlands; Meteorological Institute of the Ludwig-Maximilians-Universität, Munich, Germany; DEIMOS Space S.L., Madrid, Spain |

| Research project | Cooperation partners |
|---|---|
| Improvement of PollyXT FMI | Finnish Meteorological Institute, Kuopio, Finland |
| Inter-comparison of dust regional models | LISA - Laboratoire Interuniversitaire des Systèmes Atmosphériques, Université Paris, France; LaMP - Laboratoire de Météorologie Physique, Université Blaise Pascal Clermont-Ferrand, France |
| **IRMA**<br>*Imager Retrieval Methods and ATLID synergy* | European Space Research and Technology Center (ESTEC), The Netherlands; BMT ARGOSS, The Netherlands; University of Bremen, Germany; Deutscher Wetterdienst, Richard-Aßmann-Observatorium Lindenberg, Germany |
| Laboratory investigations in the field of liquid phase chemistry | National Institute of Chemistry Ljubljana, Slovenia; Université de Lyon, France; Université de Marseilles, France; Semenov Institute of Chemical Physics, Moscow, Russia |
| **LACIS**<br>*Leipzig Aerosol Cloud Interaction Simulator* | USA, United Kingdom, Russia, Denmark, Germany, Finland |
| Lagrangian turbulence in clouds | Max Planck Institute for Dynamics and Self-Organization, Göttingen, Germany; Ilmenau University of Technology, Germany; Michigan Technological University, USA; University of Warsaw, Poland |
| Lidar development, Measurement of Asian Aerosols | Gwangju Institute of Science and Technology (GIST), Republic of Korea |
| **MEGACITIES**<br>*Satellite-Based Aerosol Mapping over Megacities: Development of Methodology and Application in Health and Climate Related Studies* | University of Leipzig, Germany; University of Bielefeld, Germany; Peking University, China; Anhui Institute of Optics and Fine Mechanics, Chinese Academy of Sciences, Hefei, China; Sun Yat-sen University, Guangzhou, China; Taiwan National Tsing Hua University, Taiwan; Montana University, USA |
| **MEGAPOLI**<br>*Megacities: Emissions, urban, regional and Global Atmospheric Pollution and climate effects, and Integrated tools for assessment and mitigation* | MEGAPOLI-Consortium |
| Multiple scattering in Raman lidar signals | National Academy of Science of Belarus; Institute of Physics, Minsk, Republic of Belarus |
| **NASA-CALIPSO**<br>*Cloud-Aerosol Lidar and Infrared Pathfinder Satellite Observations*<br>(Lidar ground truth, EARLINET) | National Aeronautics and Space Administration (NASA), USA |
| **PAREST**<br>*PArtikel-REduktions-STrategien* | Germany, The Netherlands |

| Research project | Cooperation partners |
|---|---|
| Polar stratospheric clouds | Service d'Aéronomie CNRS/IPSL UPMC, Paris, France |
| Polly in Stockholm | Department of Applied Environmental Science (ITM), Stockholm University, Sweden |
| Polly-Measurements in China | Chinese Academy of Meteorological Sciences, Peking, China |
| Polly-Measurements in South Africa | Laser Research Institute, Faculty of Science, Stellenbosch University, South Africa |
| Polly$^{XT}$ development | Institute of Geophysics, University of Warsaw, Poland |
| Polly$^{XT}$ in Evora | Universidade de Évora, Centro de Geofísica de Évora, Portugal |
| Polly$^{XT}$ in South Korea | National Institute of Environmental Research, Air Quality Research Division, Republic of Korea |
| **PRADACS**<br>*Puerto Rico African Dust And Cloud Study* | Germany, Puerto Rico, USA, Switzerland, Mexico, Brazil |
| Relations between directly emitted wood burning emissions and ambient particle concentration in the Melbourne region | Commonwealth Scientific and Industrial Research Organization (CSIRO), Melbourne, Australia |
| Theory of Ice and Salt Crystallization in Aqueous Electrolyte and Polymeric Solutions | Georgia Institute of Technology, Atlanta, Georgia, USA; IAWPS International Association for the Properties of Water and Steam; Institute for Thermal Physics, Ekaterinburg, Russia; Joint Institute for Nuclear Research Dubna, Russia; St. Petersburg State University, Saint Petersburg, Russia; SUNY at Buffalo, Buffalo, NY, USA |
| Twinning Partnership with GAW-Stations | Korean Meteorological Service; Global Atmosphere Watch (GAW), Anmyeon, Republic of Korea; Malaysian Meteorological Service, Danum Valley, Malaysia; Bulgarian Academy of Sciences, BEO-Moussala, Bulgaria |
| **UFIPOLNET** (continuation)<br>*Ultrafine particle size distributions in air pollution monitoring networks* | Germany, Italy, Sweden, Czech Republic |
| **UFIREG - ultrafine particles & health** | Germany, Czech Republic, Slovenia, Ukraine |
| **Ultraschwarz - ultrafine particle exposure** | Germany, Czech Republic |
| **VRAME**<br>*Vertically resolved aerosol model for Europe from a synergy of EARLINET and AERONET data* | European Space Research and Technology Center (ESTEC), The Netherlands; Brockmann Consult GmbH, Germany; Aristotle University of Thessaloniki, Greece |

| Research project | Cooperation partners |
|---|---|
| **ZOTTO**<br>*Zotino Tall Tower Facility (sources and budgets of tropospheric aerosols over Siberia)* | Max Planck Institute for Biogeochemistry, Jena, Germany; Max Planck Institute for Chemistry, Mainz, Germany; IFOR-RASS, Krasnojarsk, Russia |

**National Cooperations**

| Research project | Cooperation partners |
|---|---|
| **AirShield (BMBF-Verbundprojekt)**<br>*Airborne remote sensing for hazard inspection by network enabled lightweight drones* | 8 Projektpartner |
| Analyse der grenzüberschreitenden Beiträge der Feinstaubbelastung in Deutschland | Umweltbundesamt, Dessau-Roßlau |
| **BMU Feinstaub-II**<br>*Wärme aus Holz-Feinstaubemissionen: Brennstoffeinfluss, Nutzer, Feuerungswettbewerb, Sekundärmaßnahmen, Charakterisierung, Toxizität* | Deutsches BiomasseForschungsZentrum, Leipzig; TU Hamburg-Harburg; Universität Konstanz; Technologie- und Förderzentrum im Kompetenzzentrum für Nachwachsende Rohstoffe, Straubing |
| **DFG-Forschergruppe SAMUM**<br>*Saharan Mineral Dust Experiment* | 9 Projektpartner |
| **DFG-SPP HALO**<br>Mission: ML-CIRRUS<br>Mission: ACRIDICON<br>Konzeption der HALO-Datenbank und eines HALO-Missionsplanungswerkzeugs | <br>12 Projektpartner<br>16 Projektpartner<br>World Data Center for Climate; Max-Planck-Institut für Meteorologie, Hamburg; Deutsches Zentrum für Luft- und Raumfahrt (DLR), Oberpfaffenhofen |
| **DWD-Raman-Lidar** | Kayser-Threde GmbH, München; DWD Offenbach; Meteorologisches Observatorium, Lindenberg; inqbus it-consulting, Leipzig; Loritus GmbH, München |
| Feinstaubbelastung in städtischen Ballungsgebieten am Beispiel von Dresden und Leipzig | Technische Universität Dresden (Verkehrswesen); TU Freiberg, Interdisziplinäres Ökologisches Zentrum; Umweltbundesamt Berlin |
| **GERUCH**<br>*Ermittlung der Quellen von Gerüchen und hohen Schadstoffkonzentrationen im Erzgebirge über die Modellierung der Luftmassenbahnen* | Sächsisches Landesamt für Umwelt, Landwirtschaft und Geologie, Dresden |
| **Hans Ertel Zentrum für Wetterforschung** | Deutscher Wetterdienst, Offenbach; Universität Bonn |
| Hochauflösende Modellierung von Wolken und Schwerewellen: Skalenanalyse, Numerik, Validierung (Leibniz-Pakt-Verfahren) | Leibniz-Institut für Atmosphärenphysik, Rostock; Potsdam-Institut für Klimafolgenforschung, Potsdam |

| Research project | Cooperation partners |
|---|---|
| **ICOS**<br>*Integrating Cloud Observations from Ground and Space – a Way to Combine Time and Space Information* | Universität Köln; Freie Universität Berlin |
| Influence of domestic wood stoves on particulate concentrations in rural areas of Saxony | Sächsisches Landesamt für Umwelt, Landwirtschaft und Geologie, Dresden |
| Karten der Feinstaubbelastung für den Nationalatlas aktuell | Leibniz-Institut für Länderkunde (IfL), Leipzig |
| **MARGA**<br>*Physikalisch-chemische Charakterisierung des dynamischen Verhaltens von Ammoniumsalzen im Feinstaub-Aerosol – Erprobung eines neuen zeitlich hochauflösenden Messverfahrens an der EMEP-Level 3-Station Melpitz* | Umweltbundesamt, Dessau-Roßlau |
| Messtechnische Begleitung der Umweltzone in Leipzig | Sächsisches Landesamt für Umwelt, Landwirtschaft und Geologie, Dresden |
| **OCEANET**<br>*Autonome Messplattformen zur Bestimmung des Stoff- und Energieaustauschs zwischen Ozean und Atmosphäre* | Leibniz-Institut für Meereswissenschaften IFM-GEOMAR, Kiel; GKSS-Forschungszentrum, Geesthacht; Alfred-Wegener-Institut für Polar- und Meeresforschung AWI, Potsdam; Universität Bremen |
| Paralleles Kopplungs-Framework und moderne Zeitintegrationsverfahren für detaillierte Wolkenprozesse in atmosphärischen Modellen | Technische Universität Dresden, Zentrum für Informationsdienste und Hochleistungsrechnen; Martin-Luther-Universität Halle-Wittenberg |
| Qualitätssicherung und Qualitätskontrolle der Messung ultrafeiner Partikel in der Außenluft im Jahr 2010 | Sächsisches Landesamt für Umwelt, Landwirtschaft und Geologie, Dresden |
| **REGKLAM (BMBF-Verbundprojekt)**<br>*Entwicklung und Erprobung eines integrierten regionalen Klimaanpassungsprogramms für die Modellregion Dresden* | 6 Projektpartner |
| Short-term Health Effects of Fine and Ultra-fine Particle Pollution in Beijing, China | Institut für Epidemiologie, GSF-Forschungszentrum für Umwelt und Gesundheit GmbH, Neuherberg; Helmholtz-Zentrum für Umweltforschung UFZ, Abteilung Expositionsforschung und Epidemiologie, Leipzig |
| **SOPRAN (BMBF)**<br>Surface Ocean Processes in the Anthropocene | 8 Projektpartner |
| Theory of ice and salt crystallisation in aqueous electrolyte and polymeric solutions | Institut für Polymerphysik, Universität Rostock; Institut für Ostseeforschung, Warnemünde |

| Research project | Cooperation partners |
|---|---|
| **UFOPLAN**<br>*Physikalische und chemische Charakterisierung von Fein- und Ultrafeinstaubpartikeln in der Außenluft)* | Umweltbundesamt, Dessau-Roßlau; Langen, Garmisch-Partenkirchen, Hofsgrund; Deutscher Wetterdienst, Hohenpeißenberg; IUTA Duisburg e. V.; Helmholtz-Zentrum, München; Universität Augsburg |
| Vergleich von Mobilitätsspektrometern des Typs UFP | Sächsisches Landesamt für Umwelt, Landwirtschaft und Geologie, Dresden; TSI GmbH, Aachen; Topas GmbH, Dresden; Gewerbeaufsichtsamt, Hildesheim; Helmholtz-Zentrum, München |

## Boards

### Scientific advisory board

| Name | Institution |
|---|---|
| Prof. Dr. Th. Benter **(Chair)** | Bergische Universität Wuppertal, Physikalische Chemie, FB C - Mathematik und Naturwissenschaften |
| PD Mag. Dr. F. H. Berger | Deutscher Wetterdienst, Richard-Aßmann-Observatorium, Tauche/ Lindenberg |
| Prof. Dr. A. Bott | Rheinische Friedrich-Wilhelms-Universität Bonn, Meteorologisches Institut |
| Prof. Dr. P. Builtjes | TNO Environment and Geosciences, Department of Air Quality and Climate, The Netherlands |
| Ms. Prof. Dr. S. Crewell | Universität Köln, Institut für Geophysik und Meteorologie |
| Dr. G. Ehret | Deutsches Zentrum für Luft- und Raumfahrt (DLR), Institut für Physik der Atmosphäre, Abteilung LIDAR |
| Ms. Prof. Dr. A. Flossmann | Observatoire de Physique du Globe de Clermont-Ferrand, Université Blaise Pascal, Aubière, France |
| Prof. Dr. J. Orphal | Forschungszentrum Karlsruhe GmbH, Institut für Meteorologie und Klimaforschung (IMK) |
| Prof. Dr. M. Wendisch | Institut für Meteorologie der Universität Leipzig |
| Prof. Dr. A. Wahner | Forschungszentrum Jülich GmbH ,Institut für Chemie und Dynamik der Geosphäre, ICG-2: Troposphäre |

### Boards of trustees

| Name | Institution |
|---|---|
| RR'in C. Liebner | Sächsisches Staatsministerium für Wissenschaft und Kunst, Dresden |
| RD'in Dr. G. Helbig | Bundesministerium für Bildung und Forschung, Bonn |
| Prof. Dr. C. Simmer | Rheinische Friedrich-Wilhelms-Universität Bonn, Meteorologisches Institut |

**Member of the IfT-Association**

| Name | Institution |
|---|---|
| RR'in C. Liebner | Sächsisches Staatsministerium für Wissenschaft und Kunst, Dresden |
| RD'in Dr. G. Helbig | Bundesministerium für Bildung und Forschung, Bonn |
| Prof. Dr. P. Warneck | Mainz |
| Prof. Dr. B. Brümmer | Universität Hamburg, Meteorologisches Institut |
| Prof. Dr. W. Engewald **(Chair)** | Universität Leipzig, Fakultät für Chemie und Mineralogie |

## Organigram

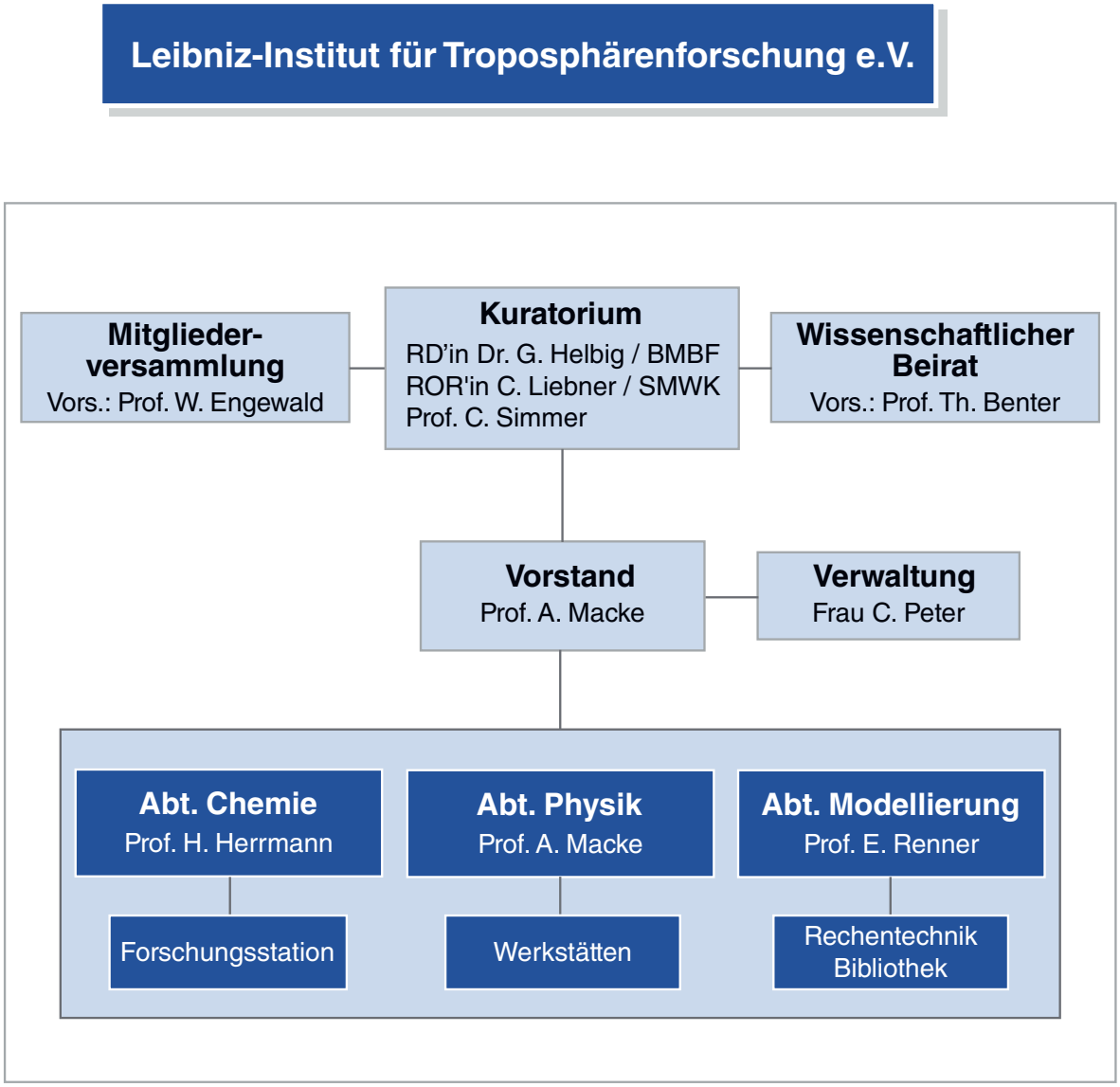

## *Leibniz Institute for Tropospheric Research & Research Park Leipzig Permoserstrasse*